PN-ABB-859
75848

7.051

PROGRAM IN SCIENCE AND TECHNOLOGY COOPERATION (PSTC)

PROGRESS REPORT NO. 6 (FINAL)

FROM SEPTEMBER 1, 1990 TO DECEMBER 31, 1990

PROPOSAL NO. 7.051

GRANT NO. 936-5542-G-00-7034-00

WELDED WIRE WALL AND EMBANKMENT SYSTEM WITH POOR QUALITY BACKFILL ON SOFT CLAY

Dr. Dennes T. Bergado
Associate Professor
Geotechnical and Transportation Engineering Division
Asian Institute of Technology
G.P.O. Box 2754, Bangkok 10501
Tel. No. 5245512
Fax No.(66-2)516-2126

THAILAND

March 1992

PROJECT PROFILE

Country : Thailand

Program : Program in Science and Technology Cooperation

Proposal No. : 7.051

Grant No. : 936-5542-G-00-7034-00

Project Durtion : Three (3) years

Reporting Period : September 1, 1990 to December 31, 1990

Project Title : Welded Wire Wall and Embankment System with Poor Quality Backfill on Soft Clay

Principal Investigator : Dr. Dennes T. Bergado

Co-Investigators : Prof. A. S. Balasubramaniam
Dr. Ramaiah Shivashankar

Project Consultant : Prof. Loren R. Anderson
Professor and Dean
College of Engineering
Utah State University
Logan, Utah 84322
U. S. A.

Prof. J. Richard Bell
Oregon State University
U. S. A.

U. S. Collaborator : Prof. Loren R. Anderson
Professor and Dean
College of Engineering
Utah State University
Logan, Utah 84322
U. S. A.

Authorized Administrator : Asian Institute of Technology

Total Project Budget : US $150,000/-

TABLE OF CONTENTS

CHAPTER	TITLE	PAGE
	PROJECT TITLE	i
	PROJECT PROFILE	ii
	TABLE OF CONTENTS	iii
1.	INTRODUCTION/BACKGROUND	1
2.	OBJECTIVES	3
	2.1 OVERALL OBJECTIVES	3
	2.2 ACCOMPLISHMENTS IN THIS REPORTING PERIOD	4
	2.3 A CONCISE LITERATURE REVIEW AND THEORETICAL CONSIDERATIONS	5
	2.3.1 HISTORICAL DEVELOPMENT	5
	2.3.2 LINE OF MAXIMUM TENSIONS, LATERAL EARTH PRESSURES, COMPACTION INDUCED STRESSES	6
	2.3.3 PULLOUT RESISTANCES OF GRID REINFORCEMENTS	7
	2.4 PREDICTIONS OF SETTLEMENTS	8
	2.5 BACKFILL SOILS	9
	2.5.1 GENERAL	9
	2.5.2 CLAYEY SAND	9
	2.5.3 LATERITIC RESIDUAL SOILS	10
	2.5.4 WEATHERED BANGKOK CLAY	10
3.	MATERIALS AND METHODS	11
	3.1 M.S.E. TEST EMBANKMENT, SUBSOIL PROFILE, IN-SITU TESTS, CONSTRUCTION, INSTRUMENTATION	11
	3.2 LABORATORY PULLOUT TEST SET-UP AND TESTING PROCEDURE	12
	3.3 FIELD PULLOUT TESTS	14
4.	RESULTS AND DISCUSSIONS	16
	4.1 WALL BEHAVIOR	16
	4.1.1 LATERAL MOVEMENTS	16
	4.1.2 VERTICAL SETTLEMENTS	17
	4.1.3 PREDICTION OF SETTLEMENTS	18
	4.1.4 STABILITY OF TEST EMBANKMENT	20
	4.1.5 POREWATER PRESSURES	21
	4.1.6 VERTICAL PRESSURE DISTRIBUTION	22
	4.1.7 TENSILE FORCES IN REINFORCEMENTS	24
	4.1.8 LATERAL PRESSURES	25
	4.1.9 COEFFICIENT OF LATERAL PRESSURES	26
	4.1.10 MAXIMUM TENSION LINE	28
	4.1.11 PLATE LOAD TEST RESULTS	28
	4.2 LABORATORY PULLOUT TEST RESULTS, INTERACTION STUDY, PREDICTION EQUATIONS	29
	4.2.1 EFFECT OF STAGE LOADING	29
	4.2.2 FRICTION PULLOUT TEST RESULTS	30

TABLE OF CONTENTS (continued)

CHAPTER	TITLE	PAGE
	4.2.3 RIBBED FRICTION PULLOUT TESTS	31
	4.2.4 SINGLE TRANSVERSE BAR PULLOUT TESTS	31
	4.2.5 GRID PULLOUT TEST RESULTS	31
	4.2.6 PREDICTION EQUATIONS	33
	4.3 FIELD PULLOUT TEST RESULTS	34
	4.4 COMPARISON BETWEEN LABORATORY AND FIELD PULLOUT TEST RESULTS	36
	4.5 PREDICTIONS USING FINITE ELEMENT PROGRAMS	37
5.	CONCLUSIONS/REMARKS	41
	5.1 WELDED-WIRE WALL/TEST EMBANKMENT PERFORMANCE AND FIELD PULLOUT RESISTANCES	41
	5.2 LABORATORY AND FIELD PULLOUT RESISTANCES OF THE WELDED WIRE REINFORCEMENTS	42
	5.3 PREDICTED RESULTS USING THE FINITE ELEMENT PROGRAMS	44
	5.4 RECOMMENDATIONS FOR FURTHER RESEARCH	44
6.	REFERENCES	46
7.	PROBLEMS ENCOUNTERED	56
8.	WORKPLAN FOR THE NEXT PERIOD	56
9.	PUBLICATIONS	56
10.	CONFERENCE/WORKSHOP ATTENDANCE	58
11.	INTERNATIONAL TRAVEL	58
12.	RESEARCH COLLABORATION	58
13.	DISTINGUISHED VISITORS	58
14.	DISSEMINATION OF RESEARCH INFORMATION	58
15.	FINANCIAL ADMINISTRATION	58
16.	OTHER PROJECTS AND GRANTS	58
17.	TABLES	59
18.	FIGURES	70

1. INTRODUCTION / BACKGROUND

Mechanically stabilized earth (MSE) is a generic term applicable to all soil reinforcing systems. MSE is a technique of reinforcing the backfill soils in embankments and walls by the inclusion of materials that are strong in tension, to form an improved composite material. Both extensible and inextensible reinforcements have been employed. The use of cohesive-frictional backfills in MSE constructions attracted much attention with the advent of the grid type of reinforcements, especially the steel grid or the welded-wire reinforcements, since they can generate high pullout resistances in these soils. Steel grid reinforcements are regarded as the inextensible reinforcements, since they can generate the required pullout resistances at small strains. Tensar geogrids are representative of the extensible reinforcements (TENSAR, 1990). Steel grids reinforcements have the unique feature of high modulus and low extensibility (FOWLER, 1986), which is particularly very desirable for embankment/wall systems with steep or vertical facing, and resting on soft clay foundations. The creep movements with such inextensible reinforcements will be less. However, the creep movements will also depend on the soil type, and with the cohesive-frictional backfills, the soil creep will be more than with the granular soils.

A few principal advantages of the MSE construction are reiterated here.

(1) Reinforcements in MSE construction not only impart sufficient tensile strength to the soil, but also the compressive and the shear strengths are improved as well.

(2) MSE construction will enable to build steeper and higher embankments. Steep embankment side slopes result in economy, while high embankments extend the economic life of MSE structures.

(3) MSE structures show extreme tolerance for large vertical deformations and lateral movements, especially while the underlying foundation subsoil is soft clay, as in the present case. MSE construction will minimize the differential movements within the backfill and reduce the occurrences of cracks on the surface.

(4) Reinforcements at the base provide restraint against lateral spreading of the backfills, thereby, increasing the bearing capacity.

(5) MSE construction provides feasible solution under constraints of limited access or right of way.

(6) MSE construction is simple, easy and quick, requiring no skilled labour. It can be done in stages. It is generally aesthetically pleasing.

(7) According to LOW & DUNCAN (1985) and BONAPARTE & CHRISTOPHER (1987), the increase in the stiffnesses of the tension reinforcements in the embankments may reduce substantially the horizontal foundation displacements and the settlements of the subsoil.

The problem of corrosion with the steel grid reinforcements can be controlled by providing sacrificial steel and/or by providing galvanizing, and ensuring a good and uniform compaction during construction. The zinc coating acts as an excellent sacrificial coating for delaying corrosion in both granular and cohesive-frictional backfill soils (CALTRANS, 1987). However, the steel reinforcements do not provide any internal drainage as would be provided in the case of the geotextiles.

2. OBJECTIVES

2.1 OVERALL OBJECTIVES

The coastal plains of Southeast Asia are covered with thick soft marine clay deposits (Fig.1) which pose considerable foundation problems to the construction activities in the region. When earth structures such as road embankments are constructed, they tend to consolidate the soft clay deposits resulting in large vertical settlements and lateral deformations. In the Chao Phraya Plain, in and around the Bangkok metropolis, the problem is further aggravated by the ground subsidence caused by the piezometric drawdown due to the excessive withdrawal of the groundwater. The rate of subsidence can be as high as about 100 mms per year.

Under the existing subsoil conditions in the Chao Phraya Plain, only low embankments of up to 2.5 m height with gentle side slopes of 3 horizontal to 1 vertical can be constructed for many applications. These embankments usually sink below the maximum flood level after about 10 years time requiring costly reconstruction and maintenance works.

In many highway projects, the right of way are restricted due to rapid urbanization and high cost of land. One of the alternatives is to utilize steep and high embankments without the normally wide stabilizing berms and flat side slopes. Steep and high embankments result in substantial savings in the construction costs, but increase further the risk of slope instability. Additional strengthening by way of mechanical stabilization will be required for the safe construction, and for the subsequent good performance of these steep and high embankments on soft ground conditions.

Granular backfills which are generally recommended in MSE construction are not readily available in many places such as the coastal plains of Southeast Asia. The use of locally-available, cohesive-frictional soils, although considered as poor to marginal in their quality, therefore, becomes imperative in such circumstances due to economic considerations. To compensate for the poor quality of the backfill materials, MSE construction is recommended.

The use of polymeric reinforcements in the Southeast Asian region are expensive due to high import taxes. Steel grid reinforcements, on the other hand, can be locally fabricated. Thus, it is appropriate to study the behavior of the steel grid reinforcements in cohesive-frictional backfill soils. Also, the behavior of the steel grid reinforcements will be very much different while using the polymeric reinforcements.

The main objective of this research project, therefore, has been to study the potential for the use of the abundantly and locally-available, poor to marginal quality cohesive-frictional backfill soils in conjunction with welded-wire (steel grids) reinforcements in MSE wall/embankment system resting on soft clay foundation. The overall objectives can be briefly summarized as follows:

(a) To study the field performance of a full-scale and an extensively instrumented welded-wire mechanically stabilized earth (MSE) embankment/wall system (AIT wall) which utilized three different locally-available, cohesive-frictional backfills in three corresponding sections along its length, resting on soft and compressible clay foundation.

(b) To study the pullout failure mechanisms and the pullout resistances of welded-wire mats. The vertical normal (confining) pressures in the laboratory pullout tests varied between 10 to 130 kPa. Field pullout tests were also conducted. Welded-wire mats of different bar sizes and mesh geometries were used. The laboratory pullout tests were conducted at three different compaction moisture conditions, namely: dry side of optimum, at optimum moisture content, and wet side of optimum; using three different locally-available, cohesive-frictional backfill soils, namely: weathered Bangkok clay, clayey sand and lateritic residual soils. To compare the laboratory and the field pullout resistances.

(c) To utilize the techniques and experiences gained in this research as a base for technology transfer to other countries having similar geologic formations and environment such as the Southeast Asian region.

2.2 ACCOMPLISHMENTS IN THIS REPORTING PERIOD

In this reporting period, the following studies/observations were made:

(i) An overall assessment of the wall behavior suggested a significant deviation from that currently established for MSE walls resting on comparatively good foundation subsoils. Compaction induced stresses affected the lateral earth pressures considerably and thereby also the tensile stresses in the reinforcements.

(ii) The factors affecting the type of bearing capacity failure mechanisms in front of the transverse bearing members and, thereby, the total pullout resistances of the steel grid reinforcement were studied. Prediction equations which are proposed for the three different backfill soils were found to have good agreement with the experimental data.

(iii) The Reinforced Earth Analysis (REA) finite element computer program was used with the concept of equivalent friction coefficient for the grid reinforcements, to predict both the laboratory pullout test results and the wall behavior. The results were also compared with the corresponding values obtained by using another finite element computer program NONLIN 1 (LO, 1990) reported in the earlier progress report.

2.3 A CONCISE LITERATURE REVIEW & THEORETICAL CONSIDERATIONS

2.3.1 HISTORICAL DEVELOPMENT

The technique of reinforcing the soils to improve their properties dates back to the earliest days of mankind. Some classic examples of those early days, and which exist even today are the "Ziggurats" or the stepped temple towers of pyramidal shape of the ancient Babylonian civilization, now in the present-day Iraq; dikes of earth and tree branches in China; bamboo fascines used to support low embankments on soft marshy lands in Southeast Asia; corduroy roads in Scandinavia and North America etc. (HOLTZ, 1978). The centuries old concept of embedding straw and branches in the clays to improve their properties also falls in this category.

Mechanically stabilized earth (MSE) in its modern form was first applied for retaining walls which utilized granular backfills and horizontally laid steel strip reinforcements connected to concrete facing units and was called "Reinforced Earth" (VIDAL, 1969) (Fig. 2). In this case, the interaction was rightly thought of to be solely due to friction generated by the normal pressures derived from gravity. After Vidal conceived the idea of "Reinforced Earth", there were a series of experimental investigations using the laboratory triaxial and direct shear tests on reinforced sands (YANG, 1972; CHAPUIS, 1972; SCHLOSSER & LONG, 1973; HAUSMANN, 1976; MCGOWN et al. 1978; INGOLD, 1984; JURAN, 1985; JEWELL & WROTH, 1987). All the studies indicated an increase in the shear strength of the soils due to the inclusion of the reinforcements.

The use of welded-wire mats made of smooth wires was patented by the Hilfiker Company of Eureka, California, in 1978, and commissioned Utah State University to do additional pullout tests (BISHOP & ANDERSON, 1979; PETERSON & ANDERSON, 1980; NIELSEN & ANDERSON, 1984). At about the same time, and consequent to the Hilfiker welded wire walls, various other reinforced soil systems were also developed such as: mechanically stabilized embankment (MSE*) developed by the California Department of Transportation (CALTRANS), VSL Corporation's VSL retained earth, Georgia stabilized earth (GASE), reinforced soil embankment (RSE) also developed by the Hilfiker Co. etc. Figure 3 shows the different components of the welded wire wall, while Fig. 4 shows the various other reinforced soil systems.

Several investigators have studied the interaction between the reinforcements and the backfill soils from pullout tests (Table 1). Field pullout test results have been reported by many research workers (LONG, 1977; CHANG et al. 1977; SCHLOSSER & ELIAS, 1978; HANNON & FORSYTH, 1984; ANDERSON et al. 1986).

2.3.2 LINE OF MAXIMUM TENSIONS, LATERAL EARTH PRESSURES AND COMPACTION INDUCED STRESSES

All measurements taken on reduced scale models or actual reinforced earth structures by several investigators have shown that the traction forces vary from one end of the reinforcement to the other. The maximum tension was found to occur at some distance behind the face (SCHLOSSER & LONG, 1974; AL HUSSAINI & PERRY, 1976). The potential failure surface was found to comply very closely with the line of maximum tensions (Fig.5).

There were a number of welded wire walls instrumented with strain gages in connection with Utah State University research program, to measure the strains periodically both during and after construction (BISHOP & ANDERSON, 1979; ANDERSON et al. 1985; ANDERSON et al. 1986; NELSON & SELVAGE, 1987). ANDERSON et al. (1986) confirmed that the "coherent gravity structure" bi-linear failure surface presented by MCKITTRICK (1978) for reinforced earth walls to be valid for grid reinforcements. BASSETT & LAST (1978) theoretically demonstrated that the failure surface of a soil reinforced with inextensible inclusions is vertical in the upper part of the wall and does not correspond to the Mohr-Coulomb failure surface.

In a reinforced earth wall, the coefficient of lateral earth pressure was assumed to vary linearly from K_o, the coefficient of lateral earth pressure in the at-rest condition, at the top, to a value corresponding to the active case, K_a, at a depth of 6 m below the top of the wall. For depths greater than 6 m, the lateral earth pressure coefficient was assumed to be a constant at K_a as shown in Fig.6 (MCKITTRICK, 1973). With the extensible type of reinforcements, the lateral earth pressure coefficients were found to reduce below the active condition (MCGOWN et al. 1988). This is due to the fact that the extensible (polymer) reinforcements are able to undergo considerable elongation and thereby allow considerable lateral displacement of the wall face. BELL (1991) suggests that many people use active K values for extensible (polymeric) reinforcements and at-rest values for inextensible (metallic) reinforcements. He also suggests that the tie-back wedge failure plane is often used for extensible reinforcements, while the coherent gravity method is used with inextensible reinforcements.

The effects of compaction induced stresses were also observed in the case of many instrumented reinforced earth structures currently in service. In all the cases the K coefficient was found to be equal to or greater than the "at rest" pressure coefficient of the soil (K_o) at the top of the wall (SCHLOSSER & DE BUHAN, 1990). INGOLD (1983c) presented a compaction theory applicable to the reinforced soil walls.

2.3.3 PULLOUT RESISTANCES OF GRID REINFORCEMENTS

The total pullout resistance of a steel grid reinforcement, F_t, comprises of two components, namely: the bearing resistances infront of the transverse members, F_b, and the frictional resistances over the longitudinal members, F_f. Therefore, the total pullout resistance can be expressed as:

$$F_t = F_b + F_f \tag{1}$$

The transverse members can be regarded as a series of deeply embedded strip footings in succession which have been rotated to the horizontal and pulled through the soil. Two types of bearing capacity failure mechanisms infront of the transverse members have been proposed. The first is the general bearing failure mechanism (PETERSON & ANDERSON, 1980) in which the slip planes are fully developed (Fig.7). The prediction equation for the pullout resistance for this case based on the Terzaghi-Buisman bearing capacity equation is as follows:

$$F_b/NWD = C*N_c + \sigma_v*N_q \tag{2}$$

where: $$N_q = e^{(\pi*\tan\phi)} \tan^2(45 + \phi/2) \tag{3}$$

and $$N_c = (N_q - 1)/\tan\phi \tag{4}$$

This prediction seems to form an apparent upper bound envelope for the pullout capacities of the grid reinforcements (PALMEIRA & MILLIGAN, 1989; JEWELL, 1990; SHIVASHANKAR, 1991). The second mechanism proposed by JEWELL et al. (1984) is based on the punching shear failure mode of deeply embedded foundations (Fig.8). The prediction equation for the bearing capacity factor, N_q, for this case based on the equation of VESIC (1963) is as follows:

$$N_q = e^{(\pi/2 + \phi)\tan\phi} \tan(45 + \phi/2) \tag{5}$$

This prediction seems to form an apparent lower bound envelope for the pullout capacities of the grid reinforcements (PALMEIRA & MILLIGAN, 1989; JEWELL, 1990; SHIVASHANKAR, 1991).

OSPINA (1988) conducted pullout tests with radiographic measurements. A predominantly general bearing failure was observed with fine sands in their loose states, while a punching shear failure was observed in the dense states. It was also observed that by increasing the confining pressures, the failure mechanism approached a general bearing failure mechanism. Ospina observed that in the dense state, a punching shear failure developed infront of the transverse members at low deformations, would become a general bearing failure at large deformations.

PALMEIRA & MILLIGAN (1989) concluded from their pullout tests using dry Leighton Buzzard sands that the failure mechanism changes from punching shear to a generalized bearing failure when D/D_{50} exceeds 7.5, where D is the diameter of the transverse bar and D_{50} is the particle size corresponding to 50% finer. It was observed that interferences between the passive resistant zones of the bearing members become negligible for S/D values beyond about 50, where S is the spacing between the transverse members and D as defined previously.

2.4 PREDICTIONS OF SETTLEMENTS

The compression of the soft foundation subsoils subjected to distributed loads from structures built above it consists of three components namely: initial compression or the immediate settlements, primary consolidation and the secondary consolidation.

The initial compression occurs simultaneously with the application of the loads. If the soil is saturated, deformation takes place at a constant volume caused by the shear strains beneath the loaded area. If the permeability of the soil is low, little drainage takes place. Under the center line of the load, the vertical compression will be accompanied by lateral expansion or lateral yield (BJERRUM, 1972). Both the primary and the secondary consolidation or drained creep are time-dependent processes and will continue beyond the construction period. The primary consolidation or simply the consolidation settlement will cause the porewater to drain out from the soil, while the stress increments are transferred to the soil skeleton. Volume changes are mainly produced. In addition, shear deformations are also involved which lead to further settlements. Secondary compression are frequently small and are generally neglected. The main part of the secondary compression settlement occurs essentially after complete dissipation of excess porewater pressures, i.e. at practically constant effective stress. In practical cases, it is often assumed that secondary compression does not start until after primary consolidation is completed (BALASUBRAMANIAM & BRENNER, 1981).

A practical and graphical approach by which it is possible to estimate the final total settlement and the settlement rates from the settlement data obtained during a certain time period was proposed by ASAOKA (1978). The method utilizes the available settlement observations and then predicts the future settlements based on the observed values. Asaoka's method was applied to a number of case histories of embankment settlements and promising results were obtained (MAGNAN & DEROY, 1980). Accordingly, with Asaoka's method, good predictions are possible after 60% consolidation has been achieved. An important feature of the method is that it allows the separate determination of the coefficient of consolidation for vertical drainage, C_v, and the final value of the settlement. Its application is limited to single layers with one-way or two-way drainage. Asaoka's graphical method involves the following steps:

(a) The observed time-settlement curve plotted to an arithmetic scale, is divided into equal time intervals, Δt (Δt usually between 30 and 100 days). The settlements ρ_1, ρ_2, ... ρ_n corresponding to times t_1, t_2,....t_n are read and tabulated (Fig.9a).

(b) The settlement values (ρ_1, ρ_2,.... ρ_n) are then plotted as points (ρ_{i-1}, ρ_i) in a coordinate system with axes ρ_{i-1} and ρ_i, as shown in Fig.9b. The 45 degree line $\rho_i = \rho_{i-1}$ is then drawn.

(c) The plotted points are then fitted by a straight line whose corresponding slope is read as β. The point of intersection of this line with the 45 degree line, gives the final consolidation settlement, ρ_f. The coefficient of consolidation (C_v) can then be calculated from:

$$C_v = \frac{-5}{12} H^2 \frac{\ln \beta}{\Delta t} \qquad (6)$$

where H is the length of the drainage path.

2.5 BACKFILLS SOILS

2.5.1 GENERAL

As stated in the objective, three locally-available cohesive-frictional soils were used in the laboratory pullout tests and in the construction of the MSE test embankment. The index properties of these backfill soils are given in Table 2. The results of the direct and the triaxial shear tests are given in Table 3 and 4, respectively. The direct shear tests were conducted at three different moisture conditions, namely: on the dry and the wet sides of optimum moisture content (OMC), with the moisture contents corresponding to 95% of the standard Proctor density, respectively; and at optimum moisture content (OMC) compacted to 100% of the standard Proctor density (See Figs.29 to 31). The UU triaxial tests were conducted on soil specimens with dimensions of 100 mm diameter and 200 mm height. The specimens were compacted to the required density at the desired moisture content in a static compaction machine. The triaxial tests were conducted only at one moisture content, closer to the optimum moisture content on the dry side of optimum and compacted to 95% of the standard Proctor density. Typical grain size distribution curves of all the three soils are shown in Fig.10.

2.5.2 CLAYEY SAND

Clayey sand used was the beach sand from Ayuththaya about 40 kms to the north-west of Bangkok. It contained about 45% fines and was found to be sensitive to moisture variations on the wet side of optimum moisture

2.5.3 LATERITIC RESIDUAL SOILS

Lateritic soils which are abundantly in many tropical countries including the Southeast Asian region, have been primarily used as construction materials (backfills) for embankments, highway fills, and dams. The lateritic soils are regarded as strong and excellent construction materials under normal conditions. They are currently being studied in the MSE test embankment at AIT which has a vertical face on one side, and in laboratory pullout tests. Direct shear tests at low normal pressures ranging from 2 to 18 kPa were conducted in a special apparatus fabricated (AMIN, 1989; MACATOL, 1990) at AIT based on the design ONITSUKA et al. (1987). Bilinear failure envelopes were obtained at all the three moisture conditions (Fig.11). This was attributed to the particle crushing phenomenon inherent in these soils under high confining stresses. This phenomenon seems to have influenced the pullout test results as well. BOONSRI (1971) studied the shear strength characteristics of lateritic soils of Thailand and concluded that these compacted samples behave similar to lightly overconsolidated soils.

2.5.4 WEATHERED BANGKOK CLAY

Weathered Bangkok clay is abundantly available as the surficial crust, about 2 m thick. It is classified as inorganic clay of high plasticity (CH). The strength, deformation, permeability characteristics of compacted weathered clay have been studied extensively at the Asian Institute of Technology (AIT) by several research workers (LEELASITHORN, 1977; HAQUE, 1977; PLANGPONGPUN, 1977; LIEW, 1979) in connection with the settlement and stability analyses of embankments. LIEW (1979) observed that the compacted weathered clay samples behave similar to the stiff clay with the coefficient of compressibility, C_c, ranging from 0.08 to 0.12. THIRAWAT (1968) reported that weathered clay is thixotropic in nature and that this behavior was found to increase with the increase in the molding water content and the energy of compaction. HAQUE (1977) concluded that compacted weathered Bangkok clay behave similar to lightly-overconsolidated clays.

3. MATERIALS AND METHODS

3.1 M S E TEST EMBANKMENT, SUBSOIL PROFILE, IN-SITU TESTS, CONSTRUCTION, INSTRUMENTATION

A 5.7 m high welded-wire wall (AIT wall), about 14.64 m long at the top (Fig.12), was built in the AIT campus resting on soft clay foundation. It has a vertical wire mesh facing on one side and a sloping back as shown in Fig.13. Three locally-available cohesive-frictional soils were used as backfills in three corresponding sections along its length. The lateritic residual soil used in the middle section (Section II) was stronger than clayey sand or weathered clay backfills used in the end sections, Sections I and III of the wall, respectively.

The typical subsoil profile of the three uppermost layers at the campus of the Asian Institute of Technology (AIT), located about 45 km north of Bangkok, is shown in Fig.14. The soft clay in the subsoil is about 6 m thick overlain by a surficial 2 m thick weathered clay crust and underlain by a layer of stiff clay. The corresponding geotechnical properties are also indicated in Fig.14. The groundwater table is found to fluctuate between 1.0 to 2.0 m depth below the ground surface, with the season. The results of the in-situ subsoil tests such as the pressuremeter tests, the vane shear tests, the Dutch cone tests, and the screw plate load tests are shown in Figs. 15 to 19.

The welded-wire mats used as reinforcements in the backfill soils were 2.44 m wide and 5.0 m long each, of W4.5 x W3.5 (6.07 mm x 5.36 mm diameters) size bars with 0.15 m x 0.225 m (6 inches x 9 inches) grid openings. The yield strength of the welded-wire bars was about 670 MPa which occurred at very low strains in the order of about 0.4 to 0.5%, and the modulus of elasticity was about 183,145 MPa. A total of seven mats were instrumented with self-temperature compensating electrical resistant strain gages for each section as shown in Fig.13. The bent-up portion of the reinforcing mats would form a part of the facing element. Backing mats and screens were provided on the inside along the vertical face of the wall. Easy to compact gravel was backfilled extending up to 0.45 m behind the wall face (See Fig.27). The objective of this was to prevent erosion of the retained soil and also for aesthetic purposes.

The first layer of reinforcing mat was laid 0.45 m below the general ground level. The fill between the reinforcing mats was placed and compacted in 3 equal lifts to a total thickness of 0.45 m corresponding to the vertical spacing between the reinforcing mats. Each lift was compacted by a combination of a hand operated impact (Wacker) compactor and a vibratory roller to densities of about 95% of the standard Proctor density, with a variation of about ±2%. Uniformity in compaction and moisture content during construction was checked with a nuclear densitometer. The placement moisture content varied by about ±1%, corresponding to that density, on the dry side of optimum. The construction guidelines set forth by the Hilfiker Company

(Hilfiker-Texas Corp. 1988) were followed. The construction took exactly a month between April 24 to May 24, 1989.

Several field instruments were installed, both in the subsurface and within the wall itself. The schematic plan view layout of the field instrumentation is given in Fig.20. Self-temperature compensating electrical resistant strain gages measured the strains in the wires, from which the tensions in the reinforcements were estimated. There were seven instrumented layers in each section. There were 12 instrumentation points on each of the bottom four instrumented mats and 10 instrumentation points on each of the top three instrumented mats (Figs.21 and 22). At each instrumentation point, two strain gages were attached diametrically opposite each other to cancel out any bending stresses (Fig.23).

Three pneumatic total earth pressure cells monitored the base pressure distributions at the mid-section of the wall beneath the lateritic backfill (Figs.24 and 20). Lateral movements of the vertical wall face, the embankment and the subsoil were monitored with the help of five SINCO inclinometers (I1 to I5). Inclinometers I1 to I3 were installed at the face, one each at the middle of each section; I4 at the center and I5 at the back (Figs. 25 and 20). The plastic casings of the inclinometer were 69.8 mm outer diameter, 58.9 inner diameter and were 3.05 m long segments. The length of the casings was extended by suitable couplings. The grooves of the casing were oriented in the directions of the principal movement, i.e., in a direction perpendicular to the face of the wall.

Nine surface and ten subsurface settlement plates were placed at different locations and at varying depths below the test embankment to monitor the settlements (Figs.26 and 20). Four pneumatic and six hydraulic piezometers were installed to monitor the porewater pressures at different locations and varying depths beneath the embankment. The locations of the hydraulic piezometers in cross section view are shown in Fig.27 (See also Fig.20). Two pneumatic piezometers were also installed in the backfill soils (Fig.24).

A total of 26 dummy mats (Fig.12) were embedded at different levels in the three backfill soils for field pullout tests. Two dummy reinforcement in each section were instrumented with strain gages at selected points.

3.2 LABORATORY PULLOUT TEST SET-UP AND TESTING PROCEDURE

Pullout tests were conducted in the laboratory at AIT in a pullout box with inside dimensions measuring 1.25 m long x 0.75 m width x 0.51 m depth. The pullout box was made up of steel plates and rolled steel beams using both welded and bolted connections. A detailed and schematic view of the laboratory pullout test set-up is shown in Fig.28. The various components shown therein are listed in Table 5.

A multistage pullout testing procedure was followed. In each set-up, three pullout tests in three corresponding loading stages were conducted by increasing the vertical normal stress at each stage. In the first stage, the reinforcing mat was pulled out under a given normal stress. After this, the pulling force was released and the normal stress was increased for the next stage. After allowing the normal stress to stabilize for about 30 minutes the mat was pulled out again. This would form the second stage. Similarly, it would be followed by a third stage. At each stage the mat was pulled out by 25 mm.

In each set-up, the soil in the pullout box was compacted in two equal lifts of 0.15 m thickness each using a hand operated impact (Wacker) compactor. After compacting the first lift, the level of the compacted soil surface reached nearly up to the centre of the pullout slot. The grid specimen was then placed in position at the centre of the slot and checked for its level and alignment. Then the second lift of backfill soil was placed over it and compacted again. The uniformity in the degree of compaction and the moisture contents in both the lifts was checked with a Troxler nuclear gauge densitometer.

Pullout tests were conducted in the laboratory at three different moisture conditions, namely: on the dry and wet sides of optimum moisture content compacted to 95% of the standard Proctor density, and also at the optimum moisture content compacted to 100% of the standard Proctor density, similar to the direct shear tests. A variation of $\pm 2\%$ about the mean value was observed on the degree of compaction, while a corresponding variation of $\pm 1\%$ was recorded on the moisture content. Figures 29, 30 and 31 show the compaction curves for weathered clay, lateritic soil, and clayey sand, respectively, along with the ranges of the moisture contents and degrees of compaction used in the laboratory pullout tests and the direct shear tests.

Two horizontal metal plates were used as sleeves on the inside part of the opening of the pullout box, extending 0.15 m behind the face. The purpose of these sleeves was to decrease the horizontal stresses on the front face near the slot during the pullout and also to minimize the arching effects over the grid specimens. These sleeves were positioned across the full width of the pullout box, above and below the reinforcements. This would also keep the normal loads off the front 0.15 m. The two sleeves were seperated by spacers 0.1 m high provided at the front corners of the pullout box to avoid any contact with the reinforcements as shown in Fig.28

After compacting the second lift of soil in the pullout box, a thin layer of clean and dry sand, about 25 to 50 mm thick was placed over it to even up the surface, especially in the case of weathered clay and lateritic soil. This would also facilitate a uniform distribution of the vertical normal stresses. The lower top cover plate, 6.35 mm thick, was then placed over the sand layer. Inflated air bag would then be placed over this, which would take reaction from I-beams above it, which were bolted on to the top of the pullout box, through an upper top cover plate.

Two strain gauges were fixed at each instrumentation point on the grid specimen, diametrically opposite each other, to cancel out any bending stresses. Before the start of the actual pullout test, a seating load of about 2 kN was applied to remove any slack in the system. During the pullout test, a uniform pullout rate of 1 mm/min. was used and maintained with the help of electronic controls, dial gage and a stop clock. All the pullout tests were conducted under undrained conditions.

The different types of pullout tests or reinforcements that were utilized are as follows:

(a) Friction pullout tests: conducted by using a reinforcement system with only the four longitudinal bars spaced 0.15 m (6 inches) laterally and no transverse bas embedded in the soil (Fig.32a).

(b) Ribbed friction pullout tests: conducted by using a reinforcement system with only the four longitudinal bars spaced 0.15 m (6 inches) laterally and no transverse bars embedded in the soil (Fig.32b). In this case, a grid reinforcement was taken and portion of the transverse bars between the longitudinal bars were clipped leaving only the transverse ribs on the longitudinal bars in place. The length of these ribs was kept at about twice the diameter of the longitudinal bars.

(c) Single transverse bar pullout tests: conducted by using a reinforcement system with four longitudinal bars and just a single transverse bearing member welded across them which was embedded and pulled through the soil (Fig.32c).

(d) Grid pullout tests: using welded-wire grid reinforcements of varying bar sizes and mesh geometries (Fig.32 d, e). The contribution of the bearing resistances in front of the transverse members was estimated by subtracting from the result of the grid pullout test (total pullout resistance), the frictional resistance derived from the corresponding friction pullout test.

3.3 FIELD PULLOUT TESTS

The field pullout tests were conducted about 8 months after the construction of the test embankment. By this time, both the foundation subsoil and the wall/embankment system had undergone substantial vertical and lateral movements. A total of 15 constant strain field pullout tests were conducted on dummy mats embedded in all the three backfill soils with varying overburden pressures, bar sizes, and mesh geometries. Three of the dummy mats tested had no transverse bars. They had only four longitudinal bars of size W4.5 (6.1 mm diameter) with short transverse ribs on them. The rest of the dummy mats had 0.15 m x 0.225 m (6 in. x 9 in.) grid openings, with 5 to 6 transverse bars. The average length of embedment of all the dummy mats was around 2.0 m behind the vertical face of the wall. The geometry

of the instrumented dummy mats together with the locations of the strain gages are shown in Fig.33.

The procedure followed in the constant strain field pullout tests was the same as adopted in the laboratory constant strain pullout tests. The dummy reinforcements were pulled out at the same laboratory strain rate of 1 mm/min. The pullout force was applied by means of an electro-hydraulic servo-controlled cylinder through a specially designed reaction frame butting against the face of the wall. A wooden platform was built to support the pullout equipment. The horizontal displacements of the dummy mats were monitored using LVDTs and dial gages. The same data acquisition system as used in the laboratory pullout tests, consisting of the 21X micrologger with multiplexer and a storage module were also employed to record the displacements of the dummy mat during pullout, pullout force (from a load cell), and axial strains in the bars. All the mats were pulled out by about 130 mm (5 inches). Figures 34 to 36 show typical constant strain field pullout test set-ups. Figure 37 shows the gripping devices used in the constant strain field pullout tests which was similar to the one used in the laboratory constant strain pullout tests.

Two constant stress field pullout tests, one each in weathered clay and lateritic backfill soils, were also conducted to determine the long-term load-strain response of the dummy reinforcements. Figure 38 shows a typical constant stress field pullout test set-up. The pullout load was applied through a direct dead loading system comprising of a flexible wire rope, a wooden frame work, a frictionless 150 mm (6 inches) diameter pulley and a weight pan or a load hanger. Concrete blocks were placed in the pan to apply the dead load and thereby the pullout force to the reinforcement. Figure 39 shows the cross sectional view of the set-up. The gripping devices used were the same as before, but for a slight modification in providing an eye to its connecting part through which the wire rope would pass and was then tightly fastened by suitable clamps (Fig.40). The dead load was maintained for a considerable length of time until the changes in the strains were very small or negligible. The strains in the reinforcements were recorded at regular intervals of time with the help of data acquisition system and the displacements of the mat were measured by mechanical dial gages mounted in front of the reinforcing mat.

4. RESULTS AND DISCUSSIONS

4.1 WALL BEHAVIOR

The extensive instrumentation program that was employed in the welded-wire wall and in the subsoil beneath it, helped to monitor its overall behavior. The performance of the wall was evaluated from this behavior and subsequent analysis carried out in this research work, based on the observed values. The very fact that the wall still continues to perform satisfactorily, nearly three years after its construction, is ample proof to show that the welded-wire steel grids can be effectively used to reinforce poor quality backfill materials in wall/embankment systems on soft and compressible clay foundations. The behavior of the wall and its foundation were generally observed in two stages. The first stage included the period during the construction of the wall/embankment system, up to the end of construction. The second stage included the period after all the construction activities had ceased. The construction period was exactly one month.

4.1.1 LATERAL MOVEMENTS:

Lateral movements of the wall face, the embankment, and the subsoil were monitored by five inclinometers I1 to I5 (Fig.20). The lateral movements at each inclinometer with depth or height are shown plotted in Figs. 41 to 45. These figures show the profiles of the lateral movements at any inclinometer location with time. The lateral movements at inclinometers I1 and I3 near the face in the end sections were similar as at I2 also near the face in the middle section. The top of inclinometer I4 in the center of the middle section moved in the same manner as I1 to I3, i.e., outward. This indicates that the whole embankment tended to move forward as a rigid body. Figures 41 to 43 indicate a continuous outward lateral movement of the wall face (I1 to I3) and of the soft clay subsoil beneath the embankment. The maximum lateral movement in the subsoil occurred at a depth of about 3 m below the general ground level in the soft clay layer, corresponding to the weakest zone in the subsoil. This weakest zone also indicates the location of the potential shear failure surface.

Most of the lateral movements in the subsoil occurred within about 100 days from the start of construction as seen in Fig.46. Thereafter, the rate of these lateral movements decreased considerably. The maximum lateral movement of the wall face occurred at the very top. Much of the lateral movements of the wall face occurred in the post-construction phase, being largely influenced by the complex subsoil movements. The rate of lateral movements of the wall face slowed down considerably about 200 days after the end of construction (Fig.46).

After 228 days from the end of construction, the maximum outward lateral movement measured at the top of the vertical wall face was about 300 mm. The maximum lateral movement in the

subsoil was about 110 mm, occurring at about 3 m depth (Fig. 46). The directions of the subsoil lateral movements at I4 and I5 were of smaller magnitudes and opposite in direction to that below the vertical face, I1 to I3. Inclinometer I4 in the center of the middle lateritic section showed virtually no lateral movement at the top after about 40 days from the end of construction, beyond about 75 mm. Inclinometer I5 recorded a lateral movement of only about 70 mm in 488 days after the end of construction, at about the same 3 m depth. Therefore, in conclusion it could be said that the soft clay subsoil moved out laterally both in the front and in the backward directions, but predominantly from the front. These lateral movements must have contributed significantly to the vertical settlements.

Figures 47 to 49 show the plots of the lateral movements versus the vertical settlements at the locations of the three inclinometers I1 to I3 near the face, at depths of 0.45 m, 3m, and 6 m. Therein, the rate of vertical movements are faster than the rate of lateral movements. It can be seen in Figs. 41 to 45 that the lateral movements at depths of 8 m or below in the stiff clay layer are very small or negligible.

4.1.2 VERTICAL SETTLEMENTS

The rate of settlements were very high initially in all the surface and the subsurface settlement plates/gages during the construction period. Settlements decreased considerably thereafter in the post-construction phase, but continued at a slow rate due to the consolidation of the soft clay subsoil. It was observed that towards the end of about 250 days after the beginning of construction, the rate of settlements had decreased to very low values at all the settlement points (Figs.50 to 56). The subsurface settlements at 3 m depth and the surface settlements still continued at a very slow rate beyond 250 days after the beginning of construction. At 3 m depth, the soft clay layer corresponds to the weakest zone in the subsoil. The lateral movements of the soft clay subsoil at this depth (3 m) were also found to be a maximum (Figs.41 to 45). The rates of settlement at 3 m depth were found to be very negligible only after about 450 days from the beginning of construction. However, the subsurface settlements at 6 m depth, had almost ceased after about 250 days since the beginning of construction.

The surface settlements at the front, i.e., at the toe below the vertical face, along the longitudinal section, indicated by the surface settlement plates S1, S2 and S3 are shown in Figs. 50 and 51. The settlements at all these three points were identical at about 0.4 m towards the end of construction, and at about 0.9 m after about 450 days since the beginning of construction. After about 600 days since the beginning of construction there was not much appreciable increase. The surface settlements in the center row comprising of S4, S5 and S6 were almost identical up to the end of construction. Since then the surface settlement at the very center (S5) has recorded the maximum surface settlement as shown in Figs. 50 and 53. The overall surface settlement pattern at the base indicated a dish-like configuration.

The subsurface settlements indicated by SS1, SS3 and SS5, all at 6 m depth near the face showed almost identical settlements with time (Fig.54). But the subsurface settlement plate, SS9, also at 6 m depth below weathered clay backfill in the center row (3 m from face), settled slightly more, probably due to the larger vertical stresses there in the center. The rates of subsurface settlements at 6 m depth were very negligible or could be said to have almost ceased after about 250 days since the beginning of construction. The maximum subsurface settlement recorded at 6 m depth was about 0.25 m at the front, while SS9 recorded a maximum of about 0.32 m. This signifies that the consolidation process of the subsoil at 6 m depth must have been completed or nearly completed due to the embankment loading by the end of about 250 days since the beginning of construction.

Subsurface settlements at 6 m depth, in the front, beneath the vertical face were identical, as mentioned earlier. However, at 3 m depth along the same longitudinal section, subsurface settlement gage, SS4 at the middle, was observed to record much lower settlements than its two adjacent subsurface settlement gages SS2 and SS6 (Fig.55). This might have been caused by the somewhat greater lateral movements of the soft clay beneath the embankment from the center of the middle section towards the front, as was observed from the inclinometer (I2) readings. The settlement at SS4 after about 600 days since the beginning of construction had been 0.51 m, while at SS2 and SS6 were 0.67 m and 0.75 m, respectively.

Along the longitudinal section at the back, surface settlement plate S8 settled more compared to its adjacent settlement gages, S7 and S9. The surface settlements have been more or less symmetrical about an axis (S2-S5-S8 axis) perpendicular to the face through the middle section. Along this axis, below the lateritic backfill soil, maximum settlements occurred at the very center, S5, as mentioned earlier, followed by the settlement near the face at S2 and the settlement at the back, S8 as shown in Fig.53. On the other hand, the end sections along the S1-S4-S7 axis below the clayey sand and along the S3-S6-S9 axis below the weathered clay, larger settlements were recorded at the front (toe) and decreasing towards the back and away from the face (Fig.52).

The magnitudes of the surface settlements were found to be the highest, followed by the subsurface settlements at 3 m depth and, lastly, the subsurface settlements at 6 m depth, at or near the same area beneath the embankment/wall system. The subsurface settlement gages SS2, SS4 and SS6 (Refer Fig. 20 for instrumentation plan) beneath the face at 3 m depth show considerable scatter as shown in Fig.55. On the other hand, the subsurface settlement points SS7 and SS8 in the center row beneath the clayey sand and the lateritic backfill soils, respectively, show almost identical settlements (also in Fig.55). The subsurface settlement gage, SS10, the lone settlement point at the back in the middle section at 3 m depth, also shows similar pattern of settlements as the other gages at the same

depth (Fig.56). The subsurface settlements at 3 m depth, along the middle section beneath the lateritic backfill soil (SS4, SS8, SS10) also followed the same trend as the surface settlements. The subsurface settlement at the center, SS8, was greater than SS10 at the back, followed by SS4 at the front near the face (Fig.56). It should, however, be noted that the subsurface settlement at SS4 is smaller than at SS10. This explains the greater lateral movements of the soft clay beneath the toe towards the front direction underneath the weathered clay crust. (The surface settlement profiles in the three sections are shown in Figs.86, 90, and 94).

4.1.3 PREDICTIONS OF SETTLEMENTS OF THE M S E WALL

The surface settlement of the center plate, at location S5, was considered in the settlement analysis in order to verify the effect of reinforcement and arching phenomenon on the settlement behavior. The stress distribution due to the embankment loading was computed using the method proposed by GRAY (1936), wherein the soil is assumed to elastic, isotropic, homogeneous, and semi-infinite in extent. Table 6 summarizes the initial settlements computed by the different methods and also shows the observed values in the field. The rate of consolidation settlement was analyzed by considering a single drainage path for the compressible layer. The coefficient of consolidation (C_v) was obtained using the graphical method of ASAOKA (1978) based from the observed time-settlement relationship of the test embankment. The time-settlement data observed from the screw plate test was also used in the Asaoka's graphical method to calculate the coefficient of consolidation (C_{vsp}). BERGADO et al. (1990b) attempted to derive an expression for C_{vsp} by accounting for the three-dimensional pore pressure dissipation during the loading of the screw plate as follows:

$$C_{vsp} = \frac{1}{\lambda} a^2 \frac{\ln \beta}{\Delta t} \qquad (7)$$

where a is the radius of the screw plate, β is a constant that represents the slope of settlement records for a given stress level, Δt is the time interval and $1/\lambda = -0.415$. The time factors used to estimate the degree of consolidation were obtained using the curves proposed by OLSON (1977) for time-dependent loading. Consequently, it was found that the 90% and 100% consolidation will take place at 389 days and 1396 days (3.92 years) after construction, respectively. This prediction seems to be reasonably good when compared with the actual observed data.

The total settlement was predicted using different methods shown in Table 7. For the method of DAVIS & POULOS (1968), the drained elastic modulus (E) and Poisson's ratio (ν) were taken as $0.26E_u$ and 0.35, respectively, as recommended by PARNPLOY (1985). Similar values were obtained through back analysis by BERGADO et al. (1990c). In the one-dimensional method, the settlement was calculated by dividing the compressible layer into

four sublayers, and the data from standard oedometer tests were used. For the SKEMPTON & BJERRUM (1957) method, the correction factor, μ , was obtained as a function of OCR using the chart presented by BALASUBRAMANIAM et al.(1985) for Bangkok soils. The secondary settlements were neglected while the subsidence effect was taken into account by adopting a subsidence rate of 40 mm/year at AIT campus (BERGADO et al. 1988). The predicted time-settlement curves were compared to the measured data in Figs. 57 and 58 using the C_v, calculated respectively, from the field observation and from the screw plate test data. All the prediction methods are seen to overestimate the settlements. The lower magnitudes of the observed settlements are the result of arching effects due to the presence of inextensible reinforcements.

4.1.4 STABILITY OF THE MSE TEST EMBANKMENT

The safety of the wall during construction (short term) was assessed using the method suggested by MATSUO & KAWAMURA (1977) for construction control of embankments on soft ground. Figure 59 shows the plots of vertical (d) and lateral (δ) deformations of the wall during its construction in d - (δ/d) coordinate system indicating that the plotted points are well below the critical boundary curves of p_j/p_f = 0.90, where p_j is the load at any jth loading stage and p_f is the load at failure.

The incumbent pullout forces in a welded-wire reinforced MSE structure are resisted by reinforcement mainly by way of passive resistance in front of the transverse members and frictional resistance over the longitudinal bars. The frictional resistances are mobilized sooner (DIMAGGIO, 1988). But the passive resistances continue to increase as the mat is being pulled out. The rate of increase in the passive resisances attain more or less a constant value after undergoing considerably large displacement of the grid mats, as was verified from the laboratory pullout tests.

For normal soft clay deposits, it is common to assume that the lowest stability condition occur during undrained conditions at the end of construction. In the post-construction phase, as the process of consolidation of the soft clay subsoil due to the dissipation of the excess pore pressures continues, the shear strength of the foundation soil and, thereby, the factor of safety increases. It was found that the rate of settlements and the rate of lateral movements of both the wall face and the subsoil decreased and the factor of safety increased with time. In addition, the inextensible reinforcements minimized the lateral spreading of the embankment fill. Thus, in spite of large settlements and lateral movements, the wall has performed well.

4.1.5 POREWATER PRESSURES

All the piezometers showed an increase in the total and the excess porewater pressures during the full period of construction. These excess porewater pressures were developed due to the increase in the self weight of the embankment during the construction period. Both the total and the excess porewater pressures showed a tendency to decrease in the post-construction phase. The dissipation of the excess porewater pressures seemed to occur at a very slow rate. The pneumatic piezometers N1, N3 and N4 ceased to function towards the end of construciton (Figs.60, 62, and 63, respectively). The hydraulic piezometers could be read reliably up to about 240 days since the beginning of construction.

Figures 60 to 69 show the porewater pressure variations monitored at different depths beneath the embankment/wall system. The dissipation of the excess porewater pressures is an indication of the consolidation process of the soft clay subsoil.

Figures 60 to 69 also show the estimated increase in the vertical stresses during construction as calculated by the method of GRAY (1936). These increase in vertical stresses correspond to the consolidating pressures due to the self weight of the embankment/wall system. To calculate the increase in the vertical stresses, the entire plan area of the wall/embankment system was transformed into an equivalent rectangular area and was then assumed to be loaded uniformly. Two perpendicular lines were drawn, parallel to the sides of the outer rectangle, through the point of interest (piezometer location). Thus, the whole plan area gets divided into four more rectangles. The net increase in the vertical stresses at the point of interest was got by the summation of contribution of increases in the vertical stresses from each of the four rectangular areas at their corner points. The subsoil was assumed to be elastic, homogenous, isotropic, and semi-infinite.

The pore water pressure coefficient, r_u, defined as the ratio of the pore pressure at depth z to the vertical stress (γz) was found to be in the range of about 0.3 to 0.35 at the end of construction. Another important factor affecting the variation of the pressures was the fluctuating water table which could be very close to the ground surface during the rainy season and as much as 2 m below the ground surface during the dry season.

In all cases, the excess porewater pressures developed were far below the increase in the vertical pressures. This may be because the soft clay layer has been reported to contain a lot sand and silt seams, as also some discontinuities and inhomogeneties (TSAI, 1981). It has also been observed that the horizontal permeabilities are twice as much as the vertical permeabilities, especially, in the soft clay layer (DUANGKHAE, 1970). The excess porewater pressures depend on Skempton's porepressure parameter, A, (which is said to approximate the porepressure parameter at failure, A_f), and the geometry of the

loading conditions. LAMBE (1962) reports that for slightly overconsolidated clays, the value of A_f should be from 0.3 to 0.7. Similar results were also reported by COX (1968) with the Bangkok subsoils. COX (1968) also reports that the excess porewater pressures vary from 50% of the increase in the vertical stresses for overconsolidated soils, to 100% of the increase in the vertical stresses for normally consolidated soils.

4.1.6 VERTICAL PRESSURE DISTRIBUTION

To determine the vertical pressure distribution at the base of the wall, three SINCO pneumatic total pressure cells (E1 to E3 in Fig.20) were placed below the middle reinforced lateritic soil section. Figure 70 shows the variation of the vertical pressure with the distance from the face of the wall, while Fig.71 shows the variation of these base pressures with time at different stages of construction. The variations of the base pressures with distance from the face of the wall are again reproduced separately in sets of similar patterns (showing the same behavior) in Figs. 72 to 75.

During the construction of the first four layers (i.e. embankment height (H) = 1.35 m above the general ground level), only the front earth pressure cell (E1) showed an increase (from 1 to 29 kPa), while those pressure cells at the center (E2) and at the back (E3) recorded very small pressures of only about 1 kPa (Fig.72). This seems to imply that the center of pressure was located near the face. But from the 5th layer up to the end of laying the 8th layer (H = 3.15 m), the center of pressure seems to have shifted to the center. The peak pressure recorded on E2 was about 35 to 40 kPa. This is probably due to the increase in the weight of the embankment and also the increase in the settlements at the center. There was a substantial increase in the values of E2 and little increase in the values of E3, while E1 remained nearly constant at 30 kPa in this period (Fig.73). At the end of the ninth layer, E3 had increased considerably and there was a slight drop in the values at E2 (Fig.74). During the laying of the 10th, 11th, and the 12th layers (H = 4.95 m), the base pressures recorded in all the three cells were nearly the same at about 55 kPa at the end of the 12th layer (Fig.74). The surface settlements near these points were also nearly the same at about 260 mm to 290 mm.

After laying the 13th and the last layer, (completed embankment height, H = 5.7 m), E2 recorded a base pressure of 70 kPa which was greater than the base pressure at E1 (63 kPa), and much greater than the base pressure at E3 (50 kPa) (Fig.75). At this instant, the surface settlement at S5 near E2, had increased well beyond the surface settlements near the face (S2) and at the back (S8).

The variation of the earth pressure with the distance from the face of the wall immediately after construction and for four different periods after construction are shown in Fig.90, and also summarized in Table 8. The different periods chosen are

those in which some major changes occurred. These changes seemed to follow some definite and repeating trends.

It had been observed throughout the post-construction phase that there would be an abrupt increase of vertical pressures at E2 followed by a decrease of pressure at E1. This is because the center of pressure being located near E2 would cause a higher rate of lateral displacement of the soft clay subsoil below it, and also higher settlements at S5. At the center, the reinforcements at the different layers being independent of each other, can settle more freely. But at the vertical face, all the reinforcement layers are interconnected together by the facing mesh to the full height and length of the wall which prevents the immediate response (in terms of settlements) of the front of the embankment/wall, whenever there is a large settlement occurring at the center. This resulted in arching effects.

This time lag in the settlement response below the vertical face decreased the contact between the bottom of the MSE embankment and the subsoil immediately below it, near the toe, around E1. The withholding forces in the facing minimized the base pressures at E1, whenever there was an abrupt increase in base pressures at E2 (Figs.75 and 90). In Fig.75, it can be seen that at the end of 8 days after construction, there was a considerable decrease in the base pressures at E1. This trend continued up to 22 days after construction when the value of base pressure at E1 was reduced to zero (Fig.90). The vertical pressures at E3 during this period were more or less a constant. From 26 days up to 89 days after construction, when sufficient settlements at the front (and also at the center and at the back) had taken place for the base of the MSE test embankment below the vertical face to increase contact with the subsoil again, the base pressures at E1 started to increase along with E2 and E3 (Fig.90). The soft clay subsoil that is moving out laterally in the front would tend to move the weathered clay crust above it upwards and, thus, increase the base pressures at E1.

The weight of the embankment would tend to push the subsurface settlement gage SS4 at the middle section in the front row at 3 m depth beneath the vertical face downwards, while the soft clay lateral movements would tend to push it upwards. The net result was that lesser settlement was recorded by SS4, than SS8 at the center row also at 3 m depth (Fig.56). SS8 below lateritic backfill was found to undergo greater settlements than below weathered clay backfill or clayey sand backfill on either side, at the same 3 m depth in the center row (Fig.55).

As the toe starts to settle gradually, E1 also starts increasing. As E1 starts increasing, there will be at first a slight decrease in the values of E2, and thereafter E2 also increases gradually at first and then at some stage, abruptly.

The base pressure monitored at E1 immediately at the end of construction was 63 kPa. But during the entire post-construction phase this value at E1 never rose beyond 19 kPa. This meant that

the contact pressures between the toe below the vertical face and the soil immediately below it, has reduced immediately after construction, due to the subsoil movements and the arching effects caused by the interconnecting facing mesh and the inextensible reinforcements. At 203 days after construction, there was again an abrupt increase in the value of E2, followed by a decrease in the value of E1 to nearly zero at the end of about 286 days after construction (Fig. 90).

The measured earth pressure distribution at the base of the middle section immediately after construction was compared to the trapezoidal, MEYERHOF (1953), and uniform vertical pressure distributions as shown in Fig.76. It is evident that the theoretical values are higher than the measured values of the earth pressures in the field. Due to foundation deformations caused by the subsoil movements, the measured base pressures are lower than any of the above theoretical predictions. The other factors reducing the contact pressure distributions are the arching effects due to the presence of the inextensible reinforcements which are also caused by the subsoil movements and the relative stiffness of the embankment and the foundation subsoil. The MSE test embankment at best could be considered only as a semi-rigid structure on a highly compressible foundation. Also, the total earth pressure cells that were used by virtue of their high stiffness tend to register lower vertical pressures than the actual values (DUNNICLIFF & GREENE, 1988). Trapezoidal or MEYERHOF (1953) pressure distributions presuppose that the front face of the structure will tend to rotate about the toe with an active mechanism away from the fill.

4.1.7 TENSILE FORCES IN THE REINFORCEMENTS

The initial readings on the strain gages were taken corresponding to zero tension (strains) in the reinforcements at the time of its installation, before being subject to any loads. Subsequent readings were then taken as the wall was constructed and for several periods after the completion of the construction at regular intervals of time. Most of the strain gages were damaged about one year after the end of construction probably due to excessive and sustained strains, or the strain measurements did not seem to be very reliable after this period. From the strains calculated thus, the tensions in the wires can be computed as:

$$T = \varepsilon * E * A \qquad (8)$$

where:
- T = axial tension in the reinforcing wires
- ε = axial strain in the reinforcing wires
- E = modulus of elasticity of steel, and
- A = cross-sectional area of the reinforcing wire

The measured strains in the reinforcements, and therefore, the tensile forces were found to be continually changing in response to the subsoil movements. The variation of the strains were found to be in conformity with the variation in the base

pressures, particularly for the bottom 4 instrumented mats. Typical variations of the tensions for instrumented mat No. 1 during construction as each lift of the backfill was placed are given in Figs. 77 to 79 for the three types of backfills. Also shown in these figures are the lines corresponding to the different values of K (K = 0.2 to 2.0). The variations of the tensile forces in the reinforcements with distance from the face of the wall during construction are shown in Figs.80 to 82 for the three types of backfills. The tension in the wires did not indicate a consistent increase with the height of the test embankment. One of the attributes can be the varying amounts of compression of the soft foundation subsoil.

Figures 83 to 85; 87 to 89; and 91 to 93 show the reinforcement tensions after 4, 8, and 12 layers of fill were placed, respectively, during construction in each of the three backfill soils. The corresponding settlements and the base pressures (for the middle lateritic section only) are also shown therein.

Typical reinforcement tensions immediately after construction and for four different periods after construction for the three types of backfills are depicted in Figs. 86, 90, and 94, respectively. After 22 days from the end of construction, it was seen that some reinforcing mats displayed a sudden increase in stresses at small distances behind the facing and a decrease of stresses at distances far behind the facing in all the sections. At this stage, there was an abrupt decrease in the earth pressure readings near the face (E1). However, near the middle (E2), the earth pressure readings remained at about the same magnitude it had immediately after construction. E3 recorded some small reduction. After 89 days from the end of construction, the earth pressures at all the 3 locations were found to increase, especially at E2, which resulted in high reinforcement stresses far behind the facing as recorded for all the layers. Since then, the reinforcement stresses for any mat never went down significantly below this level. However, the reinforcement stresses at small distances behind the facing showed a considerable drop. At 203 days after construction, the reinforcement stresses even at small distances behind the facing increased considerably and were never found to drop considerably thereafter. At 286 days after construction, E1 decreased without causing any significant variation in the tensile stresses in the reinforcing mats. This may be due to the fact that all the subsoil movements had reduced considerably by this time.

4.1.8 LATERAL PRESSURES

The lateral pressures were computed from the strain measurements in the longitudinal wires from the following relationships:

$$T = \varepsilon * E * A = K * \sigma_v * (a) * (z) \qquad (9)$$

where: $(K*\sigma_v)$ will constitute the lateral pressures and
- T = tension in the wire
- ε = net axial strain
- E = modulus of elasticity of steel
- A = area of cross section of the longitudinal wire
- K = lateral earth pressure coefficient
- σ_v = $\gamma*y$, where γ is the unit weight of the backfill material and y is the depth of the reinforcing mat measured from the top of the wall
- a = horizontal spacing of the longitudinal wires in a layer
- z = vertical spacing of mats in the different layers

The maximum lateral pressures immediately after construction are plotted with distance below the top of the wall in Figs. 95 to 97 for the three sections. It is interesting to note that the arching effect altered significantly the lateral pressures in the lateritic section which is supposed to be the strongest of all the backfills used in the wall by yielding lower measured lateral pressures than the other two sections. This was also confirmed from the field pullout tests on the dummy mats located at the center section which indicated contrasting results to the theoretical expectations. Lateritic backfill not only yielded lower pullout resistances when compared to weathered clay and clayey sand, but also the pullout resistances decreased with the increase in the overburden pressures. The laboratory pullout tests with all the three backfill soils clearly confirmed increasing pullout capacities with the increase in the normal pressures.

The measured values of the lateral pressures were compared with the existing earth pressure theories on reinforced soil structures. The measured values immediately after construction were found to higher than either the coherent gravity or the tie-back structure hypotheses, but seemed to be closer to the predictions by either the compaction theory proposed by INGOLD (1983c) or the hysteritic model proposed by DUNCAN & SEED (1986) (See Figs. 95-97).

4.1.9 COEFFICIENT OF LATERAL PRESSURES

The lateral earth pressure coefficients during construction were computed from the strain measurements from equation 9. The maximum values of K during the construction of wall was obtained for the different heights of the backfills above each of the seven instrumented mats in all the 3 sections and plotted in Figs. 98 to 100. The trend observed in all the sections were similar. The values of K increase as the top of the wall is approached, with most of these K values being larger than the active value (K_a), K_a being determined from the expression $K_a = (1 - \sin \phi)/(1 + \sin \phi)$. ϕ was determined from UU triaxial shear tests on partially saturated and compacted backfill soil samples (compacted to 95% of standard Proctor's density on the dry side of optimum). This variation is significantly different from those reported for welded-wire walls using high quality granular

backfills on comparatively firm foundations (ANDERSON et al. 1987) as well as for reinforced earth walls (MCKITTRICK, 1978). In this study, however, it was found that the K values near the top of the wall exceeded the at-rest K values, similar to the observations made in earlier studies on unreinforced and reinforced soil walls (CARDER et al, 1980; MURRAY & BODEN, 1979; MURRAY & FARRAR, 1990). These deviations may be attributed to the combined effects of compaction induced stresses, highly compressible foundation, poor quality backfill, inextensible reinforcements, etc.

Foundation compressibility can enhance lateral displacement of the wall face as the wall is constructed. The lateral movement necessary to develop the fully active case (K_a) has been reported to be only a minimal fraction (1/1000) of the wall height (TERAZGHI, 1934). Any further movement of the face will increase the lateral pressure (CARDER et al. 1977; CARDER et al. 1980; TERZAGHI, 1934). In this study, the maximum lateral movement measured for the wall, immediately after construction, amounted to about 0.15 m which is much higher than the required displacement of 0.0057 m to develop the fully active case. For a grid-reinforced soil wall, this continuous outward wall movement may cause the full mobilization of the passive resistance in front of the transverse members, thereby inducing larger strains in the longitudinal members. On the other hand, experimental evidence using compacted sand and silty clay backfills have shown that the maximum lateral earth pressures throughout the height of the wall are significantly higher than were calculated from the at-rest (K_o) values, especially at the top meter of the wall (CARDER et al. 1977; CARDER et al. 1980; MURRAY & BODEN, 1979). These high values were attributed to the stresses induced by compaction.

The compaction induced stresses depend on the type and the size of the compaction plant employed. The maximum stresses at the very top of the wall are not to exceed the lateral pressure calculated using the coefficient of earth pressure for unloading, K'_o (BROMS, 1974; ROWE, 1954). CARDER et al. (1977) assumed the value of K'_o as equal to $1/K_o$, where K_o is calculated from the equation: $K_o = 1 - \sin\phi$. Using this limiting value of the lateral pressure coefficient at the top of the wall, it was considered appropriate to express an upperbound envelope of K with the height of the wall, to be linearly increasing from the active value (K_a) to a value of K'_c at the top of the wall for the three sections as shown in Figs. 98 to 100.

By considering the commonly accepted notion that the compaction of the soil is a form of overconsolidation (DUNCAN & SEED, 1986), the at-rest coefficient K_o can be expressed as a function of the OCR of the compacted soil (MAYNE & KULHAWY, 1982; WROTH, 1975). A limited amount of experimental data on the shear strength of compacted lateritic soil (BOONSRI, 1971) reports that these compacted samples behaved like heavily overconsolidated soils. From a series of triaxial tests on compacted weathered Bangkok clay, HAQUE (1977) indicated that these compacted samples

behaved like lightly overconsolidated samples. Thus, an OCR value of 8 was assumed to estimate the value of K_o. Therefore, for walls constructed up to 6 m height on soft and highly compressible foundation utilizing poor quality cohesive-frictional backfill materials, the above mentioned envelope for K (K_a to K'_o) may be recommended. This may be overconservative for walls which will undergo only very small lateral movements.

4.1.10 MAXIMUM TENSION LINE

The potential failure surface in a reinforced soil wall is supposed to closely comply with the line of maximum tensions. It has been reported to define either a Coulomb/Rankine linear failure plane or a bilinear failure plane or a logarithmic spiral failure plane. These were empirically derived for embankments on rigid and good foundations, with maximum pressures at the toe. In this study, wherein the foundation subsoil is highly compressible, it was observed that the maximum tension line does not comply well with any of the aforementioned failure planes. The tensile forces as mentioned earlier showed considerable variations. Sometimes there would be more than one peak (maximum point) on some of the reinforcing mats. Even with these variations, it was generally observed that the measured maximum tension line agreed with the log spiral failure plane (farther from face than the Coulomb/Rankine (tie-back wedge) failure plane) at the lower half of the wall, and to the coherent gravity plane (closer to the face than the Coulomb/Rankine failure plane) for the upper half of the wall. However, it is rather difficult to draw a well-defined failure plane. Therefore, in Figs. 86, 90, and 94, both the Coulomb/Rankine (tie-back wedge) failure plane and the coherent gravity failure plane are shown for comparison with the measured tensions.

4.1.11 PLATE LOAD TESTS ON REINFORCED AND UNREINFORCED FILL

To study the effects of the reinforcements on the stress distribution and settlements, plate load tests were conducted on both the reinforced and the unreinforced embankment fills (SHIVASHANKAR, 1991; HARDIYATIMO, 1990). The MSE embankment was provided with two earth pressure cells at the top (back) in the weathered clay section, at depths of 0.55 and 1.0 m, respectively, from the top of the embankment (Fig. 24). The unreinforced earth fill, on the other hand, was constructed at a site close to the welded wire wall using the same weathered clay backfill and employing the same compaction process. Two more earth pressure cells were placed at the center of the unreinforced fill at the same depths of 0.55 and 1.0 m, respectively. Figures 101 and 102 show the detailed set-up of the plate load tests. A uniform compressive load was applied on the surface through a rigid plate, by means of a 150 kN capacity hydraulic jack and a hand pump. The jack would take reaction against a loading frame which transferred the load uniformly on the rigid plate. The load was measured by means of a proving ring. The pressure below, in the two earth pressure cells, was measured with the help of a digital pressure indicator which was

connected to the leads of the earth pressure cell. The settlements were measured by means of two dial gages mounted diametrically opposite of each other on to a reference beam by means of a magnetic base.

Figures 103 and 104 show the results of the plate load tests on the unreinforced and the reinforced fills. It was observed that the stresses beneath the unreinforced fill were only slightly larger. This, however, proves that the effect of having the reinforcements is to distribute the loads over a larger area. In the case of sands, plate load tests show an increase in the ultimate bearing capacity by a factor of about 2 with the reinforcements (HOLTZ, 1991). Therefore, the effect of reinforcements is to reduce the stress concentrations, increase the load carrying capacity and also reduce the total and the differential settlements. The observed settlements in the case of the unreinforced fill were higher as shown in Fig.105.

4.2 LABORATORY PULLOUT TEST RESULTS, INTERACTION STUDY, PREDICTION EQUATIONS

4.2.1 EFFECT OF STAGE LOADING

The rate of increase in the total pullout resistance with the grid displacement was higher in the earlier phases of the grid pullout tests conducted in the laboratory. After this initial phase, i.e., after about 8 to 12 mm displacement of the grid specimen, the rate of increase slowed down considerably and the pullout resistances would attain more or less constant values (Fig.106). For a given displacement, at a given normal stress and compaction moisture condition, the pullout resistances of the grid reinforcements during the first stage, especially on the dry side of optimum, would be lower than during the latter or higher stages (Fig.106). However, the difference in the maximum pullout resistances at the end of 25 mm pull was found to be very small. Therefore, it was concluded from this study that irrespective of the stage in a multistage pullout testing program, the maximum pullout resistance at the end of 25 mm pull for a given normal stress and moisture condition were more or less the same. The only difference was in the manner in which these peak values were attained. The first stage load-displacement curves were found to be flatter and smoother depicting a lower modulus, unlike the latter stages (Fig.106). The second stage results, i.e., maximum pullout resistances of the grid reinforcements at the end of 25 mm pull, of any set-up at a given moisture condition, adopting the three stage pullout testing program for each set-up, were found to lie on the regression line for the total pullout resistances at that moisture condition (Fig.107).

MOTALEB & ANDERSON (1988) concluded that the load-displacement curves for the multi-stage tests were continuations of the post-yield portion of the first stage curve, which was also found to be quite relevant to the results obtained from this study.

4.2.2 FRICTION PULLOUT TEST RESULTS

The frictional resistances over the longitudinal members of the grid were found to contribute on an average of only about 10 to 15% of the total pullout resistance, while the bearing resistances infront of the transverse members would contribute the rest (SHIVASHANKAR, 1991). Figures 108 to 110 show the friction pullout test results in clayey sand, lateritic soil, and weathered clay, respectively, at all the three moisture conditions. The increase in the frictional resistances ($F_f/\pi LMd$) with the increase in the applied normal stresses, at all the three moisture conditions, is very small especially with weathered clay and clayey sand. However, the frictional resistances ($F_f/\pi LMd$) were found to decrease with the increase in the bar sizes, especially in the case of weathered clay and lateritic soil.

The apparent friction coefficient on the longitudinal wires has been defined as:

$$\mu^* = f/\sigma_{ave} \tag{10}$$

$$f = \frac{F_f}{M\pi dL} \tag{11}$$

F_f is the maximum pullout force from the friction pullout tests at the end of 25 mm pull.

The apparent friction coefficient, μ^*, as defined in equation (10) was found to decrease with the increase in the applied normal stress level. Figures 111 to 113 show plots of the apparent friction coefficient, μ^*, versus the applied normal stresses with all the three backfill soils. The curves flatten out beyond a normal stress of about 100 kPa in all the three soils. This trend is similar to that obtained by SCHLOSSER & ELIAS (1978) from the pullout tests of strip reinforcements from reinforced earth walls, which was attributed to the effects of soil dilatancy at the soil/reinforcement interface.

The stress normal to the surface of the wires or the average overburden pressure, σ_{ave}, was taken as 1.15 times the applied vertical normal stress (σ_v), to account for the compaction induced stresses and also the circular cross-section of the longitudinal wires (Fig.114). An OCR value of 8 was found to be quite appropriate for the compacted soils used in this study, which correspond to lightly overconsolidated soils (WROTH, 1975; DUNN et al. 1980; MAYNE & KULHAWY, 1982; BERGADO et al. 1991a, b). This corresponds to a coefficient of lateral earth pressure at rest (K_o) value of 1.3.

4.2.3 RIBBED FRICTION PULLOUT TESTS

The ribbed longitudinal bars gave considerably higher pullout loads than the smooth longitudinal bars, especially on the dry side and at optimum moisture content. In the case of the ribbed longitudinal bars, the total pullout resistance comes partly from the frictional resistances over the longitudinal bars and partly from the passive resistances in front of the transverse ribs. The passive resistances in front of the ribs were found to increase with the increase in the applied normal stresses for all bar sizes and moisture conditions, and also with the increase in the diameter of the transverse ribs due to the increase in the rigidity of these ribs. The passive resistances (F_b/NWD) in front of the ribs were found to be larger than in front of the full transverse bars of a grid reinforcement at the same overburden stress on the dry side and at optimum moisture content, and about the same on the wet side. Thus, the presence of the ribs was found to increase the total pullout resistances considerably. However, it is not practically feasible and economical to have such a reinforcement system with steel wherein the ribs will have to be welded on top of the longitudinal bars.

4.2.4 SINGLE TRANSVERSE BAR PULLOUT TESTS

Only four tests were conducted at each moisture condition using 6.35 mm (1/4 in.) diameter bars and 0.15 m x 0.225 m (6 in. x 9 in.) mesh in weathered clay and clayey sand backfill soils. The bearing resistances mobilized infront of the transverse bar at the end of 25 mm (1 in.) pull from the single transverse bar pullout tests were about 75 to 80% of the upper bound value estimated from equations 2 to 4.

4.2.5 GRID PULLOUT TEST RESULTS

The pullout results with the grid reinforcements in all the three backfills basically agreed with the earlier mentioned apparent upper bound (general bearing failure mechanism) and lower bound (punching shear failure mechanism) envelopes. The bearing resistances infront of the transverse bars of the grid reinforcement, and, thereby, the total pullout resistances were found to vary considerably with the spacing to diameter (S/D) ratios of the transverse bars. The transverse bars of the grid can be considered as a succession of bearing elements that can interfere with each other (PALMEIRA & MILLIGAN, 1989). When the transverse bars are closely spaced (i.e. for small values of S/D) the passive resistant zones of the successive transverse bars interfere with each other. Therefore, the bearing resistances mobilized infront of the transverse bars will be lower. As the (S/D) ratio is gradually increased, the interference decreases. At a limiting value of the spacing to diameter ratio ($(S/D)_{lt}$), the interferences become zero. Any further increase in the spacing of the transverse bars or increase in the S/D ratios will have no effect on the bearing resistances $(F_b/NWD)_{lt}$. The values of ($(S/D)_{lt}$) for the weathered Bangkok clay and lateritic soil were found to vary with the moisture content. The value of

$(S/D)_{lt}$ in the case of clayey sand was found to be around 100 at all three moisture conditions (Fig.115). The values of $((S/D)_{lt})$ for lateritic soil on the dry side of optimum, at optimum moisture content, and on the wet side of optimum were found to about 75, 100 and 60, respectively (Fig.116), while the values of $((S/D)_{lt})$ for weathered clay on the dry side of optimum, at optimum moisture content, and on the wet side of optimum were found to be about 60, 40 and 30, respectively (Fig.117). PALMEIRA & MILLIGAN (1989) concluded that for dry sands, when S/D ratio exceeds 50, the interference effect becomes negligible. Figures 115 to 117 show a decrease in the degree of interferences (DI) with the increase in the (S/D) ratios in all the three soils. Although there is some scatter in the data, the trend is clearly seen. In calculating the values of DI from the grid pullout test data, the maximum bearing resistance that can be generated infront of the transverse bars with no interference $((F_b/NWD)_{lt})$ was obtained from equations 2 to 4. The degree of interference (DI) from the grid pullout test data as shown in Figs.115 to 117 was calculated as:

$$DI = 1 - \frac{(F_b/NWD)_{ave}}{(F_b/NWD)_{\ell t}} \qquad (12)$$

where $((F_b/NWD)_{ave})$ is the average bearing resistance mobilized in front of all the transverse bars of the grid reinforcement obtained from the grid pullout test, and $((F_b/NWD)_{lt})$ is the upper bound value for the bearing resistances. It was assumed that the first transverse bar will have no interference effects and that the bearing resistances mobilized infront of the other transverse bars $((F_b/NWD)_{grid})$, are proportional to the S/D ratios of the grid reinforcement. Therefore, the degree of interference (DI) can also be expressed in terms of only the grid parameters, for a grid with N number of transverse bars, similar to JEWELL (1990) as:

$$DI = \left\{1 - \frac{1}{N}\right\}\left\{1 - \frac{(S/D)}{(S/D)_{\ell t}}\right\} \qquad (13)$$

The pullout tests with all the three backfill soils revealed that with large values of S/D ratios, especially at higher confining normal stresses, the pullout resistances after 25 mm pull approached the prediction of the general bearing failure mechanism (Figs.118 to 126). On the other hand, in the case of the grid mats with lower values of S/D ratios, especially at lower confining normal stresses, the pullout resistances after 25 mm pull approached the prediction of the punching shear failure mechanism (Figs.118 to 126). The data points, especially with the weathered clay, on the wet side were found to have moved closer to the prediction by the general bearing failure mechanism which is the apparent upper bound envelope. Thus, the increase in the moisture content seems to steer the pullout failure mechanism infront of the transverse bars more towards a general bearing failure mechanism.

4.2.6 PREDICTION EQUATIONS

The frictional resistance, F_f, has been expressed as:

$$F_f = \pi LMd \{ C_a^p + \sigma_{ave} * \tan(\delta^p) \} \quad (14)$$

Dividing both sides of equation (14) by NWD yields the following expression:

$$F_f/NWD = \pi S_f \{ C_a^p + \sigma_{ave} * \tan(\delta^p) \} \quad (15)$$

where S_f is the grid shape factor. The terms C_a^p and $\tan \delta^p$ were obtained by a simple linear regression of the friction pullout test data with F_f/NWD as the dependent variable and the average overburden pressure, $\sigma_{ave} = 1.15\sigma_v$, as the independent variable. The values of C_a^p and $(\tan \delta^p)$ obtained for clayey sand were respectively as follows: 70 kPa and 0.18 on the dry side, 37 kPa and 0.05 at optimum moisture content, and 14 kPa and 0.04 on the wet side. The values of C_a^p and $(\tan \delta^p)$ obtained for lateritic soil were respectively as follows: 92 kPa and 0.25 on the dry side, 51 kPa and 0.15 at optimum moisture content, and 38 kPa and 0.23 on the wet side. The values of C_a^p and $(\tan \delta^p)$ obtained for weathered clay were respectively as follows: 44 kPa and 0.0 on the dry side, 35 kPa and 0.01 at optimum moisture content, and 10 kPa and 0.07 on the wet side.

The bearing resistance infront of the transverse bars has been expressed in the general form as:

$$F_b/NWD = \{ C*N_c + \sigma_v*N_q \}*(1 - DI) \quad (16)$$

The term F_b/NWD represents the bearing resistance per unit area of the transverse members normal to the direction of pullout. The bearing capacity factors, N_q and N_c, were obtained from equations 3 and 4, respectively. The shear strength parameters were derived from the direct shear tests. The degree of interference (DI) in the above prediction equation (equation 16) can be estimated from equation 13, by considering a suitable value of the $((S/D)_{lt})$. The prediction lines which are also shown in Figs.118 to 126 were found to have good agreement with the experimental data.

The total pullout resistance can be expressed in the general form as:

$$F_t/NWD = [\{(C*N_c + \sigma_v*N_q)*(1 - DI)\} + \pi S_f \{C_a^p + \sigma_{ave}*\tan(\delta^p))\}] \quad (17)$$

4.3 FIELD PULLOUT TEST RESULTS

The load-displacement curves and the strain-displacement curves obtained from the field pullout tests are shown in Figs. 127 to 130 and Figs.131 to 134, respectively. The pullout resistances obtained in the case of the three dummy mats with no transverse bars (dummy mat Nos. 10,11 and 13 in Fig.12) were nearly the same, as shown in Figs.130. In all these three pullout tests of the reinforcements without the transverse members, it was observed that after reaching a peak value and holding on to this peak value for a while, the maximum pullout resistances tend to decrease with further displacement. The peak values in the case of weathered clay were attained after about 25 mm displacement, whereas in the case of lateritic soil and clayey sand the peak values were obtained after about 50 and 80 mm displacements (pullouts), respectively. Assuming that all the pullout force is resisted by friction over the longitudinal bars in these three tests, the friction coefficient using equations 10 and 11 would work out to be about 2.45.

In the case of weathered clay and clayey sand, it was observed that increase in the overburden pressures or the bar sizes or the number of transverse bars definitely increased the pullout resistances, as per theoretical expectations. However, the same was not true with the lateritic backfill soil.

In the case of weathered clay, all the load-displacement curves (Fig. 127) show a yield point and a peak load. The peak pullout forces were nearly approaching the tension capacity of the reinforcements. The results are also tabulated in Table 9. Comparing dummy mat Nos. 26 and 8, both in weathered clay (Fig.127) and having the same bar sizes of W7 X W4.5 (longitudinal X transverse; 7.6 mm X 6.07 mm diameters) and about the same length of embedment, but with different overburden heights of 0.6 and 3.93 m, respectively, the peak pullout resistances obtained were, respectively, 38.39 and 64.28 kN. Again comparing dummy mat No.26 of bar sizes W7 X W4.5 and dummy mat No.22 of bar sizes W4.5 X W3.5 (6.07 mm X 5.36 mm diameter bars), both in weathered clay (Fig.127), even though the bar sizes decreased in the latter case, but due to the increased overburden pressure, there was a considerable increase in the maximum pullout resistances as seen in Table 9. Comparing dummy mat No. 22 comprising of W4.5 X W3.5 having a overburden height of 2.043 m, with dummy mat No.17 comprising of W12 X W5 (9.93 mm X 6.4 mm size bars) having a overburden height of 2.116 m, both in weathered clay (Fig.127), the sizes of bars are increased considerably in the latter case and also the number of transverse bars are increased to 6, but the increase in the maximum pullout resistance is not very appreciable.

In the case of pullout of a grid reinforcement (dummy mat No.22) from weathered clay backfill, a peak value was reached at about 100 mm displacement and, thereafter, the total pullout resistances tend to decrease (Fig.127). But in the case of clayey sand (dummy mat No. 20, having about the same overburden

height as dummy mat No.22), the pullout resistance was still increasing at the end of 60 mm pull, when the tension capacity of the longitudinal bars had been reached. The reinforcing mat failed by tension simultaneously in the middle two longitudinal bars, some distance behind the grips outside the face of the welded-wire wall. Comparing dummy mat No. 8 in weathered clay (Fig.127) and dummy mat No. 7 in clayey sand (Fig.129), it can be seen that with the same size of bars and mesh, and nearly the same overburden pressures, the maximum pullout resistance in case of clayey sand is considerably higher. Thus, clayey sand backfill has been found to give higher pullout resistances than weathered clay backfill from the field pullout tests, all other conditions being the same.

Dummy mat No. 9 (W12 X W5) and dummy mat No.7 (W7 X W4.5) both in clayey sand (Fig.129) can also be taken to illustrate that in the case of clayey sand also the maximum pullout resistance increased with the increase in the overburden pressures. Even though the bar sizes have decreased in the latter case, there is a considerable increase in the maximum pullout resistance which can be attributed to the increased overburden stress.

It was observed during the field pullout tests of the dummy mats that the axial strains in the longitudinal bars decreased with the increase in the distance from the face of the wall. In most cases during the field pullout tests, the strains with the W4.5 (6.07 mm diameter) size bars were beyond the yield strains, especially near the face. The strains recorded in the reinforcements during the field pullout tests with clayey sand were considerably larger than that with weathered clay, especially near the face. There was even a tension failure just outside the face of the welded wire wall with clayey sand as mentioned earlier (dummy mat No.20).

The middle section of the test embankment showed a decrease in the maximum pullout resistances with the increase in the overburden pressures, contrary to what was observed in the laboratory pullout tests on the same soil. Also, when compared with the other two backfills i.e., clayey sand and weathered Bangkok clay, the lateritic soil gave somewhat lower values of field pullout resistances for the same height of overburden, with the same reinforcement geometry and size. The maximum pullout resistance obtained from the field pullout test at the top level dummy mat (dummy No.23) in lateritic soil was quite good as expected. However, due to the arching effects, the backfill in the lower portions of the wall, especially near the facing, must have decreased drastically in its degree of compaction.

Dummy mat No.23 with a overburden height of 1.5 m and made of large size bars (W12 x W5, with 9.93 mm X 6.4 mm diameters of the longitudinal and transverse bars, respectively), with 5 transverse bars and embedment length of 2.117 m, gave a maximum pullout resistance of 108.83 kN at the end of 136.7 mm pull. While dummy No.12 having the same size bars and the same number

of transverse bars, embedment length of 2.046 m, overburden height of 3.8 m, gave only a maximum pullout resistance of 54.82 kN at the end of 126 mm pull. Thus, the maximum pullout resistance of dummy No.12 had reduced to about 50% of that obtained with dummy No.23. A comparison with the laboratory and field test results are shown in Tables 10 to 12 and Figs.135 to 137 for the three soils used in this study. Comparing dummy mat Nos. 21 and 15 (Fig.128), wherein the bar sizes and the overburden height were larger in the case of the latter and the number of transverse bars were also increased to 6, still there was a decrease in the maximum pullout resistance.

The results of the constant stress field pullout tests are shown in Figs. 138 to 141. The time-dependent load-strain behavior of the reinforcements under sustained and/or repetitive loads are important for their satisfactory performance. For example, an earth wall reinforced with inclusions may fail by excessive deformation due to creep of the reinforcement, although adequate factors of safety are provided against reinforcement rupture and pullout. It can be observed that the creep strains varied with time, although there was considerable scatter in the results, which may be due to effects of temperature, possible errors in instrumentation, arching effects, stress concentration at the gravel facing and other effects.

4.4 COMPARISON BETWEEN LABORATORY AND FIELD PULLOUT TEST RESULTS

The reinforcement mats used in both the laboratory and the field pullout tests had 0.15 m x 0.225 m mesh openings with varied bar diameters, and most of them had 5 transverse bars. The length of embedments of the reinforcements in the laboratory pullout tests was about 1.0 m, while the length of embedments of the dummy reinforcements in the field pullout tests was around 2 m. In the case of the dummy mats, a regular 0.15 m x 0.225 m mat about 2.0 m long was used with some of the transverse bars clipped, with only 5 or 6 transverse bars left.

The field pullout tests yielded higher pullout resistances than the laboratory pullout tests in the case of weathered clay and clayey sand (Figs.135 and 137). The interconnection of all the reinforcement layers at the facing for the full length and height of the wall, and also due to the fact that the settlements at the middle lateritic soil section were relatively higher than at the two end sections (clayey sand and weathered clay sections), must have caused arching effects. These arching effects in turn must have caused the vertical stresses or the overburden pressures from the middle section to be redistributed to the two end sections. This could have resulted in higher field pullout resistances in the end sections as compared to the laboratory (BERGADO et al. 1992).

During the laboratory pullout tests, the interaction between the soil/reinforcement system and the rigid boundaries of the laboratory pullout box, especially the front face, in the small scale tests can affect the generated pullout resistances.

Compaction and moisture can be controlled better in the laboratory.

4.5 PREDICTIONS USING FINITE ELEMENT PROGRAMS

Two finite element computer programs REA and NONLIN 1 were used to predict the laboratory pullout test results and the wall behavior. The Reinforced Earth Analysis (REA) program was used with the concept of equivalent friction coefficient (LIU, 1988) for the grid reinforcements. The laboratory pullout tests were treated as plane strain problems, similar to that of an externally loaded sheet pile, with the reinforcements being treated as discrete bending elements (SHIVASHANKAR, 1991). These results were compared with the corresponding values obtained by using the program NONLIN 1 (LO, 1990).

REA is a general two-dimensional soils and reinforced earth analysis program developed by HERRMANN (1978) at the University of California, Davis. The finite element mesh used to model the pullout test in the laboratory is shown in Fig.142. Bending members are assumed to be elastic-plastic with isotropic linear strain hardening. It is also assumed that when the material is in the plastic range, the bending stiffness is solely determined by the value of the plastic modulus. The soil was being represented by continuum elements. The interface between the reinforcement and the soil was represented by friction, by assigning a suitable friction factor in the REA input format. A displacement of 25 mm (1 in.) was specified at the free end of the projecting bending element 67, at node 85. Relative element of node 85 with respect to soil continuum was prevented, while the relative movement was prescribed for the rest of the bending elements. Modified Duncan' characterization (WONG & DUNCAN, 1974) were employed for the soils and the properties of the soils used in this finite element analysis are shown in Table 13.

In this study, NONLIN 1 was modified and used to model the soil-reinforcement interaction a laboratory pullout test (LO, 1990). NONLIN 1 is a two-dimensional program that used the initial stress method to represent the nonlinear behavior of the soil. The program is based on an analytical method suggested by OCHIAI & SAKAI (1987). The soil was represented by triangular and quadrilateral elements with a nonlinear elastic model criterion (DUNCAN and CHANG, 1970). The soil parameters are given in Table 13. The interface properties between the soil and the reinforcement were modelled by one-dimensional joint elements and the relative displacement between the soil and the reinforcement was allowed if the mobilized shear stress at the interface equalled or exceeded the shear strength at the interface. This shear strength at the interface was obtained from Mohr-Coulomb strength theory. The parameters C and Ø of the interface were set to be the same as those of the surrounding soil.

The reinforcement was represented by one-dimensional bar elements in the NONLIN 1 program. The three-dimensional discrete

bar mats were converted into two-dimensional representation (SCHMERTMANN et al. 1989). The modulus of elasticity and the yield stress of the steel grids were set equal to the known standard values for steel. Figure 143 shows the finite elements for the reinforcement and the reinforcement-soil interface. A typical finite element mesh used for analyzing the laboratory pullout tests is shown in Fig.144.

In order to define completely the load-displacement response during a pullout test with the NONLIN 1 program, five displacement increments were considered. The displacements were specified at the nodal point at the free end of the reinforcement, just outside the front face of the pullout box. The comparison between the predicted load-displacement curves and those obtained from the actual laboratory pullout tests for 0.15 m x 0.225 m (6 in. x 9 in.) mesh and 6.35 mm (1/4 in.) diameter steel bars with weathered clay backfill are presented in Fig. 145. The predictions from the finite element analyses (NONLIN 1) are comparable with the experimental results for all the three types of backfills, with a maximum difference of about 15% in terms of the pullout force. Figures 146 to 148 show the results of the finite element analyses using REA and NONLIN 1 programs for the three backfill soils along with the laboratory pullout test data. Figures 149 and 150 show some typical tensile forces in the reinforcements from the REA program compared with the the observed data.

The finite element mesh used to model the welded wire wall using REA and NONLIN 1 are shown in Figs. 151 and 152, respectively. Only the middle lateritic section was considered in the analysis. Table 14 shows the parameters used for the different subsoils and the backfill soil while using the program REA. The welded wire wall was first transformed to a strip reinforced wall to suit the format in the REA program. The values of the friction coefficients for the different layers were not the same, higher near the top of the wall and decreasing with the increase in the overburden pressures. The typical wall face of the Hilfiker's welded wire wall consisting of a bent pronged mat, backing mat, and screen was adopted in the analysis to calculate the needed input data for the facing plate. The elastic modulus (E), the plastic modulus (E_p), and the yield stress (Y) were adopted as 2.11×10^8 kPa, 1.41×10^6 kPa, 4.23×10^5 kPa, respectively which are similar to the main reinforcements in the wall (Table 15). A failure strain of 0.025 was assigned to the facing plate; the cross-sectional area, A and the moment of inertia per unit width I were adopted as 0.66 mm^2/mm and 10.23 mm^4/mm, respectively. The boundary spring coefficient, K, of 6.7×10^7 $kN/m/m^2$ was found by its definition and employed to adjust the edge effects (LIU, 1988). The main reinforcements in the wall that were being represented as discrete bending elements were free to undergo relative movement including slippage, but not so with the facing elements which were assigned only a spring resisted rotation.

The program REA allows for the construction sequence to be adopted in the analysis. The construction sequence as followed in the actual wall construction at the site was also adopted in the analysis. There were sixteen solution increments. The initialization of the soil stress state of the subsoils was the first solution increment, then the excavation of the top of crust of soil of about 0.45 m was the second solution increment and replacing the excavated volume with compacted backfill soil after laying the first layer of reinforcement at -0.45 m level was the third increment, and thereafter there were thirteen more solution increments corresponding to each layer of reinforcement and soil (18 in. or 0.45 m thick) placed up to the top of the wall. The finished height of the wall was taken as 19.5 feet (5.95 m).

The settlements were found to be very sensitive to the values of the bulk moduli (B) of the subsoils. However, the bulk moduli of the backfill soils seemed to have very little influence on the tension forces in the reinforcements. The tensions in the reinforcements seemed to depend mainly on the values of the friction coefficients selected. The results also depend on the parameters selected and the mesh configuration and size. The behavior of this wall resting on soft clay foundation has been a very complex one, and a very unique interaction between the subsoil movements and the response of the embankment/wall system, especially the reinforcement forces, was taking place. The settlements at the end of the construction as obtained from the finite element analysis using the program REA, agreed fairly closely with the observed values immediately after the construction (Fig.153 and 154).

The lateral movements of the wall face are underestimated, while the subsoil lateral lateral movements at the front below the vertical face are overestimated (Fig.155). This is probably because a single set of parameters representative for the soft clay subsoil were used. The parameters used corresponded to the properties of the soft clay subsoil at about 3 m depth below the general ground surface, which is the weakest zone in the subsoil. However, the actual shear strength of the subsoil beneath the embankment was found to be increasing with depth, for instance, as observed from the vane shear tests. Therefore, a more rigorous analysis should include several varying sets of soil parameters in the input for the soft clay subsoil with depth. A model more suited to represent the behavior of soft clays, e.g., the cam clay model could be used (CHAI, 1992). This could bring the observed and the predicted values closer. Similar observations were also made at the center of the middle section at the location of the inclinometer I4. The observed values of the lateral movements of the embankment are higher than the finite element prediction, but the observations made with regard to the subsoil movements are the opposite (Fig.156). The direction of the lateral movement in the subsoil is opposite to that of the embankment above the ground level. The observed subsoil lateral movement at I4 were quite small. The actual observations showed maximum lateral movement of the wall face (I1 to I3) and of the embankment as monitored at I4 occurred at the very top, but the

finite element prediction from REA shows the maximum lateral movements of the wall face or the embankment at some distance below the top. The subsoil movements at the back near the heel are also overestimated, although the observed values were quite small (Fig.157).

The observed tensions immediately after construction agree fairly well with the finite element prediction from REA (Fig.153). Due to arching effects and delay in response of the settlements at the toe, there would be a higher tensile force in the reinforcements just behind the facing and this would also cause some decrease in the tensile forces at distances far behind the facing. Moreover, the tensile forces were found to be continually fluctuating right from the beginning of construction influenced greatly by the subsoil movements.

The AIT Welded Wire Wall was modeled using the program NONLIN 1 by LO (1990) (Fig.152). The mesh was established based on the geometry of the structure, zones of expected high stress gradients, zones of interest for computed stresses and deformations, practical limitations of the program capacity and required run times. Mesh boundary conditions were selected to appropriately model the expected deformations and were set far enough from the reinforced soil zone so as to have negligible influence on the zone of interest. A suitable one-dimensional bending (Hermitian) element was introduced to simulate the typical wall face of the Hilfiker's welded wire wall.

The results of the analysis from the NONLIN 1 program were used for comparison with the results of the analysis from REA and the observed values. The tensile forces in reinforcing mat No. 1 in the middle lateritic backfill section obtained from the NONLIN 1 analysis are much higher than those obtained by either the REA analysis or the observed values (Fig.153).

The lateral movements of the wall face were computed with the program NONLIN 1 and are shown in Fig.155. The lateral movements of the wall face from NONLIN 1 agreed very well with the observed values. The shape of the curve was also very close. However, the foundation subsoils were being represented by suitable springs instead of continuum elements or soil elements. Moreover, no allowances were made for the compaction induced stresses while using the NONLIN 1 program.

5 CONCLUSIONS/REMARKS

5.1 WELDED-WIRE WALL / TEST EMBANKMENT PERFORMANCE AND FIELD PULLOUT RESISTANCES

(1) The wall showed no signs of instability both during construction and also in the post-construction phases, despite the large settlements and lateral movements. Its overall performance was satisfactory.

(2) The subsoil movements and the arching effects within the wall due to the presence of the inextensible reinforcements greatly influenced the variations in the vertical pressures beneath the wall.

(3) The magnitudes and the variations of the strains, and thereby, the tensile forces in the reinforcing members were found to be dictated by the foundation deformations, arching effects and lateral movements of the vertical wall face. The welded wire mesh facing also had a major role in the arching effects.

(4) Compaction induced stresses increased the lateral earth pressures considerably, and thereby, also the tensile forces in the reinforcements.

(5) The tensions in the different layers of the reinforcements increased considerably, throughout their lengths, in the post-construction phase. The tensions near the rear end of the mats were also high. Increase in the reinforcement tensions in the post-construction phase also implies an increase in the values of K.

(6) The lateral earth pressure coefficients K measured during the wall construction were found to vary from a value corresponding to the active condition, K_a, at the base of the wall, to a value in excess of the at-rest condition, but not exceeding $1/K_o$ at the top of the wall. By considering the appropriate OCR of the compacted samples, the K value at the top would probably lie closer to the observed values.

(7) The location of the maximum tension line was found to be severely affected by the foundation compressibility, arching effects and the effects of compaction induced stresses. These features caused the overall behavior to depart from the behavior of reinforced walls with granular backfill constructed on relatively rigid foundations.

(8) The line of maximum tensions at the end of construction did not agree well with either the Rankine or the coherent gravity or the logarithmic or the logarithmic spiral failure planes. It was found rather difficult to draw a well-defined failure plane. Also, in the post-construction phase, there would be more than one peak in a mat.

(9) Steel grids reinforcements can be effectively used to reinforce poor to marginal quality backfill soils in walls and embankments on soft clay foundations. The laboratory and the field pullout tests support this conclusion.

(10) The arching severely affected the field pullout resistances from the lateritic backfill soil used in the middle section. The pullout resistances were found to decrease with the increase in the overburden pressures, contrary to the theoretical expectations and what was observed from the laboratory pullout tests using the same backfill soil.

(11) Weathered clay and clayey sand backfill soils gave higher pullout resistances from the field pullout tests than from the laboratory pullout tests. Thus, in general, the laboratory pullout tests provide conservative values of the pullout resistances.

(12) During the field pullout tests, the axial strains were found to decrease more or less linearly with the increasing distance from the face of the wall.

(13) If the subsoil were also stabilized by some effective method, it would have drastically reduced the total and differential settlements as also the lateral movements, resulting in improved stability of the embankment/wall system.

5.2 LABORATORY AND FIELD PULLOUT RESISTANCES OF THE WELDED-WIRE REINFORCEMENTS

(1) Pullout resistances comparable to that of the good quality granular backfill materials can be generated with the compacted cohesive-frictional soils on the dry side of optimum, while using welded wire grid reinforcements.

(2) Frictional resistances on an average provide only about 10 to 15% of the total pullout resistances of the grid reinforcements in poor to marginal quality backfill soils and maybe nearly zero, while the bearing resistances infront of the transverse bars of the steel grid constitute the rest.

(3) The pullout failure mechanisms in front of the transverse members of the grid, and thereby, also the magnitudes of the total pullout resistances were found to be a function of both the soil and the grid parameters.

(4) Only either the general bearing failure mechanism or the punching shear failure mechanism is possible at any instant in front of the transverse members of the grid during pullout, depending on the grid and the soil parameters.

(5) The pullout failure mechanism was found to be a function of the spacing to diameter (S/D) ratios of the transverse bars, compaction moisture content of the soil and the relative stiffness of the soil compared to that of the transverse member. Increase in either the moisture content or the vertical normal stresses or the (S/D) ratios were found to steer the pullout failure mechanism more towards a general bearing failure mechanism. Otherwise, the failure mechanism tends to move towards a punching shear failure mechanism.

(6) Interferences between the passive resistant zones of the successive transverse members in a steel grid reinforcement become less significant for spacing to diameter (S/D) ratios greater than about 50 to 75 for the cohesive-frictional soils used in this study.

(7) The total pullout resistances of the grid reinforcements in cohesive-frictional backfill soils increase linearly with the confining vertical normal stresses, similar to that in the granular soils for the range of normal pressures 10 to 130 kPa employed in the laboratory pullout tests. This was also confirmed from the field pullout tests in the two end sections comprising of the weathered clay and the clayey sand backfills.

(8) Pullout resistances of the lateritic residual backfill soils at high normal stresses (greater than about 50 kPa) were greatly affected by the particle crushing phenomenon, inherent in these soils. Clayey sands were found to be more sensitive to moisture changes on the wet side of optimum. Lateritic soil gave almost the same pullout capacities at the optimum moisture content, as on the dry side. However, the weathered clay gave higher pullout capacities on the dry side of optimum.

(9) Predictions by the general bearing failure mechanism and the punching shear failure mechanism give, respectively, the upper and the lower bound values for the pullout capacities of grid reinforcements.

(10) With the increase in the particle size, the pullout failure mechanism in front of the transverse members of the grid approaches the punching shear failure mechanism. Increase in the moisture content was found to steer the pullout failure mechanism more towards a general bearing failure mechanism.

(11) Bar diameters of around 6.35 mm (1/4 in.) for both the longitudinal and the transverse members forming the grid with mesh openings of about 0.15 m to 0.225 m to 0.15 to 0.3 m (i.e., 6 in. x 9 in. to 6 in. x 12 in.) have been found to be the most convenient in practice. The vertical spacing can be provided as per the design requirements.

(12) The laboratory pullout tests provide conservative values of the pullout resistances compared to the field pullout tests.

5.3 PREDICTED RESULTS USING THE FINITE ELEMENT PROGRAMS

(1) The prediction of the total (laboratory) pullout resistances of the grid reinforcements at the end of 25.4 mm (1 in.) pull using the program REA with the concept of equivalent friction coefficient by a discrete analysis was found to be comparable with the actual observed values. The predicted tension forces were closer to the observed values, except at the rear end of the mat wherein the tension forces were underestimated. The prediction of the total pullout resistances at the end of 1 in. (25.4 mm) pull using the program NONLIN 1 was also found to be comparable. Both these predictions were found to lie between the upper and the lower bound envelopes for the pullout resistances of the grid reinforcements.

(2) Regarding the prediction of the behavior of the wall immediately after construction using the programs REA and NONLIN 1, the lateral movements of the subsoil were overpredicted and that of the wall face were slightly underpredicted with REA. The lateral movements of the wall face agreed fairly well with the prediction from the program NONLIN 1. The actual observed surface settlements and subsurface settlements beneath the embankment were lower than the corresponding predicted settlements from REA.

(3) Using the modified finite element program NONLIN 1 to model the laboratory pullout tests, the load-displacement curves could be predicted comparably well with the experimental results.

5.4 RECOMMENDATIONS FOR FURTHER RESEARCH

The following suggestions are being made for further research and for a better understanding of the soil-reinforcement interactions in mechanically stabilized earth structures, especially while using poor quality cohesive-frictional backfill soils and welded wire (steel grids) reinforcements.

(1) More pullout tests of the grid reinforcements over a wide range of S/D ratios and also single transverse bar pullout tests are required to be conducted to confirm and clearly identify the value of $(S/D)_{lt}$ above which there will be no interference effects, in the case of cohesive-frictional soils such as the ones used in this study. It is also necessary to identify the various factors affecting the value of $(S/D)_{lt}$.

(2) The effect of shape of reinforcements, especially the transverse members, on the pullout failure mechanisms and the pullout resistances in cohesive-frictional soils could also be studied.

(3) Study the effect of degrees of compaction and the rates of pullout on the pullout failure mechanisms and the pullout resistances.

(4) The effects of the extensibility of the reinforcements could be studied by comparing the findings of this research work, both the laboratory pullout test results and the behavior of the AIT wall, with similar results obtained while using polymeric reinforcements.

(5) This research work dealt with only the peak pullout resistances for varying soil and grid parameters. These peak values are being utilized in the limit equilibrium methods of analysis of MSE structures, incorporating a factor of safety. However, it would also be interesting and useful to numerically model the load-displacement response during pullout to obtain the pullout resistances at a particular strain level i.e., under working stress conditions.

(6) In the numerical modeling of the AIT wall, Duncan's characterization were used to represent the different soils in the present study. Therefore, it can at best predict only the behavior of the wall at the end of construction. In order to predict the long-term behavior, a model more suited to represent the behavior of the soft clay subsoils, including the effects of consolidation and creep (such as the critical state models, e.g. the cam clay model using the CRISP computer program) could be used.

(7) Corrosion studies can be made on the welded-wire (steel grids) reinforcements embedded in different types of backfill materials. Predictions for long-term corrosion rates can be verified.

6. REFERENCES

AL-HUSSAINI, M.M. & PERRY, E.B. (1976), Effect of Horizontal Reinforcement on Stability of Earth Masses, Technical Report S-76-11, Soils and Pavement Laboratory, US Army Engineer Waterway Experiment Station, Vicksburg, Mississippi, USA, 105pp.

AL-HUSSAINI, M.M. & JOHNSON, L.D. (1978), Numerical Analysis of a Reinforced Earth Wall, Proc. ASCE Symp. on Earth Reinforcement, Pittsburg, Pennsylvania, pp.98-126

AMIN, NOOR UL (1989), Direct Shear and Pullout Tests on Lateritic Soil at Low Pressure, AIT M.Eng. Thesis No.GT-88-4.

ANDERSON, L.R., SHARP, K.D., WOODWARD, B.L. & WINWARD, R.F.(1985), Performance of Rainier Avenue Welded-Wire Retaining Wall, Seattle, Washington, Report Prepared for the Hilfiker Company, Centerville, Utah, Utah State Uni., Logan, Utah, U.S.A.

ANDERSON, L.R., LIU, J. & BAY, J.A. (1986), Experimental Evaluation and Design Recommendations for Syro Anchored Retaining Wall System, Report Prepared for Syro Steel Co., Centerville, Utah, Department of Civil and Environmental Engineering, Utah State University, Logan, Utah, U.S.A.

ANDERSON, L.R., SHARP, K.D. & HARDING, O.T. (1987), Performance of a 50-feet high Welded Wire Wall, Soil Improvement - A Ten Year Update, Geotechnical Special Publication No.12, ASCE (1987) pp.280-308.

ASAOKA, A. (1978), Observational Procedure for Settlement Prediction, Soils and Foundations, Vol.18, No.4, pp.87-101.

BALASUBRAMANIAM, A.S. & BRENNER, R.P. (1981), Consolidation and Settlement of Soft Clay, Soft Clay Engineering, Developments in Geotechnical Engineering 20, (Editors: E.W.Brand & R.P.Brenner), Elsevier Scientific Publishing Company

BALASUBRAMANIAM, A.S., BERGADO, D.T., LEE, Y.H., CHANDRA, S. & YAMADA, Y. (1985), Stability and Settlement Characteristics of Structures on Soft Bangkok Clay, Proc. 11th Intl. Conf., Soil Mech. Foun. Eng'g., ISSMFE, Vol.3, pp1641-1648.

BASSETT, R.H. & LAST, N.C. (1978), Reinforcing Earth Below Footings and Embankments, Symp. on Earth Reinforcements, ASCE Annual Convention, Pittsburg, Pennsylvania, U.S.A., pp. 202-231.

BELL, J. R. (1991), External Examiner's Report of Doctoral Candidate- R.Shivashankar

BERGADO, D.T., BUKKANASUTA, A. & BALASUBRAMANIAM, A.S. (1987), Laboratory Pullout Tests Using Bamboo and Polymer Geogrids including a Case Study, Geotextiles and Geomembranes, 5(1987), pp.153-189.

BERGADO, D.T., NUTALAYA, P., BALASUBRAMANIAM, A.S., APAIPONG, W., CHANG, C.C. & KHAW, L.G. (1988), Causes, Effects and Predictions of Land Subsidence in AIT Campus, Chao Phraya Plain, Thailand, Bull. Assoc. Eng'g. Geol., Vol.25, No.1, pp.57-81.

BERGADO et al (1988-90), Welded-Wire Wall and Embankment System with Poor Quality Backfill on Soft Clay, Progress Report Nos. 1 to 5, Submitted to USAID, Bangkok, Thailand.

BERGADO, D.T., SAMPACO, C.L., SHIVASHANKAR, R., ALFARO, M.C., ANDERSON, L.R. & BALASUBRAMANIAM, A.S. (1990a), Interaction of Welded Wire Reinforcement with Poor Quality Backfill, Proc. 10th SEA Geotech. Conf., Taipei, Vol.1, pp.29-34.

BERGADO, D.T., DARIA, P.A.M., ALFARO, M.C., SAMPACO, C.L. & CHONG, J.C. (1990b), Prediction of Settlements of AIT Test Embankments Using Screw Plate and Pressuremeter Tests, Proc. 10th SEA Geotech. Conf., Taipei, pp.261-264.

BERGADO, D.T., AHMED, S., SAMPACO, C.L. & BALASUBRAMANIAM, A.S. (1990c), Settlements of Bangna-Bangpakong Highway on Soft Bangkok Clay, J.Geotech. Eng'g. Div. (ASCE), Vol. 116, No.1, pp.136-155.

BERGADO, D.T., SAMPACO, C.L., SHIVASHANKAR, R., ALFARO, M.C., ANDERSON, L.R. & BALASUBRAMANIAM, A.S. (1991a), Performance of a Welded Wire Wall With Poor Quality Backfills On Soft Clay, ASCE Geotechnical Engineering Congress at Boulder, Colorado, U.S.A., pp.909-922.

BERGADO, D.T., SHIVASHANKAR, R., SAMPACO, C.L., ALFARO, M.C. & ANDERSON, L.R. (1991b), Behavior of a Welded Wire Wall With Poor Quality, Cohesive-Frictional Backfills on Soft Bangkok Clay (A Case Study), Canadian Geotechnical Eng'g Journal, December 1991 Issue

BERGADO, D.T., LO, K.H., CHAI, J.C., SHIVASHANKAR, R., ALFARO, M.C. & BALASUBRAMANIAM, A.S. (1992), Pullout Tests Using Steel Grids Reinforcement With Low-Quality Backfill, Accepted for publication in the ASCE J. of Geotech. Eng'g., July, 1992 Issue

BISHOP, J.A. & ANDERSON, L.R. (1979), Performance of Welded Wire Retaining Wall, Research Report Submitted to Hilfiker Pipe Company, Department of Civil and Environmental Engineering, Utah State University, Logan, Utah, U.S.A.

BJERRUM, L. (1972), Embankments on Soft Ground, Proc. Spec. Conf. Performance of Earth and Earth-Supported Structures, Lafayette, Ind., 2:1-54

BONAPARTE, R. & CHRISTOPHER, B. R. (1987), Design and Construction of Reinforced Embankments Over Weak Foundations, Transportation Research Record, 1153, Transportation Research Board, National Research Council, Washington, D.C., pp. 26-39.

BONCZKIEWICZ, C., CHRISTOPHER, B.R. & ATMATZIDIS, D.K. (1988), Evaluation of Soil-Reinforcement Interaction by Large Scale Pullout Tests, Transportation Research Board, 67th Meeting, Washington, U.S.A., Paper No.87.

BOONSRI, N. (1971), Shear Strength Characteristics of Compacted Lateritic Soils, AIT M.Eng. Thesis No.399.

BRAND, S.R. & DUFFY, D.M. (1987), Strength of Pullout Testing of Geogrids, Proc. Geosynthetics'87 Conference, New Orleans, Louisiana, U.S.A., pp.226-236.

BROMS, B.B.(1974), Lateral Earth Pressures due to Compaction of Cohesionless Soils, Proc. 4th Budapest Conference on SMFE, pp.373-384.

"CALTRANS" (1987), Investigation of Corrosion at 14 Mechanically Stabilized Embankment Sites, California Department of Transportation Report No.CA/TL-87/12.

CARDER, D.R., POCOCK, R.G. & MURRAY, R.T. (1977), Experimental Retaining Wall Facility - Lateral Stress Measurements with Sand Backfill, Transpn. and Road Res. Laboratory Report No. LR-766, Crawthorne, 19pp.

CARDER, D.R., MURRAY, R.T. & KRAWCZYK, J.V.C. (1980), Earth Pressures against an Experimental Retaining Wall Backfilled with Silty Clay, Transpn. and Road Res. Laboratory Report No. LR-946, Crawthorne, 21 pp.

CHAI, JINCHUN (1992), Performance of Reinforced Cohesive-Frictional Soil with Varying Reinforcement Stiffness on Soft Ground, AIT D.Eng. Dissertion in Progress

CHANG, J.C., HANNON, J.B. & FORSYTH, R.A. (1977), Pullout Resistance and Interaction of Earthwork Reinforcement and Soil, Transpn. Res. Record No.640, pp.1-7.

CHAPUIS, R. (1972), Rapport De Recherche De DEA Institut De Mecanique De Grenoble, Unpublished Internal Report.

COX,J.B. (1968), A Review of the Engineering Characteristics of the Recent Marine Clays in Southeast Asia, Research Report No.6, AIT, Bangkok.

DAVIS, E.H. & POULOS, H.G. (1968), The Use of Elastic Theory for Settlement Prediction Under Three-Dimensional Conditions, Geotechnique, Vol.18, No.1, pp.67-91.

DIMAGGIO, J.A. (1988), Mechanically Stabilized Earth: Walls and Slopes, Federal Highway Administration, U.S. Department of Highways.

DUANGKHAE, S. (1970), The Permeability of Bangkok Clay, AIT M.Eng. Thesis No.340

DUNCAN, J.M. & CHANG, C.Y. (1970), Nonlinear Analysis of Stress and Strain in Soils, Journal of Soil Mech. Found. Div., ASCE, Vol.96, No.SM5, pp.1624-1653

DUNCAN, J.M. & SEED, R.B. (1986), Compaction-induced Earth Pressures under K_o-Condition, J. Geotech. Eng'g. Div., ASCE, Vol.112, No.1., pp1-22.

DUNN, I.S., ANDERSON, L.R. & KIEFER, F.W. (1980), Fundamentals of Geotechnical Analysis, John Wiley and Sons Inc., New York.

DUNNICLIFF, J. & GREEN, G.E.(1988), Geotechnical Instrumentation For Monitoring Field Performance, John Wiley & Sons

FABIAN, K.J. (1987), Clay-Geotextile Interaction in Drained and Undrained Shearing and Pullout Tests, Proc. of the Intl. Symp. on Geosynthetics, Kyoto, Japan, pp.93-102.

FOWLER, J., PETERS, J. & FRANKS, L. (1986), Influence of Reinforcement Modulus on Design and Construction of Mohicanville Dike No.2, 3 ICG, Vienna, Austria, pp.267-271.

GRAY, H. (1936), Stress Distribution in Elastic Solids, Proc. 1st Intl. Conf. Soil Mech. & Found. Eng'g., Vol.2, p.157.

HANNON, J.B., FORSYTH, R.A. & CHANG, J.C. (1982), Field Performance Comparison of Two Earthwork Reinforcement Systems, Transportation Research Record 872, pp.24-32.

HANNON, J.B. & FORSYTH, R.A. (1984), Performance of an Earthwork Reinforcement System Constructed with Low Quality Backfill, Transpn. Res. Record No.965.

HAQUE, M.A. (1977), Some Engineering Properties of Compacted Rangsit Clay Evaluated on the Basis of Laboratory Tests, AIT M.Eng. Thesis No.1005.

HARDIYATIMO, H.C. (1990), Behavior of Mechanically Stabilized Embankment on Soft Bangkok Clay, AIT M.Eng Thesis No. GT-89-9.

HAUSMANN, M.R. (1976), Strength of Reinforced Soil, Proc. 8th Australian Road Res. Conf., Vol.8, Section 13, pp.1-8.

HAUSMANN, M.R. (1990), Engineering Principles of Ground Modification, McGraw-Hill International Editions, Civil Engineering Series.

HERMANN, L.R. (1978), User's Manual for REA (General Two Dimensional Soils and Reinforced Earth Analysis Program), University of California, Davis, California, U.S.A.

"HILFIKER WALLS" (1987,88), Welded Wire Wall Construction Guide, 7th and 8th Editions, Hilfiker Co., Eureka, CA.

HOLTZ, R.D. (1973), Laboratory Studies of Reinforced Earth Using a Woven Plastic Material, Technical Report (Unpublished).

HOLTZ, R.D. (1978), Special Applications of Reinforced Earth - State of the Art and General Report, Symp. on Earth Reinforcement, ASCE Annual Convention, Pittsburg, Pennsylvania, U.S.A., pp.77-97.

HOLTZ, R.D. (1991), External Examiner's Report of Doctoral Candidate- R.Shivashankar.

INGOLD, T.S. (1979), The Effects of Compaction on Retaining Walls, Geotechnique, Vol.29, No.3, pp.265-283.

INGOLD, T.S. (1981), Reinforced Earth - Theory and Design, The Highway Engineer, No.7, pp.2-14.

INGOLD, T.S. (1982), Reinforced Earth, Thomas Telford Ltd., London, U.K.

INGOLD, T.S. (1983 a), Laboratory Pullout Testing of Grid Reinforcements in Sands, ASTM Geotechnical Testing Journal, Vol.6, No.3, pp.101-111.

INGOLD, T.S. (1983 b), A Laboratory Investigation of Grid Reinforcements in Clay, ASTM Geotechnical Testing Journal, Vol.6, No.3, pp.112-119.

INGOLD, T.S. (1983 c), The Design of Reinforced Soil Walls by Compaction Theory, The Structural Engineer, Vol.61A, No.7, pp.205-211.

INGOLD, T.S. (1984), A Laboratory Investigation of Soil-Geotextile Friction, Ground Engineering, Vol.17, No.8, pp21-28.

JEWELL, R.A., MILLIGAN, G.W.E., SARSBY, R.W. & DUBOIS, D. (1984), Interaction Between Soil and Geogrids, Conf. on Polymer Grid Reinforcement, London, U.K., Thomas Telford Publishers, pp.18-30.

JEWELL, R.A. & WROTH, C.P. (1987), Direct Shear Tests on Reinforced Sand, Geotechnique, Vol.37, No.1, pp.53-68.

JEWELL, R.A. (1990), Reinforcement Bond Capacity, (Technical Note), Geotechnique 40, No.3, pp.513-518.

JURAN, I. (1985), Reinforced Soil Systems - Applications in Retaining Structures, Geot. Eng'g. Journal, ASCE, Vol.16, No.1, pp.39-82.

LAMBE, T.W. (1962), Pore Pressures in a Foundation Clay, J. Soil Mech. and Found. Div., A.S.C.E., v. 88, SM2, pp.19-47.

LEELASSITHORN, T. (1978), Strength Characteristics of Compacted Clay, AIT M.Eng. Thesis No.1286.

LESCHINSKY, D. & FIELD, D.A. (1987), In Soil Load Elongation, Tensile Strength and Interface of Non Woven Geotextiles, Proc. Geosynthetics'87 Conference, New Orleans, Louisiana, pp.238-249.

LIEW, Y.Y. (1979), Compressibility and Permeability Characteristics of Compacted Clay, AIT M.Eng. Thesis No.GT-78-12.

LIU, J.S. (1988), Analysis of Mechanically Stabilized Retaining Walls, Ph.D. Dissertation, Utah State University, Logan, Utah, U.S.A.

LO, K.H. (1990), Modelling of Laboratory and Field Pullout Test of Steel Grid Reinforcements, AIT M.Eng. Thesis No.GT-89-5.

LONG, N.T. (1977), Some Aspects About Fill Materials in Reinforced Earth, Proc. Heriott Watt Uni. Symp. on Reinforced Earth and Other Techniques, Edinburg, U.K., pp.246-249.

LOW, B.K. & DUNCAN, J. M. (1985), Analysis of the Behavior of Reinforced Embankments on Weak Foundations, Report VPI/CE-GT-85-11, Virginia Polytechnic Institute, Blacksburg.

MACATOL, K.C.B. (1990), Interaction of Lateritic Backfill and Steel Grid Reinforcements at High Vertical Stresses Using Pullout Tests, AIT M.Eng. Thesis, No.GT-90-12

MAGNAN,J._P. & DEROY,J._M. (1980), Analyse graphique des tassements observes sous les ouvrages, Bull. Liais. Lab. Ponts Chauss., No.109, pp.45-52

MATSUO, M. & KAWAMURA, K. (1977), Diagram for Construction Control of Embankments on Soft Ground, Soils and Foundations, Vol.17, No.3, pp.37-52.

MAYNE, P.W. & KULHAWY, F.H. (1982), K_o-OCR Relationships in Soil, J. of Geotech. Eng'g. Div., ASCE, Vol.108, No.GT6, pp.851-872.

MCGOWN, A., ANDRAWEZ, K.Z. & AL-HUSSAINI, M.M. (1978), Effects of Inclusion Properties on the Behavior of Sand, Geotechnique (28), pp.327-346.

MCGOWN, A., ANDRAWEZ, K. Z. & MURRAY, R. T. (1988), Controlled Yielding of the Lateral Boundaries of Soil Retained Structures, Geosynthetics for Soil Improvement (Edited by R. D. HOLTZ), ASCE Geotechnical Special Publication No. 18, pp. 193-210.

MCKITTRICK, D.P. (1978), Reinforced Earth: Application of Theory and Research to Practice, Proc. Symp. on Soil Reinforcing and Stabilizing Techniques, Sydney, Australia.

MEYERHOF, G.G. (1953), The Bearing Capacity of Foundations Under Eccentric and Inclined Loads, Proc. 3 Intl. Conf. Soil Mech. Zurich, 1, 440-445

MITCHELL, J.K. & VILLET, W.C.B. (1987), Reinforcement of Earth Slopes and Embankments, Transportation Research Record No.290.

MOTALEB, ALAA A. ABDEL & ANDERSON, L.R. (1989), Pullout Resistance of Welded Wire Mats Embedded in Clayey Silt Backfill, Utah State Uni., Logan, Utah.

MURRAY, R.T. & BODEN, J.B. (1979), Reinforced Earth Wall Constructed with Cohesive Fill, Proc. Intl. Conf. on Soil Reinforcement, Paris, Vol.2, pp.569-577.

MURRAY, R.T. & FARRAR, D.M. (1990), Reinforced Earth Wall on the M-25 Motorway at Waltham Cross, Proc. Inst. Civil Engrs. Vol.88, Part 1, pp.261-282.

NELSON, K.J. & SELVAGE, J.R. (1987), Design Applications of the Welded Wire Wall, Proc. 23rd Symp. on Eng'g. Geology and Soil Eng'g., Utah State University, Logan, Utah.

NIELSEN, M.R. & ANDERSON, L.R. (1984), Pullout Resistance of Welded Wire Mats Embedded in Soil, Research Report Submitted to the Hilfiker Co., Department of Civil and Environmental Eng'g., Utah State University, Logan, Utah, U.S.A.

OCHIAI, H. & SAKAI, A. (1987), Analytical Method For Geogrid Reinforced Soil Structures, Proc. of the Intl. Symp. on Geosynthetics, Kyoto, Japan, (Organized by the Japanese Chapter of IGS), pp.483-486

OLSON, R.E. (1977), Consolidation Under Time Dependent Loading, J. Geotech. Eng'g. Div., ASCE, Vol.103, No.1, pp.55-60.

ONITSUKA, K., YOSHITAKE, S. & BERGADO, D.T. (1987), Shear Characteristics of Decomposed Granite Soil Under Low Pressure and Stability Analysis of Surface Failure, Saga University, Japan.

OSPINA, RAFAEL I. (1988), An Investigation on the Fundamental Interaction Mechanism of Non-extensible Reinforcement Embedded in Sand, Unpublished MS Thesis, Georgia Institute of Technology, Atlanta, GA, U.S.A.

PALMEIRA, E.M. & MILLIGAN, G.W.E. (1989), Scale and Other Factors Affecting the Results of the Pullout Tests of Grids Buried in Sand, Geotechnique, Vol.39, No.3, pp.551-584.

PARNPLOY, U. (1985), Deformation Analysis and Settlement Prediction of Bangna-Bangpakong Highway (Section 1), AIT, M.Eng. Thesis No.GT-84-40.

PETERSON, L.M. & ANDERSON, L.R. (1980), Pullout Resistance of Welded Wire Mesh Embedded in Soil, Research Report Submitted to the Hilfiker Pipe Co., Department of Civil and Environmental Engineering, Utah St.Uni., Utah, U.S.A.

PLANGPONGPUN, S. (1977), Strength Characteristics of Bangkok Clay in Relation to Pavement Design, AIT M.Eng ThesisPs No.1014.

POULOS, H.G. & DAVIS, E.H. (1974), Elastic Solution for Soil and Rock Mechanics, John Wiley and Sons Inc., New York.

ROWE, P.W. (1954), A stress-strain Theory for Cohesionless Soil With Application to Earth Pressure at Rest and Moving Walls, Geotechnique, Vol.4, No.2, pp.70-88.

SALAMONE, W.G., BOUTRUP, E., HOLTZ, R.D.,KOVACS, W.D. & SULTON, C.D. (1980), Fabric Reinforcement Designed Against Pullout, The Use of Geotextiles For Soil Improvement, ASCE National Convention, Portland, Oregon, U.S.A. pp.80-177.

SCHLOSSER, F. & LONG, N.T. (1973), Etude Du Comportement Du Maeriau Teree Armee, Annles De L'Inst Techq Du Battiment Et Des Trav Publ. Suppl. No. 304, Ser Mater. No.45.

SCHLOSSER, F. & LONG, N.T. (1974), Recent Results in French Research on Reinforced Earth, Journal of Construction Division, ASCE, 100 (CO3) pp.223-237

SCHLOSSER, F. & ELIAS, V. (1978), Friction in Reinforced Earth, Symp. on Earth Rein. ASCE Annual Convention, Pittsburg, Pennsylvania, U.S.A., pp.735-762.

SCHLOSSER, F. (1982), Reinforced Earth - Mechanism, Behaviour and Design Methods, Symp. on Soil and Rock Improvement Techniques Including Geotextiles Reinforced Earth and Modern Piling Methods, Bangkok, Thailand, pp.F-1-1 to pp.F-1-26.

SCHLOSSER, F. & DE BUHAN, P. (1990), Theory and Design Related to the Performance of Reinforced Soil Structures, State of the Art Report, Performance of Reinforced Soil Structures, Proceedings of the Internal Reinforced Soil Conference, Glasgow, (Edited by MCGOWN et al.), Thomas Telford, London, pp.1-14.

SCHMERTMANN, G.R., CHEW, S.H. & MITCHELL, J.K. (1989), Finite Element Modelling of Reinforced Soil Wall Behavior, Geotechnical Eng'g. Rep. No. UCB/GT/89-01, University of California, Berkeley, California.

SCHWAB, E. F., PREGL, O. & BROMS, B. B.(1977) Deformation Behavior of Reinforced Sand at Model Tests Measured by the X-Ray Technique, Proceedings of the International Conference, Fabrics in Geotechnics, Paris, Vol. 1, pp.101-112.

SHIVASHANKAR, R. (1991), Behavior of a Mechanically Stabilized Earth (MSE) Embankment and Wall System with Poor Quality Backfills on Soft Clay Deposits, Including a Study of the Pullout Resistances, AIT Doctoral Dissertation No.GT-90-3, Asian Institute of Technology, Bangkok, Thailand.

SKEMPTON, A.W. & BJERRUM, L. (1957), A Contribution to the Settlement Analysis of Foundations on Clay, Geotechnique, Vol.7, No.4, pp.168-178.

"SLOPE INDICATOR CO. (SINCO)" (1984a), Digitilt Inclinometer Manual - Model 50309-M Indicator with 50325-M Sensor.

"SLOPE INDICATOR CO. (SINCO)" (1984 b), Instrumentation Manual for Total Pressure Cell, Model 51482 with Model 514178 Transducer.

"SLOPE INDICATOR CO. (SINCO)" (1984 c), Instruction Manual for Pneumatic Pressure Transducer Model 514177 or 514178.

"SLOPE INDICATOR CO. (SINCO)" (1987), Instruction Manual for Digital Pneumatic Pressure Indicator Model 514209.

TENSAR (1990), A Case Study, Netlon Limited, Kelly Street, Blackburn, England.

TERZAGHI, K. (1934), Large Retaining Wall Tests (I): Pressure of Dry Sand, Eng'g News Record, Vol.112, pp.136-140.

TERZAGHI, K. (1943), Theoretical Soil Mechanics, John Wiley and Sons Inc., New York.

THIRAWAT, S. (1968), Thixotropic Characteristics of Compacted Bangkok Clay, AIT M.Eng. Thesis No.211.

TSAI, CHOW-YUAN (1981), A Monograph on the Engineering Properties of Bangkok Subsoil, AIT M.Eng. Thesis No.GT-81-15.

TUMAY, M.T., MARIO ANTONINI & ARA ARMAN (1979), Metal Versus Non-Woven Fiber Fabric Earth Reinforcement in Dry Sands: A Comparative Statistical Analysis of Model Tests, Geotechnical Testing Journal, ASTM, Vol.w, No.1, pp.44-56.

TZONG, W.H & CHENG-KUANG, S. (1987), Soil-Geotextile Interaction Mechanism in Pullout Test, Proc. Geosynthetics'87 Conference, New Orleans, Louisiana, pp.250-259.

"UNIVERSITY OF CALIFORNIA, DAVIS, DEPARTMENT OF CIVIL ENG'G." (1984), Large Scale Pullout Tests on Tensar SR-2 Geogrids, Report Submitted to Tensar Corporation, U.S.A.

VESIC, A. (1963), Bearing Capacity of Deep Foundations in Sand, Highway Research Record 39 pp.112-153

VIDAL, M.H. (1969), The Principle of Reinforced Earth, Highway Research Record 282, pp.1-16, Washington, D.C., U.S.A.

WONG, K.S. & DUNCAN, J.M. (1974), Hyperbolic Stress-Strain Parameters For Nonlinear Finite Element Analysis of Stresses and Movements in Soil Masses, Geotechnical Eng'g Report No.TE-74-3, University of California, Berkeley, California, USA

WROTH, C.P. (1975), In-situ Measurement of Initial Stresses and Deformation Characteristics, Proc. 6th ASCE Spec. Conf. on Analysis and Design in Geotech. Eng'g. Vol.2, pp.181-230.

YANG (1972), Strength and Deformation Characteristics of Reinforced Sand, Ph.D. Thesis, UCLA.

7. PROBLEMS ENCOUNTERED

The problems encountered during the course of this research work were mainly related to the setting up of the pullout testing program, i.e., apparatus and its accessories; laboratory and field pullout testing procedures, reliability and performance of the strain gages and other field instrumentation as emphasized in the earlier progress reports. It was possible to run only strain-controlled pullout tests by the manual operation of the potentiometer pot, interfaced on the power supply module having a linear displacement output, due to the absence of the Temposonics analog output module with velocity controls.

The inclinometers functioned well only up to about 228 days from the end of construction. Most of the pneumatic piezometers were ineffective before the end of construction, except for N2 at 2 m depth. The hydraulic piezometers performed well and reliably up to about 280 days from the beginning of construction. The settlement gages and the earth pressure cells were found to be working satisfactorily even after about 600 days from the beginning of construction. Most of the strain gages were damaged about one year after the end of construction, or the strain measurements did not seem to be consistent and reliable after this period.

8. WORKPLAN FOR THE NEXT PERIOD

Although the duration of this project is over and the main objectives mentioned earlier have been achieved, the infrastructure that have been procured with the help of this project such as the pullout box and its accessories, the advanced data acquisition system, and other instrumentation help to continue the research in various related fields of soil reinforcement and soil improvement techniques at the Asian Institute of Technology, by way of Master's theses, Doctoral dissertation topics, and others.

9. PUBLICATIONS

The following technical papers related to this project have been accepted for publication:

Bergado, D. T., Shivashankar, R. & Chai, J. C. (1990), Mechanically Stabilized Earth (MSE) Embankments on Soft and Subsiding Ground in Bangkok, Thailand, Proc. Intl. Seminar on Geotechnical and Water Problems in Lowland, Saga University, Japan, November 1990.

Bergado, D. T., Lo, K. H., Sampaco, C. L., Alfaro, M. C., Shivashankar, R. & Anderson, L. R. (1990), Behavior of Mechanically Stabilized Earth (MSE) Wall on Soft Ground, Proc. Philippine Institute of Civil Engineers National Convention, November 1990.

Bergado, D. T., Hardiyatimo, H., Lo, K.H., Sampaco, C. L. & Balasubramaniam, A. S. (1990), Interaction of Steel Geogrids and Low-Quality, Cohesive-Frictional Backfill and Behavior of Mechanically Stabilized Earth (MSE) Wall on Soft Ground, Proc. Symp. Developments Laboratory and Field Tests in Geotechnical Engineering Practice, Bangkok, Thailand, December, 1990

Bergado, D.T., Shivashankar, R., Sampaco, C.L., Alfaro, M.C. & Anderson, L.R. (1991), Behavior of a Welded-Wire Wall with Poor Quality Cohesive-Frictional Backfills on Soft Bangkok Clay - A Case Study, Canadian Geotechnical Engineering Journal, Vol 28, December 1991.

Shivashankar, R. (1991), Behavior of a Mechanically Stabilized Earth (MSE) Embankment and Wall System with Poor Quality Backfills on Soft Clay Deposits, Including a Study of the Pullout Resistances, AIT Doctoral Dissertation No.GT-90-3, Asian Institute of Technology, Bangkok, Thailand (Advisor: Dr. D. T. Bergado).

Bergado, D. T., Lo, K. H., Chai, J. C., Shivashankar, R., Alfaro, M. C. & Anderson, L. R. (1992), Laboratory and Field pullout Tests Using Steel Grid Reinforcement With Cohesive-Frictional Backfill, Journal of Geotechnical Engineering Division, ASCE, July 1992.

Bergado, D. T.,Hardiyatimo, H. C., Cisneros, C. B., Chai, J. C., Alfaro, M. C., Balasubramaniam, A. S. & Anderson, L. R. (1992), Pullout Resistance of Steel Geogrid With Weathered Clay Backfill material, Geotechnical Testing Journal, March 1992.

Bergado, D. T., Shivashankar, R., Alfaro, M. C. & Balasubramaniam, A. S. (1992), Pullout Resistance and Interaction of Steel Grid Reinforcements in Weathered Bangkok Clay, Proceedings of IS Kyushu'92 Symp. on Soil Reinforcement Techniques, Fukuoka, Japan, September 1992.

* The following technical papers related to this project have been submitted for possible publication in journals:

Bergado, D. T., Shivashankar, R., Alfaro, M. C. & Balasubramaniam, A. S. (1992), Pullout Resistances of Steel Grid Reinforcements in a Clayey Sand, Submitted to Geotechnique, U.K.

Shivashankar, R. & Bergado, D. T. (1992), Lateritic Soil-Steel Grid Reinforcement Interaction in Pullout Tests, Submitted to J. of Geotech. Eng'g. Div. ASCE, U. S. A.

Bergado, D. T. & Shivashankar, R. (1992), Interaction of Welded-Wire Steel Grid Reinforcements with Weathered Bangkok Clay, Submitted to Soils and Foundations, Japan.

10. CONFERENCE/WORKSHOP ATTENDANCE

(a) November, 1990 - International Seminar on Geotechnical and Water Problems in Lowland, Saga University, Saga, Japan. (Dr. D. T. Bergado attended and presented a paper on MSE wall behavior).

(b) November, 1990 - Philippine Institute of Civil Engineers National Convention, Manila, Philippines. (Dr. D. T. Bergado attended and presented a paper on MSE wall behavior).

(c) December, 1990 - Symposium on Developments in Laboratory and Field Tests in Geotechnical Engineering Practice, Bangkok, Thailand. (Dr. D. T. Bergado attended and presented a paper on steel grids research results and MSE wall behavior).

11. INTERNATIONAL TRAVEL

No international travel has been charged to the project for this period.

12. RESEARCH COLLABORATION

The research collaboration has been limited to discussions with the research consultant, Prof. Anderson, regarding data analysis and subsequent publications.

13. DISTINGUISHED VISITORS

There were no distinguished visitors in this period.

14. DISSEMINATION OF RESEARCH INFORMATION

Research information has been disseminated through lectures in conferences (see item 10 above), as well as, through technical publications (see item 9 above).

15. FINANCIAL ADMINISTRATION

The project finally showed a net deficit of Bahts 69,759.00. This deficit included the currency exchange loss of Bahts 18,397.00. The deficit has to be paid from the Geotechnical Engineering (GTE) Division to the AIT Central Fund. The expenses exceeded the budget due to the large amount of equipment purchases, increase in the volume of backfill materials used in the wall/embankment system, and escalation in the prices of the equipments during time of their purchase, freight and customs clearance costs, etc. Some of the overexpenditure was drawn from the overhead costs.

16. OTHER PROJECTS AND GRANTS

No financial assistance was obtained from any other projects or grants during this period.

TABLES

TABLE 1 SUMMARY OF PULLOUT TESTING BY SEVERAL RESEARCH WORKERS

AUTHOR	BOX SIZE inches (LxWxD)	PULLOUT RATE per minute in inch. or as stated	NORMAL LOADING	TYPE OF REINFORCEMENT TESTED	TYPE OF SOIL TESTED
HOLTZ (1973)	42 x 10 x 11	0.18	Flexible	Woven Geotextile	Sand
CHANG et al (1977)	54 x 36 x 18 Large Scale	0.002	Rigid	Bar Mesh, long smooth bars, solid steel plate, steel strips	Poorly Graded Gravelly Sand
CHANG et al (1977)	Modified Shear Box (Small Scale)			Bars & Strips	Poorly Graded Gravelly Sand
SCHLOSSER & ELIAS (1978)	36 x 36 x18	1.8 mm	Flexible	Metal Strips	Sand
TUMAY et al (1979)	48 x 18 x 39	Pulled until sliding occurred	Rigid	Aluminium & Fibre Fabric Strips	Sand
BISHOP & ANDERSON (1979)				Welded Wire Mats	Silty Sand
PETERSON & ANDERSON (1980)		Stress Controlled (pulled by 1/2")	Rigid	Welded Wire Mats	Silty Sand
SALAMONE et al (1980)	75 x 27 x 24		Flexible	Woven Geotextile	Sand
INGOLD (1983a,b)	20 x 11 x 12	0.04	Flexible	Geogrid	Sands, clays
JEWELL et al (1984)			Rigid	Geogrid	Sand
NIELSEN & ANDERSON (1984)	Refer Fig.2.12	0.0333 (Pulled up to 1")	Rigid	Welded Wire Mats	Sands & Pea Gravels
UNIVERSITY OF CALIFORNIA, Davis (1984)	54 x 36 x 20	2% per minute	Rigid	Tensar SR2, Geogrids	Sand
HANNON & FORSYTH (1984)			Rigid	Welded Wire Mats	Low Quality Backfills
BERGADO et al (1987)	39 x 32 x 36	0.04	Rigid	Bamboo and Tensar geogrids	Poor Quality Backfills
FABIAN (1987)	60 mm SHEAR BOX	0.9 mm/min. for Undrained Tests 0.0033 mm/min. for Drained Tests	Rigid	Geotextiles and Geogrids	Silty Clay

Note: 1 m = 3.28 feet & 1 foot = 12 inches; 1 inch = 25.4 mm

TABLE 1 (CONTD.) SUMMARY OF PULLOUT TESTING BY SEVERAL RESEARCH WORKERS

AUTHOR	BOX SIZE inches (LxWxD)	PULLOUT RATE per minute in inch. or as stated	NORMAL LOADING	TYPE OF REINFORCEMENT TESTED	TYPE OF SOIL TESTED
LESCHINSKY & FIELD (1987)	8 x 8 x 2	0.04	Rigid	Non Woven Geotextile	Ottawa Sand
BRAND & DUFFY (1987)	12 x 12 x 3 Reinforcement pulled out from top, Normal stresses applied on one side	0.004	Rigid	Geogrid	Clay (Low moisture Content Expansive Soil) and Concrete
TZONG & CHENG-KUANG (1987)	48 x 24 x 57	Load Increments	Rigid	Non Woven Geotextile	Sand
BONCZKIEWICZ et al (1988)	50 x 27 x 18	0.04	Flexible	Geotextiles Geogrids, Fibre &	Varying Soils Mostly Sands
OSPINA (1988) at Geogria Inst. of Tech.	54 x 19 x 15 (Large Scale)			GASE Meshes	Sands
OSPINA (1988)*	44 x 8 x 8	10 lb/sec load		GASE Meshes	Sands
PALMIERA & MILLIGAN (1989)	10 x 6 x 8 (Medium Size)		Flexible	Mild Steel & Galvanized Steel Grids	Three types of Leighton Buzzard Sand (dry)
PALMIERA & MILLIGAN (1989)	40 x 40 x 40 (Large Size)		Flexible	Mild Steel & Galvanized Steel Grids	Three types of Leighton Buzzard Sand (dry)

* with Radiographic Measurements X-Ray Techniques were also used by SCHWAB et al. (1977) with Geotextiles in Sands.

Note: 1 m = 3.28 feet & 1 foot = 12 inches; 1 inch = 25.4 mm

TABLE 2

	CLAYEY SAND	
1.	COLOUR	Brownish
2.	SIEVE ANALYSIS	
	percent passing U.S standard Sieve No.200	45%
3.	ATTERBERG LIMITS	
	liquid limit	32%
	plastic limit	12%
4.	STANDARD PROCTOR COMPACTION TEST	
	optimum moisture content (OMC)	14.4%
	maximum dry density	17.9 kN/m^3
5.	SPECIFIC GRAVITY OF SOIL PARTICLES	2.55
	WEATHERED CLAY	
1.	COLOUR	Reddish Brown
2.	SIEVE ANALYSIS	
	percent passing U.S standard Sieve No.200	85%
3.	ATTERBERG LIMITS	
	liquid limit	45%
	plastic limit	21%
4.	STANDARD PROCTOR COMPACTION TEST	
	optimum moisture content (OMC)	22.3%
	maximum dry density	16.0 kN/m^3
5.	SPECIFIC GRAVITY OF SOIL PARTICLES	2.67
	LATERITIC SOIL	
1.	COLOUR	Reddish
2.	SIEVE ANALYSIS	
	percent passing U.S standard Sieve No.200	18%
3.	ATTERBERG LIMITS (of finer fraction only)	
	liquid limit	39%
	plastic limit	23%
4.	STANDARD PROCTOR COMPACTION TEST	
	optimum moisture content (OMC)	11.5%
	maximum dry density	19.3 kN/m^3
5.	SPECIFIC GRAVITY OF SOIL PARTICLES	2.61

Table 3

DIRECT SHEAR TEST RESULTS FROM THIS STUDY

SAMPLE	STD. PROCTOR DENSITY	WATER CONTENT (%)	DRY UNIT WT. (t/cu.m.)	ϕ (degrees)	c (tsm)
Weathered Clay	95% Dry Side	16.0	1.52	32.20	8.90
Weathered Clay	100% OMC	22.3	1.60	24.25	14.71
Weathered Clay	95% Wet Side	28.0	1.52	22.15	11.50
Clayey Sand	95% Dry Side	10.0	1.70	37.15	5.93
Clayey Sand	100% OMC	14.4	1.79	32.00	7.70
Clayey Sand	95% Wet Side	20.2	1.70	17.00	6.00
Lateritic Soil (Low, ≤2 tsm)	95% Dry Side	8.5	1.83	57.18	3.48
Lateritic Soil (>2 tsm)	95% Dry Side	8.5	1.83	38.51	5.08
Lateritic Soil (Low, ≤0.5 tsm)	100% OMC	11.5	1.93	66.19	2.65
Lateritic Soil (>0.5 tsm)	100% OMC	11.5	1.93	41.44	3.21
Lateritic Soil (Low, ≤2 tsm)	95% Wet Side	14.0	1.83	47.67	1.95
Lateritic Soil (>2 tsm)	95% Wet Side	14.0	1.83	37.21	2.03

Note: 1 t/cu.m. = 10 kN/m

Table 4

TRIAXIAL SHEAR TEST RESULTS FROM THIS STUDY

SAMPLE	STD. PROCTOR DENSITY	WATER CONTENT (%)	DRY UNIT WT. (t/cu.m.)	ϕ (degrees)	c (tsm)
Weathered Clay	95%	21.34	1.55	31.50	11.80
Clayey Sand	95%	13.20	1.70	33.00	5.60
Lateritic Soil	95%	10.64	1.83	32.50	8.00

TABLE 5

COMPONENTS OF PULLOUT TESTING PROGRAM (REFER FIG. 28 FOR DETAILS)

1. Compacted Soil in the Pullout Box, Compacted With a Wacker Hand Compactor, Density and Moisture Contents checked with a Troxler Nuclear Gage
2. Reinforcing Mat Being Tested (Refer to Fig. 32)
3. Strain Gages (2 in number) at Each Instrumentation Point
4. Flexible Plate (1/4" thick) Placed Over Compacted Soil
5. Air Bags For Applying Normal Pressures
6. Dial Gages at Top
7. Airloc Pads
8. Clamping Mechanism
9. Swivel Joint
10. Load Cell
11. Adjustable Height Mount or Rest For Load Cell
12. Piston Pump & Motor with, Filters and Valves
13. Hydraulic Cylinder
14. Servo Valve
15. Wooden Table Rest For the Cylinder
16. Analog Output Module
17. Dial Gage For Measuring Front Displacements
18. LVDT For Measuring Front Displacements
19. Stop Clock
20. 21X Data Logger with Multiplexer
21. EMRS Power Supply Module and EMD Amplifier Module
22. Air Compressor
23. Regulator
24. Stiff Tubing Connecting Air Compressor to Air Bag through Regulator
25. Lead Wire Connecting Load Cell to Datalogger
26. Lead Wire Connecting LVDT to Datalogger
27. Lead Wires Connecting all the Strain Gages to the Datalogger through the Multiplexer

TABLE 6

REFERENCES	FORMULA	IMMEDIATE SETTLEMENTS (m
Janbu et al (1956) and D'Appolonia et al (1971)	$p_i = \mu_0 \mu_1 \frac{q\,B}{SR \times E_u}$	0.58
Davis and Poulos (1968) and D'Appolonia et al (1971)	$p_i = \Sigma \left[\frac{\sigma_z - 0.5(\sigma_x + \sigma_y)}{SR \times E_u} \right] \Delta H$	0.57
Observed Settlement		0.53

TABLE 7

REFERENCE	FORMULA	TOTAL SETTLEMENTS (1
Davis and Poulos (1968)	$p_t = \Sigma \left[\frac{z' - \nu'(\sigma_x + \sigma_y)}{E'} \right] \Delta H$	1.35
(Terzaghi, 1943)	$p_t = p_i + p_{oed}$	1.59
Skempton and Bjerrum (1957)	$p_t = p_i + \mu p_{oed}$	1.36
Asaoka (1978)	Graphical Method	1.32

Table 8

N	S2 (m)	S5 (m)	S8 (m)	E1 (kN/m²)	E2 (kN/m²)	E3 (kN/m²)	δ_{top} (m)	δ_{-3m} (m)
0	0.448	0.553	0.383	62.0	70.0	50.0	0.12	0.05
22	0.518	0.621	0.424	00.0	68.0	41.0	0.21	0.09
89	0.698	0.806	0.557	19.0	92.0	50.0	0.35	0.12
203	0.825	0.924	0.637	05.0	100.0	42.0	0.45	0.14
286	0.886	0.977	0.659	01.0	82.0	32.0	0.46	–

N IS NUMBER OF DAYS AFTER CONSTRUCTION

δ IS LATERAL MOVEMENT AT TOP OF WALL AND AT 3 m BELOW GROUND LEVEL

TABLE 9

FIELD PULLOUT TESTING

TESTED ON JULIAN DAY	DUMMY NO. (REFER FIG. NO.) 12	NO. OF TRANS-VERSE BARS	GALVA-NISED/ INSTRU-MENTED	BAR SIZES	AVERAGE LENGTH OF EMBED-MENT (Metres)	HEIGHT OF OVER-BURDEN (Metres)	PULLOUT (Cms)	MAXIMUM PULLOUT RESIST-ANCE in (Tons)	MAXIMUM AXIAL STRAINS L1% BACK	L2% MIDDLE	L3% FRONT
WEATHERED CLAY											
362	26	5	G-I	W7 XW4.5	2.046	0.60	12.550	3.839	0.036	0.094	0.166
9	22	5	G-I	W4.5XW3.5	2.043	2.35	13.230	6.015	0.080	0.258	0.337
2	17	6	B-NI	W12 X W5	2.116	3.27	13.820	7.806	-	-	-
4	13	0	G-NI	W4.5=4Nos	2.047	3.80	12.530	2.389	-	-	-
3	8	5	G-NI	W7 XW4.5	2.041	3.93	13.600	6.428	-	-	-
LATERITE											
12	23	5	B-NI	W12 X W5	2.117	1.50	13.670	10.883	-	-	-
10	21	5	G-I	W4.5XW3.5	2.035	2.40	14.750	5.713	Strains recorded not good		
11	15	6	G-I	W7 XW4.5	2.037	3.33	14.430	4.055	0.007	0.086	0.094
5	12	5	B-NI	W12 X W5	2.046	3.80	12.600	5.482	-	-	-
6	11	0	G-NI	W4.5=4Nos	2.045	3.80	12.670	2.537	-	-	-
CLAYEY SAND											
354	24	5	G-I	W7 XW4.5	2.091 2.086	0.60	3.625 4.600	* 2.366‡	not realistic-due to slippage		
356	20	5	G-I	W4.5XW3.5	2.085 2.078	2.40	4.730 6.150	5.650‡ 7.382@	0.069 0.102	0.163 0.216	0.242 0.510
8	10	0	G-NI	W4.5=4Nos	2.045	3.75	12.700	2.466	-	-	-
360	9	5	B-NI	W12 X W5	2.046	3.80	12.600	9.400	-	-	-
359	7	5	G-NI	W7 XW4.5	2.045	4.23	12.750	10.352	-	-	-

Note : All mats except 10,11,13 are of 6"X9" mesh size

* no peak
‡ not peak value
@ tension failure

TABLE 10 FIELD AND LABORATORY PULLOUT TEST RESULTS
(Clayey Sand Backfill)

Details	DUMMY MAT NOS. (REFER TO FIG.12)				
	24	20	10	9	7
Mat Size (LXT)	W7XW4.5	W4.5XW3.5	W4.5XW3.5	W12XW5	W7 XW4.5
Mesh Size	6"X9"	6"X9"	6"X9"	6"X9"	6"X9"
M X N	4 X 5	4 X 5	4 X 0	4 X 5	4 X 5
Overburden (m)	0.50	2.40	3.75	3.80	4.23
Pullout (mms)	46.0	61.5	127.0	126.0	127.5
Embedment (m)	2.086	2.078	2.045	2.046	2.045
Pt-field (KN)	23.66*	73.82#	24.66	94.0	103.5
Pt-Lab (KN)	31.90	50.4	20.9	69.6	67.2

(LXT)=Longitudinal X Transverse; Pt is Total Pullout Force;
M is Number of Longitudinal Bars & N is Number of Transverse bars
* indicates not a peak value
# indicates tension failure at grips

TABLE 11 FIELD AND LABORATORY PULLOUT TEST RESULTS
(Lateritic Backfill Soil)

Details	DUMMY MAT NOS. (REFER TO FIG.12)				
	23	21	15	12	11
Mat Size (LXT)	W12XW5	W4.5XW3.5	W7XW4.5	W12XW5	W4.5XW3.5
Mesh Size	6"X9"	6"X9"	6"X9"	6"X9"	6"X9"
M X N	4 X 5	4 X 5	4 X 6	4 X 5	4 X 0
Overburden (m)	1.50	2.40	3 33	3.80	3.80
Pullout (mms)	136.7	147.5	144.[illegible]	126.0	126.7
Embedment (m)	2.117	2.035	2.037	2.046	2.045
Pt-field (KN)	108.83	57.13	40.55	54.82	25.37
Pt-Lab (KN)	95.60	81.50	102.20	133.30	56.20

TABLE 12 FIELD AND LABORATORY PULLOUT TEST RESULTS
(Weathered Clay Backfill)

Details	DUMMY MAT NOS. (REFER TO FIG.12)				
	26	22	17	13	8
Mat Size (LXT)	W7XW4.5	W4.5XW3.5	W12XW5	W4.5XW3.5	W7 XW4.5
Mesh Size	6"X9"	6"X9"	6"X9"	6"X9"	6"X9"
M X N	4 X 5	4 X 5	4 X 6	4 X 0	4 X 5
Overburden (m)	0.60	2.35	3.2	3.80	3.93
Pullout (mms)	125.5	132.3	138.2	125.3	136.0
Embedment (m)	2.046	2.043	2.116	2.047	2.041
Pt-field (KN)	38.39	60.15	78.06	23.89	64.28
Pt-Lab (KN)	43.40	46.40	63.30	15.70	57.11

TABLE 13

Parameter	Symbol	Clayey Sand	Lateritic Soil	Weathered Clay
Unit Weight (kN/m³)	γ	19.2	20.3	18.8
K_o Value	K_o	0.59	0.57	0.56
Cohesion (kPa)	C	42.0	80.0	118.0
Friction Angle (deg.)	ϕ	23.5	32.5	31.5
Modulus Number	K	360	1400	630
Modulus Exponent	n	0.31	0.34	0.15
Failure Ratio	R_f	0.96	0.96	0.84
Poisson's Ratio	ν	0.36	0.36	0.36

TABLE 14 SOIL PARAMETERS USED IN FINITE ELEMENT ANALYSIS OF THE WELDED-WIRE WALL (REA)

PARAMETER	SYMBOL	SOFT CLAY SUBSOIL	WEATHERED CLAY SUBSOIL	LATERITI SOIL BACKFILL
(1) Unit Weight (T/m^3)	γ	1.50	1.60	2.00
(2) Cohesion (T/m^2)	C	0.49	1.10	5.08
(3) Angle of Internal Friction (Degrees)	ϕ	13.50	20.00	38.50
(4) Primary Loading Modulus Number	K	60	70	1600
(5) Modulus Exponent	n	2.50	-0.40	0.35
(6) Failure Ratio	R_f	0.92	0.82	0.96
(7) Bulk Modulus in PSI	B	150	650	26000

1 T/m^2 = 10 kPa = 1.42 PSI & 1 T/m^3 = 10 kN/m^3

TABLE 15 BENDING ELEMENT PROPERTIES USED IN THE FINITE ELEMENT ANALYSIS OF THE WALL (REA)

BENDING ELEMENT TYPE NO.	ELASTIC MODULUS (PSI)	PLASTIC MODULUS (PSI)	YIELD POINT (PSI)	ULTIMATE STRAIN	AREA PER UNIT WIDTH (IN^2/IN	MOMENT OF INERTIA PER UNIT WIDTH (IN^4/IN)	BOND SPRING COEFF.	FRICTION COEFF.
1	30×10^6	200,000	60,000	0.025	0.0075	2.67E-05	0.652	2.71
2	30×10^6	200,000	60,000	0.025	0.0075	2.67E-05	0.652	2.96
3	30×10^6	200,000	60,000	0.025	0.0075	2.67E-05	0.652	3.44
4	30×10^6	200,000	60,000	0.025	0.0075	2.67E-05	0.652	4.63
5	30×10^6	200,000	60,000	0.025	0.0075	2.67E-05	0.652	7.40
6	30×10^6	200,000	60,000	0.025	0.0075	2.67E-05	0.652	12.94
7	30×10^6	200,000	60,000	0.025	0.026	6.24E-04	-	-

FOR BENDING ELEMENT 7, BOUNDARY SPRING COEFFICIENT = 242,000 LBS/IN/IN^2/ (WELDED-WIRE WALL FACING)
BENDING ELEMENT TYPE[1] FOR MAT NOS.8,1,2; TYPE[2] FOR 9,3,10; TYPE[3] FOR 4,11,5; TYPE[4] FOR 12,6,13;
TYPE[5] FOR MAT NO.7; TYPE[6] FOR MAT NO.14
(FOR MAT NOS. REFER TO FIG.12)

NOTE: 1 T/m^2 = 1.42 PSI = 10 kPa & 1 inch = 25.4 mm

FIGURES

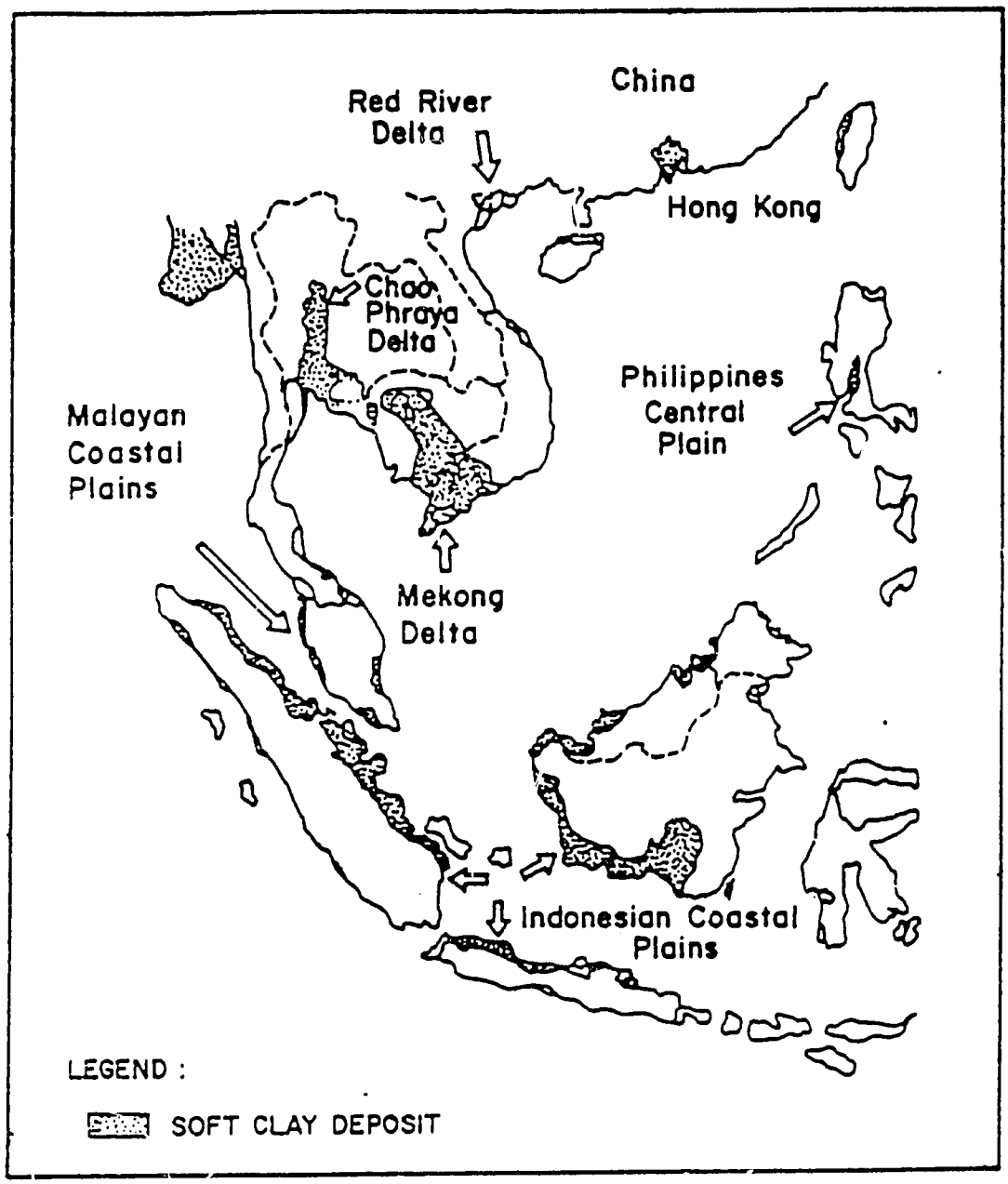

Fig.1 The Distribution of Recent Marine Clays in Southeast Asian Region

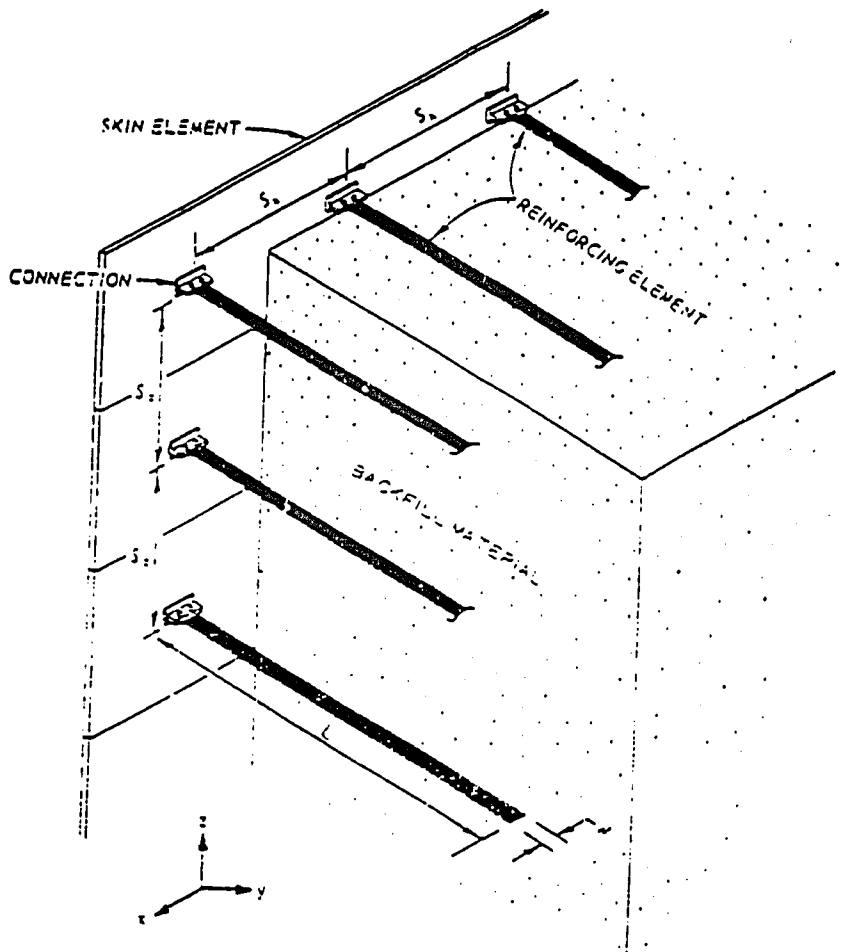

Fig.2 Vidalean Concept of Reinforced Earth (After AL HUSSAINI & JOHNSON, 1978)

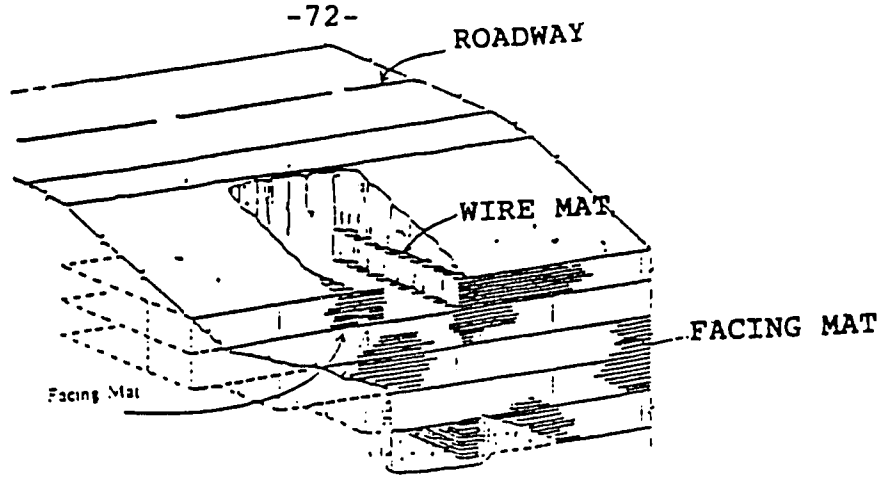

After PETERSON & ANDERSON, 1980

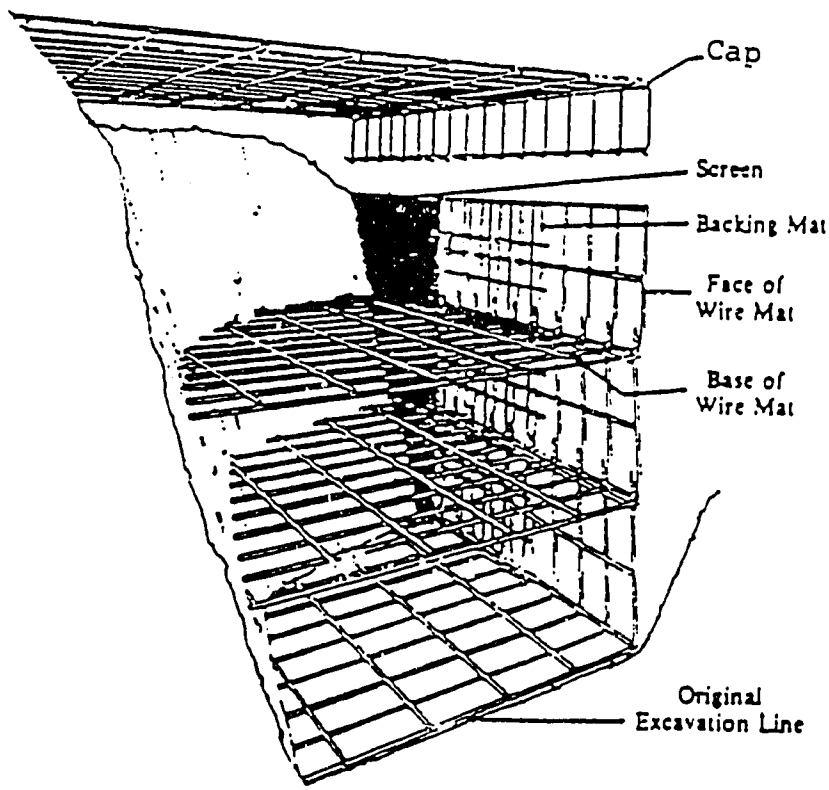

After DIMAGGIO, 1988

Fig. 3 Schematic Drawing of Welded Wire Wall Components

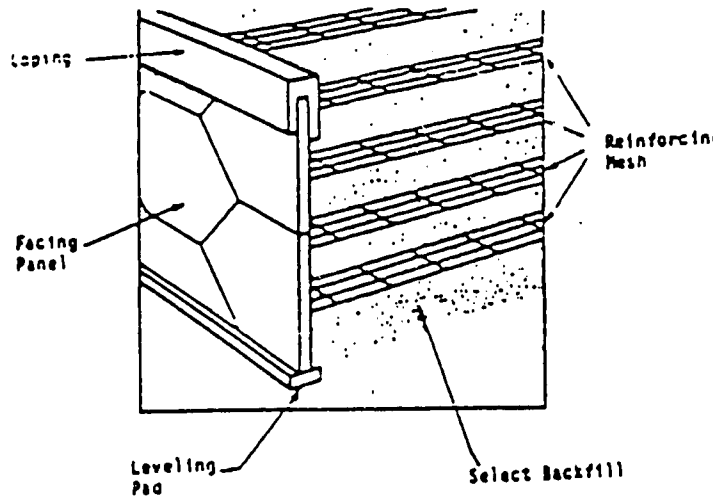

VSL's RETAINED EARTH

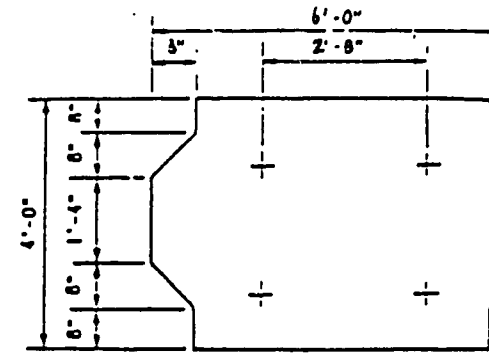

Elevation
GEOGIA STABILIZED EARTH FACING PANEL

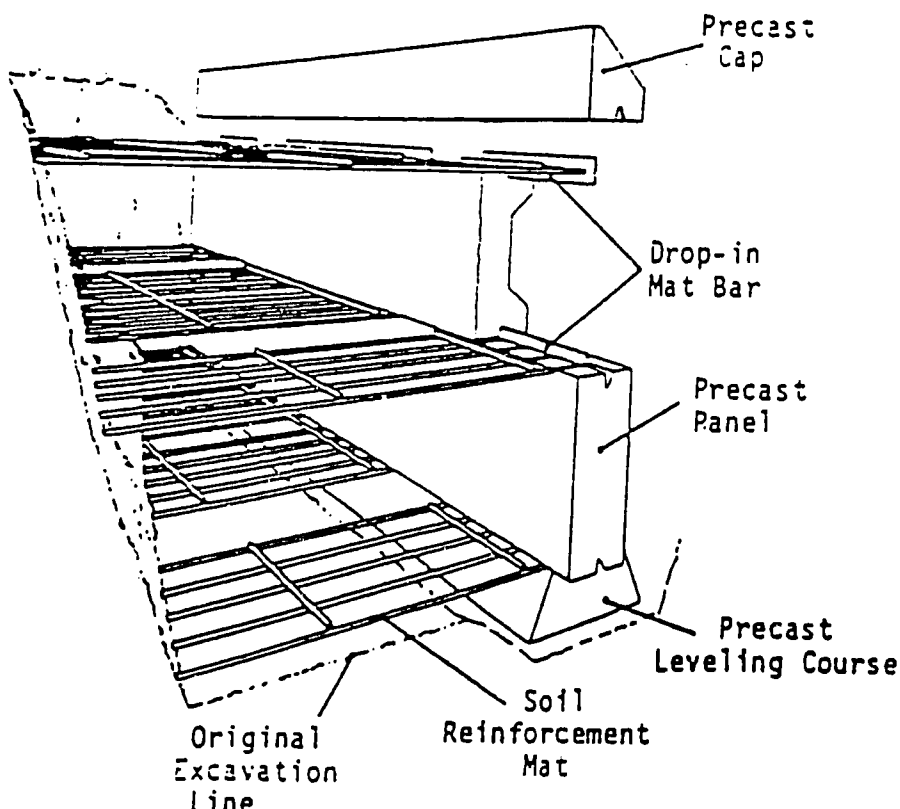

REINFORCED SOIL EMBANKMENT

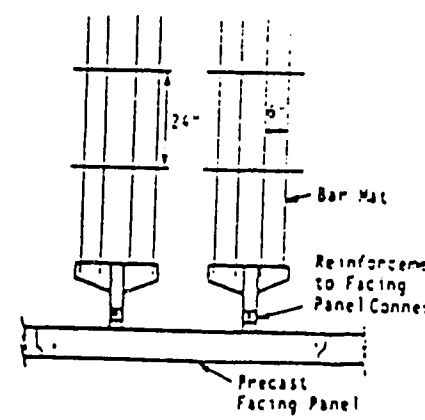

Plan
GEORGIA STABILIZED EARTH (GASE) MESH & CONNECTION TO FACING

Fig. 4 Various Reinforced Soil Systems

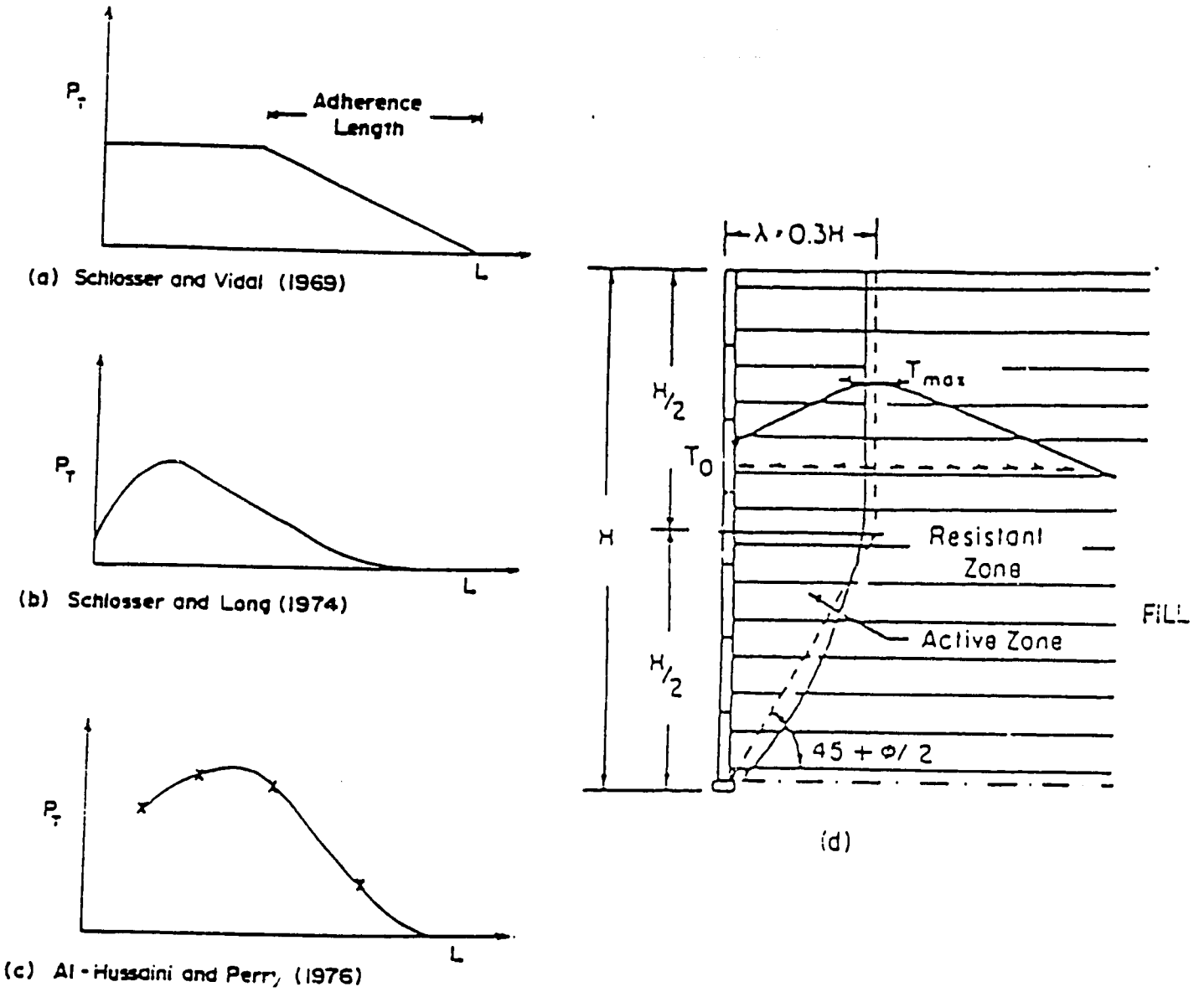

Fig. 5 Distribution of Traction Forces on the Reinforcements

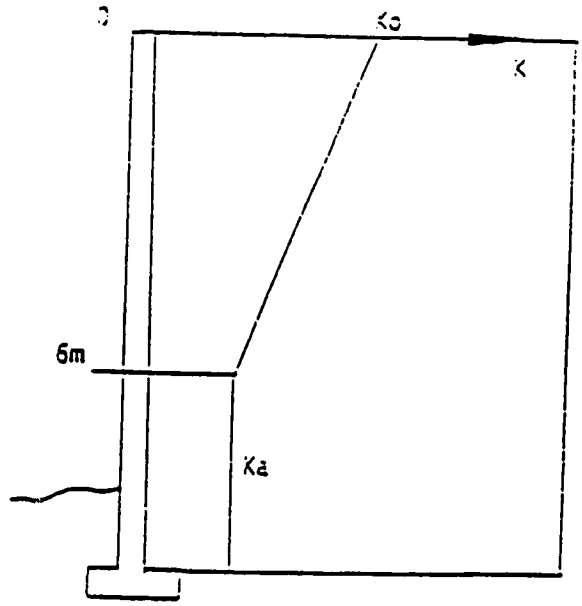

Fig. 6 Variations of Coefficients of Lateral Earth Pressures in Reinforced Earth Walls (After MCKITTRICK, 1978)

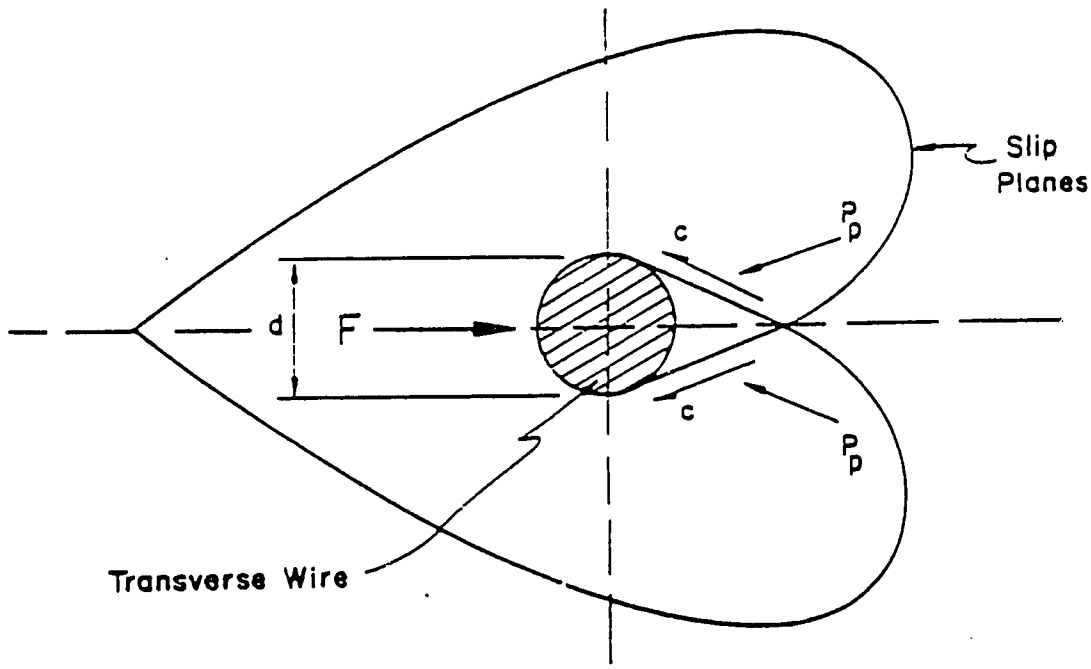

$$N_q = e^{(\pi \tan \phi)} \tan^2 (45 + \phi/2)$$

Bearing Capacity Failure (After Peterson & Anderson, 1980)

Fig. 7 Suggested Failure Planes During Pullout (After PETERSON & ANDERSON, 1980)

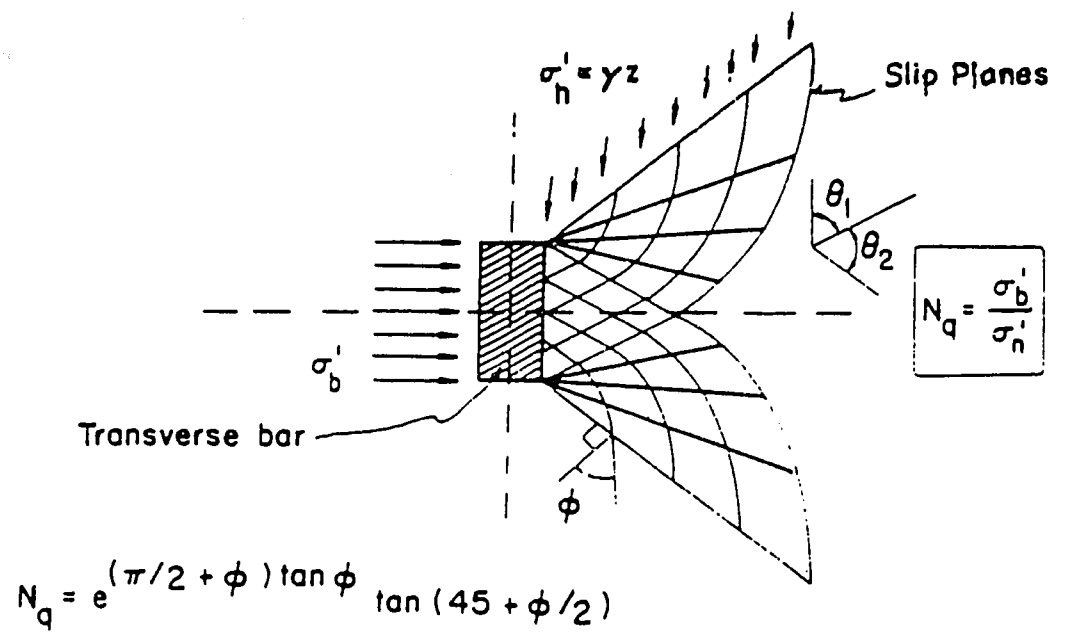

Punching Shear Failure (After Jewell et al, 1984)

Fig. 8 Punching Shear Failure Mechanism (After JEWELL et al. 1984)

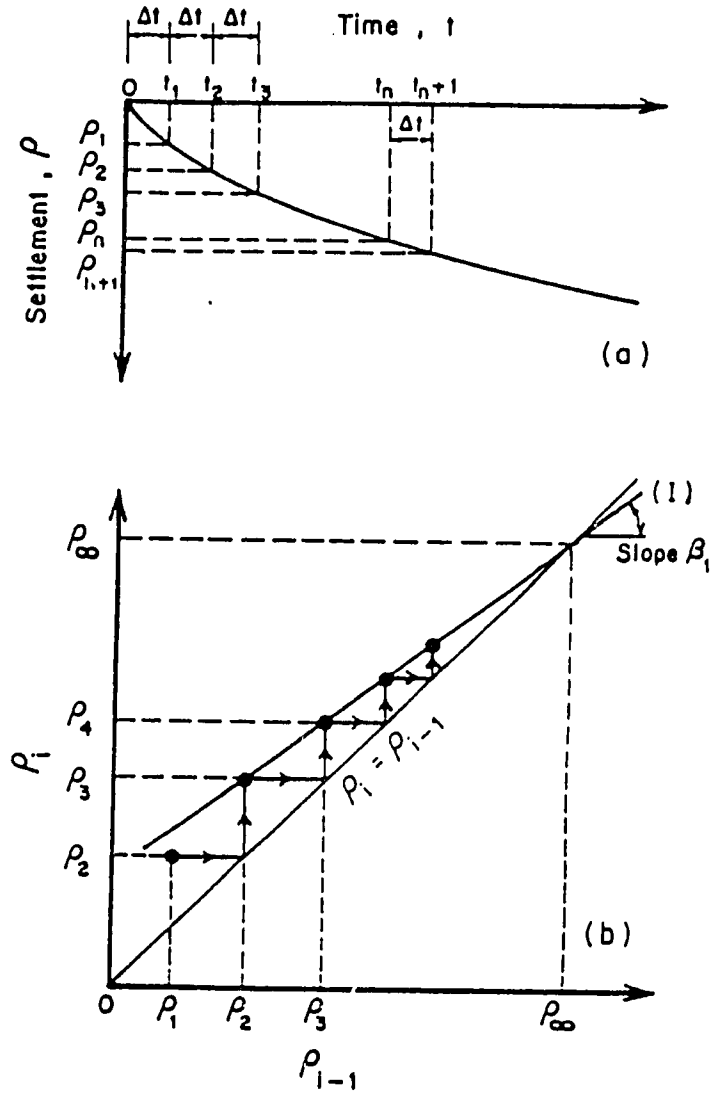

Fig. 9 Steps For the Use of ASAOKA's Method: (a) Partition of Settlement Record into Equal Time Intervals, (b) Plot of Settlement Values and Fitting of Straight Line (After MAGNAN & DEROY, 1980)

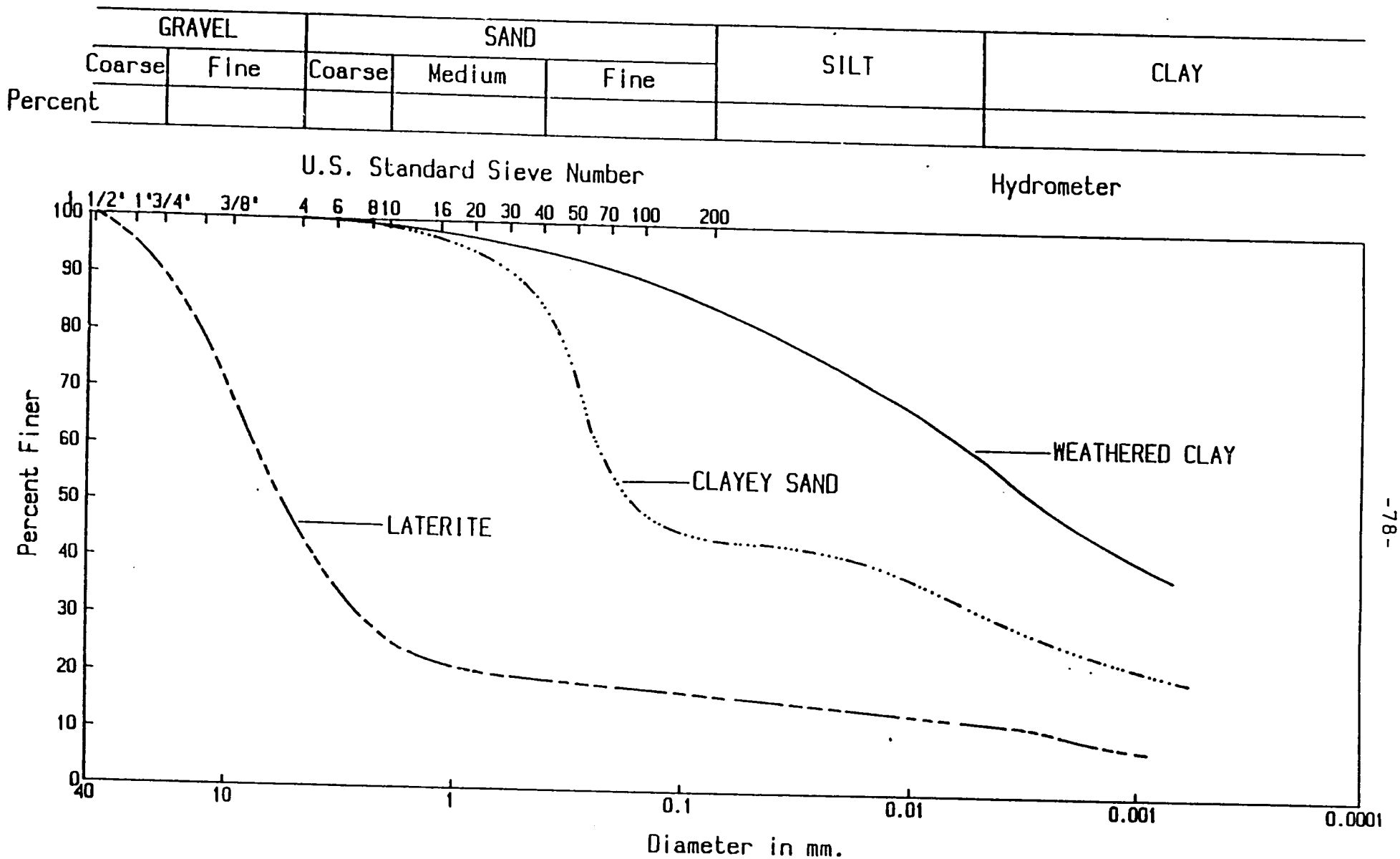

Fig.10 Grain Size Distribution Curves of the three Backfill Soils used from this Study

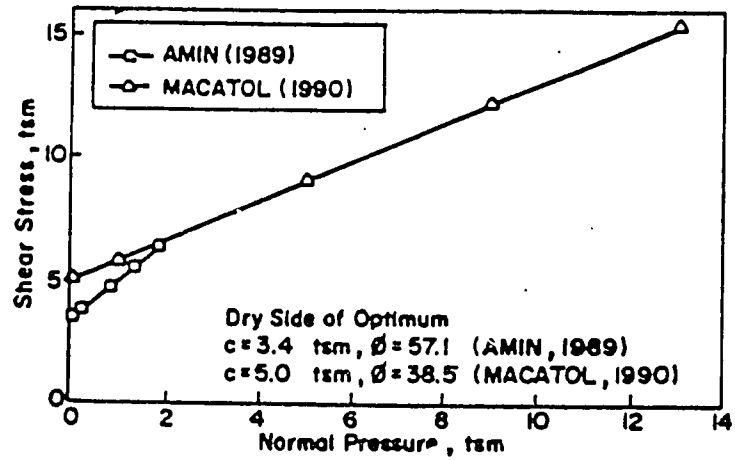

1 tsm = 10 kPa

Fig. 11a Direct Shear Test Results for Lateritic Soil (Dry of Optimum)

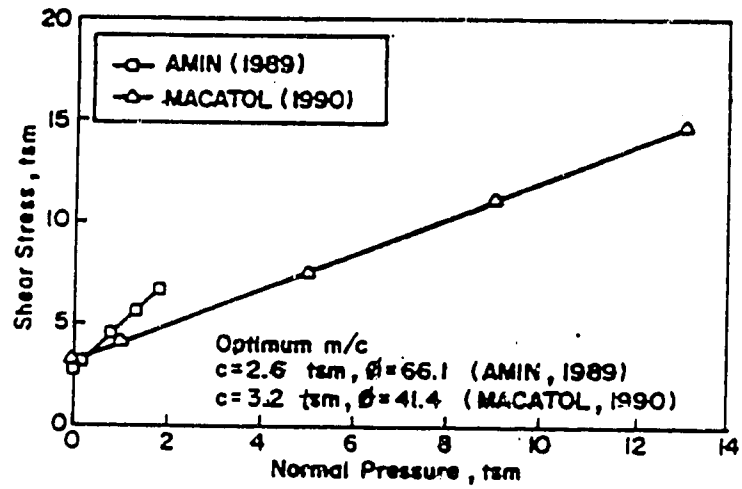

Fig. 11b Direct Shear Test Results for Lateritic Soil (at Optimum Moisture Content)

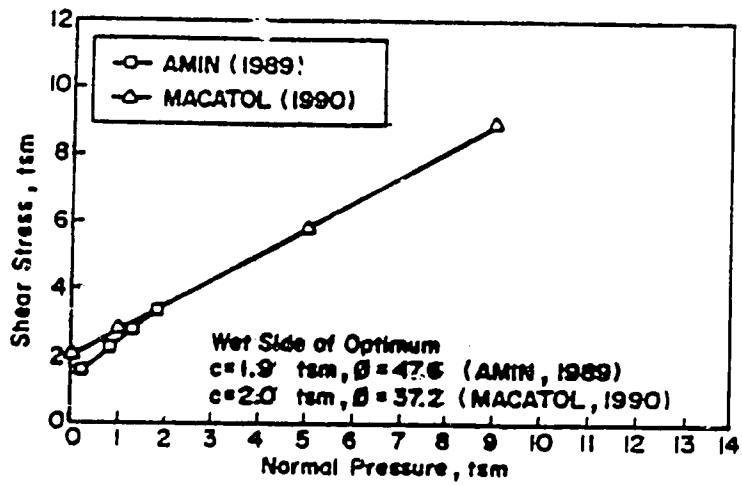

Fig. 11c Direct Shear Test Results for Lateritic Soil (Wet of Optimum)

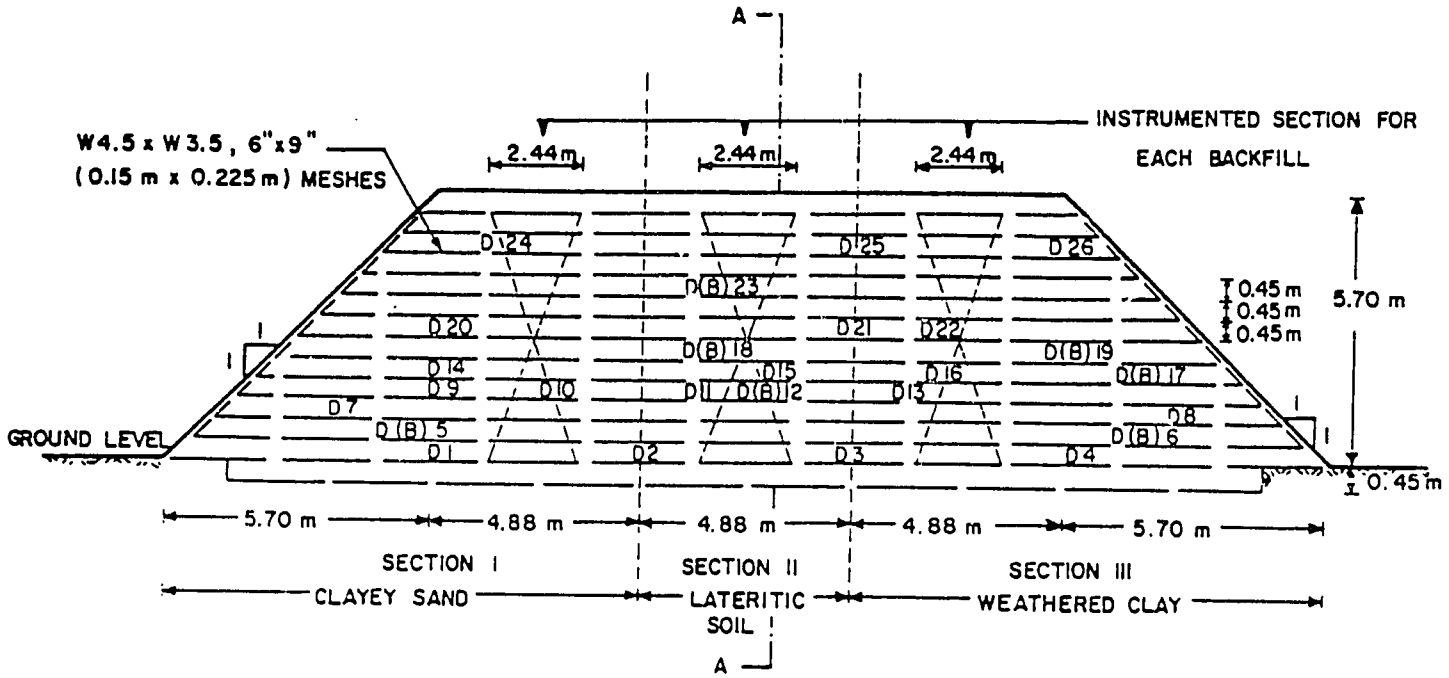

Fig.12 Front View of the Welded Wire Wall

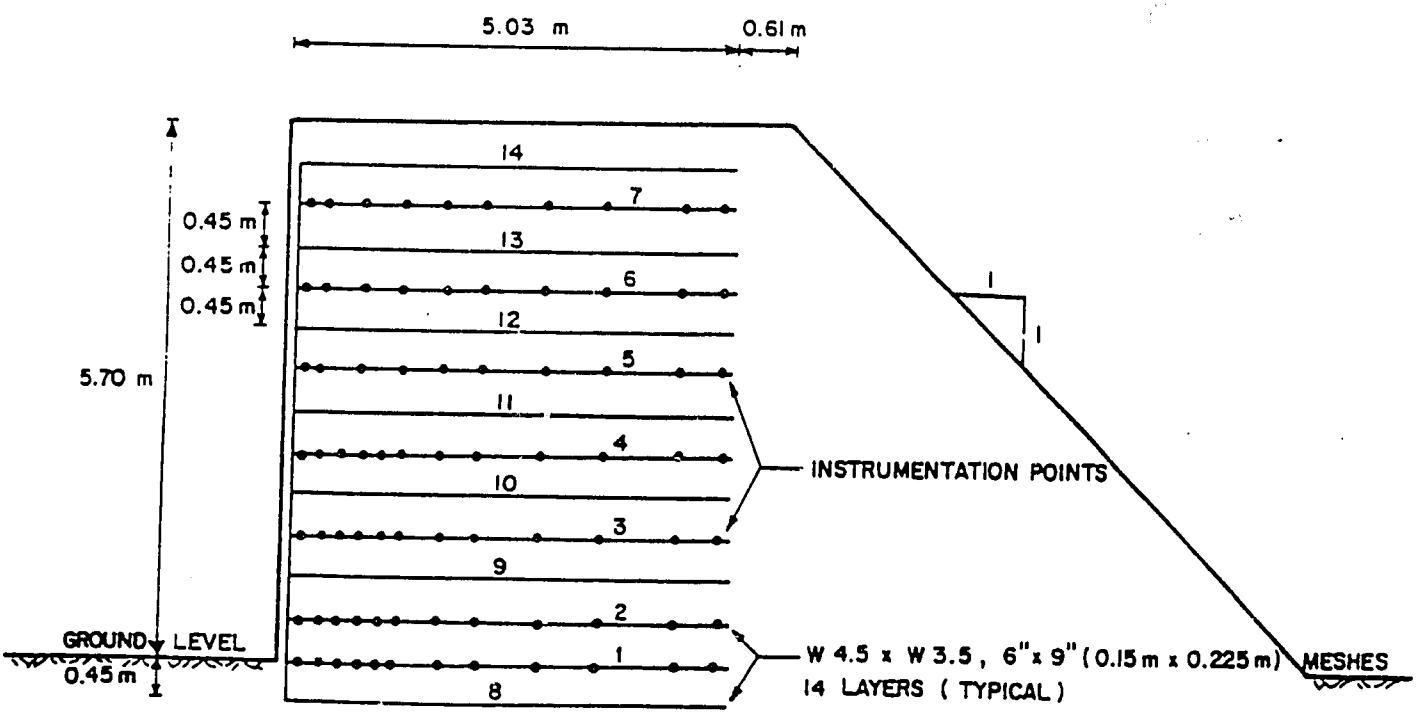

NOTE : MAT NOS. 1 TO 7 ARE INSTRUMENTED
MAT NOS. 8 TO 14 ARE NOT INSTRUMENTED

Fig.13 Typical Section View of the Wall

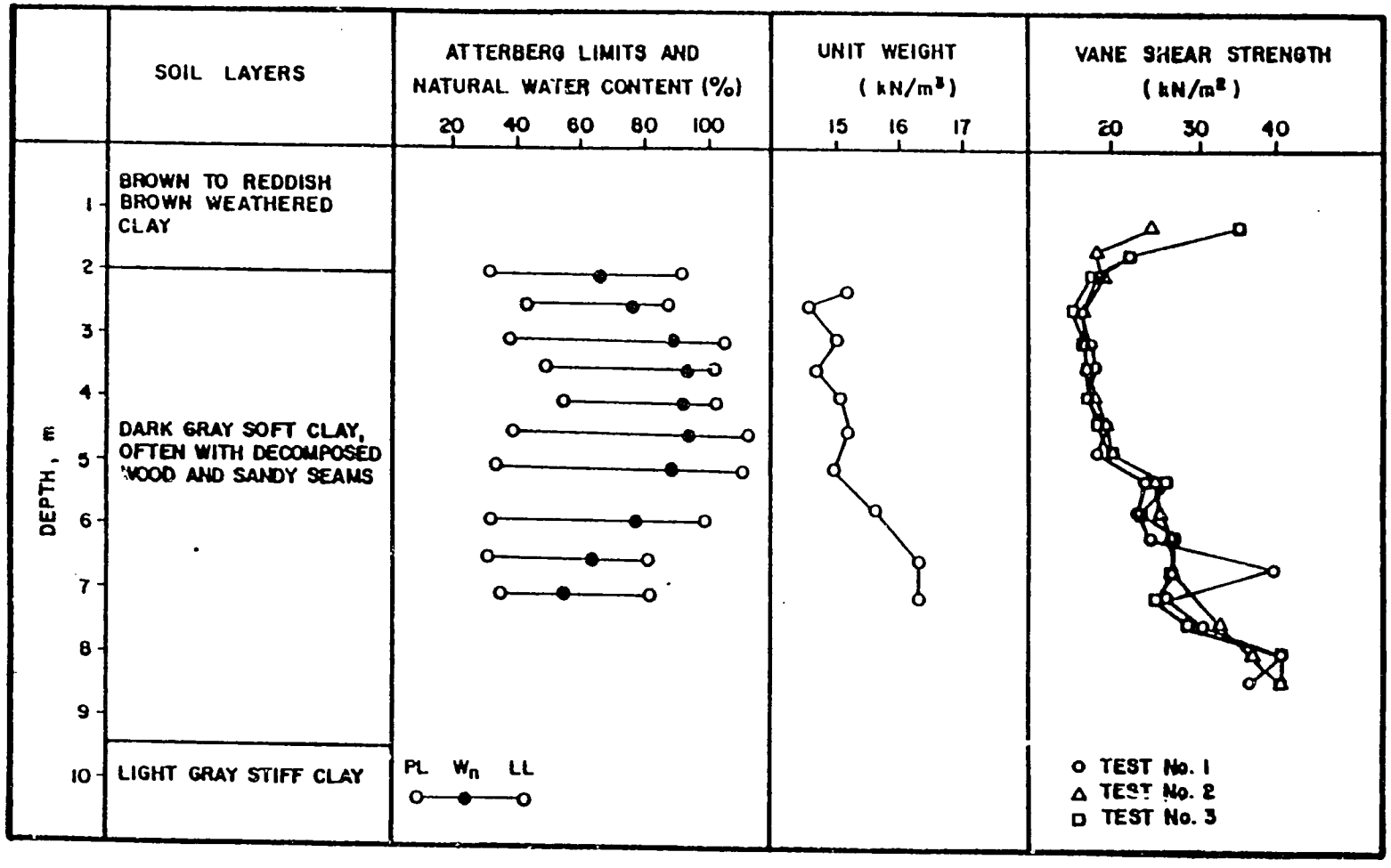

Fig. 14 Typical Geotechnical Properties of the Subsoil in the Uppermost Three Layers at the AIT Campus in Bangkok

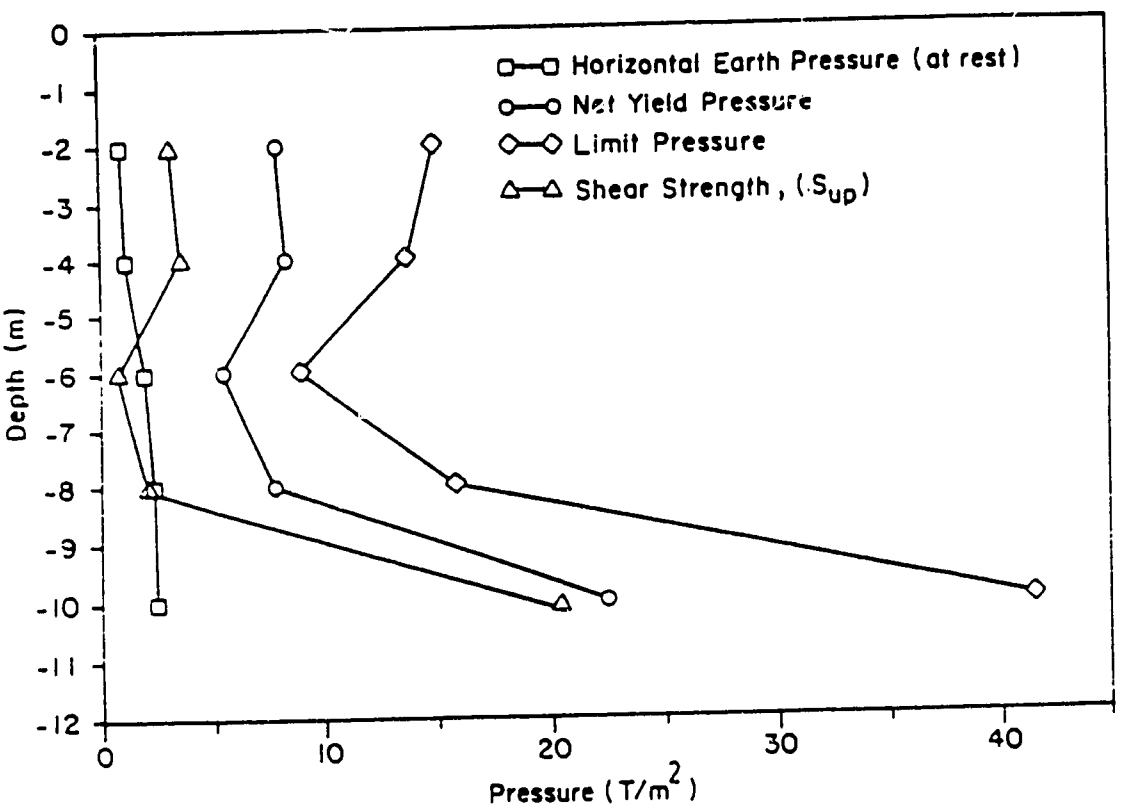

Fig.15 Results of Pressuremeter Tests

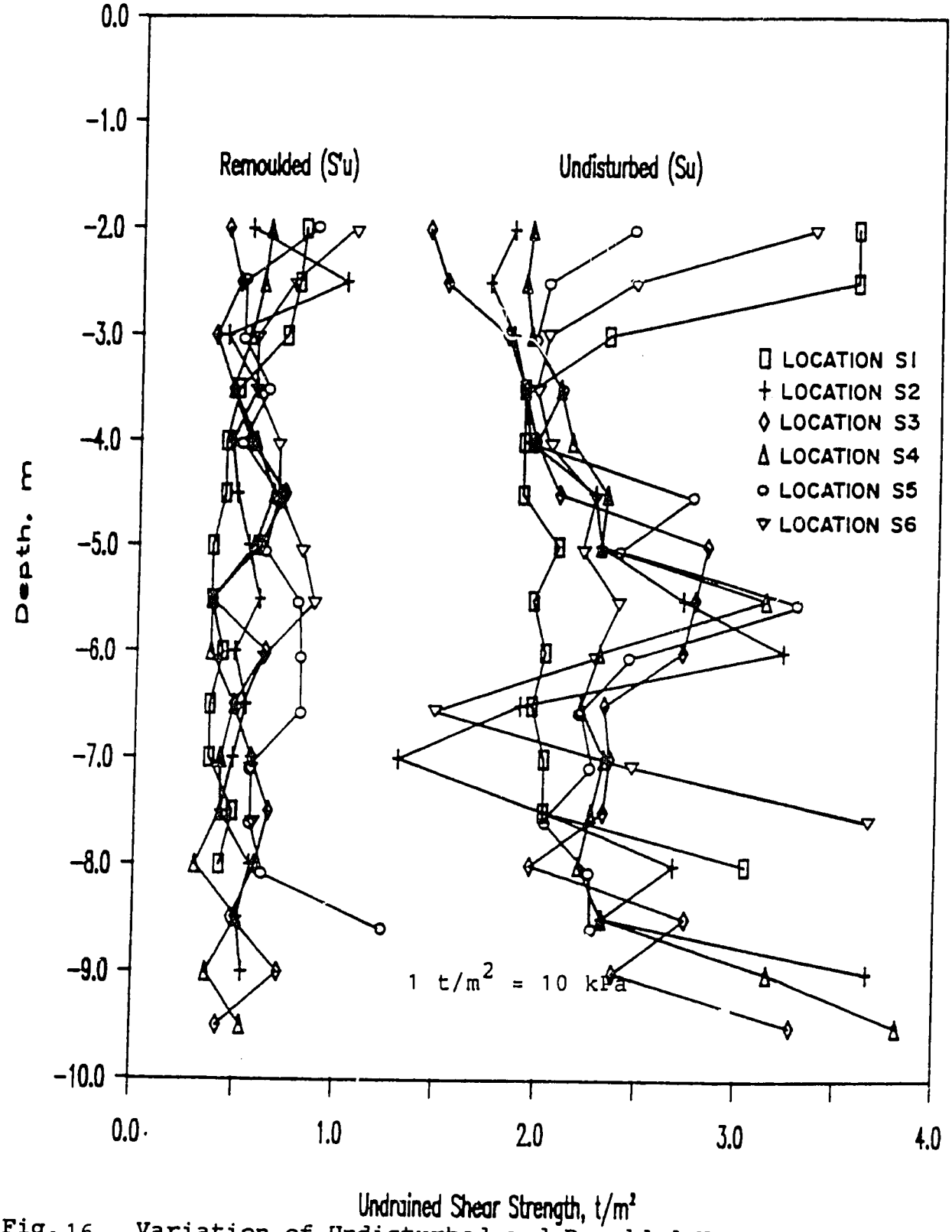

Fig. 16 Variation of Undisturbed and Remolded Vane Shear Strengths With Depth at Different Locations (Locations S1 to S6 are different points at the Site of the Welded Wire Wall, Behind the ET Building)

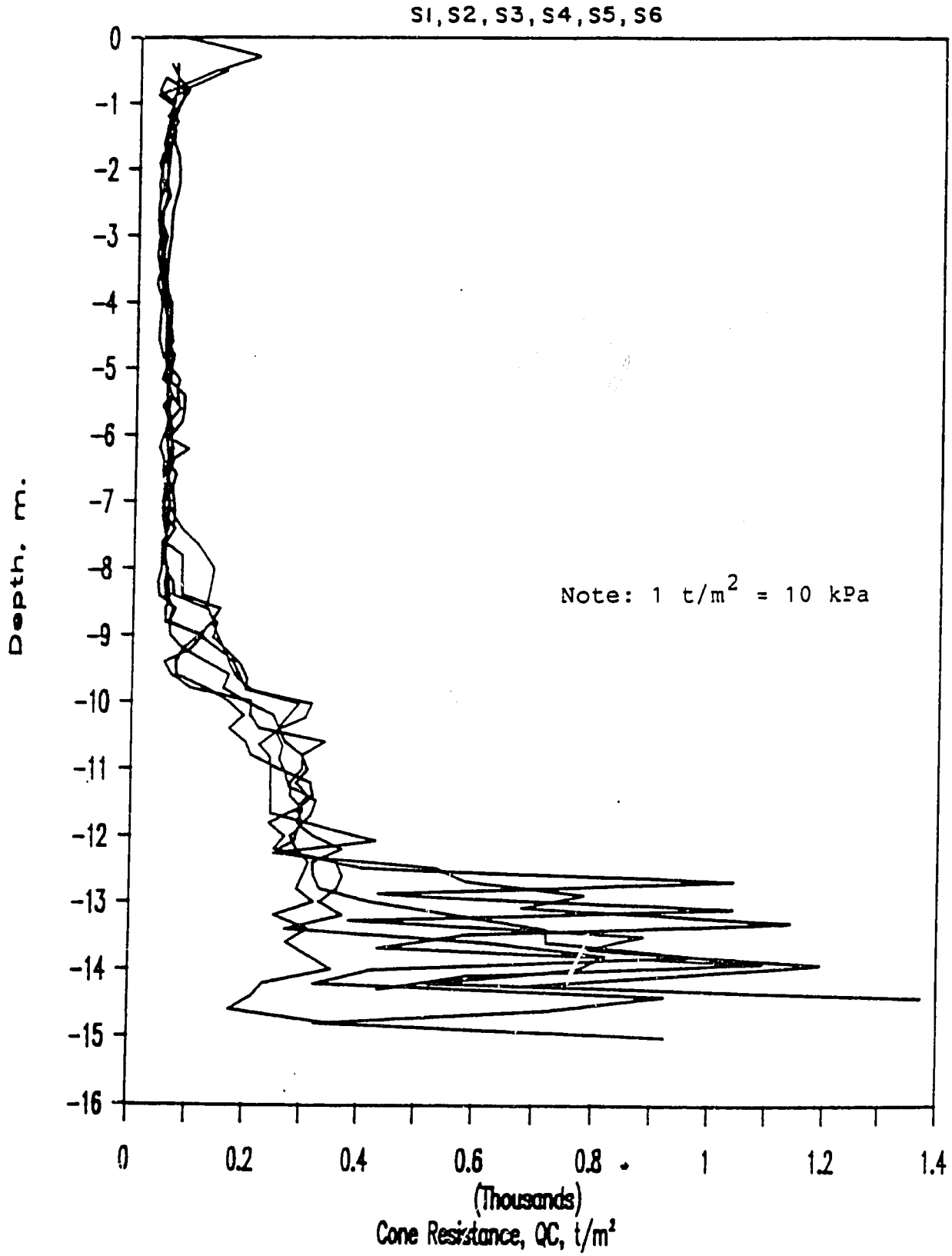

Fig. 17 Variation of Cone Resistances With Depth From Dutch Cone Tests at Different Locations

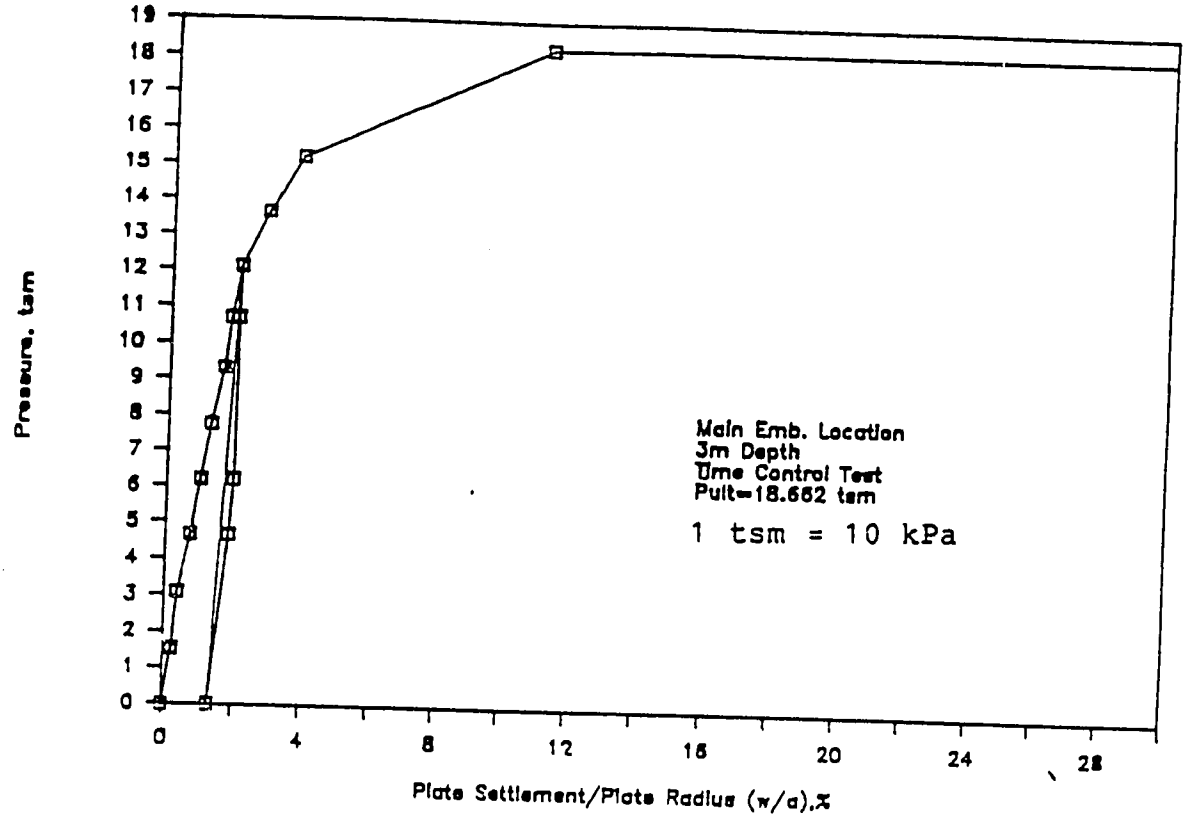

Fig.18 Screw Plate Load Test Result at 3 m Depth

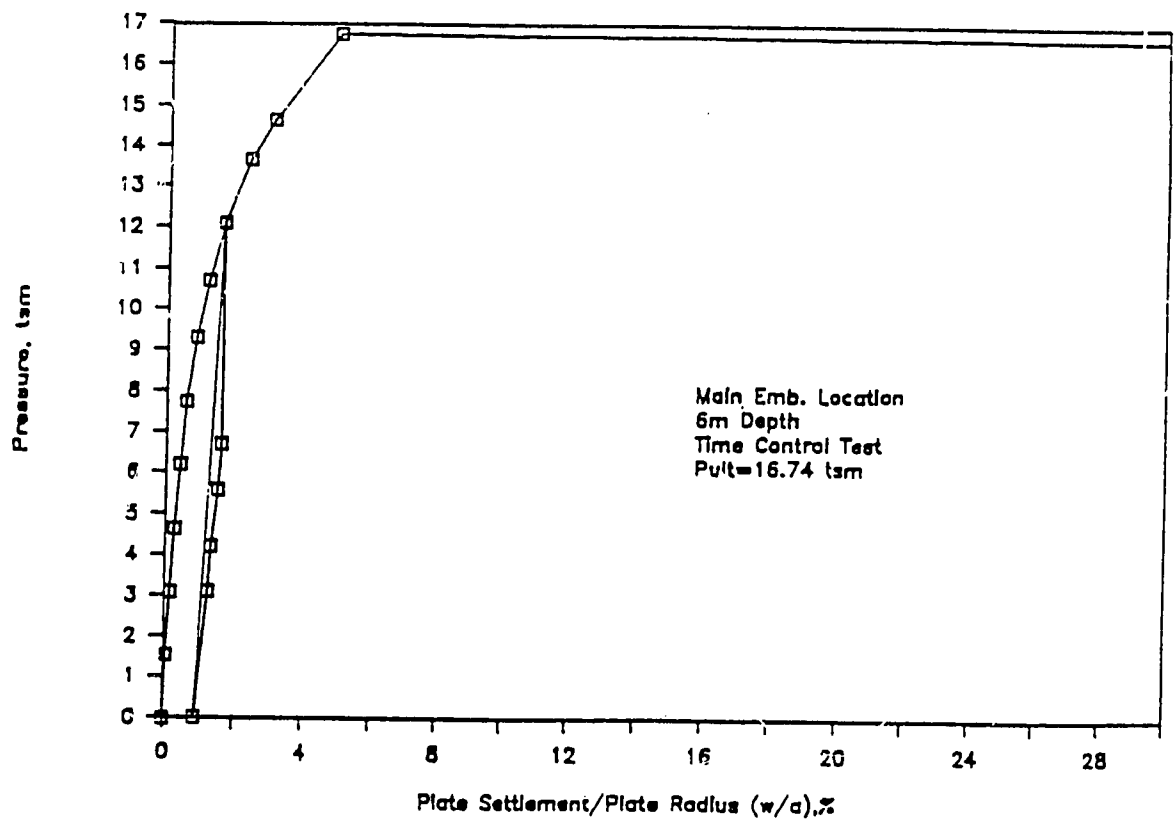

Fig. 19 Screw Plate Load Test Result at 6 m Depth

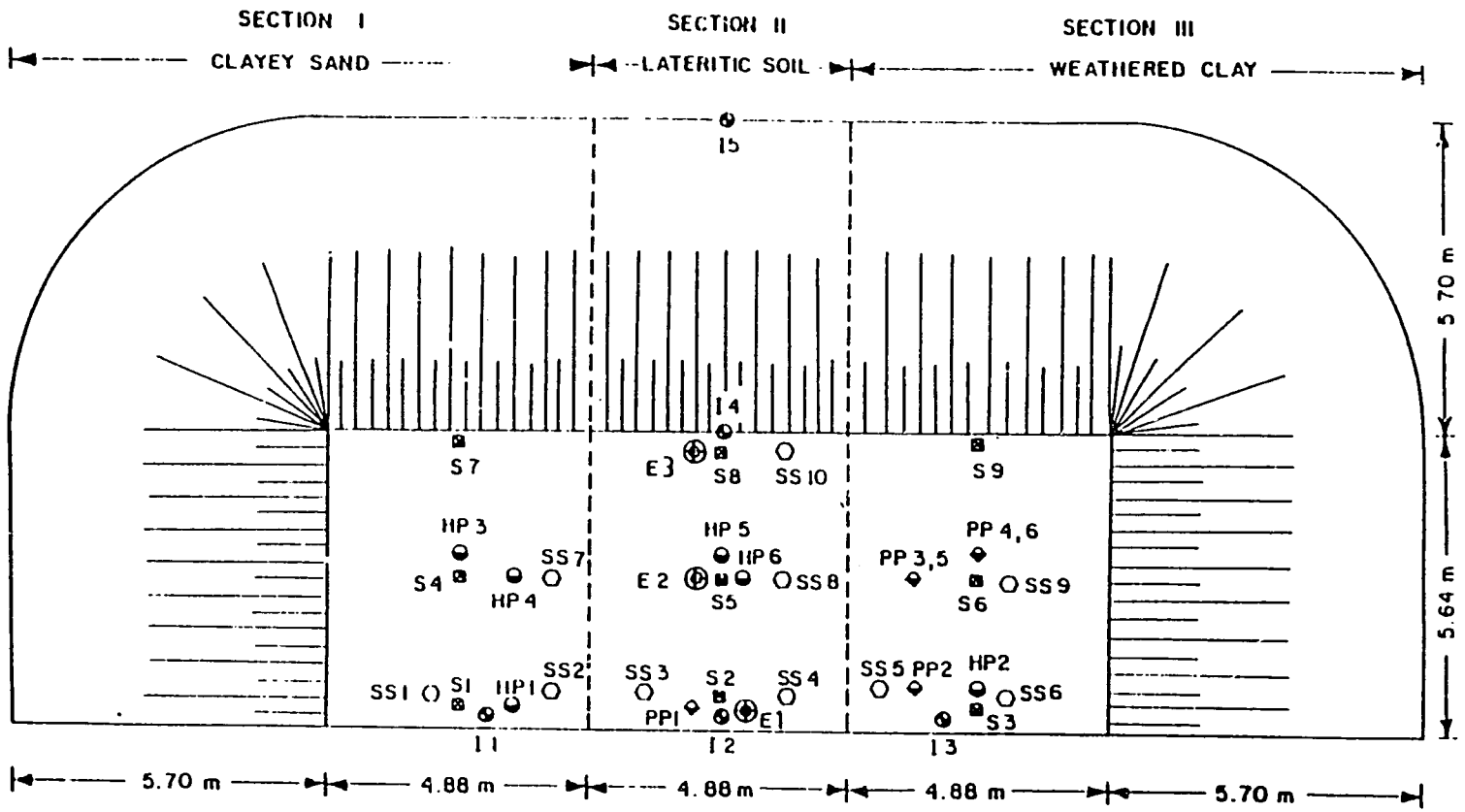

DEPTH OF INSTRUMENTATION IN METERS (BELOW GROUND SURFACE)

LEGEND	No. OF INSTRUMENTATIONS									
	1	2	3	4	5	6	7	8	9	10
■ SURFACE SETTLEMENT PLATES (S)	0.45	0.45	0.45	0.45	0.45	0.45	0.45	0.45	0.45	—
○ SUBSURFACE SETTLEMENT PLATES (SS)	5.30	3.00	6.00	3.00	6.00	3.00	3.00	3.00	6.00	3.00
⊕ INCLINOMETER CASINGS (I)*	10.85	10.85	10.25	8.50	8.50	—	—	—	—	—
● HYDRAULIC PIEZOMETERS (HP)	5.00	5.00	3.00	6.00	7.00	4.00	—	—	—	—
◆ PNEUMATIC PIEZOMETERS (PP)	5.00	2.00	3.00	6.00	(2.00)†	(4.00)†	—	—	—	—
⊕ EARTH-PRESSURE CELLS (E)	0.45	0.45	0.45	—	—	—	—	—	—	—

* UP TO TOP OF EMBANKMENT

† 5 & 6 IN EMBANKMENT

Fig.20 Schematic Plan View Layout of Field Instrumentation

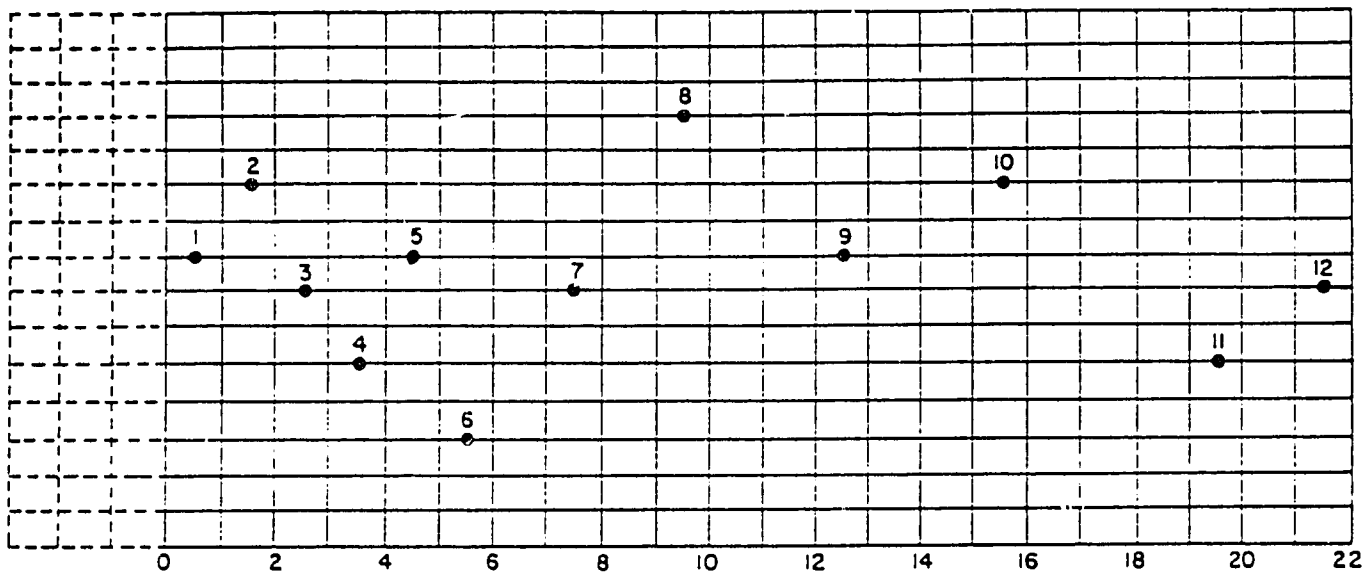

Fig.21 Location of Strain Gages Along the Welded Wire Mat For the Bottom Four Instrumented Layers

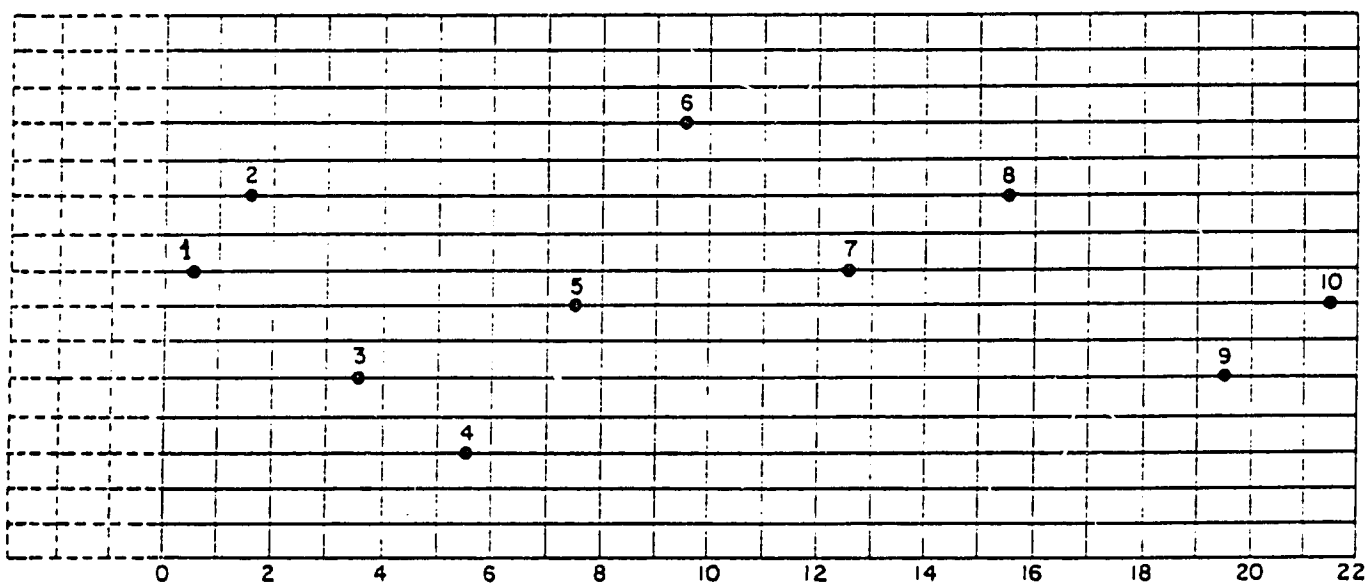

Fig.22 Strain Gage Locations Along the Welded Wire Mat For the Top Three Instrumented Mats

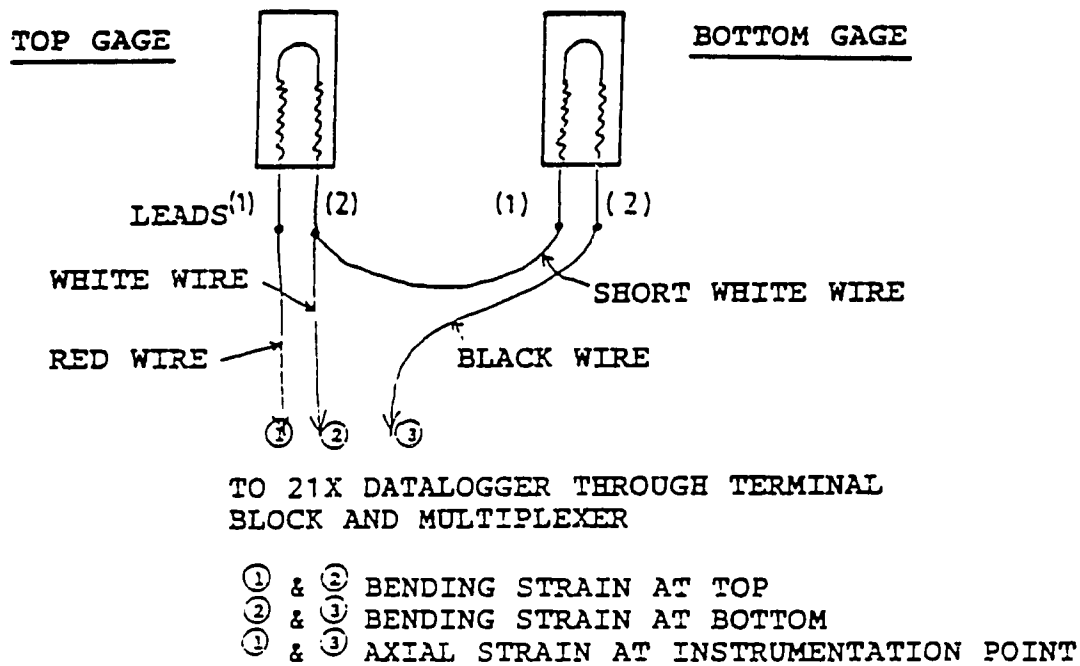

Fig. 23 Wiring System of the Two Strain Gages at Each Instrumentation Point

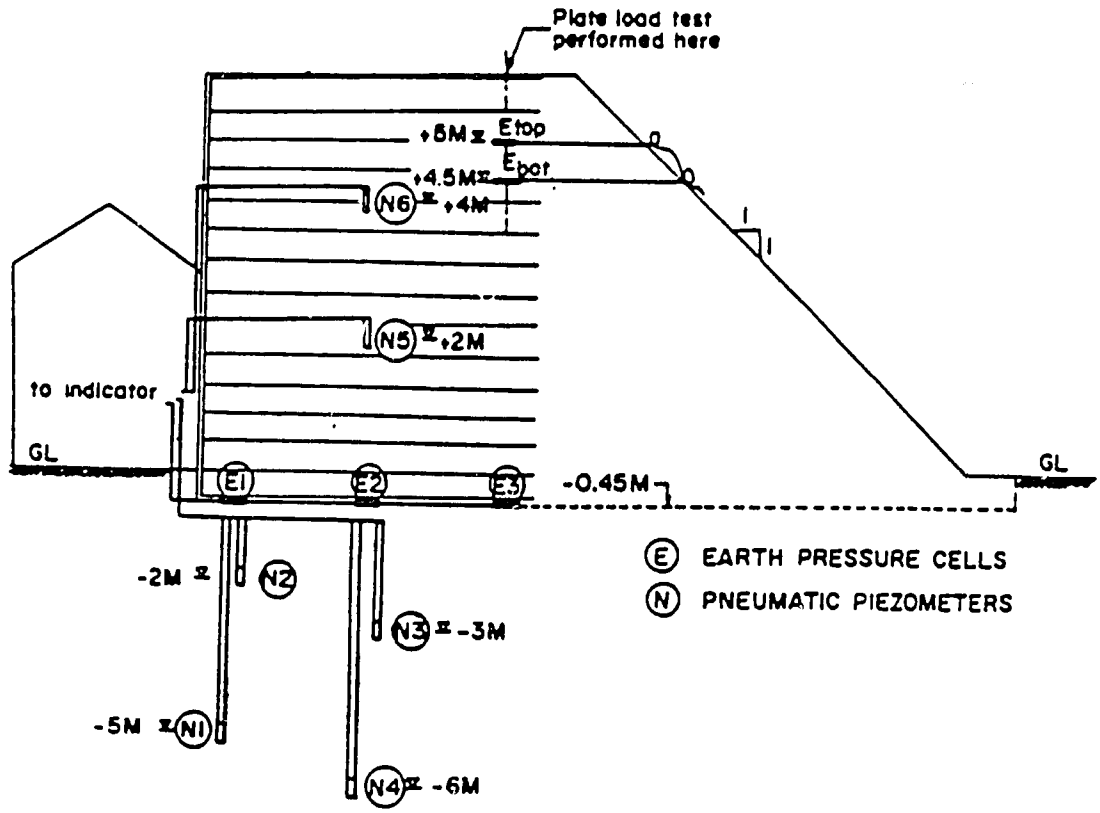

Fig. 24 Cross Section View of the Wall Showing Locations of Pneumatic Piezometers and Earth Pressure Cells

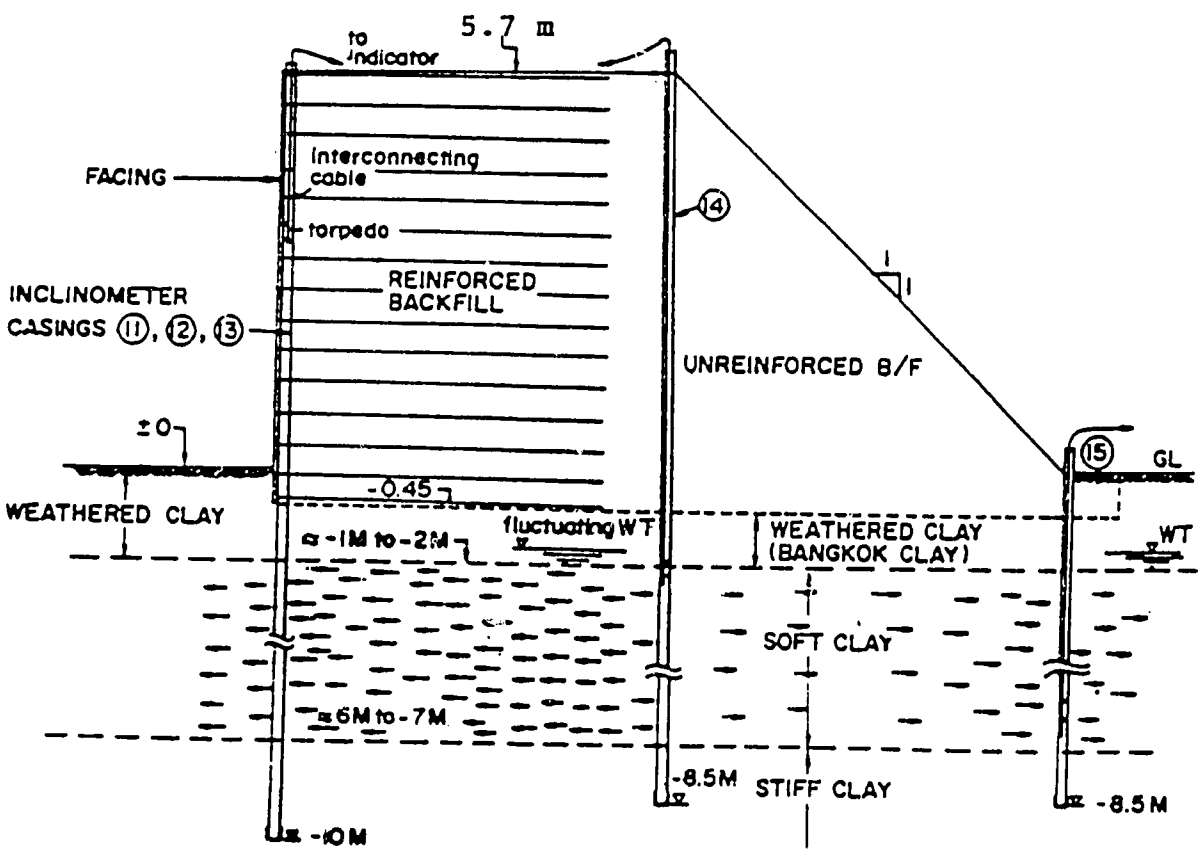

Fig. 25 Cross Section View of the Wall Showing Locations of Slope Indicators or Inclinometers

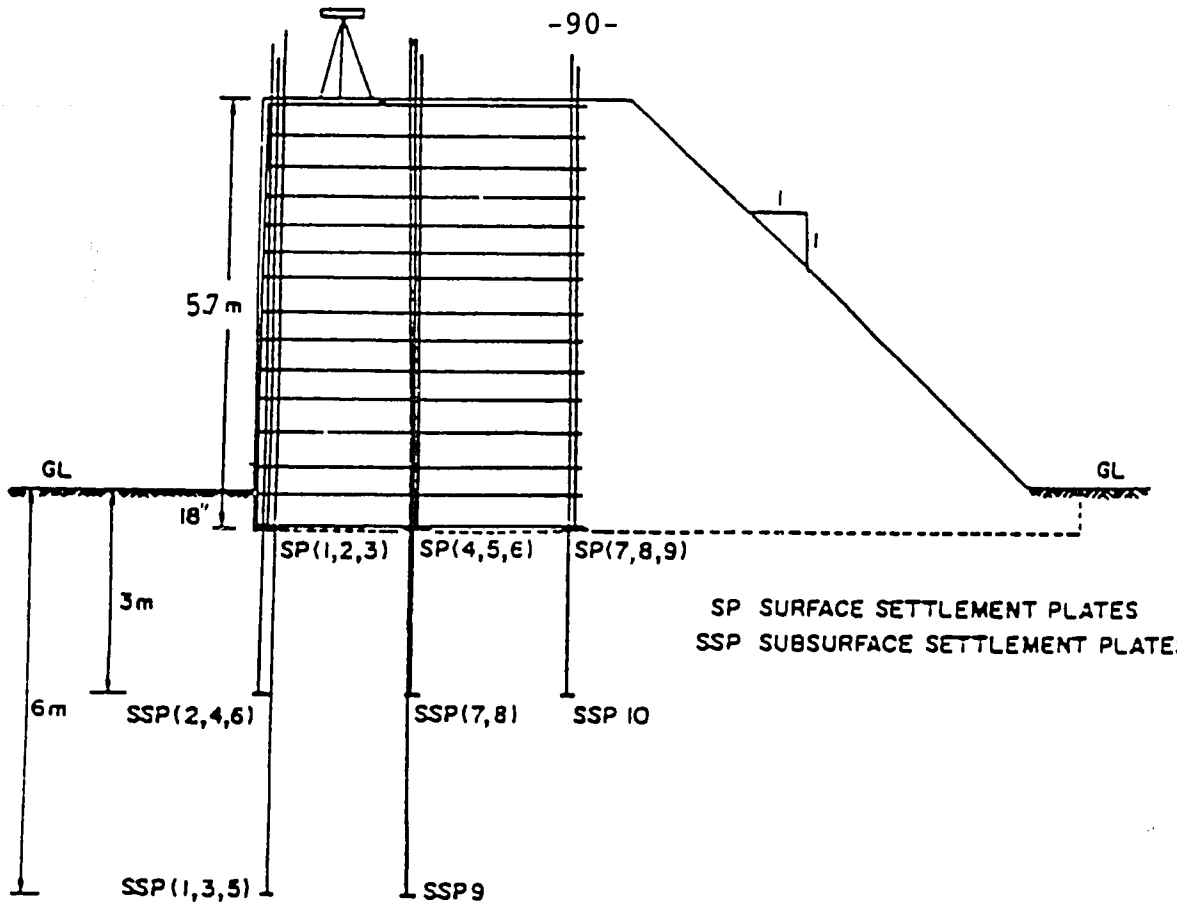

Fig. 26 Location of Settlement Points

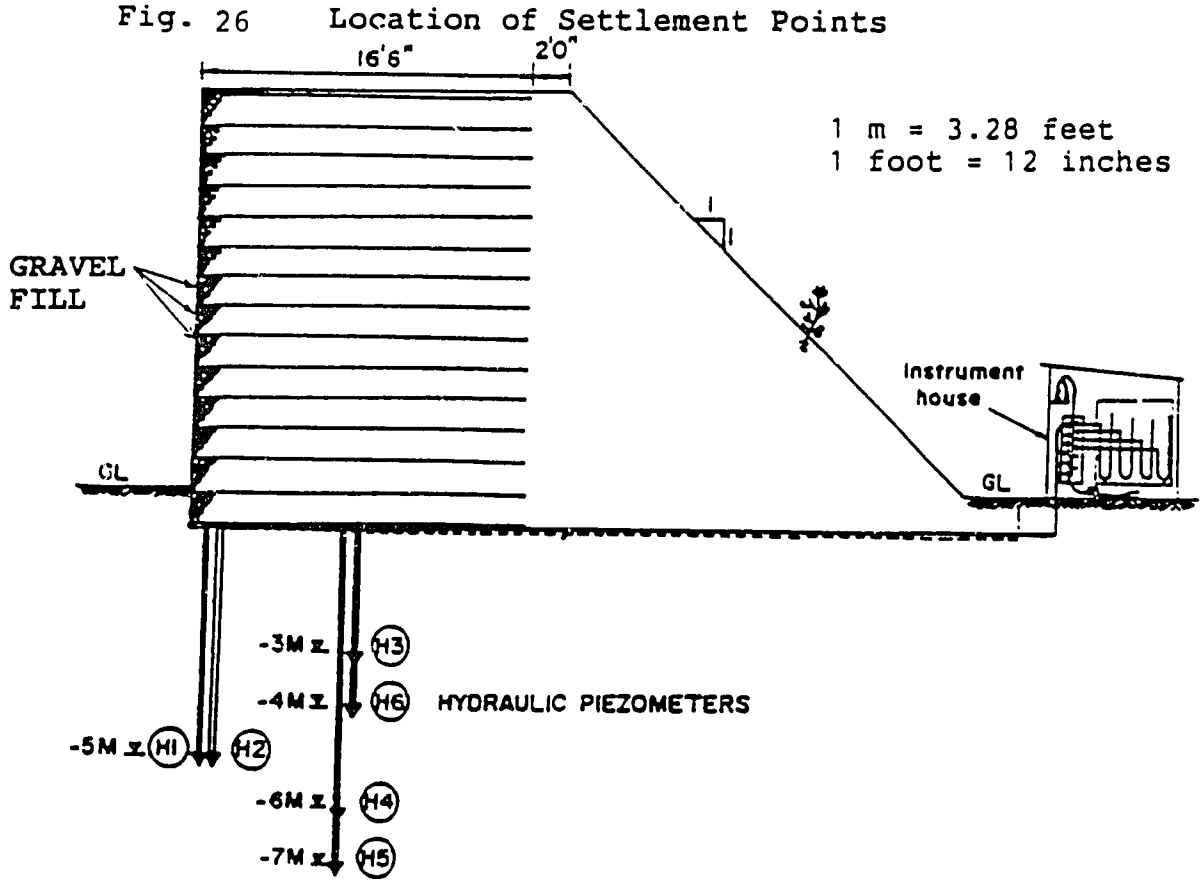

Fig. 27 Cross Section View of the Wall Showing Locations of Hydraulic Piezometers

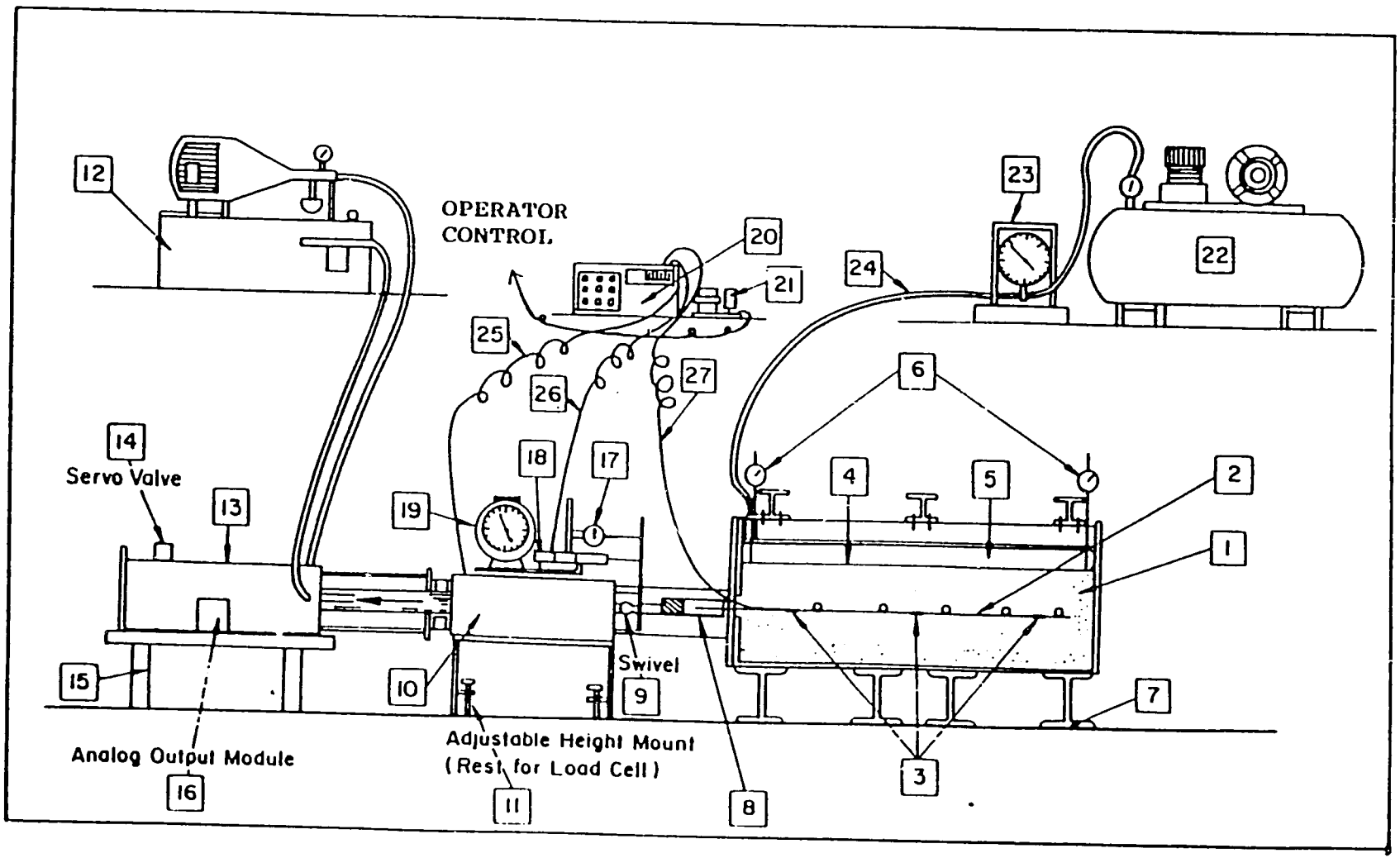

FIG. 28 DETAILED SET-UP OF LABORATORY PULLOUT TEST
(SEE TABLE 5 FOR DETAILS)

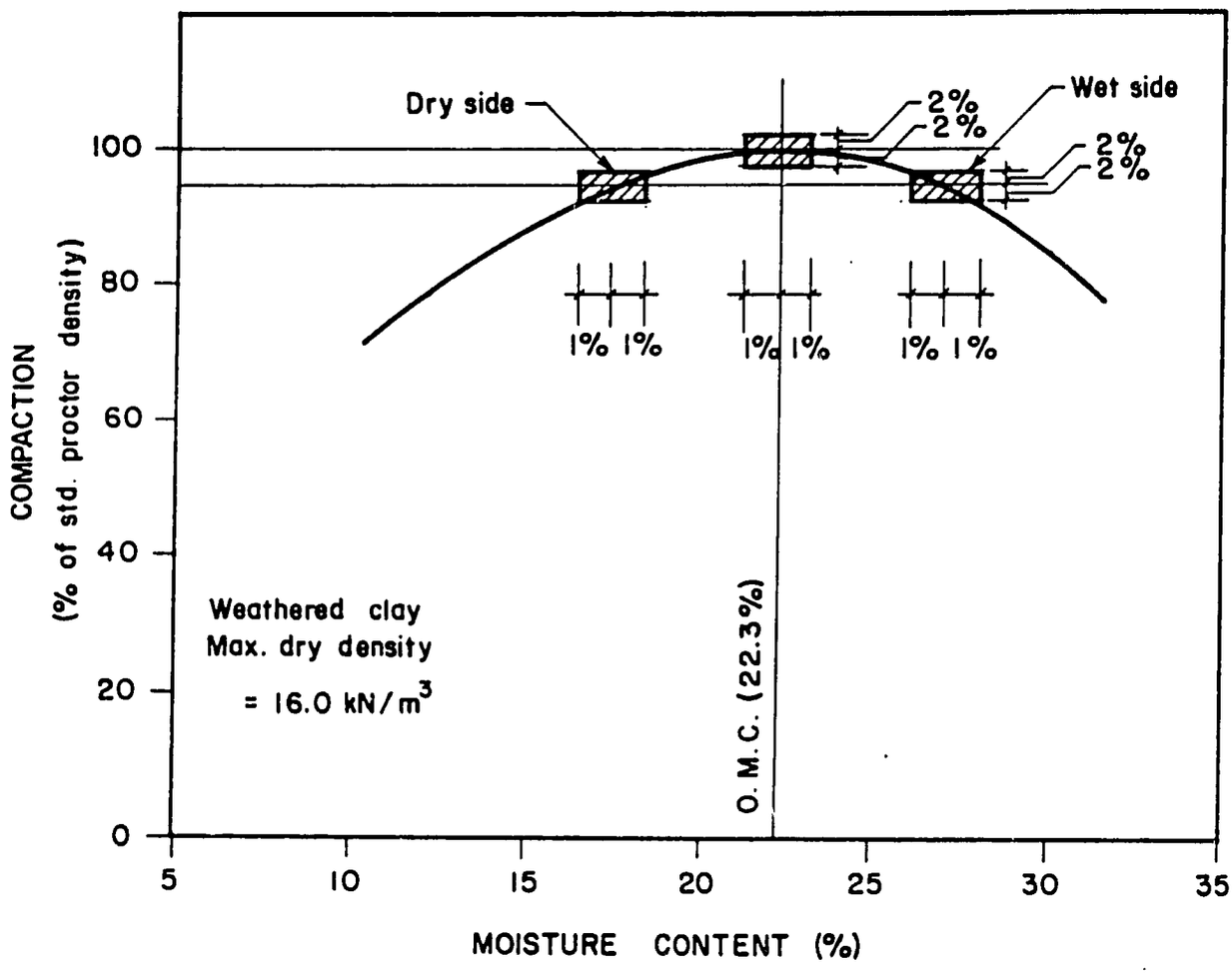

Fig.29 Compaction Curve of Weathered Bangkok Clay Showing Ranges of Compaction and Moisture Content Used in the Laboratory Pullout Tests and Direct Shear Tests

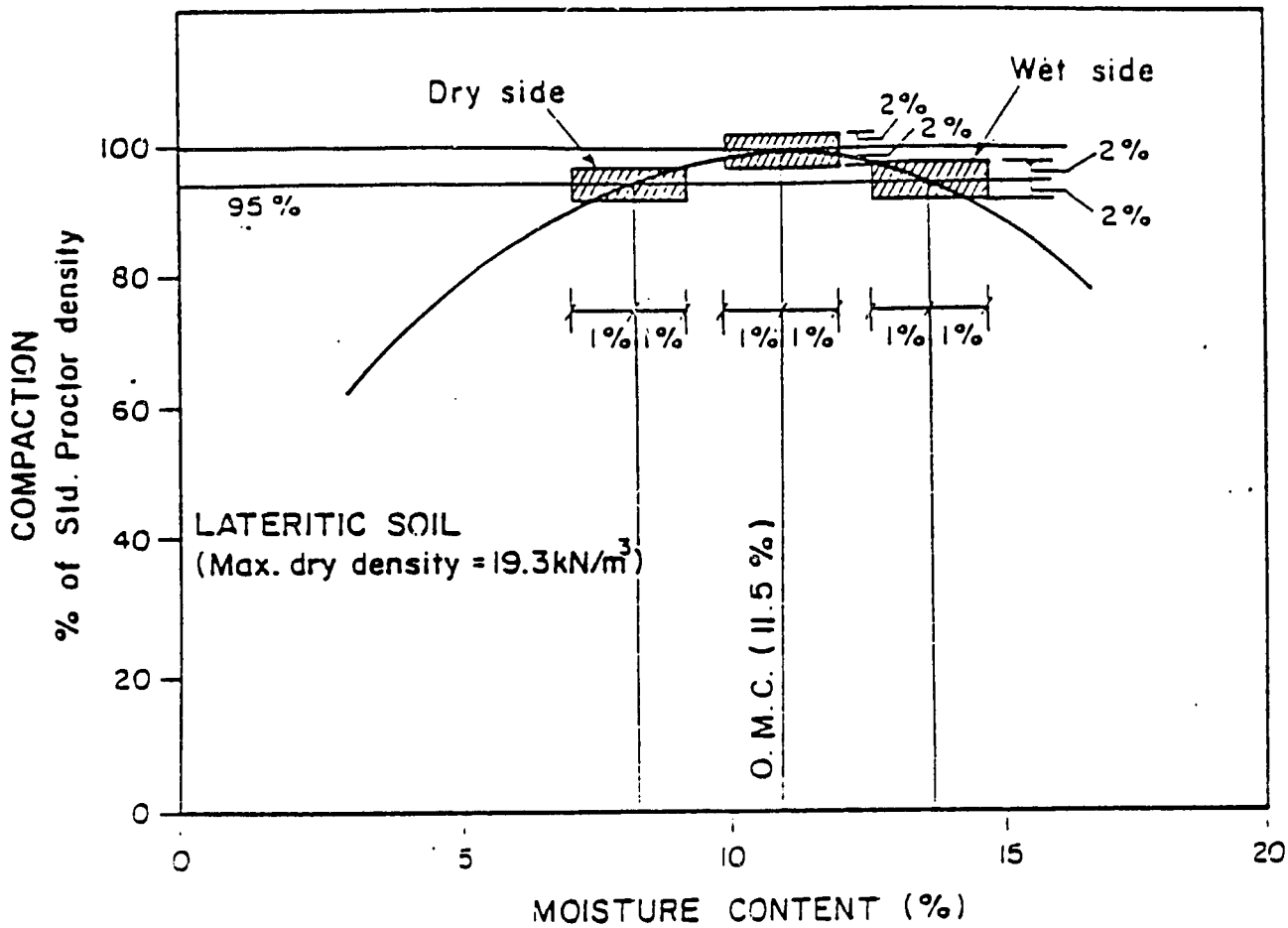

Fig.30 Compaction Curve of Lateritic Residual Soil Showing Ranges of Compaction and Moisture Content Used in the Laboratory Pullout Tes

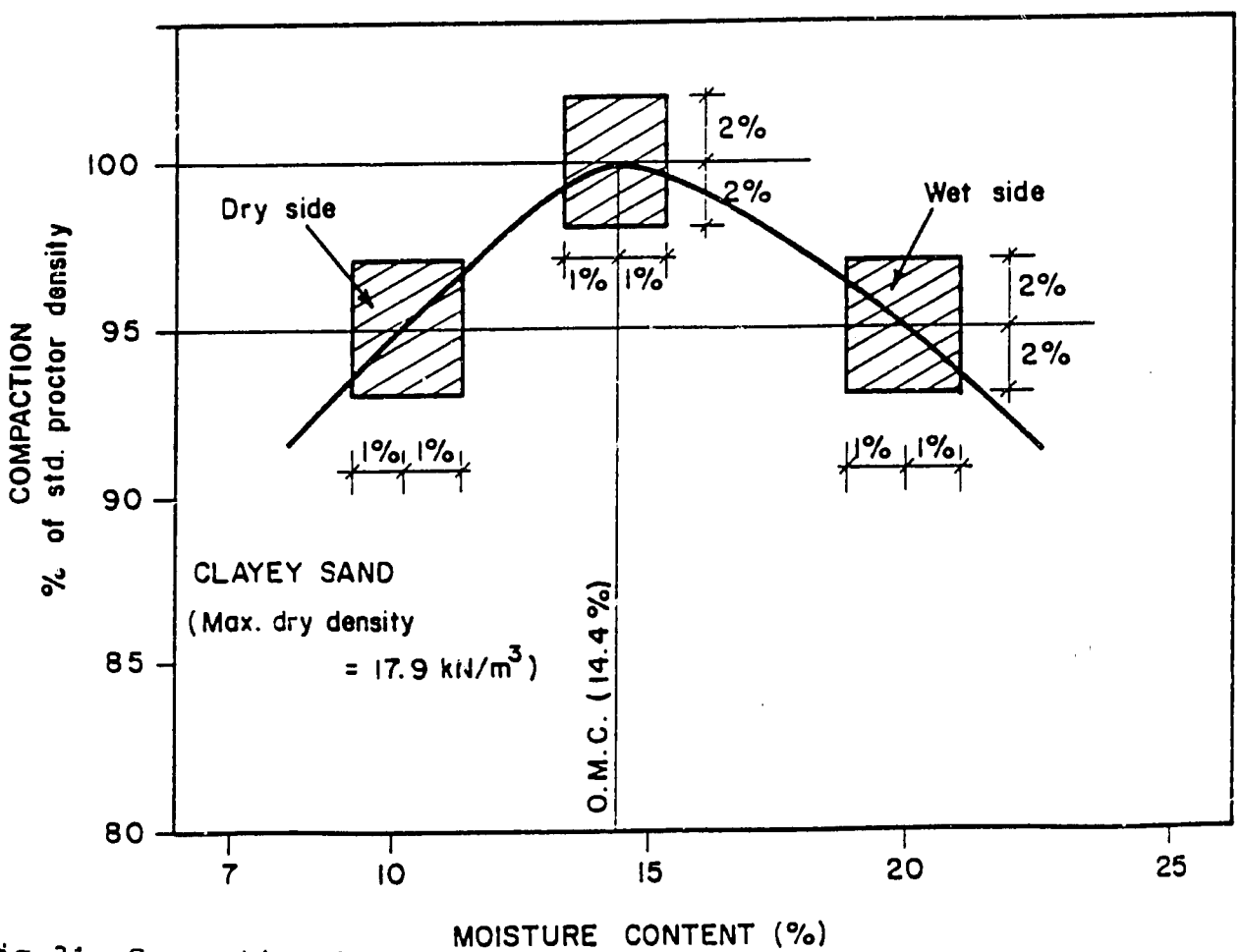

Fig.31 Compaction Curve of Clayey Sand Showing the Ranges of Compaction

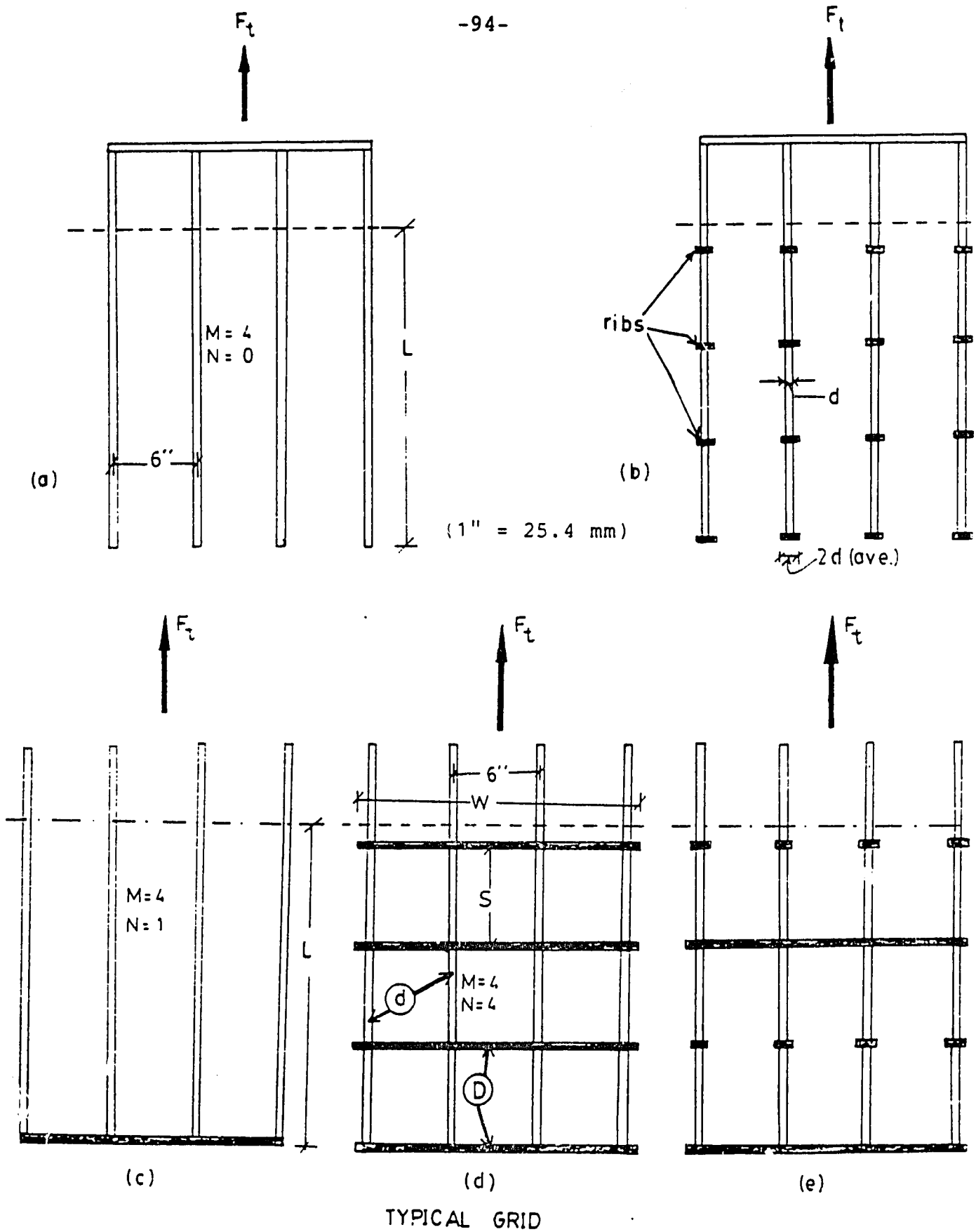

Fig. 32 Different Types of Reinforcements used in the Pullout Tests (Laboratory)

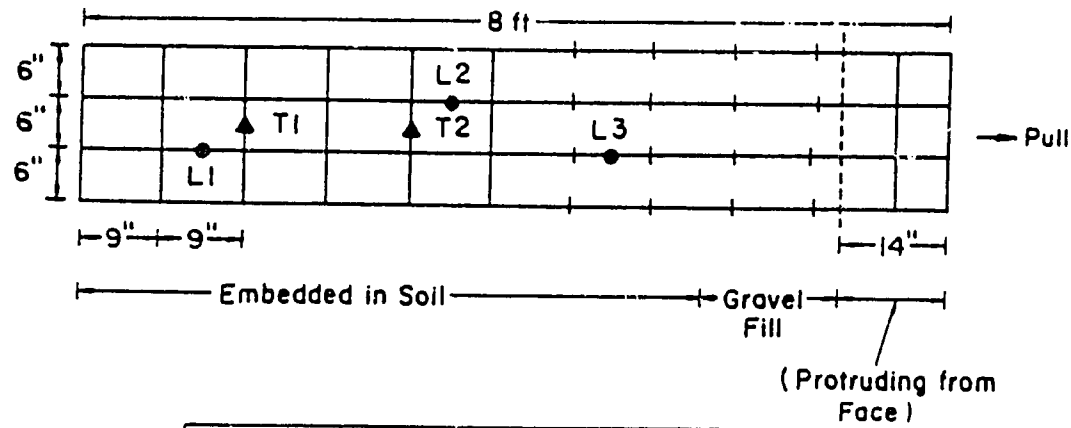

(a) FD-14 and FD-16 (W7 x W4.5)

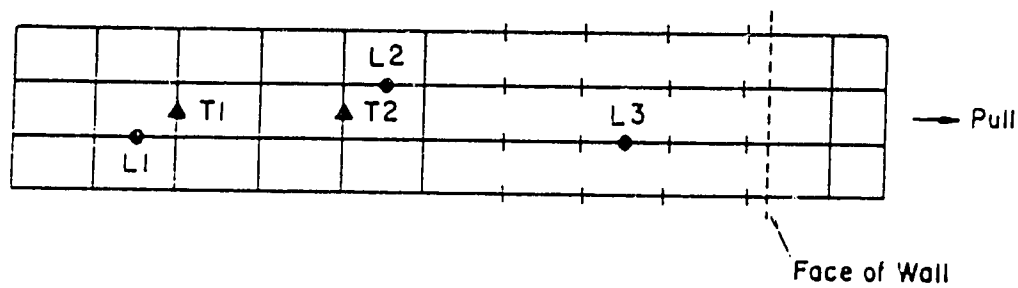

(b) FD-15 (W7 x W4.5)

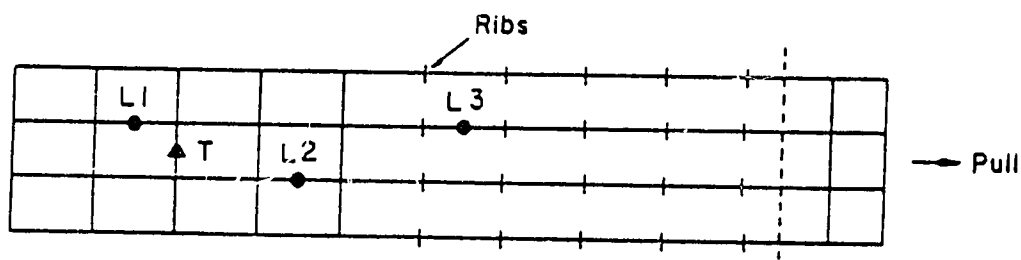

(c) FD-20, FD-21 & FD-22 (W4.5 x W3.5)
FD-24, FD-25 & FD-26 (W7 x W4.5)

- ● Strain Gauge on Longitudinal Bar
- ▲ Strain Gauge on Transverse Bar

Note : 1" = 25.4 mm ; 1' = 0.3048 m ; 1 m = 1000 mm

Fig. 33 Dummy Mats Used in Field Pullout Tests

Fig.34 Set-up for the Field Constant Strain Pullout Test at Low Level with the Reaction Frame Resting on the Ground (A Front View)

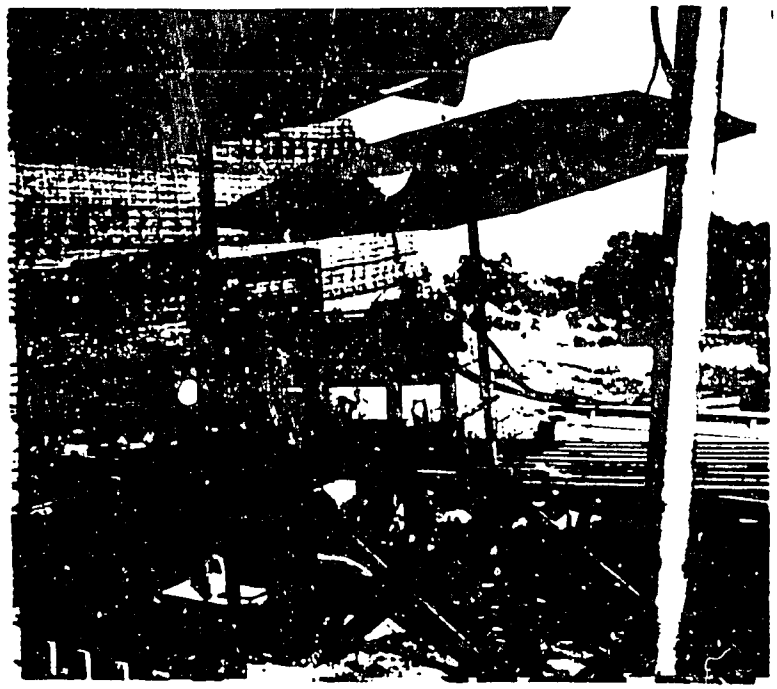

Fig.35 Set-up for the Field Constant Strain Pullout Test at an Intermediate Level

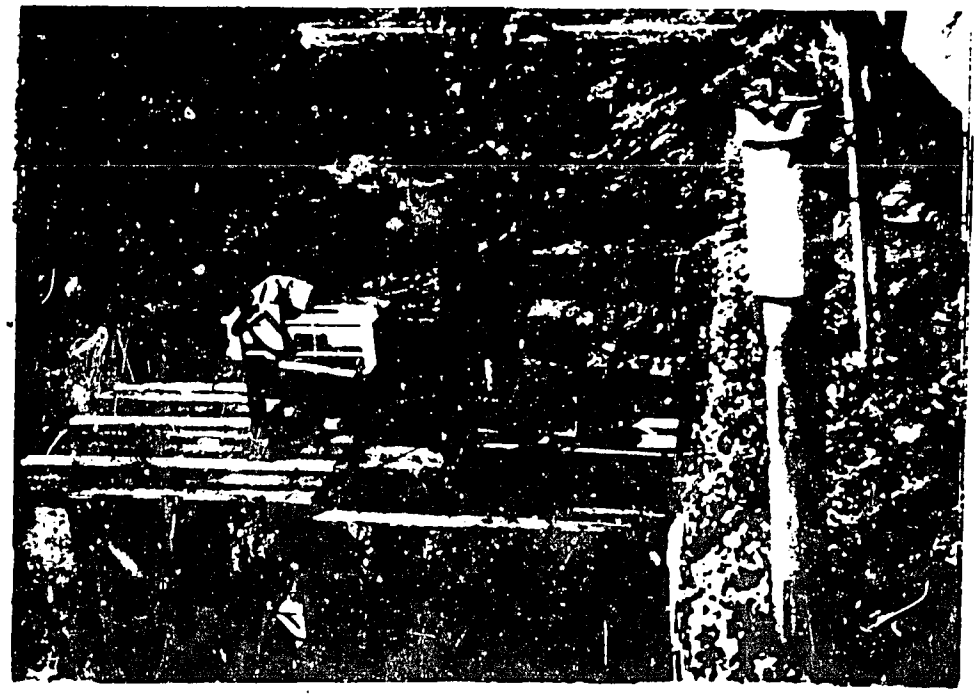

Fig.36 A View of the Set-up for the Field Constant Strain Pullout Test at the Highest Level

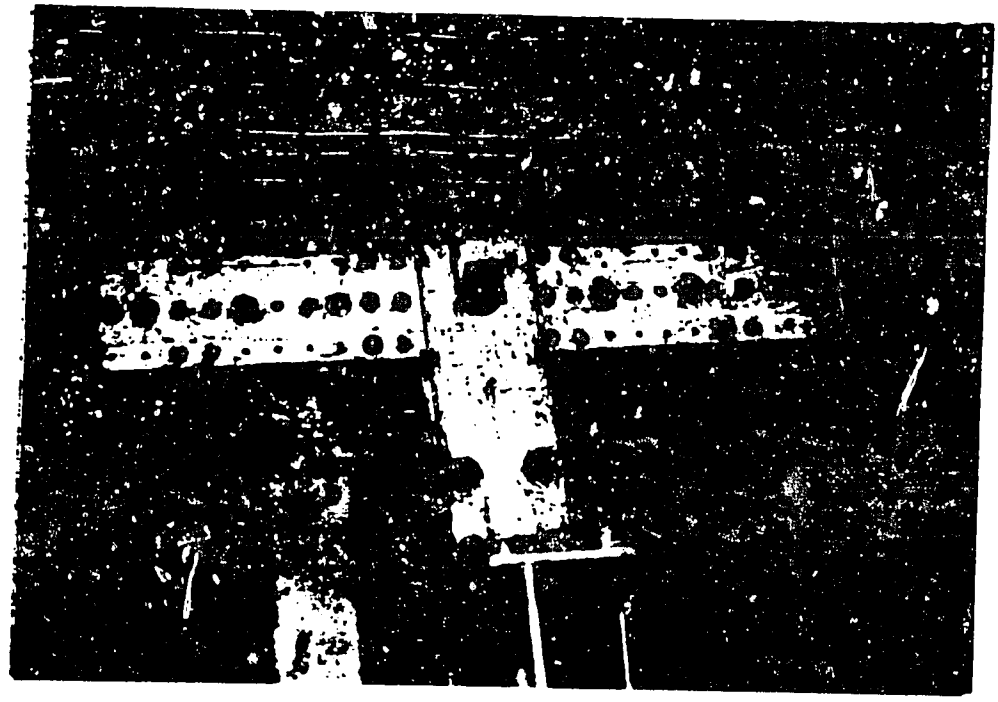

Fig.37 The Gripping Devices Used in the Field Constant Strain Pullout Tests, Similar to the Laboratory Pullout Tests

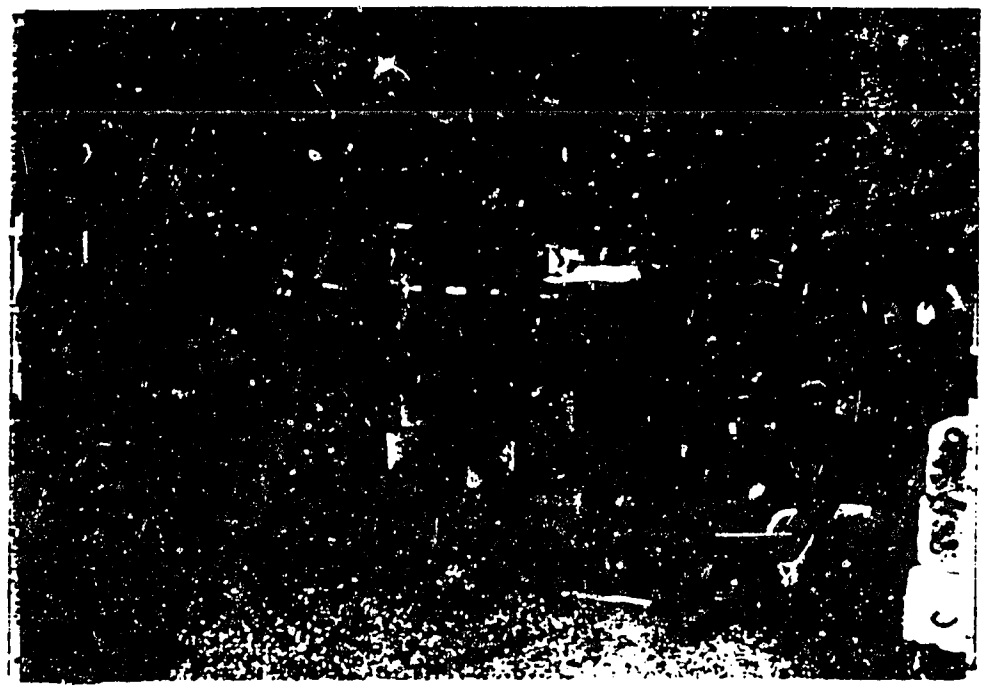

Fig.38 A View of the Constant Stress Field Pullout Test Set-up Showing the Loading Pan and Concrete Blocks

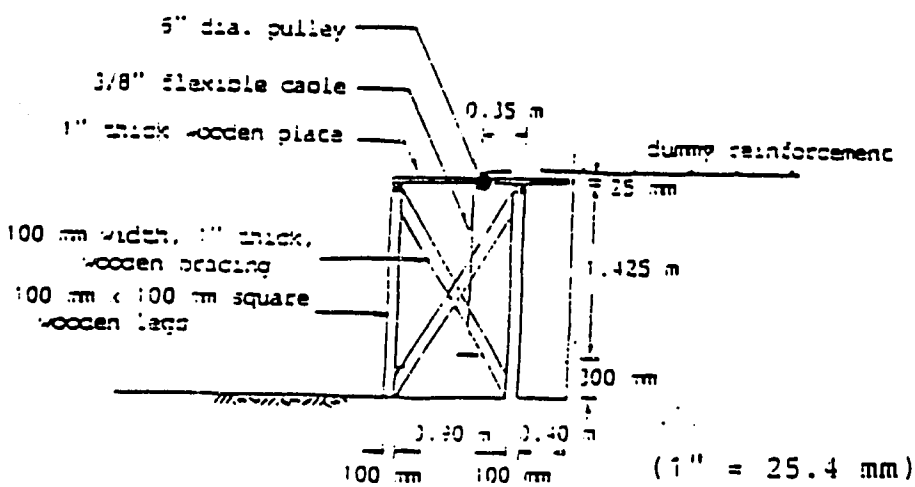

Fig.39 A View of the Constant-Stress Field Pullout Test Set-up

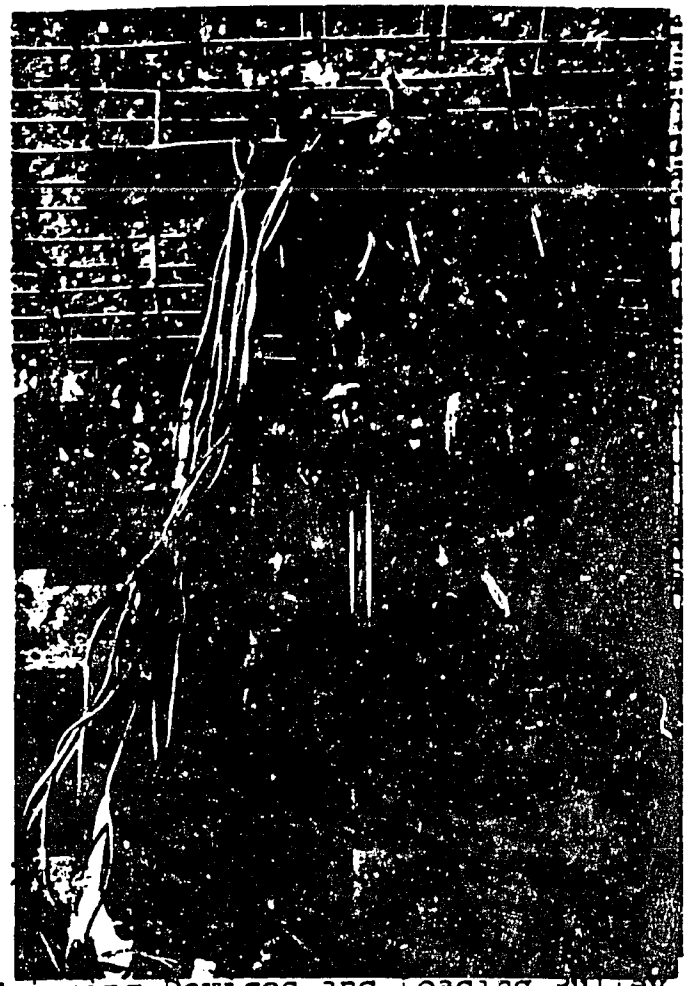

Fig.40 Gripping Devices and Loading Pulley For Constant Stress Field Pullout Tests (Top View)

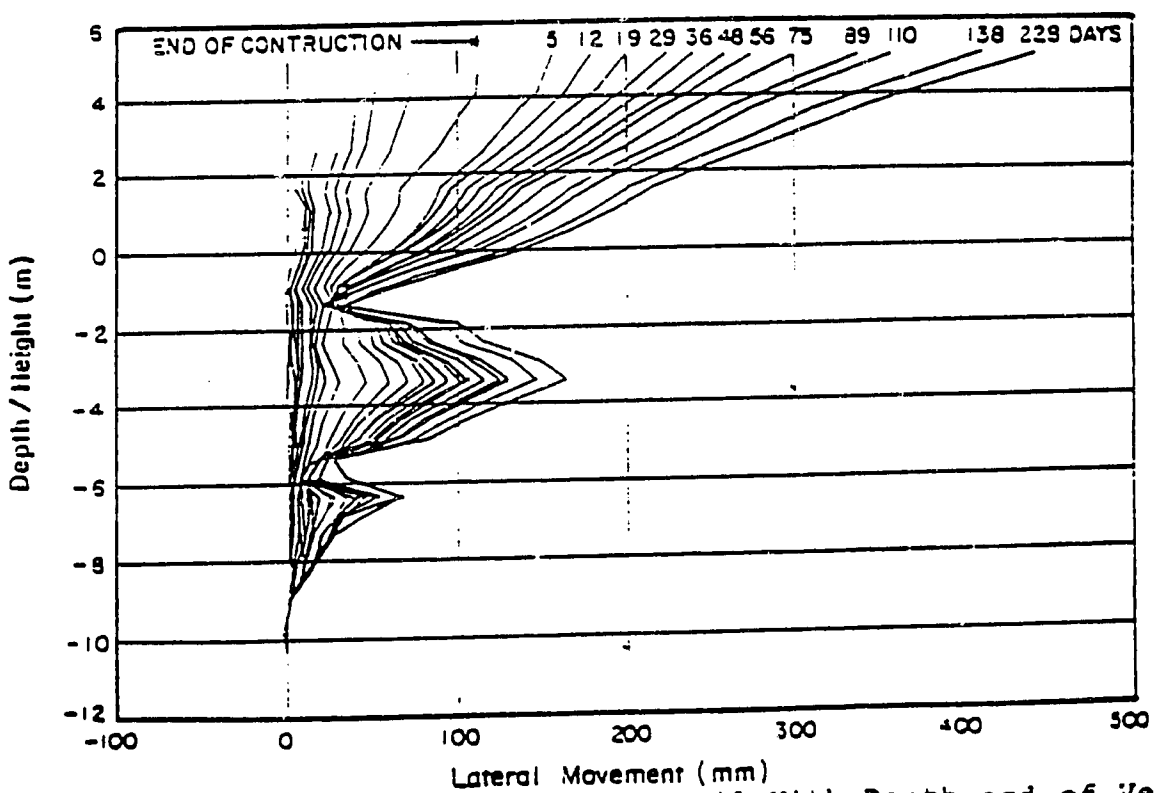

Fig.41 Lateral Movements of Subsoil With Depth, and of Vert ca Wall Face With Height, For Different Time Intervals During and After Construction at I1

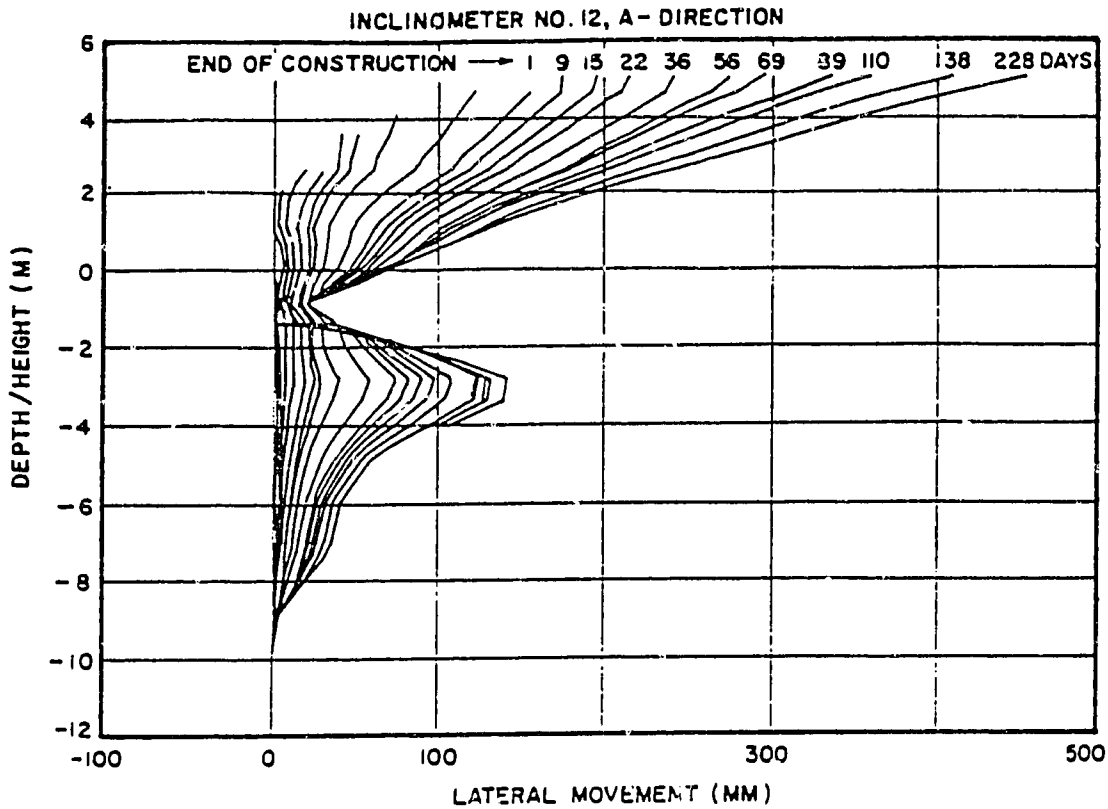

Fig.42 Lateral Movements of Subsoil with Depth and Vertical Wall Face with Height For Different Time Interval During and After Construction at I2

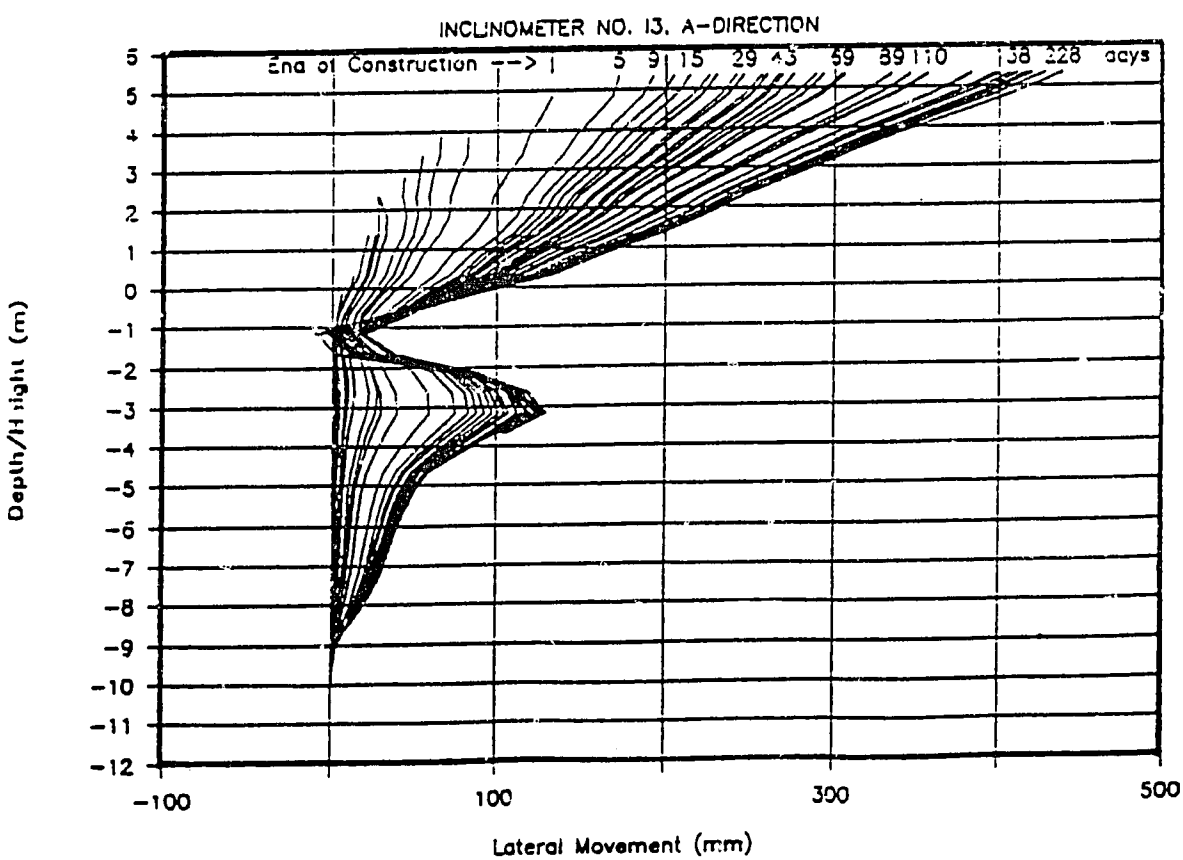

Fig.43 Lateral Movements of Subsoil with Depth and Vertical Wall Face with Height For Different Time Interval During and After Construction at I3.

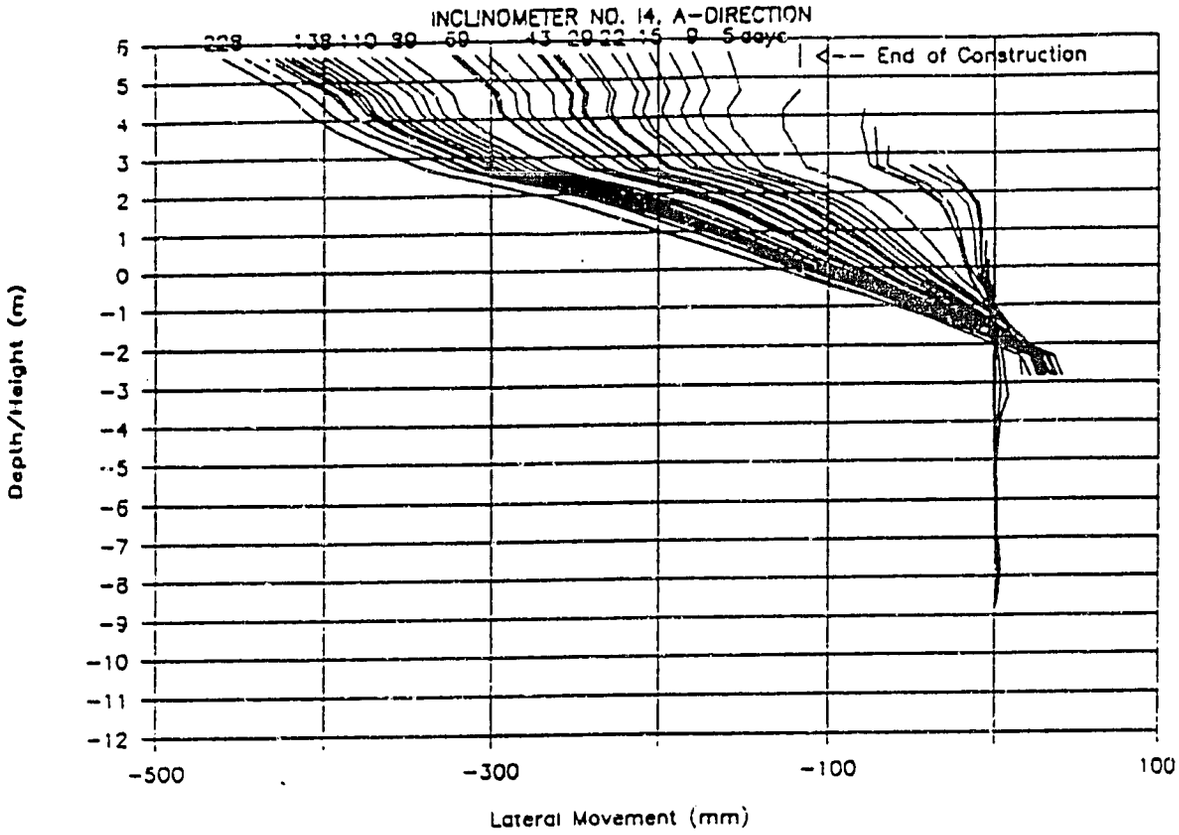

Fig. 44 Lateral Movements of Subsoil with Depth and Embankment in the Center with Height For Different Time Intervals During and After Construction at I4

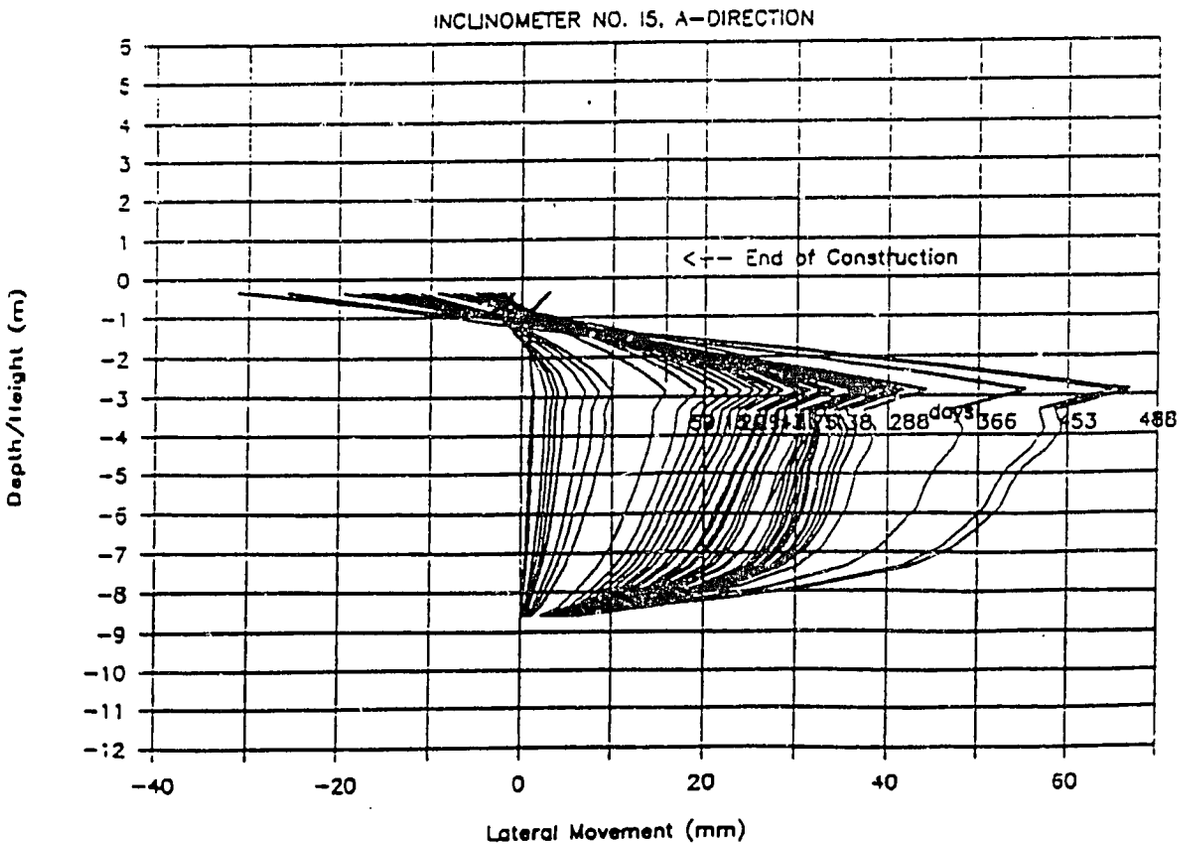

Fig. 45 Lateral Movements of Subsoil with Depth For Different Time Intervals During and After Construction at I5

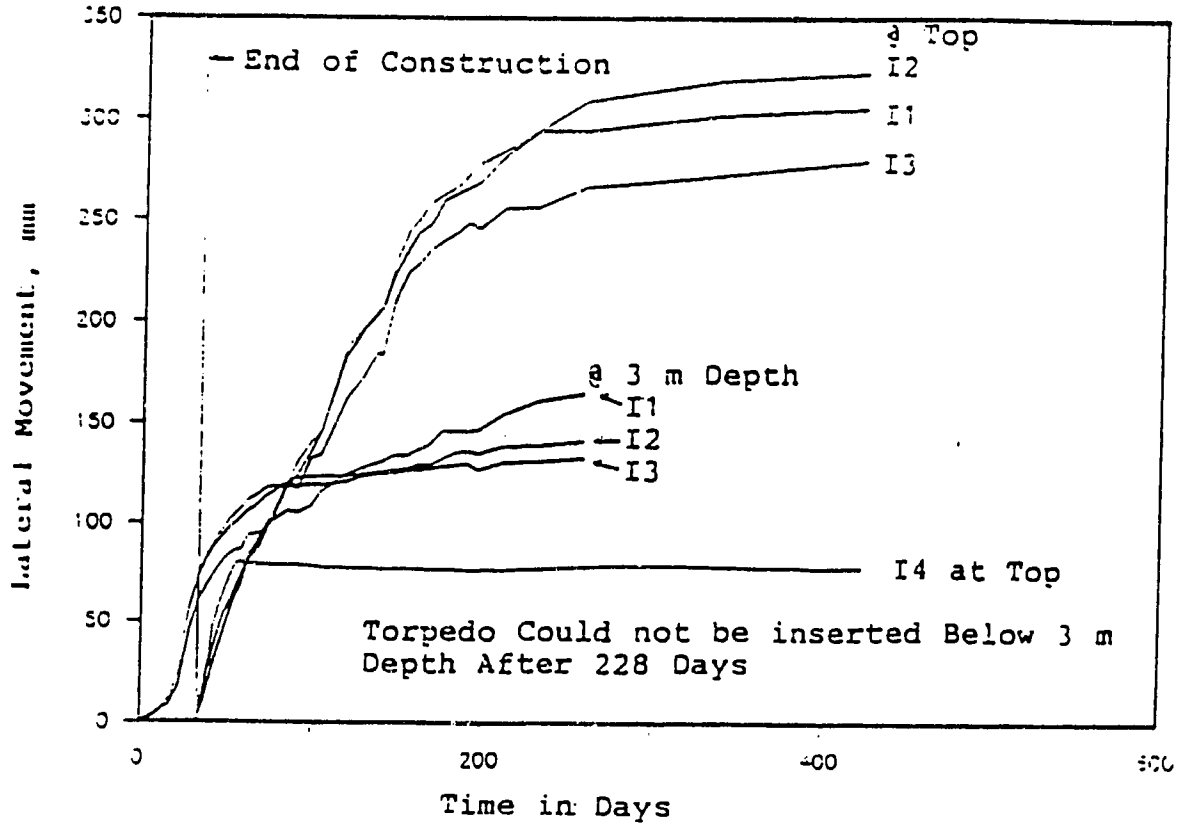

Fig. 46 Maximum Lateral Movements of the Wall Face and in the Subsoil at 3 m Depth Plotted With Time

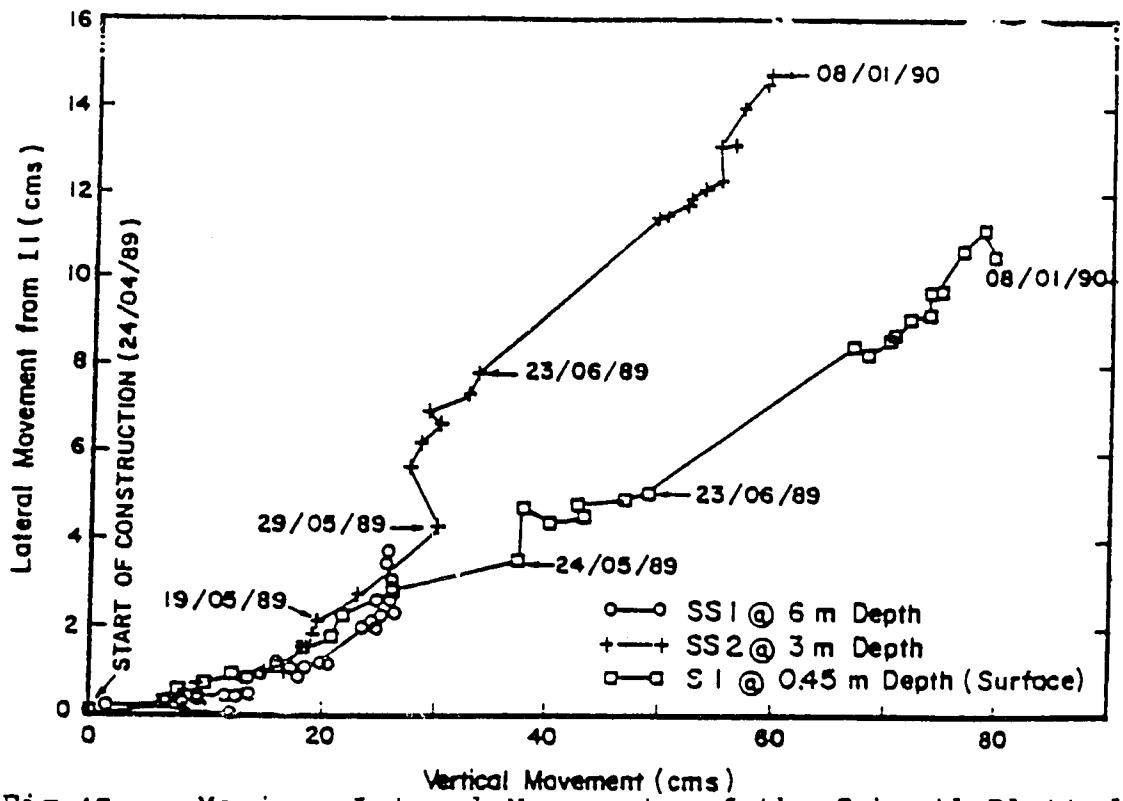

Fig.47 Maximum Lateral Movement of the Subsoil Plotted Against the Vertical Movement of the Wall (Inclinometer No.1) (1 cm = 0.01 m)

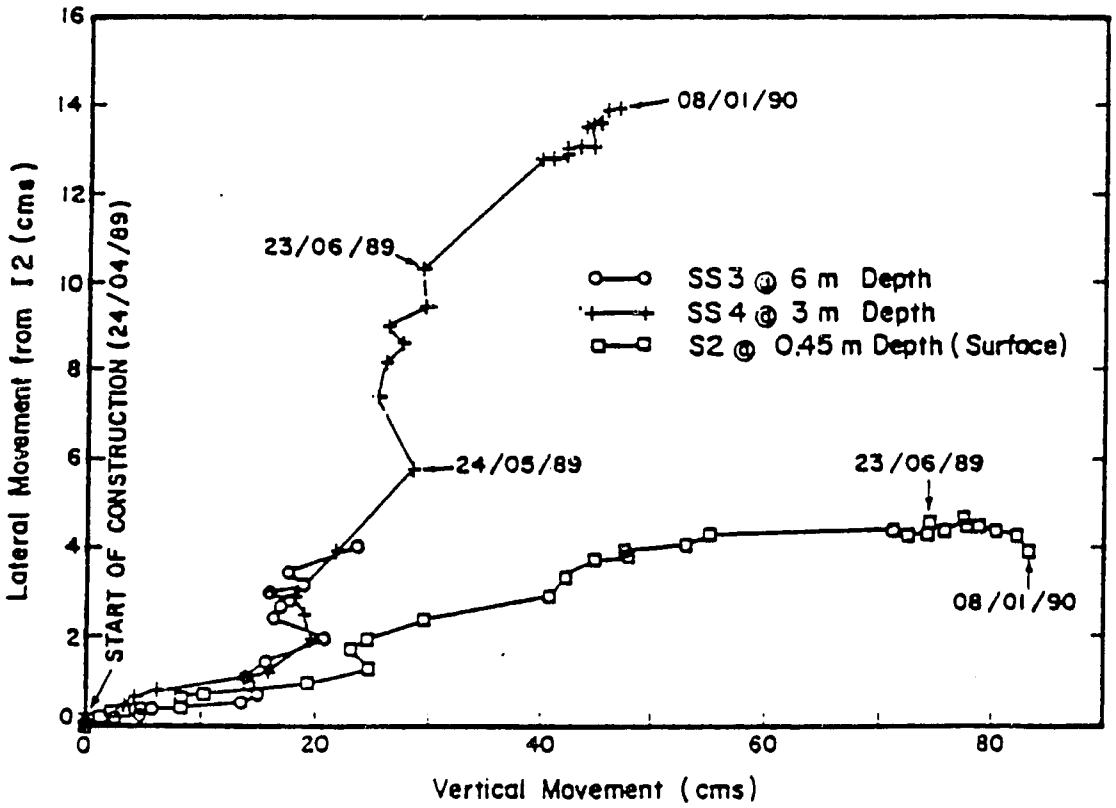

Fig.48 Maximum Lateral Movement of the Subsoil Plotted Against the Vertical Movement of the Wall (Inclimeter No.2)

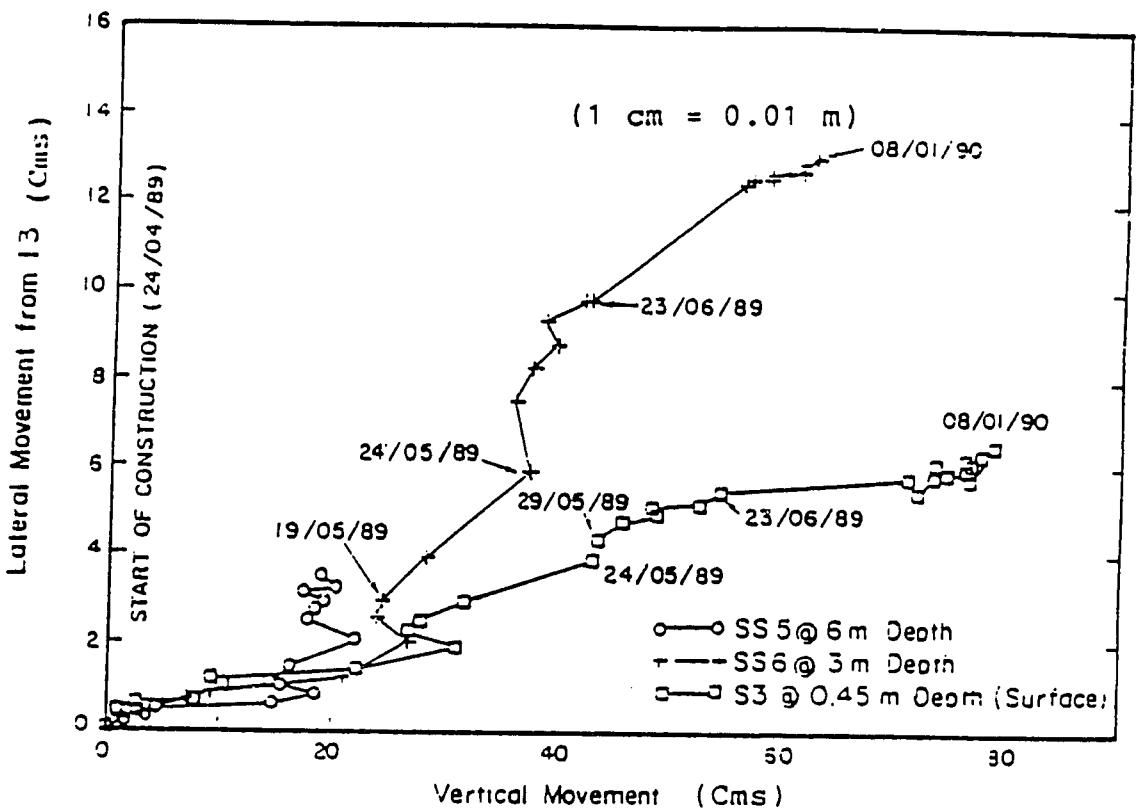

Fig.49 Maximum Lateral Movement of the Subsoil Plotted Against the Vertical Movement of the Wall (Inclinometer No.I3)

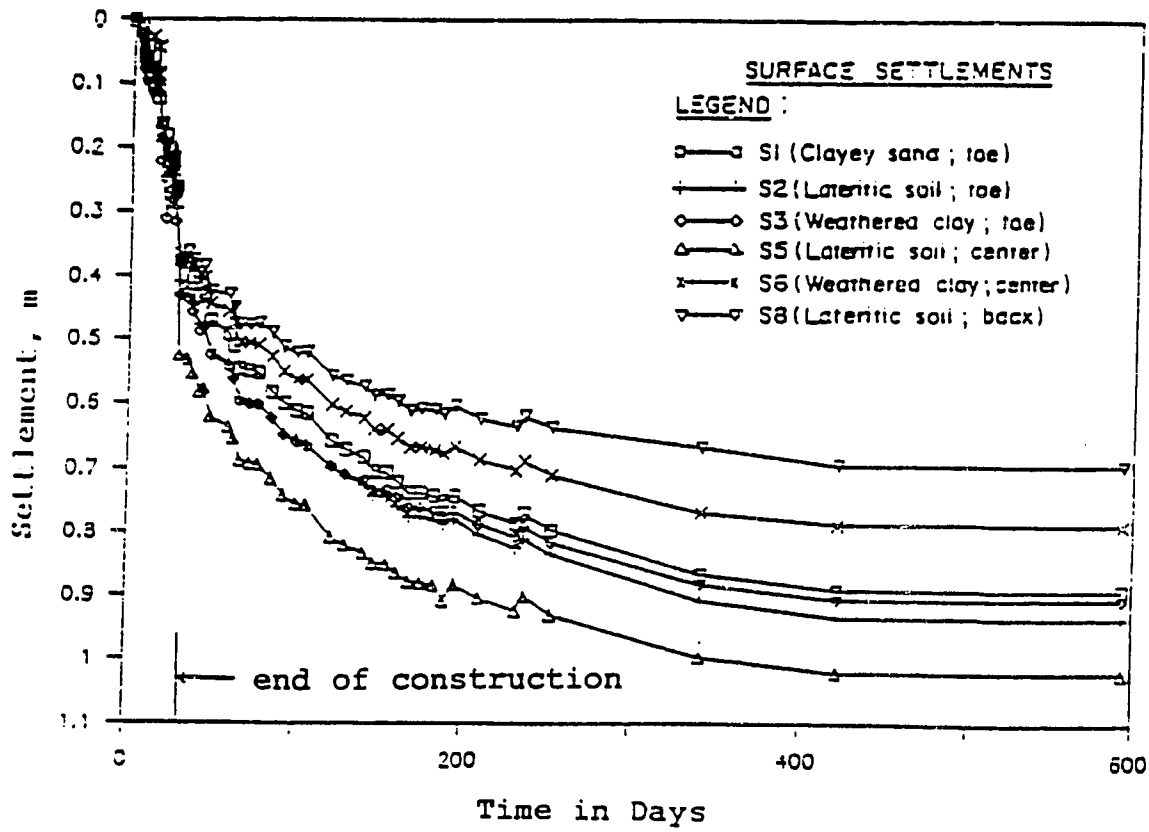

Fig. 50 Surface Settlements Beneath the Embankment

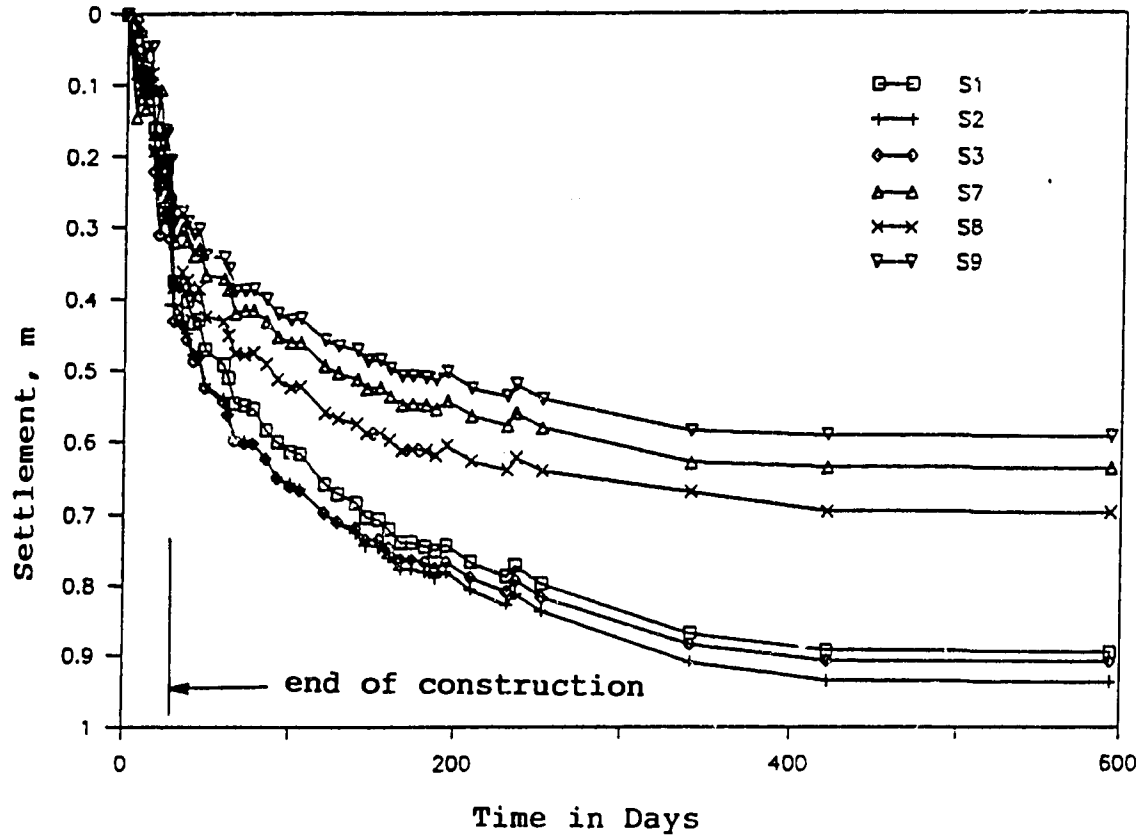

Fig. 51 Surface Settlements Beneath the Embankment at the Front (S1-S2-S3) and at the Back (S7-S8-S9) of the Reinforced Zone

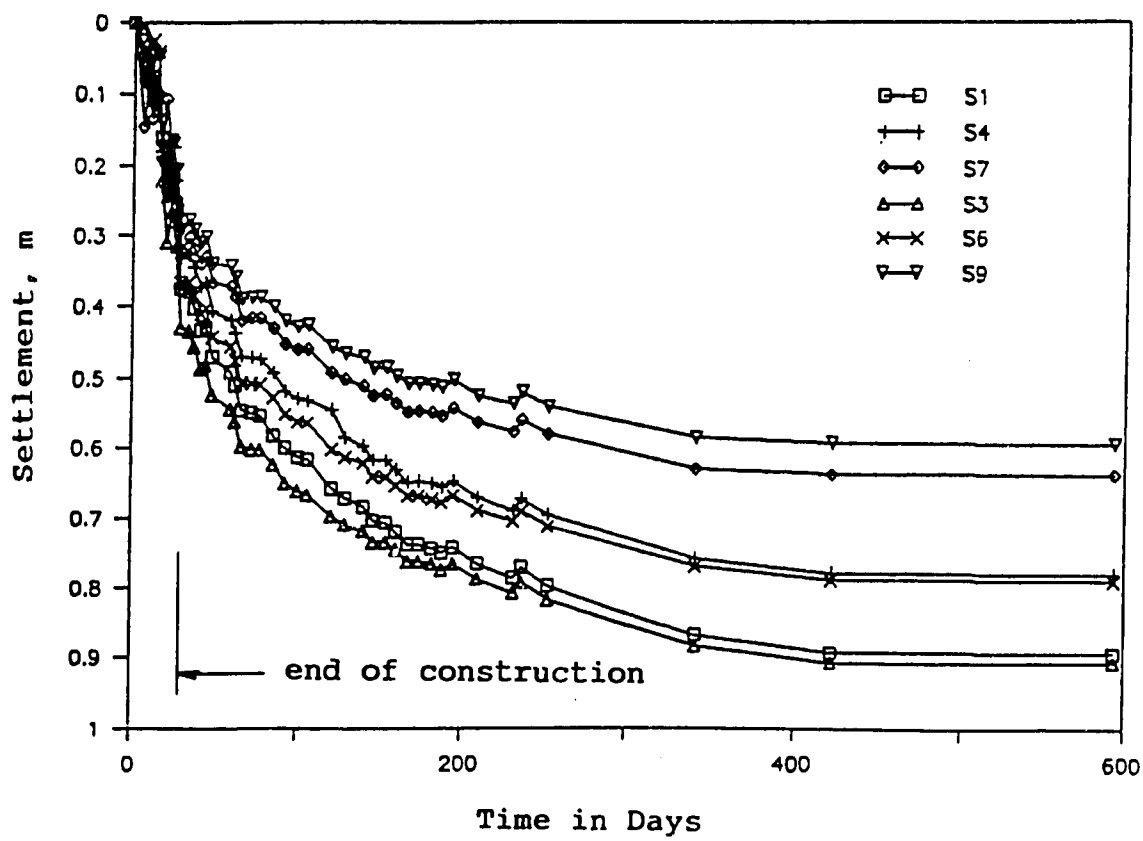

Fig.52 Surface Settlements Beneath the Embankment, Below Clayey Sand Backfill (S1-S4-S7) and Below Weather Clay Backfill (S3-S6-S9)

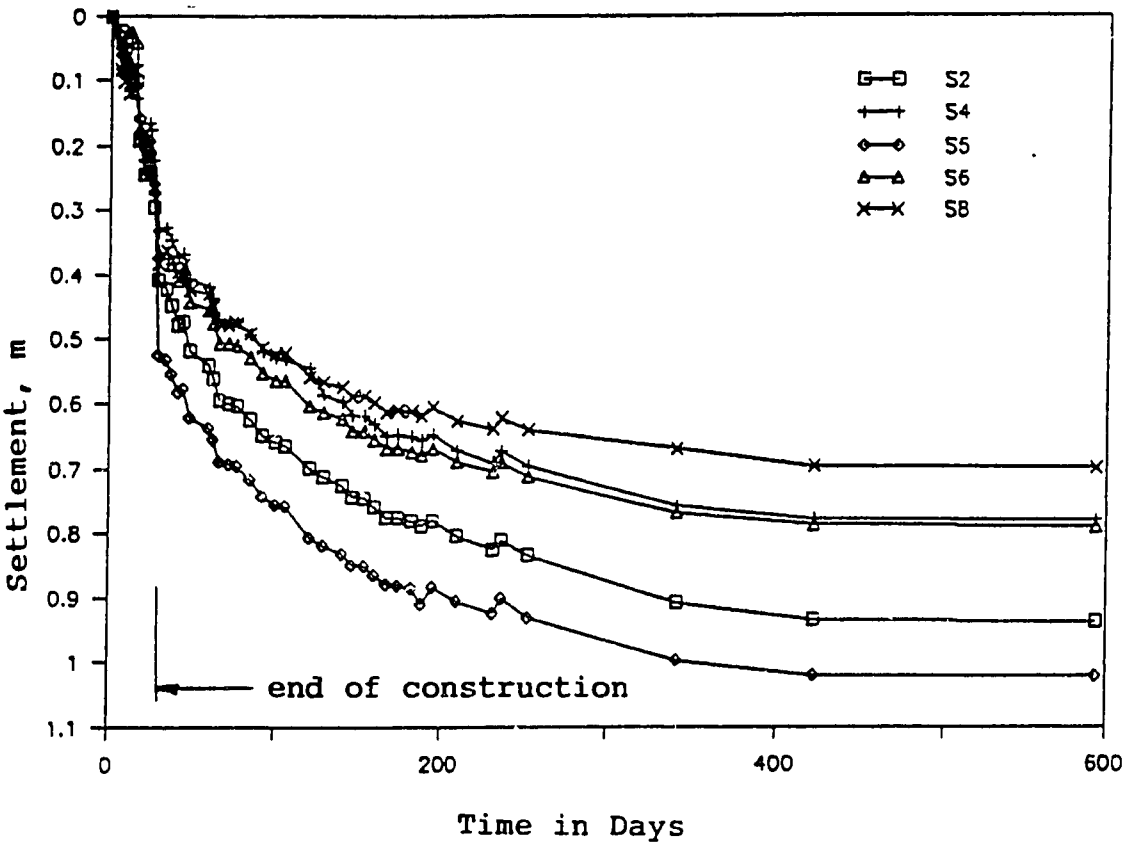

Fig. 53 Surface Settlements Beneath the Embankment, Showing the Maximum Surface Settlement at S5

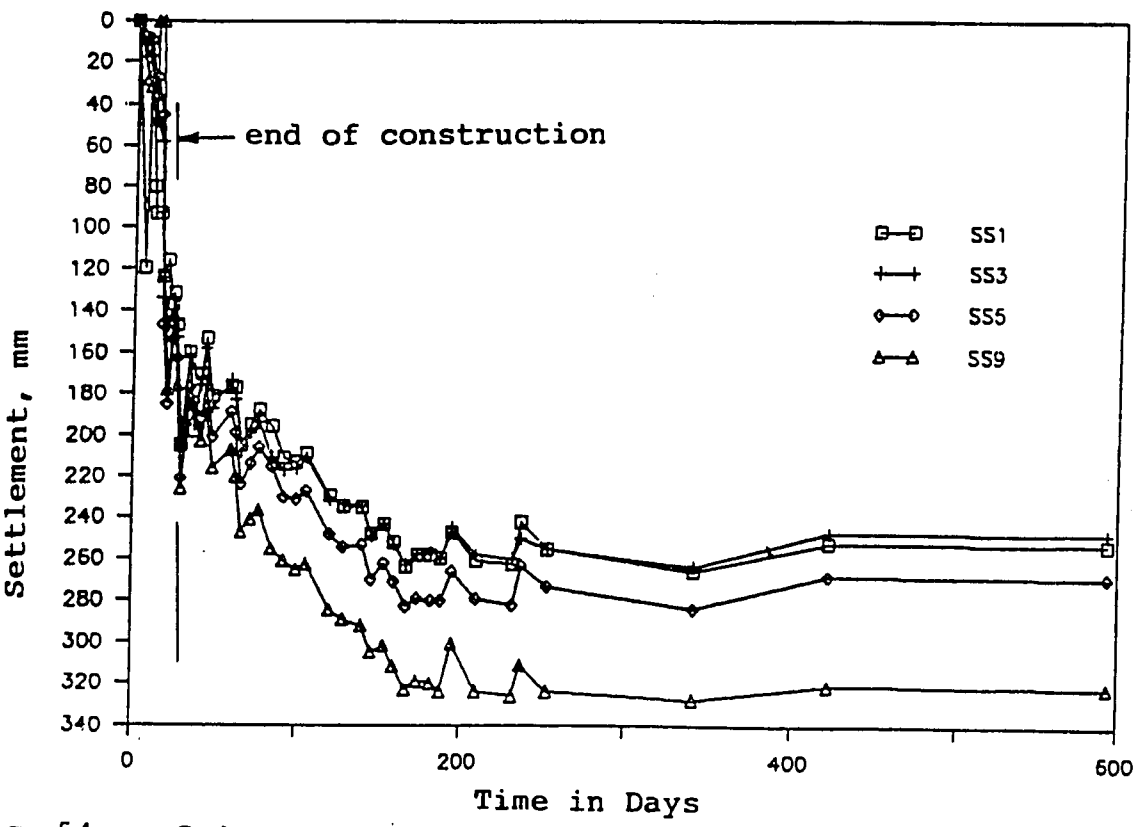

Fig. 54 Subsurface Settlements at 6 m Depth Beneath the Embankment

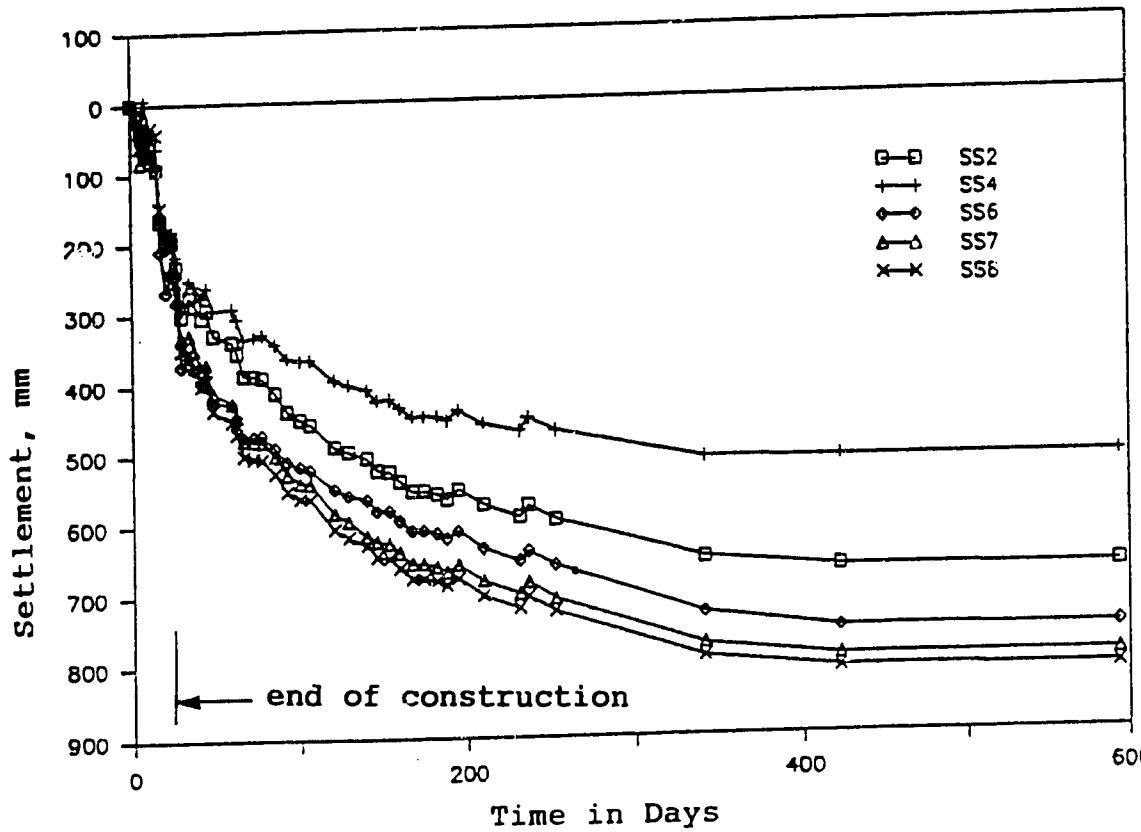

Fig. 55 Subsurface Settlements at 3 m Depth Beneath Embankment at the Front and in the Middle Rows

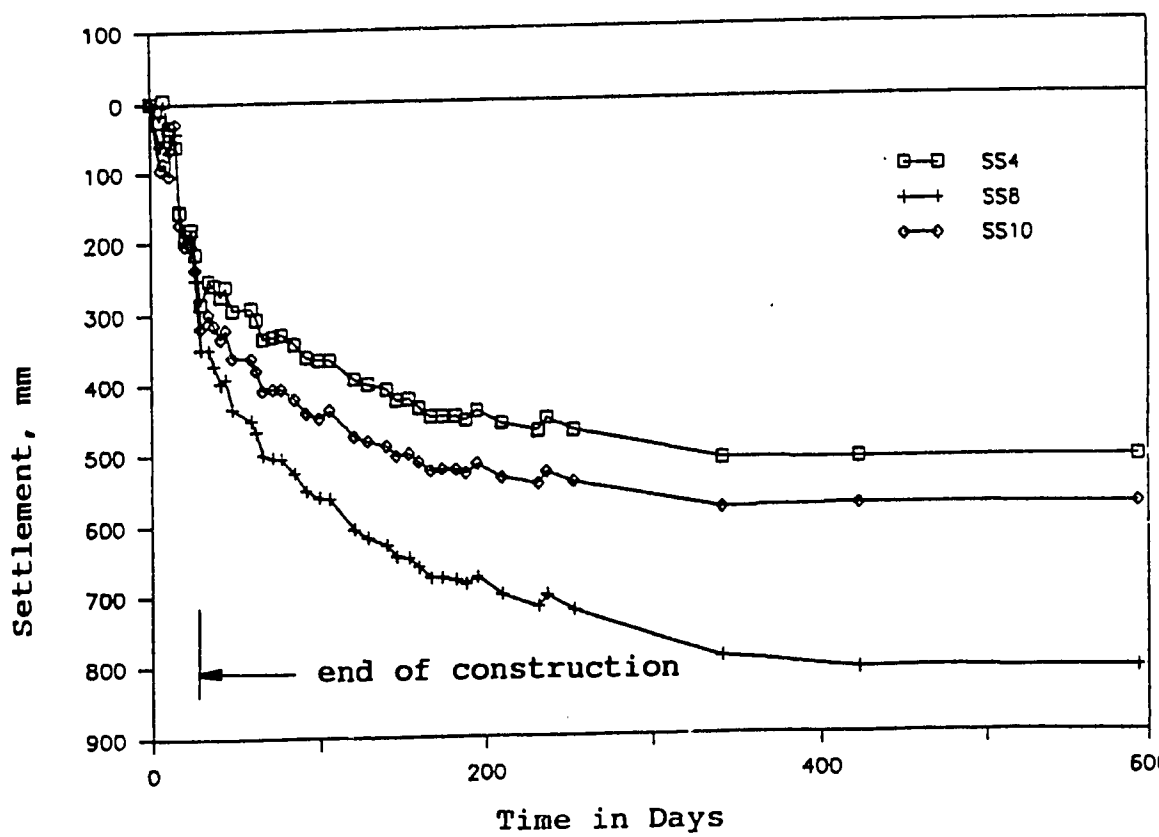

Fig.56 Subsurface Settlements at 3 m Depth Beneath the Embankment in the Middle Section Below Lateritic Soil

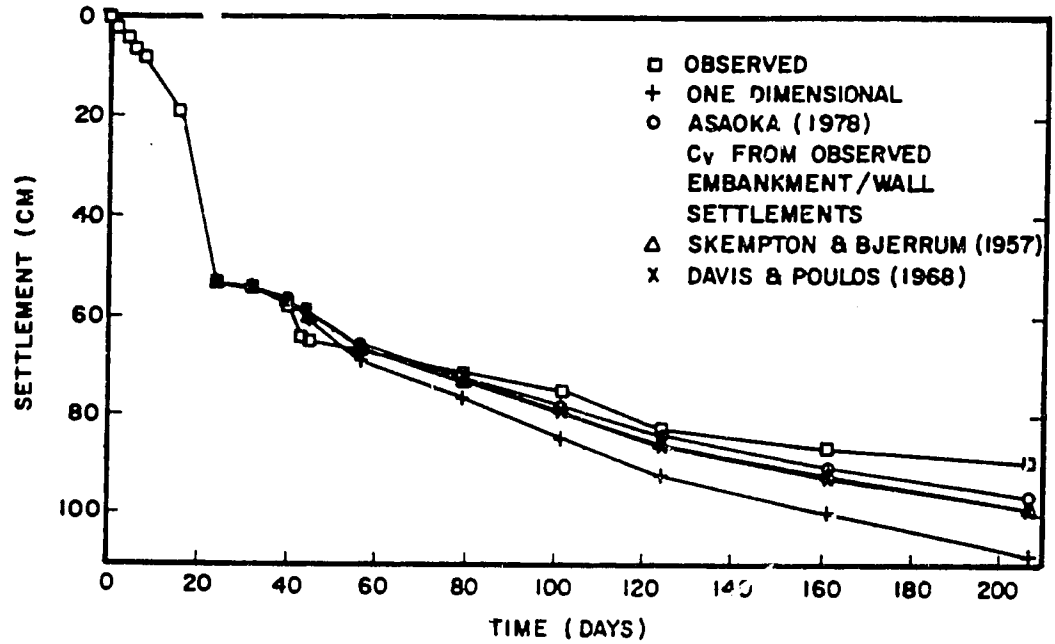

Fig.57 Observed and Predicted Time-Settlement Curves (using C_v From Observed Settlements in Asaoka's Method)

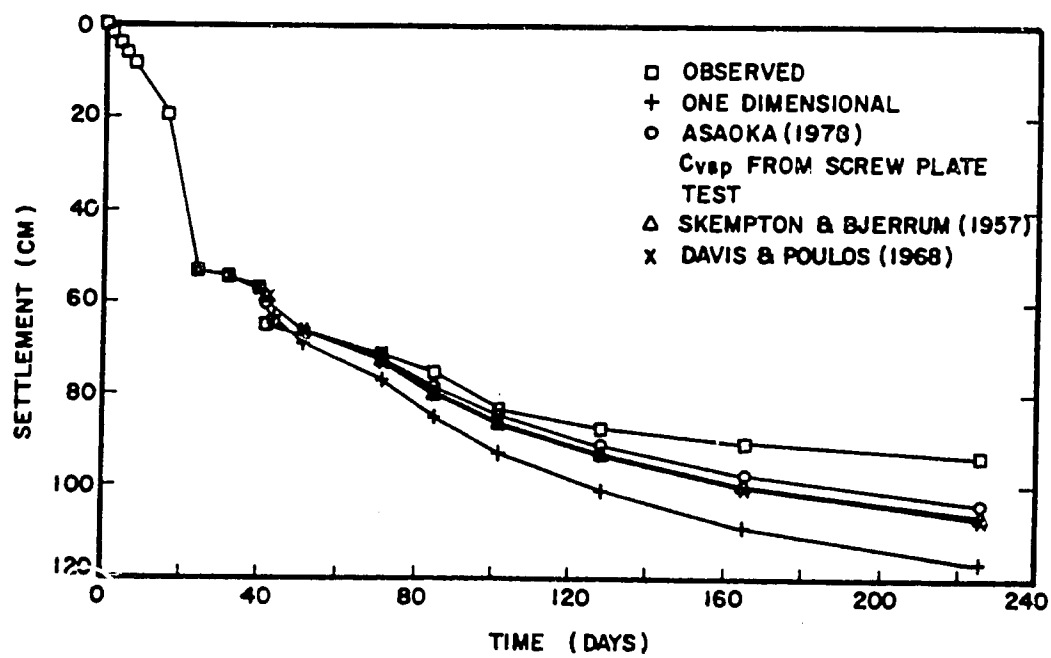

Fig.58 Observed and Predicted Time-Settlement Curves (using C_v From Screw Plate Test Results in Asaoka's Method)

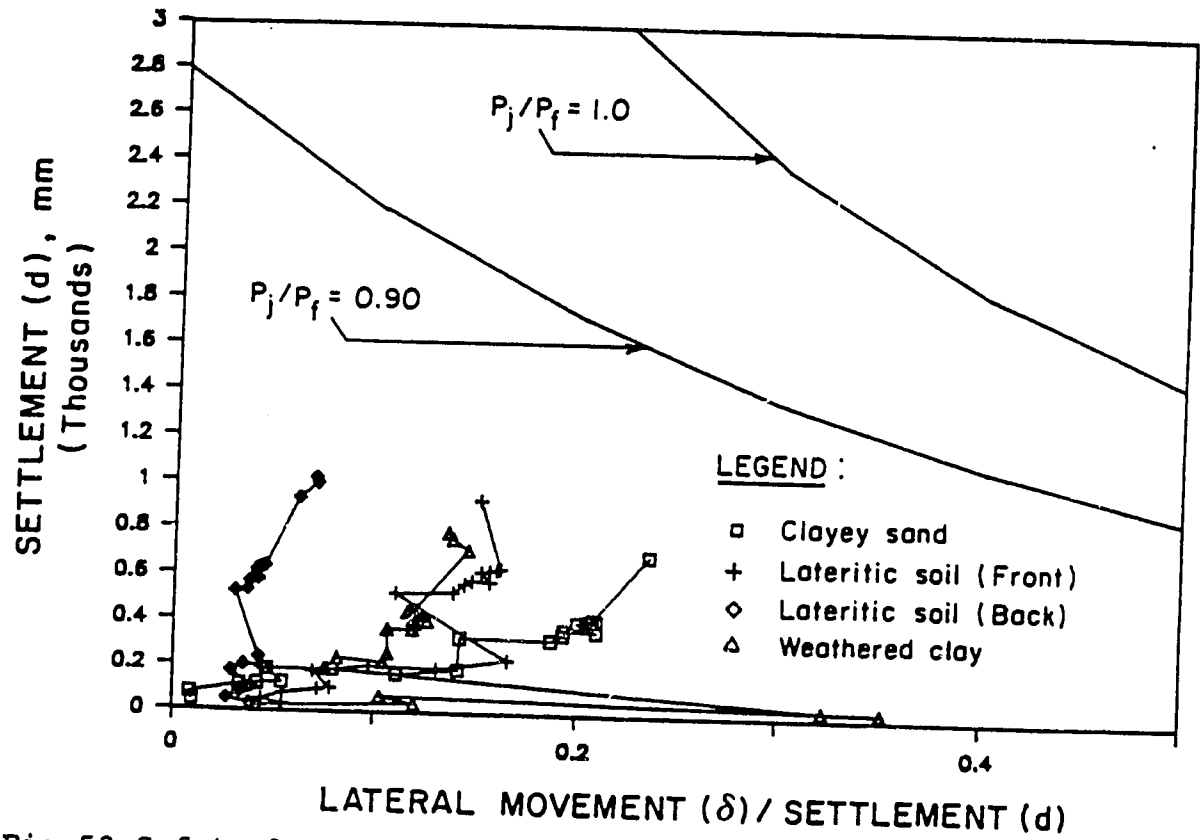

Fig.59 Safety Assessment of the Wall on Soft Ground During construction (After MATSUO & KAWAMURA, 1977)

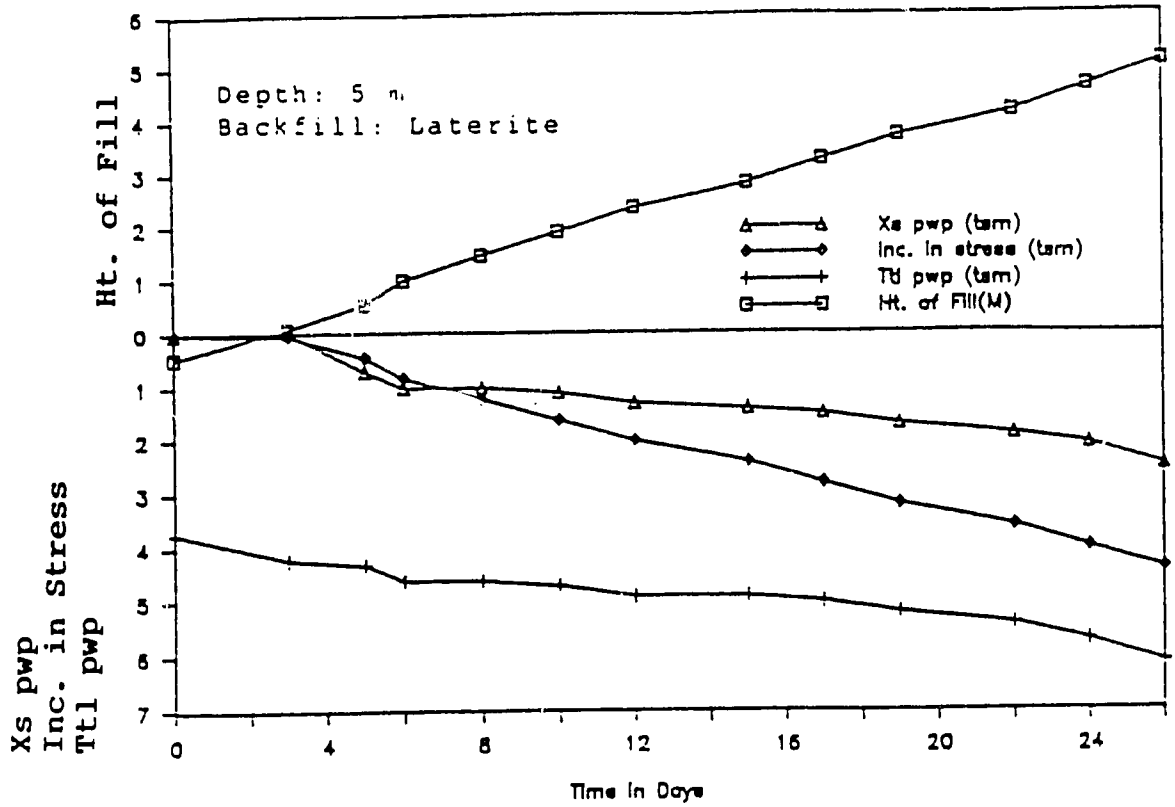

Fig. 60 Forewater Pressures From Pneumatic Piezometer N1 at 5 m Depth Below the Surface During Construction

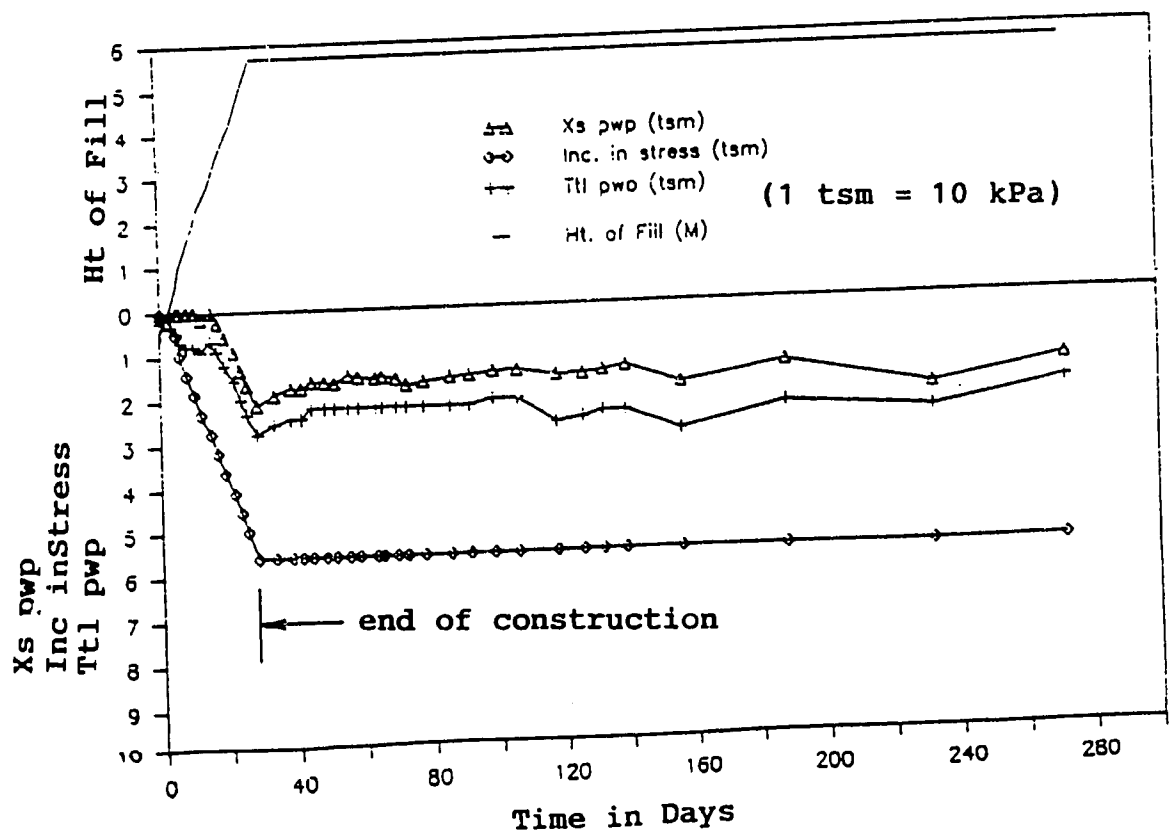

Fig. 61 Porewater Pressures From Pneumatic Piezometer N2 at Depth Below the Surface During Construction & Subsequently

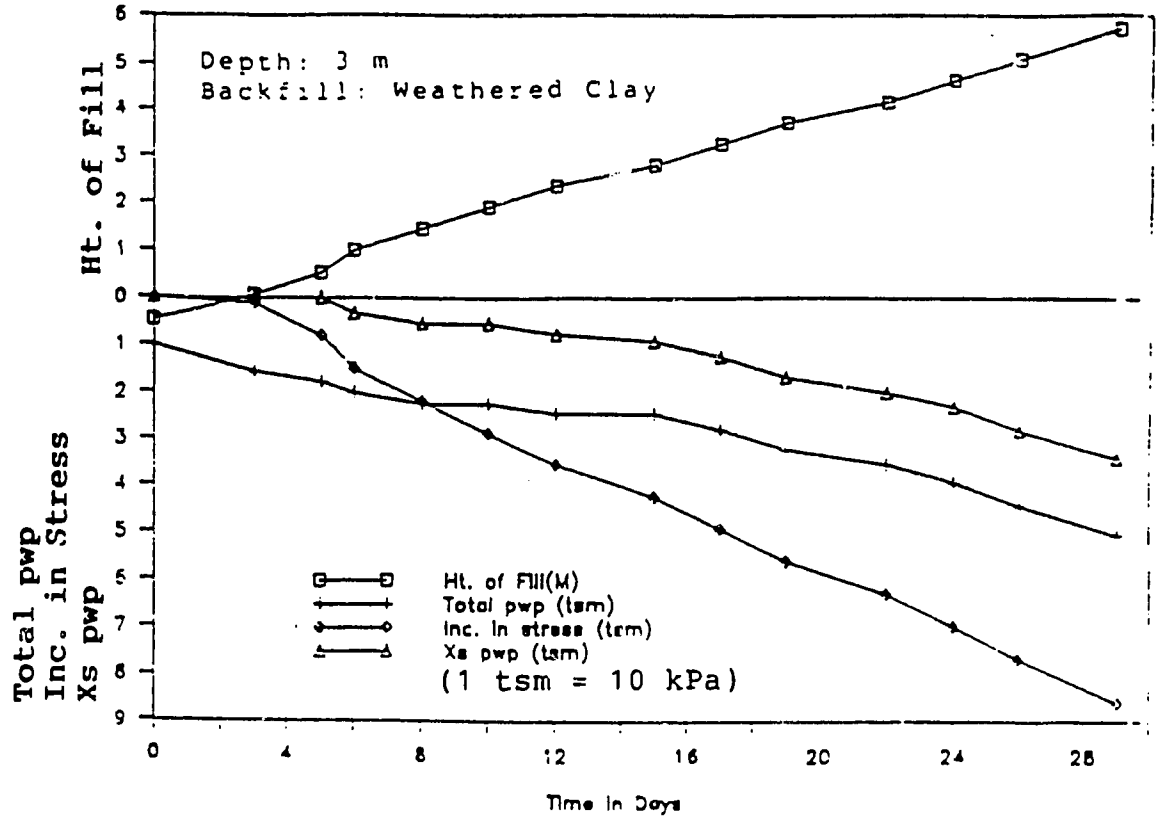

Fig. 62 Porewater Pressures From Pneumatic Piezometer N3 at 3 m Depth Below the Surface During Construction

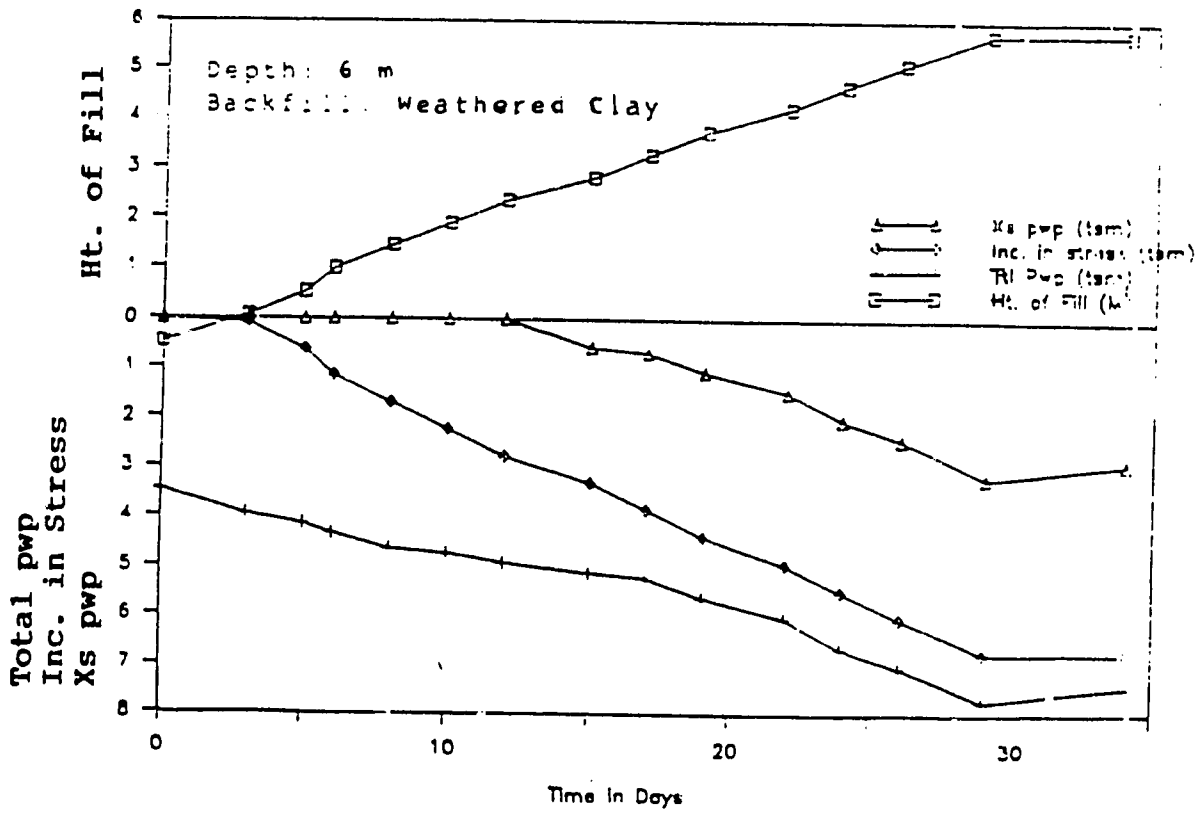

Fig. 63 Porewater Pressures From Pneumatic Piezometer N4 at 6 m Depth Below the Surface During Construction

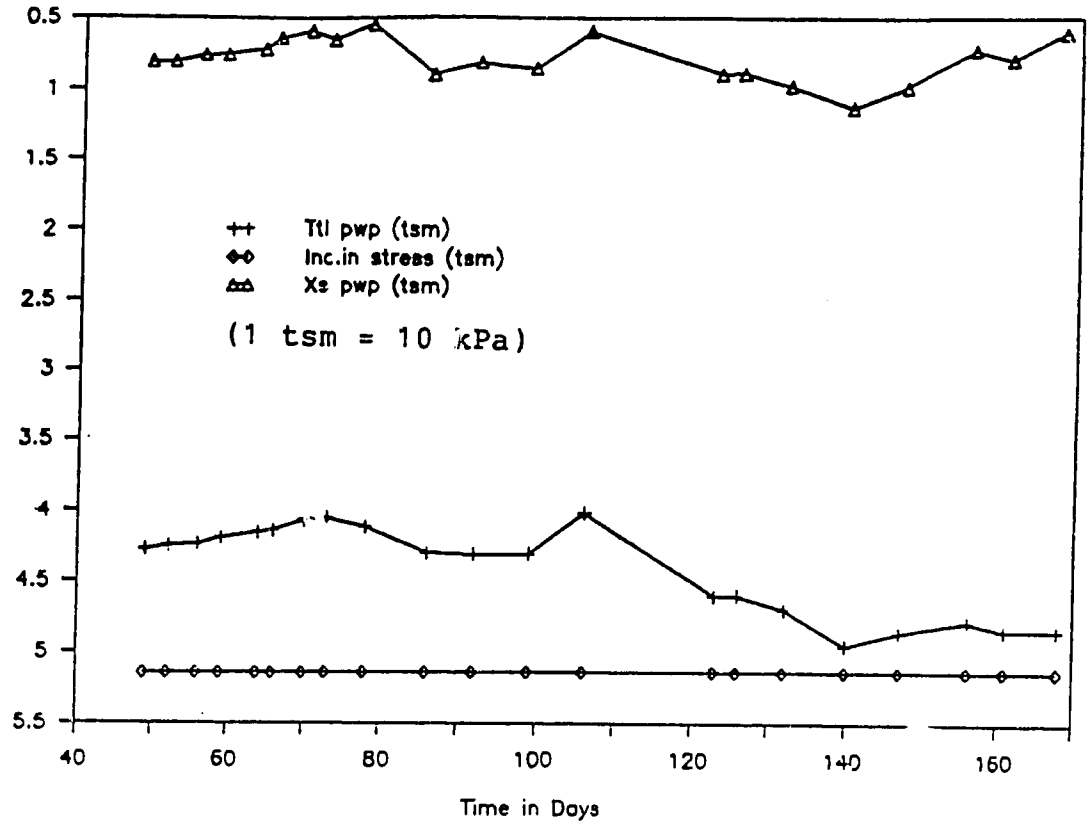

Fig. 64 Porewater Pressures From Hydraulic Piezometer H1 at 5 m Depth Below the Surface After Construction

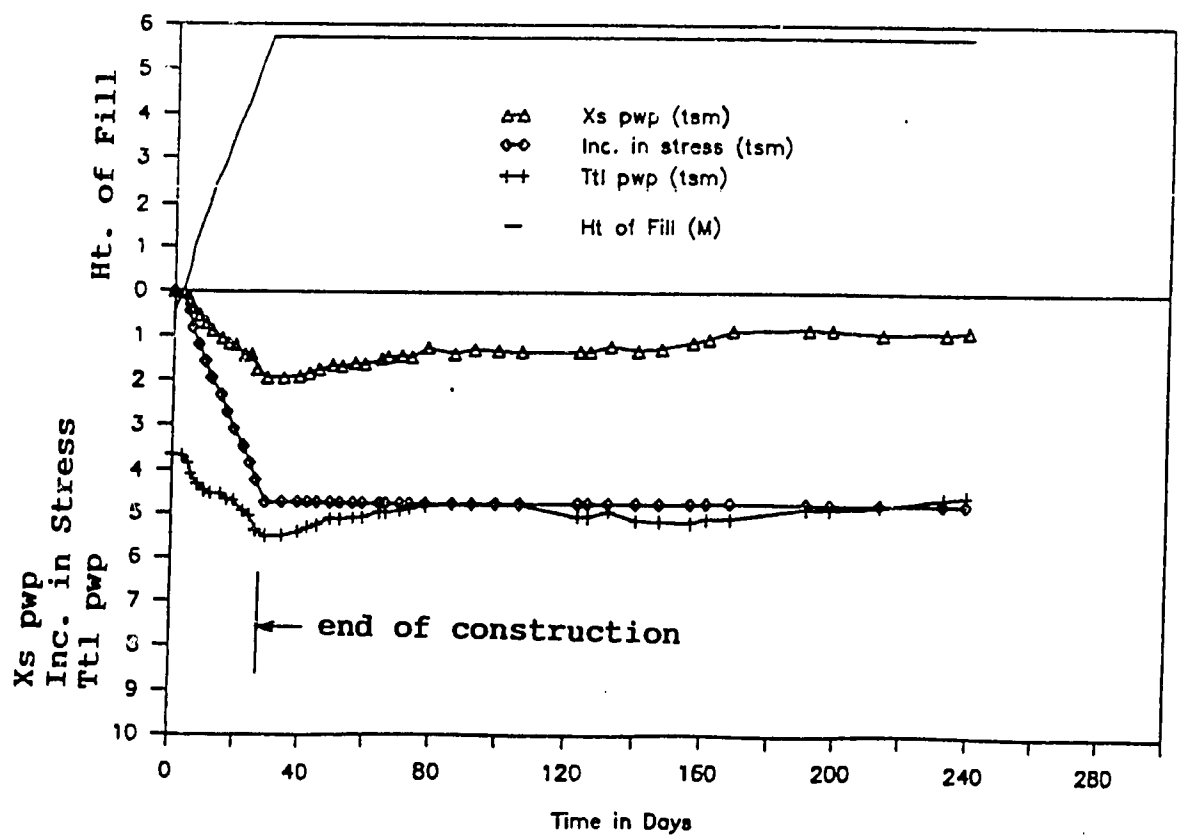

Fig. 65 Porewater Pressures From Hydraulic Piezometer H2 at 5 Depth Below the Surface During Construction and Subsequently

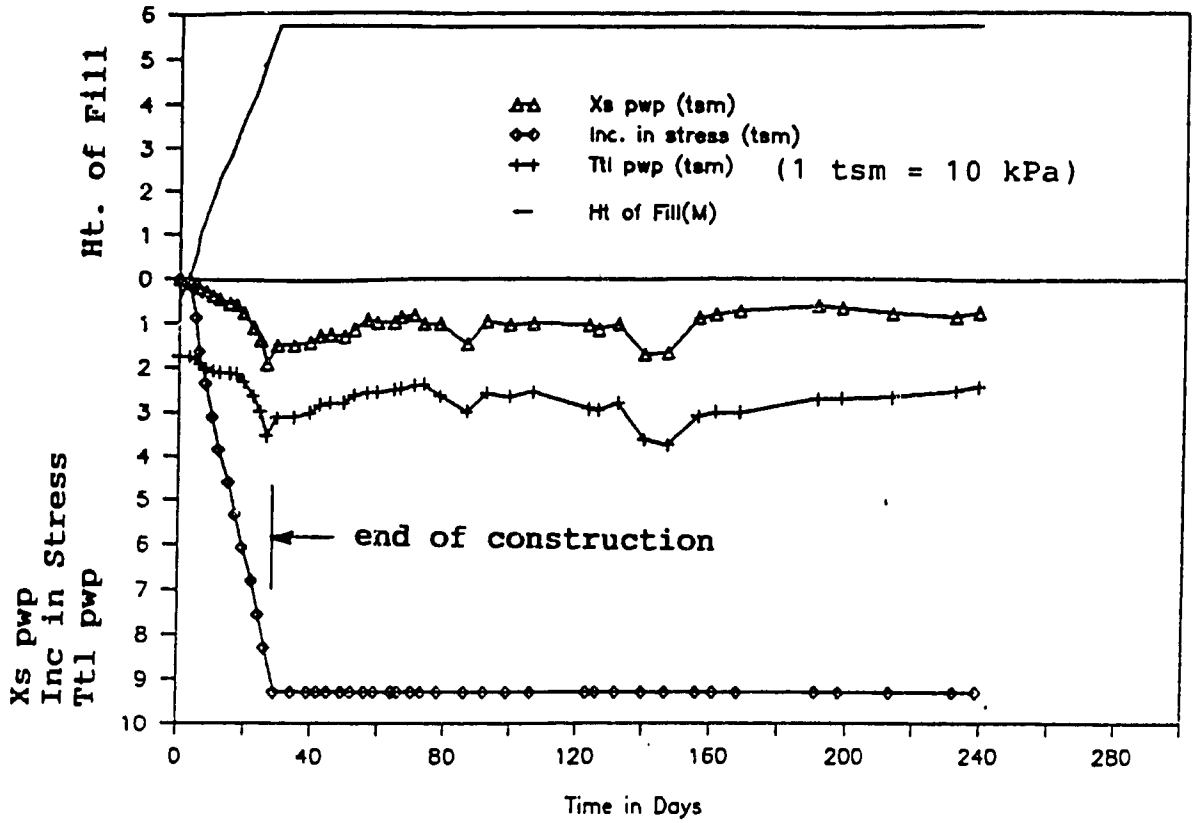

Fig.66 Porewater Pressures From Hydraulic Piezometer H3 at 3 m Depth Below the Surface During Construction and Subsequently

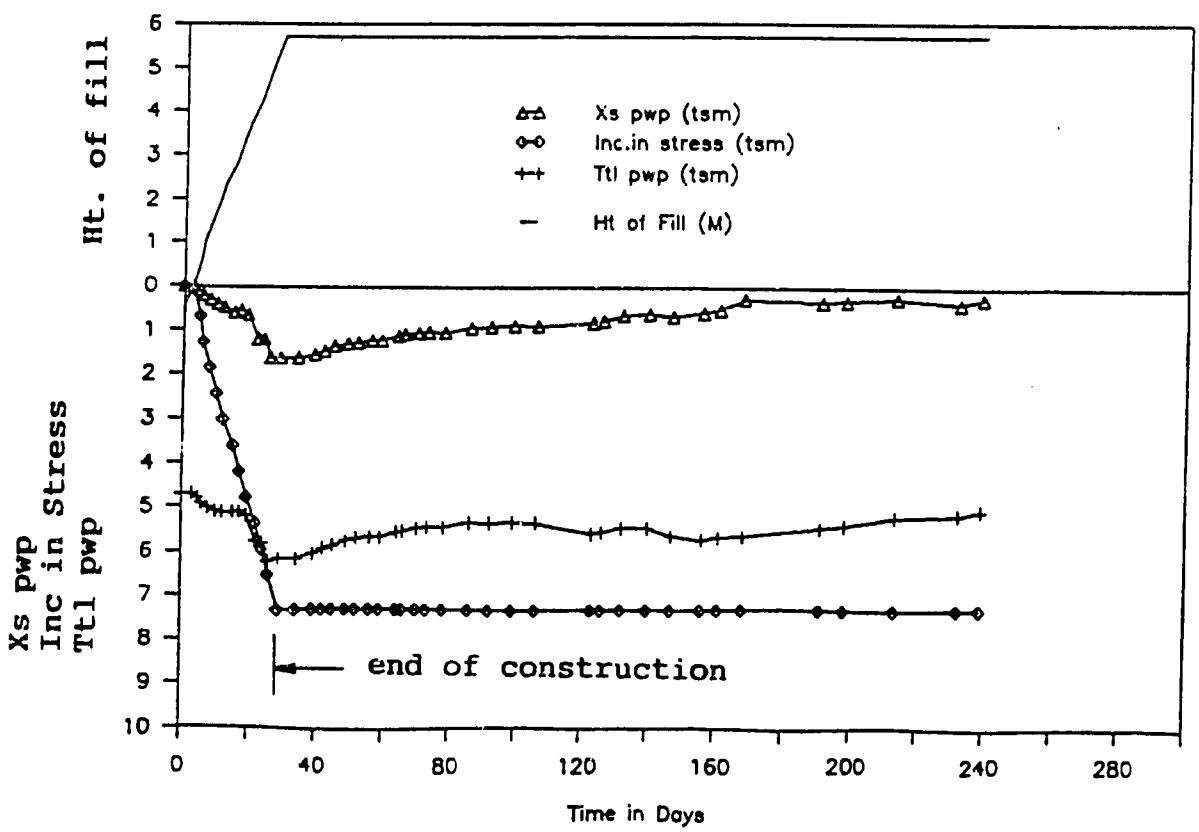

Fig. 67 Porewater Pressures From Hydraulic Piezometer H4 at 6 m Depth Below the Surface During Construction and Subsequently

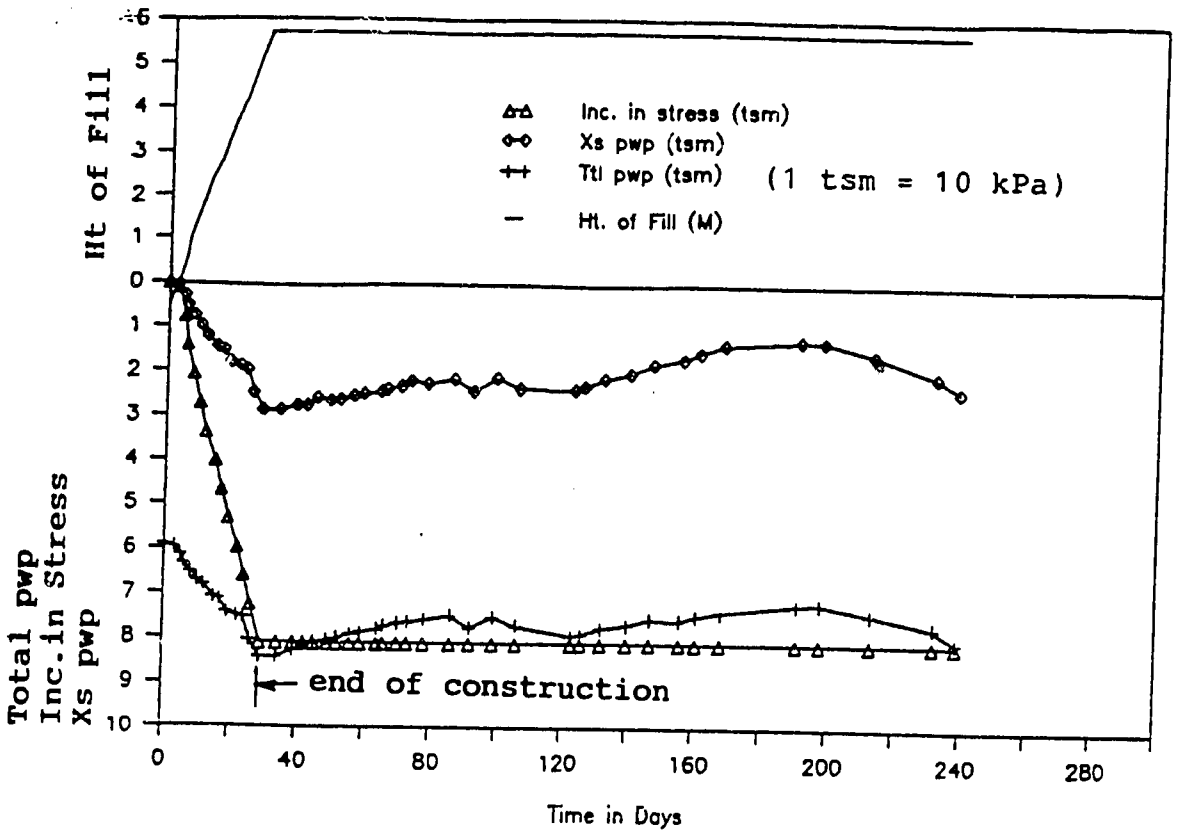

Fig.68 Porewater Pressures From Hydraulic Piezometer H5 at 7 m Depth Below the Surface During Construction and Subsequently

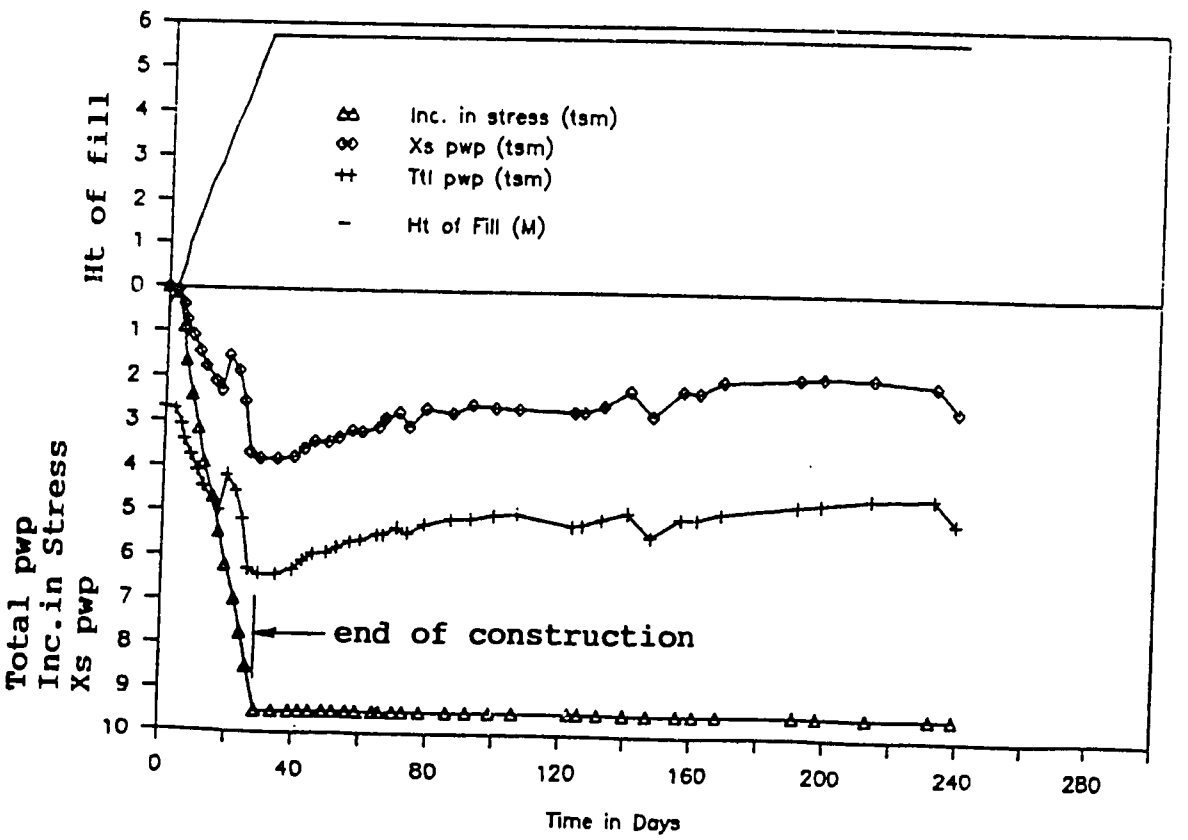

Fig.69 Porewater Pressures From Hydraulic Piezometer H6 at 4 m Depth Below the Surface During Construction and Subsequently

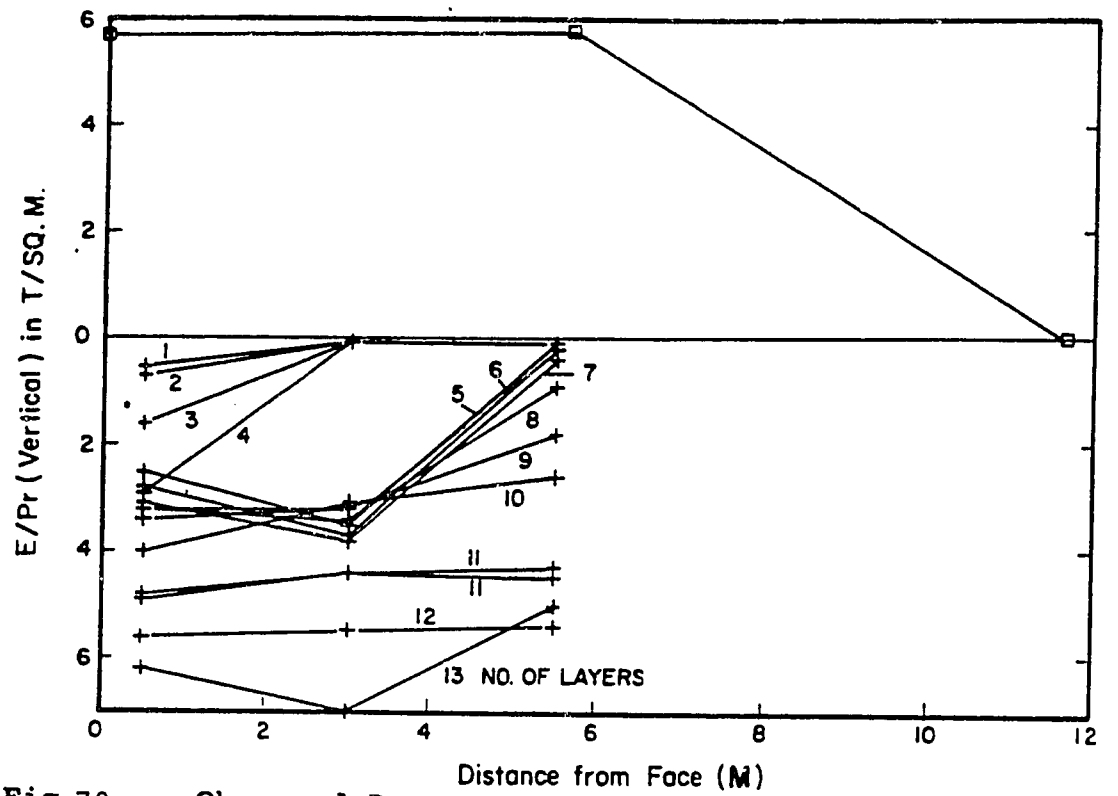

Fig.70 Observed Pressure at the Base of the Wall During Construction Plotted With Distance From the Face of the Wall

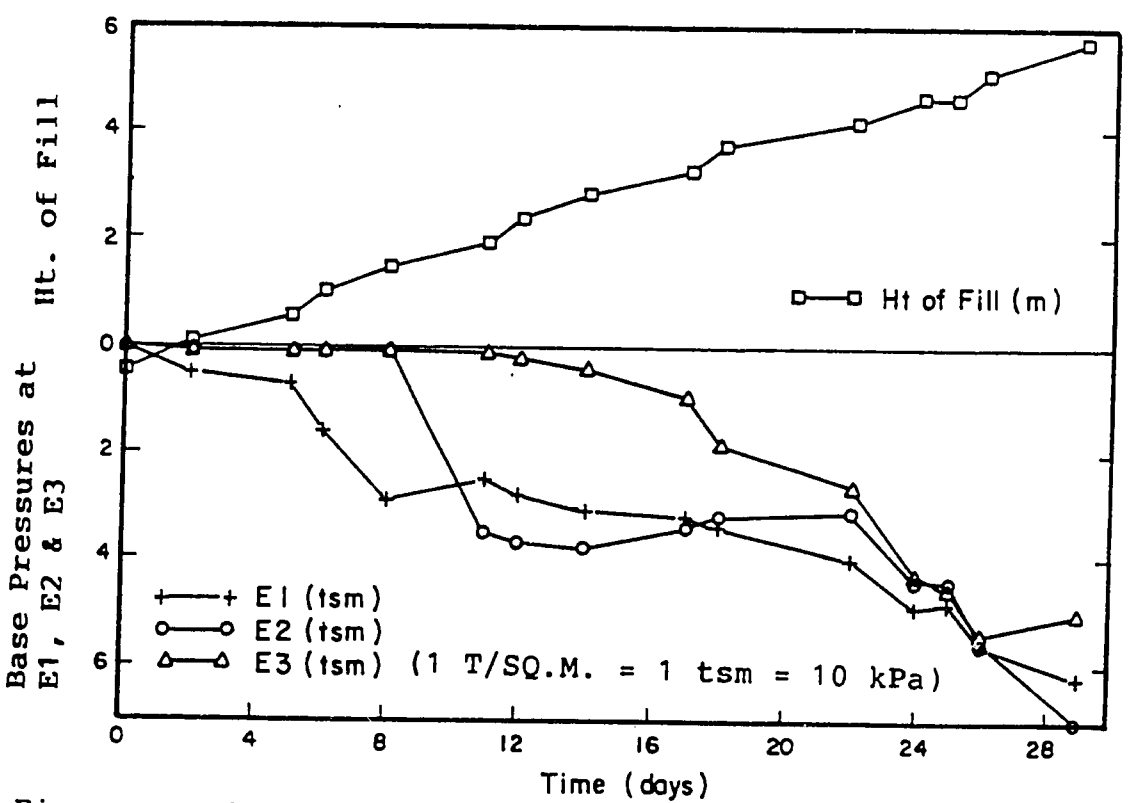

Fig. 71 Plots of the Pressure at the Base Wall Against Time During Construction

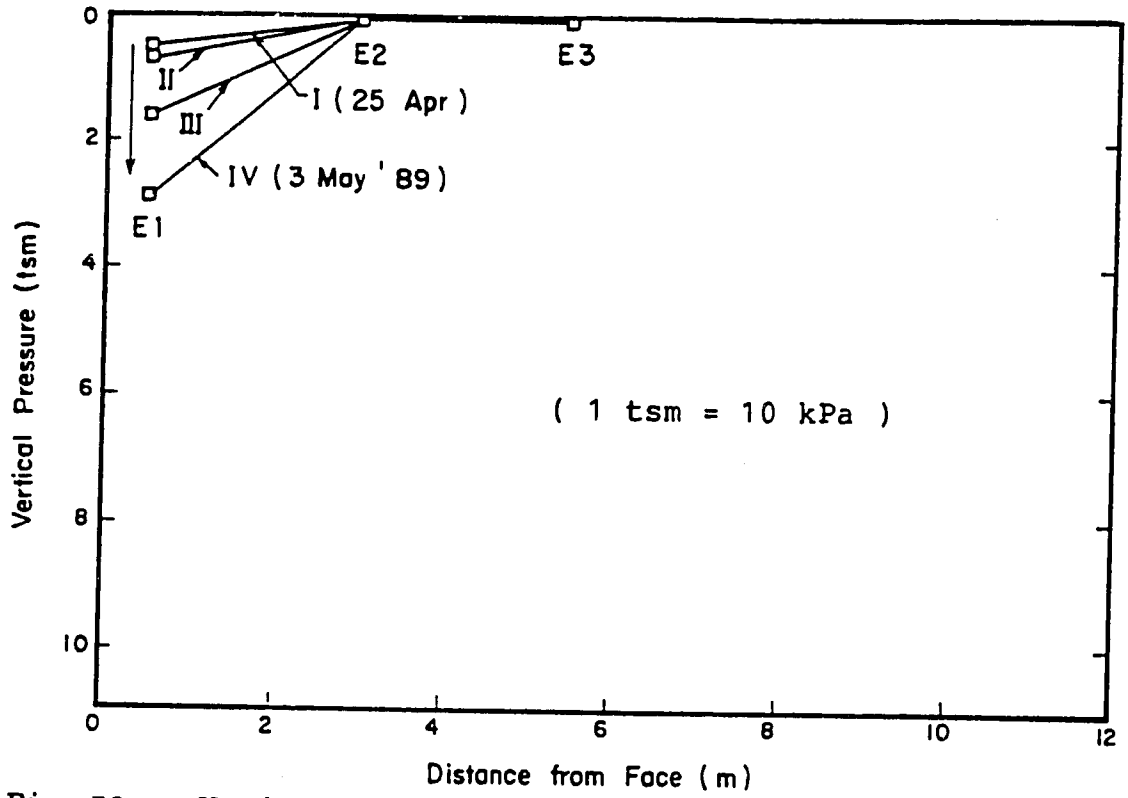

Fig. 72 Variation of Base Pressures With Distance From the Face of the Wall During the Laying of the First Four Layers During Construction

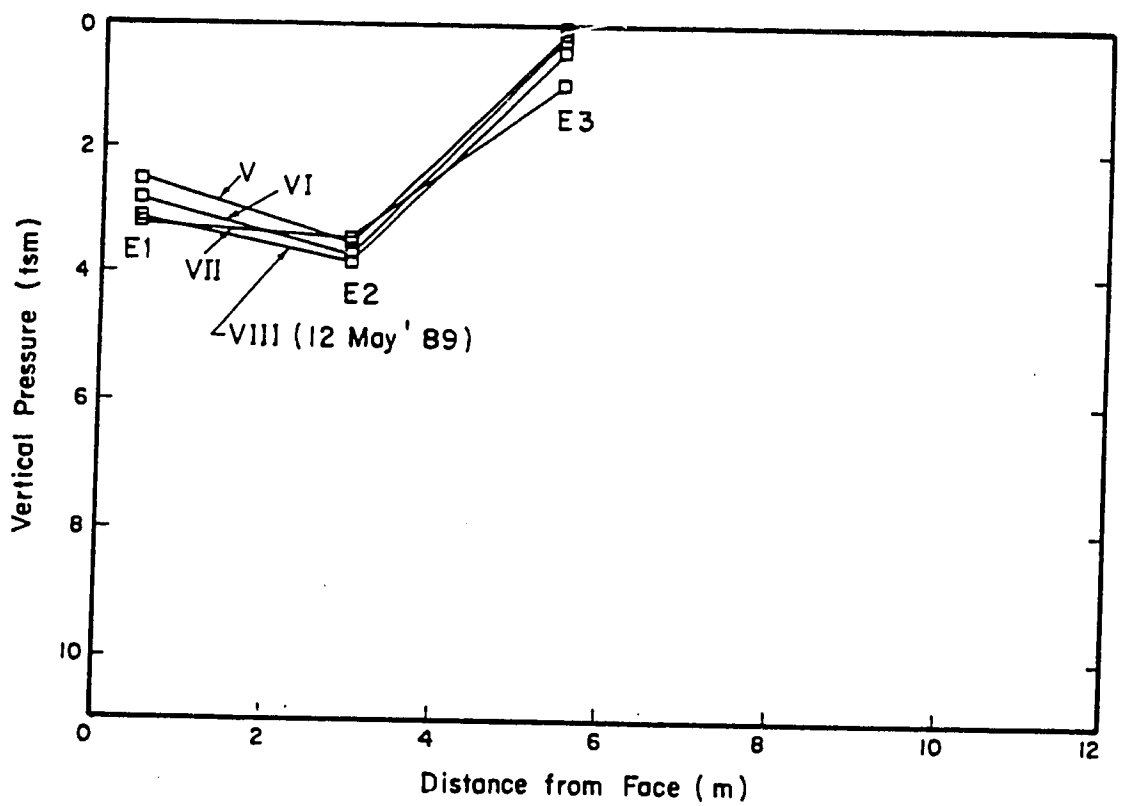

Fig. 73 Variation of Base Pressures With Distance From the Face of the Wall From the Fifth to the Eighth Layers During Construction

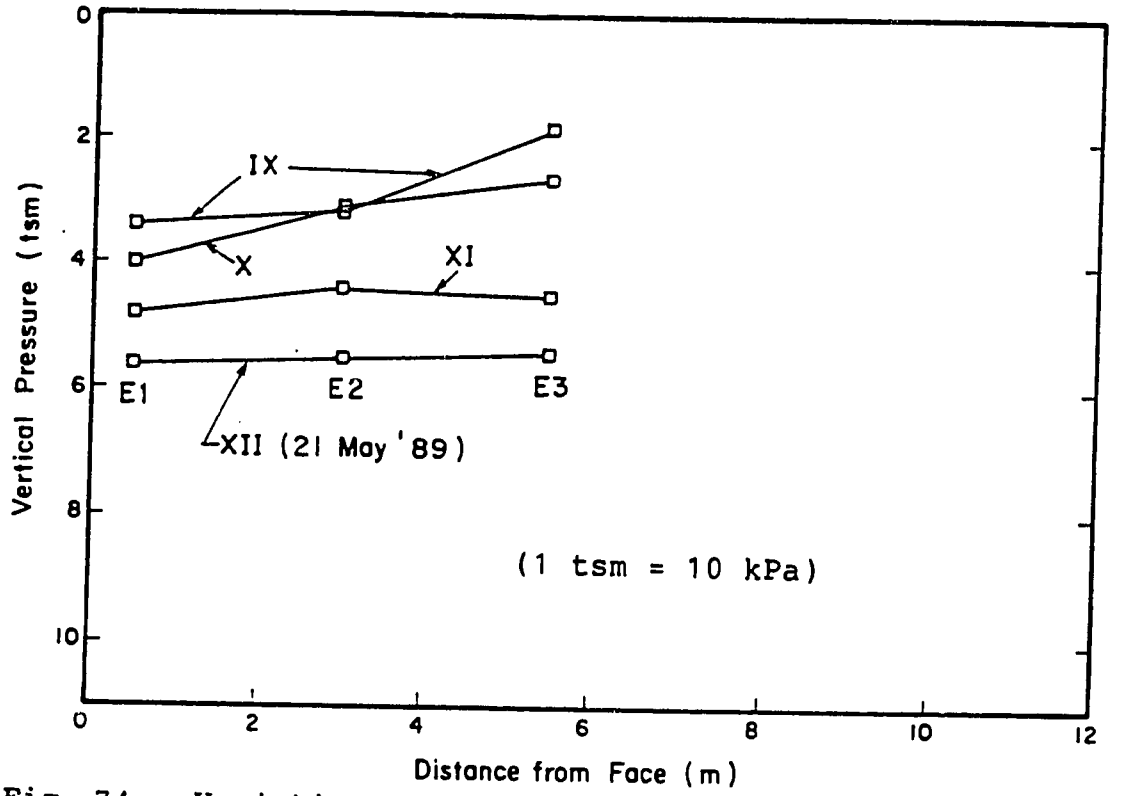

Fig. 74 Variation of Base Pressures With Distance From the Face of the Wall From the Ninth to the Twelfth Layers During Construction

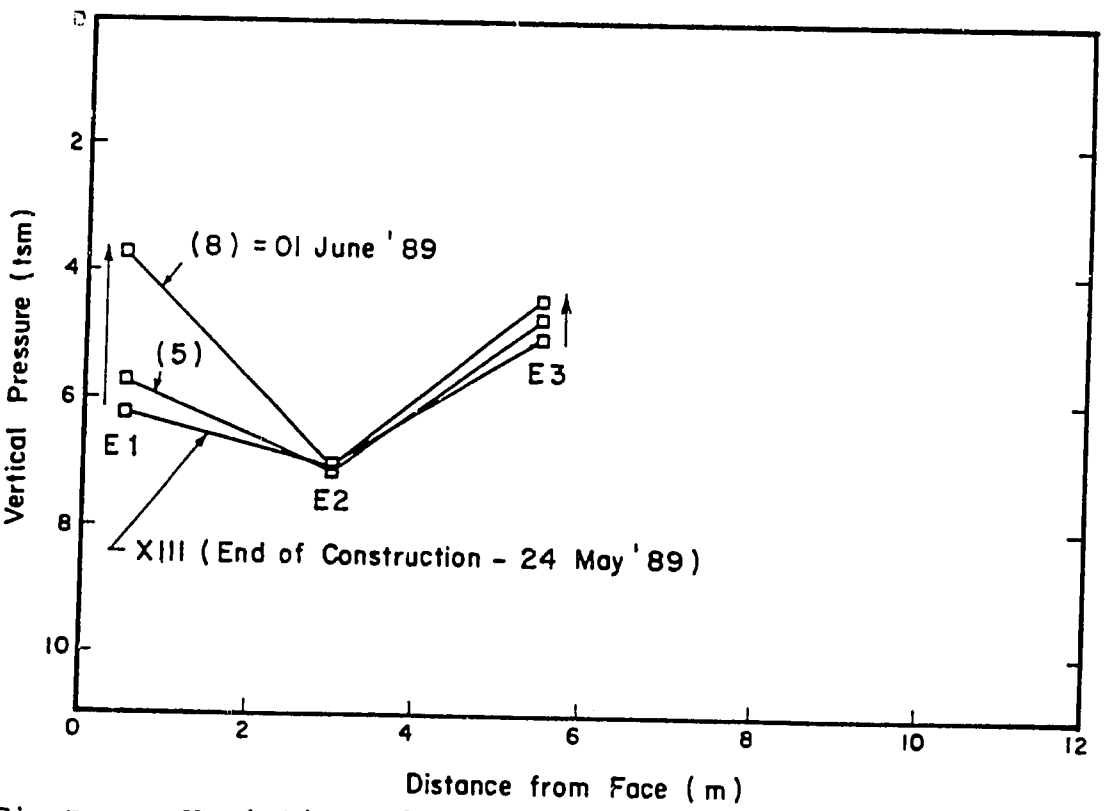

Fig.75 Variation of Base Pressures With Distance From the Face of the Wall Immediately After Construction (13 Layers) and Up To 8 Days Thereafter

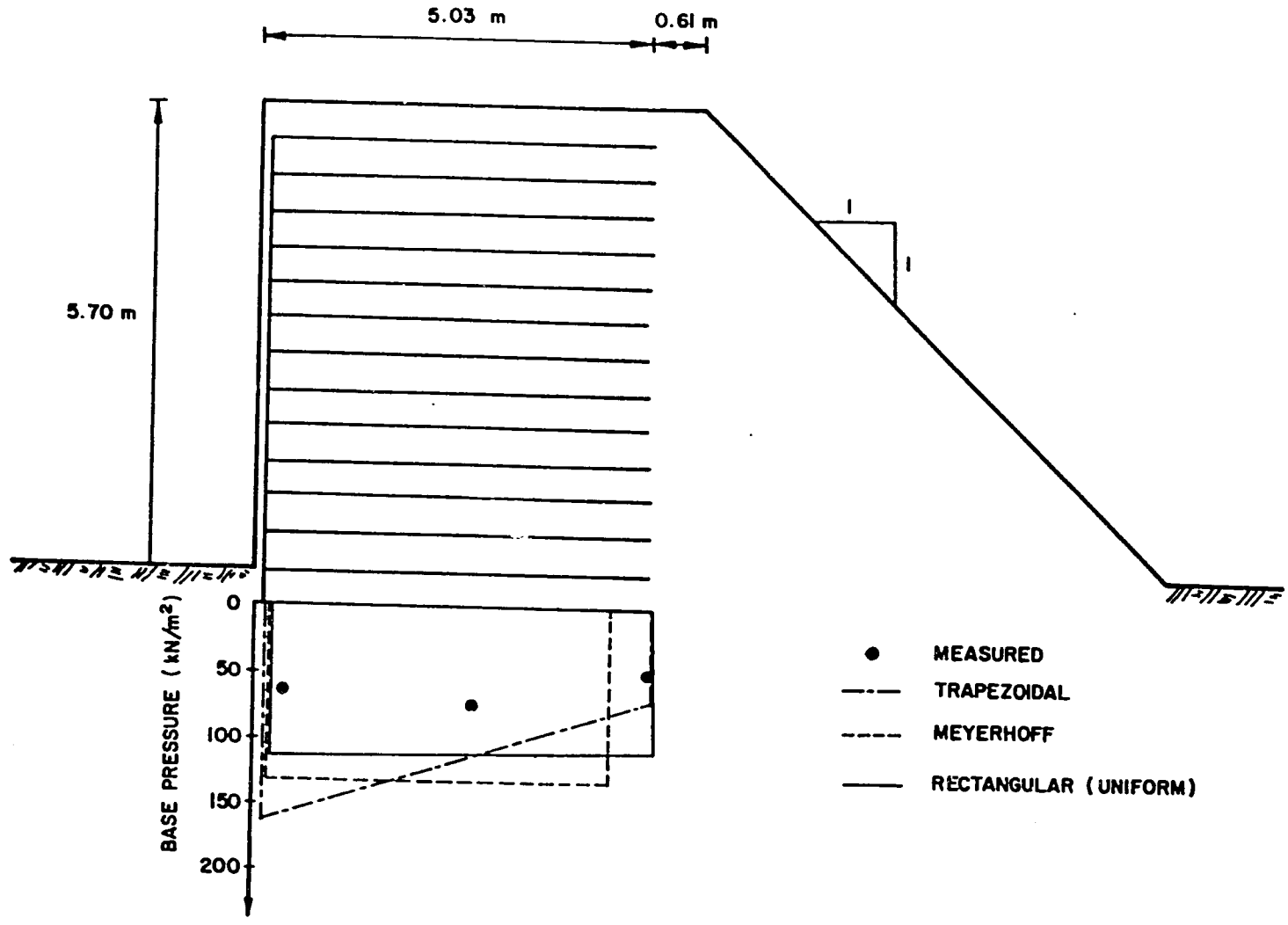

Fig.76 Observed and Predicted Base Pressure Distributions Beneath the Embankment in the Middle Lateritic Section Immediately After Construction

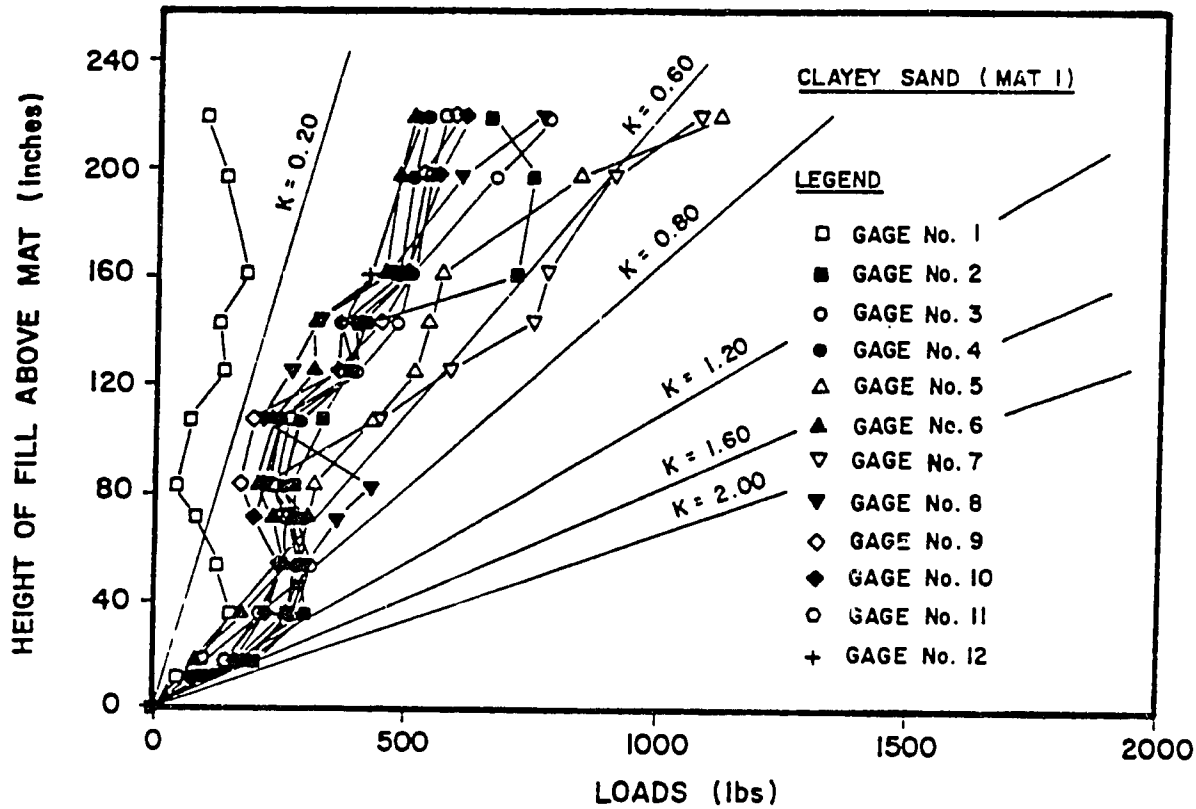

Fig.77 Typical Variations of the Tensile Forces in the Reinforcements During Construction (Clayey Sand)

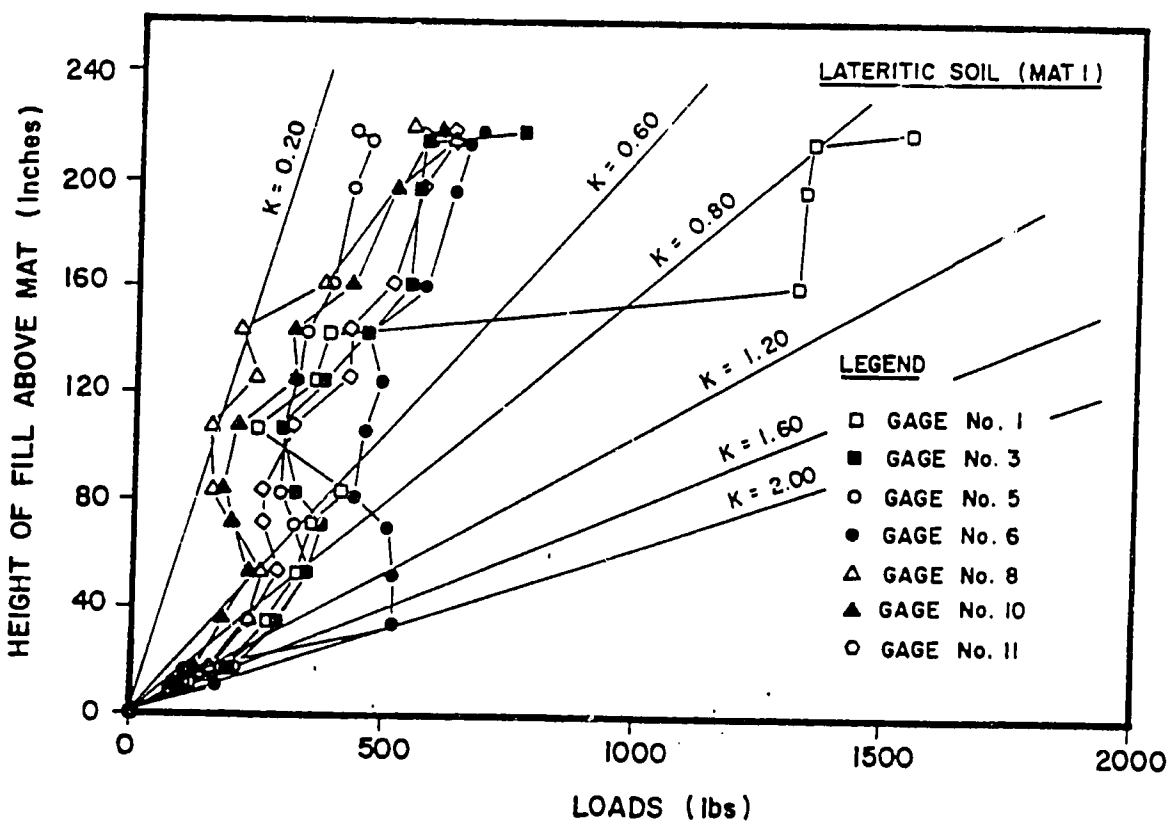

Fig.78 Typical Variations of the Tensile Forces in the Reinforcements During construction (Lateritic Soil)

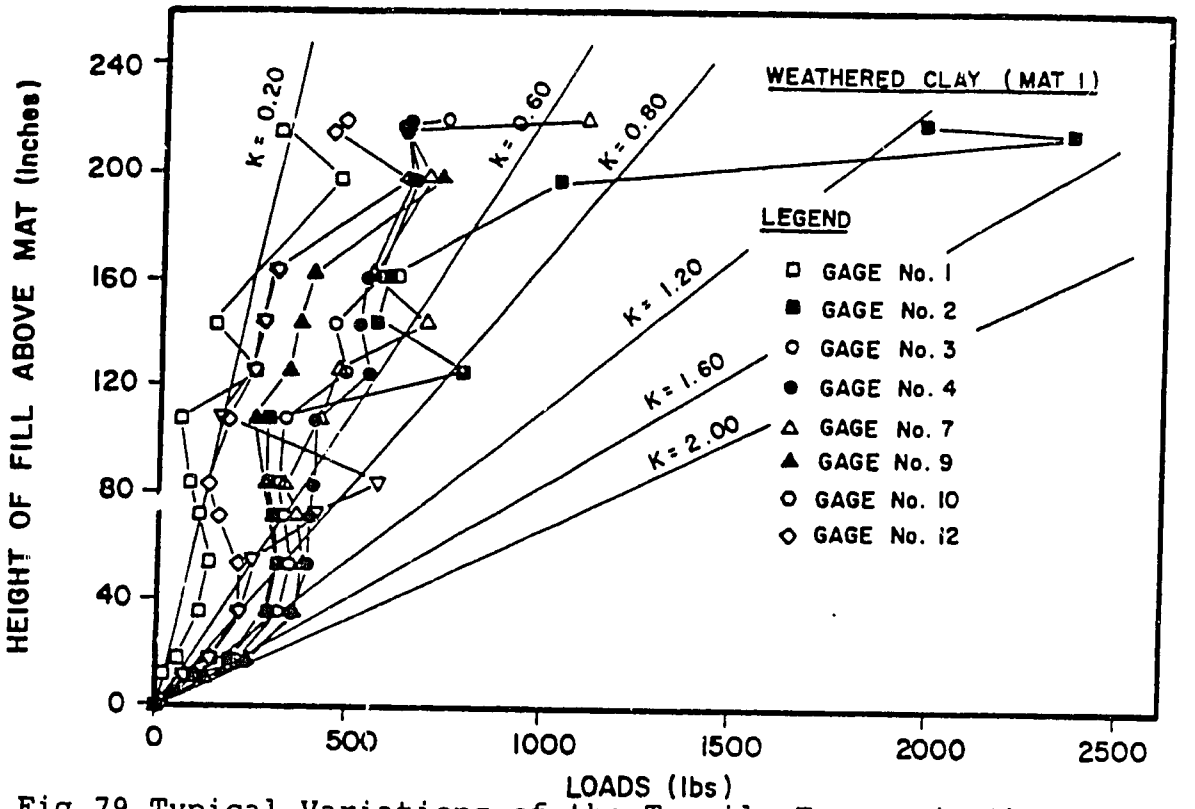

Fig.79 Typical Variations of the Tensile Forces in the Reinforcements During Construction (Weathered Clay)

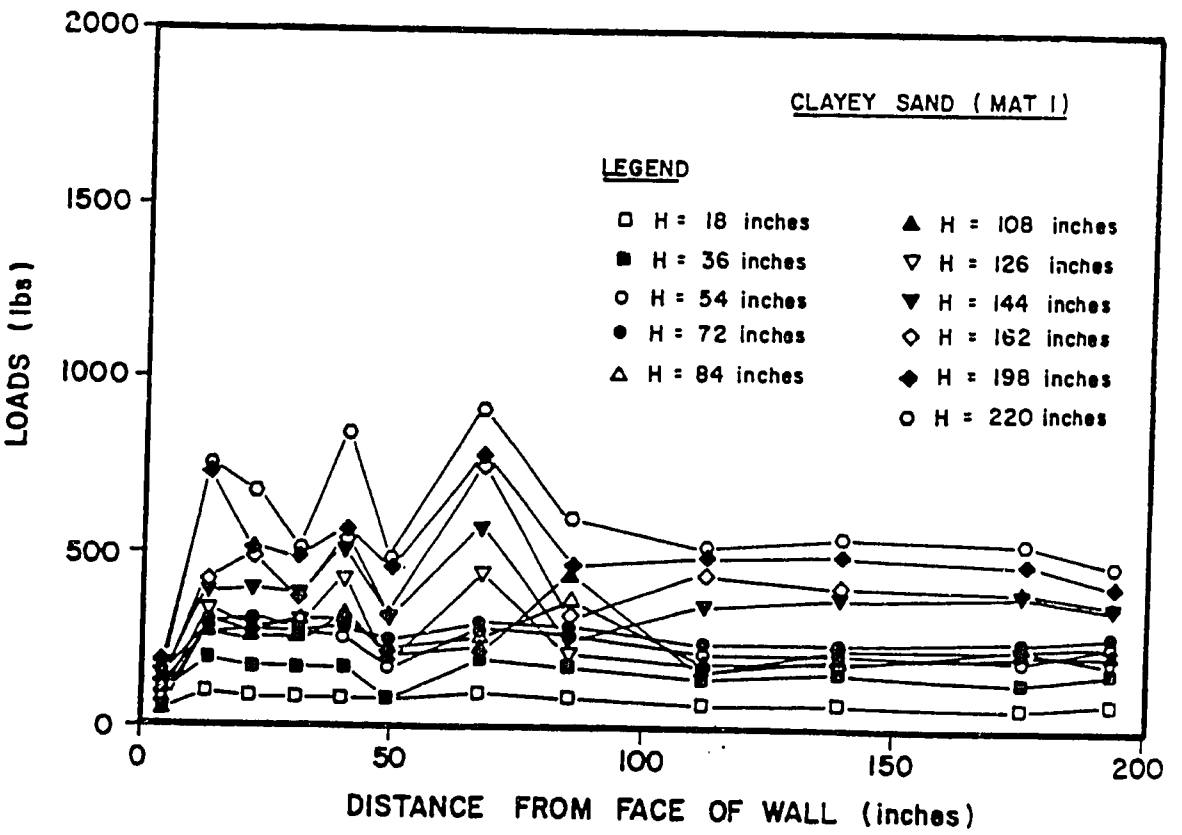

Fig.80 Typical Variations of the Tensile Forces in the Reinforcements With distance From the Face of the Wall During Construction (Clayey Sand)

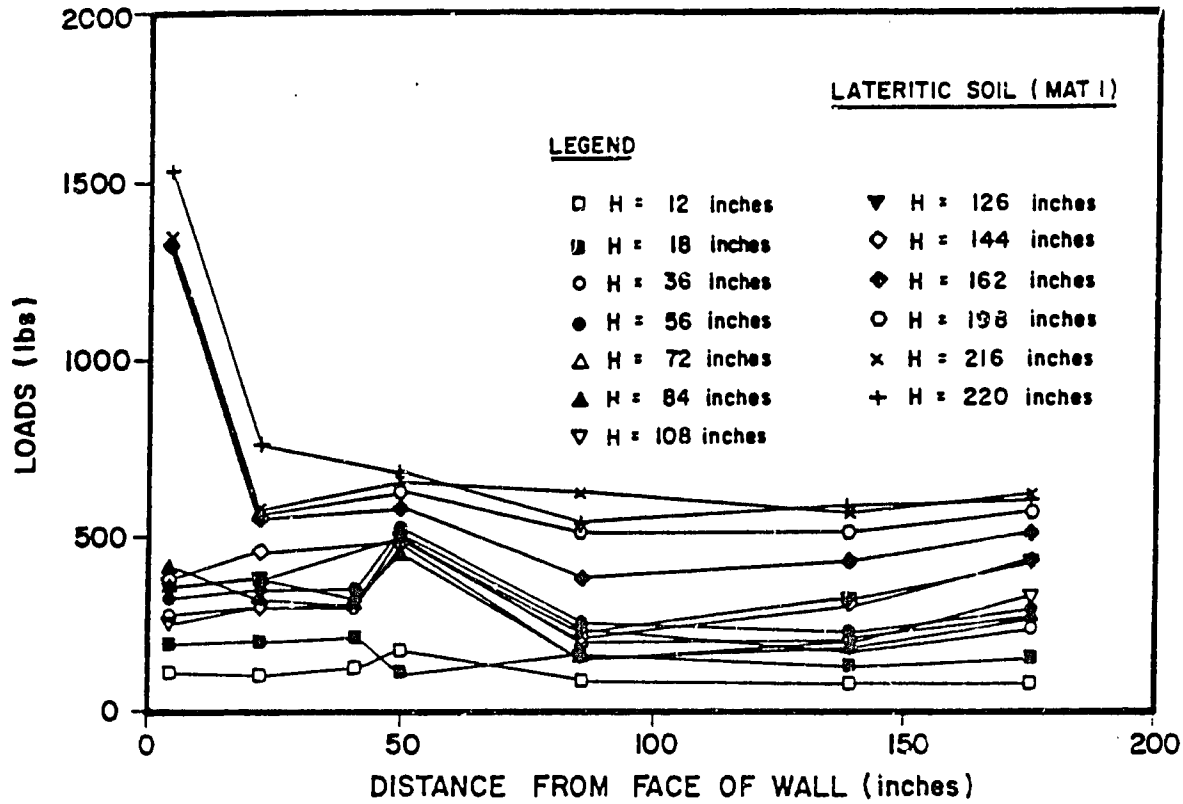

Fig.81 Typical Variations of the Tensile Forces in the Reinforcements with distance From the Face of the Wall During Construction (Lateritic soil)

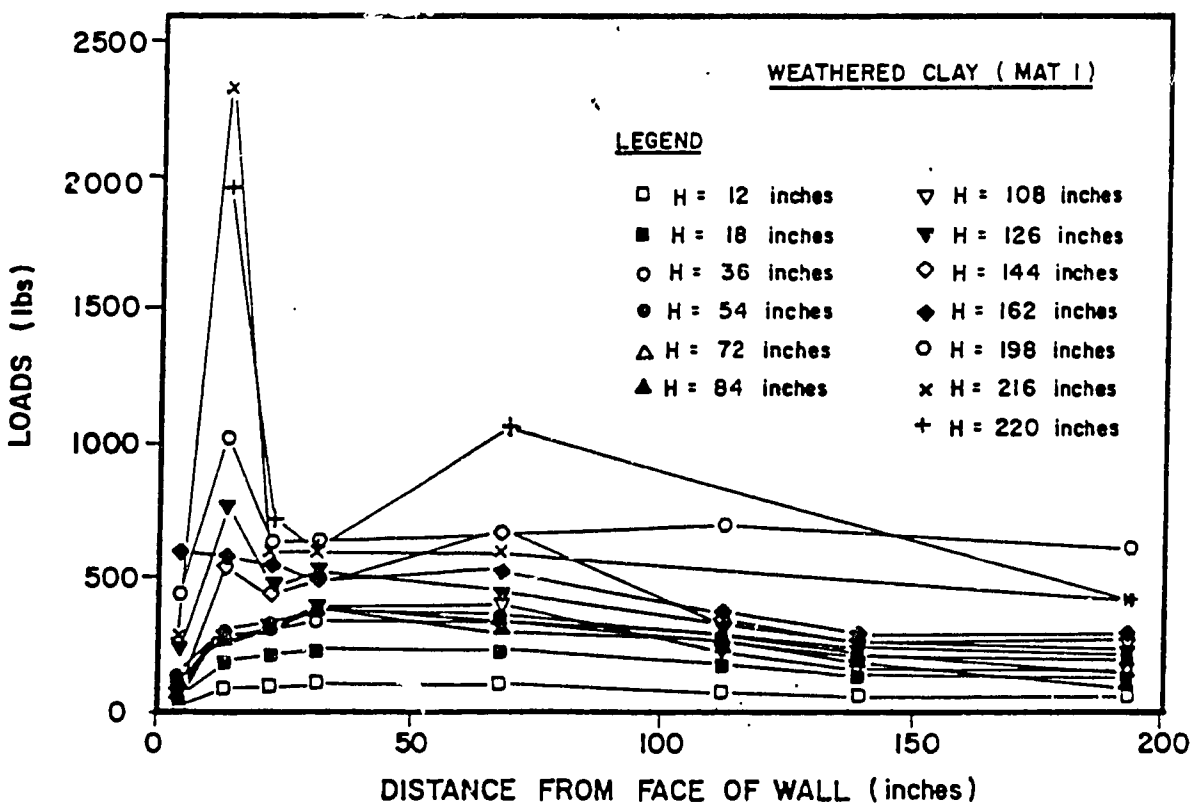

Fig.82 Typical Variations of the Tensile Forces in the Reinforcements With Distance From the Face of the Wall During Construction (Weathered Clay)

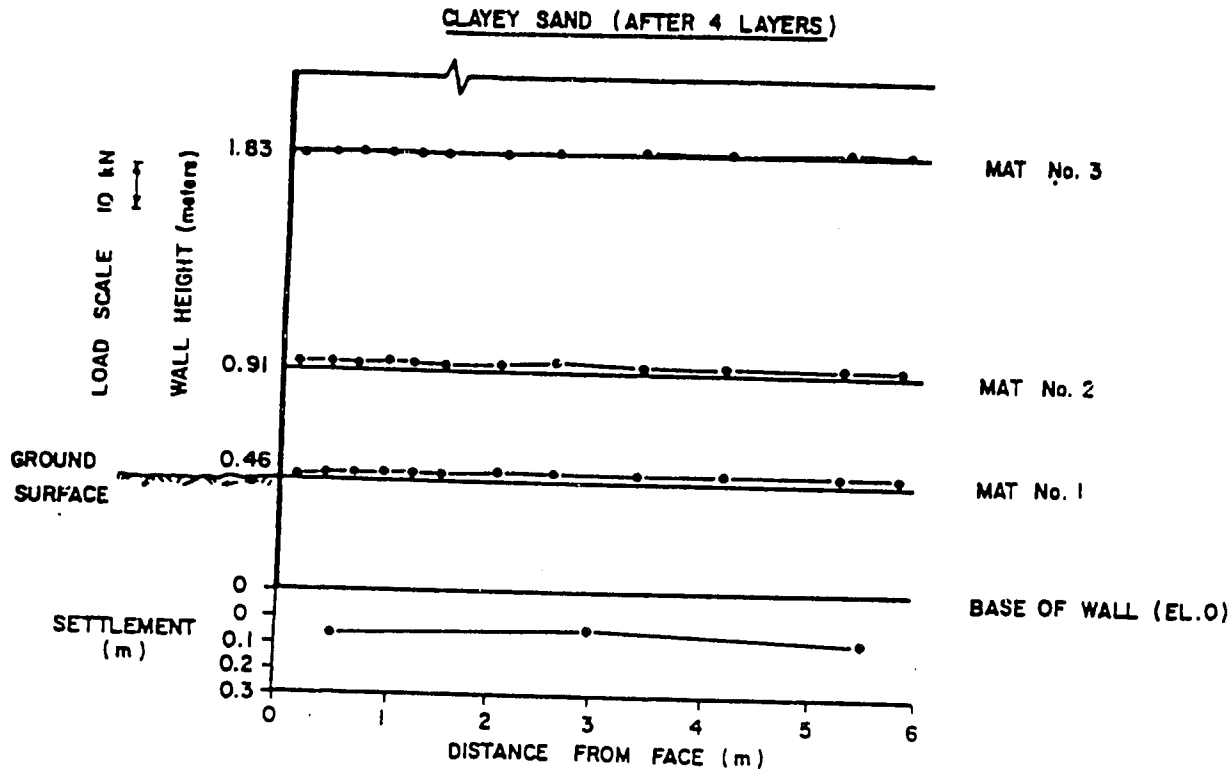

Fig. 83 Reinforcement Tensions During Construction

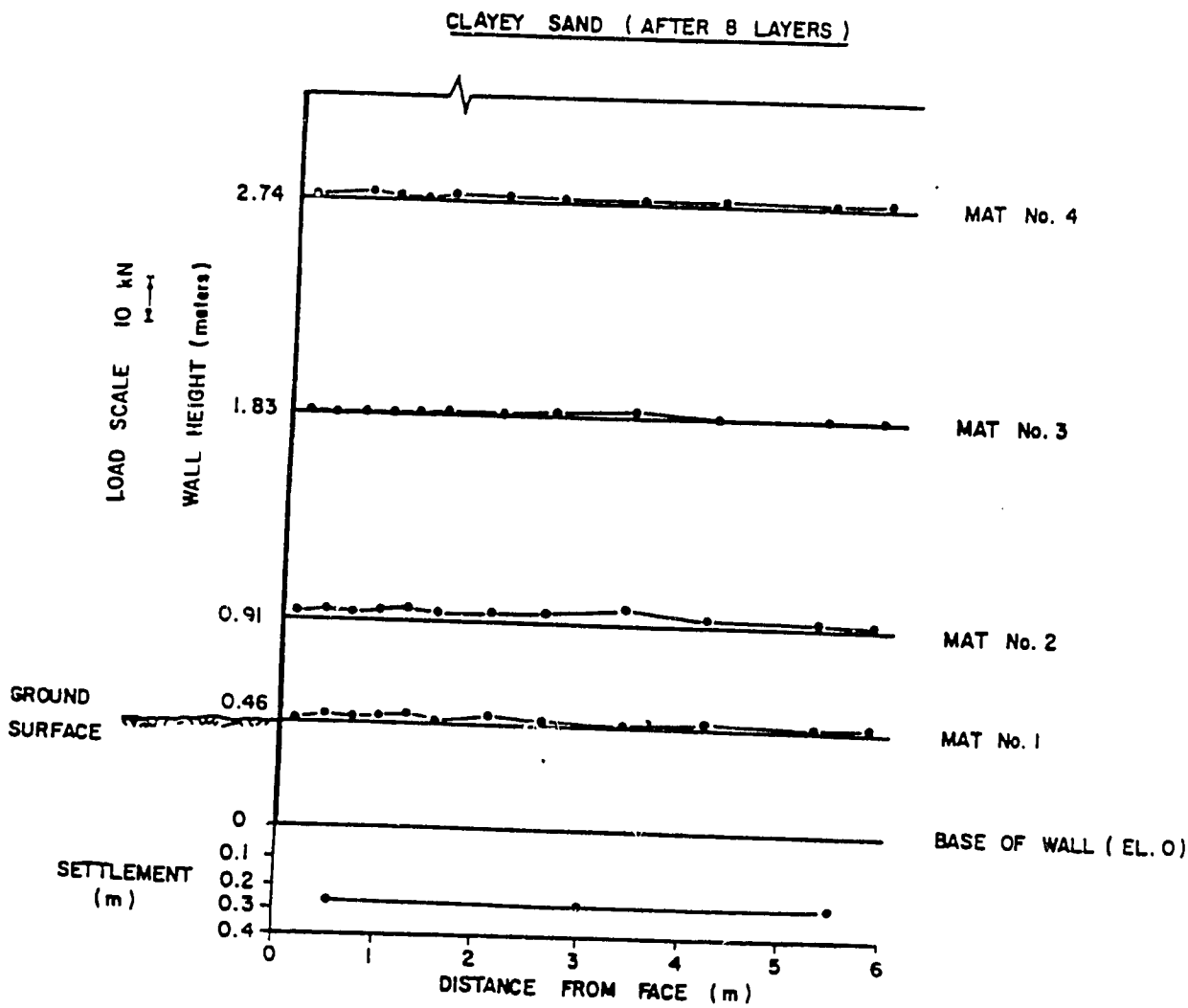

Fig. 84 Reinforcement Tensions During Construction

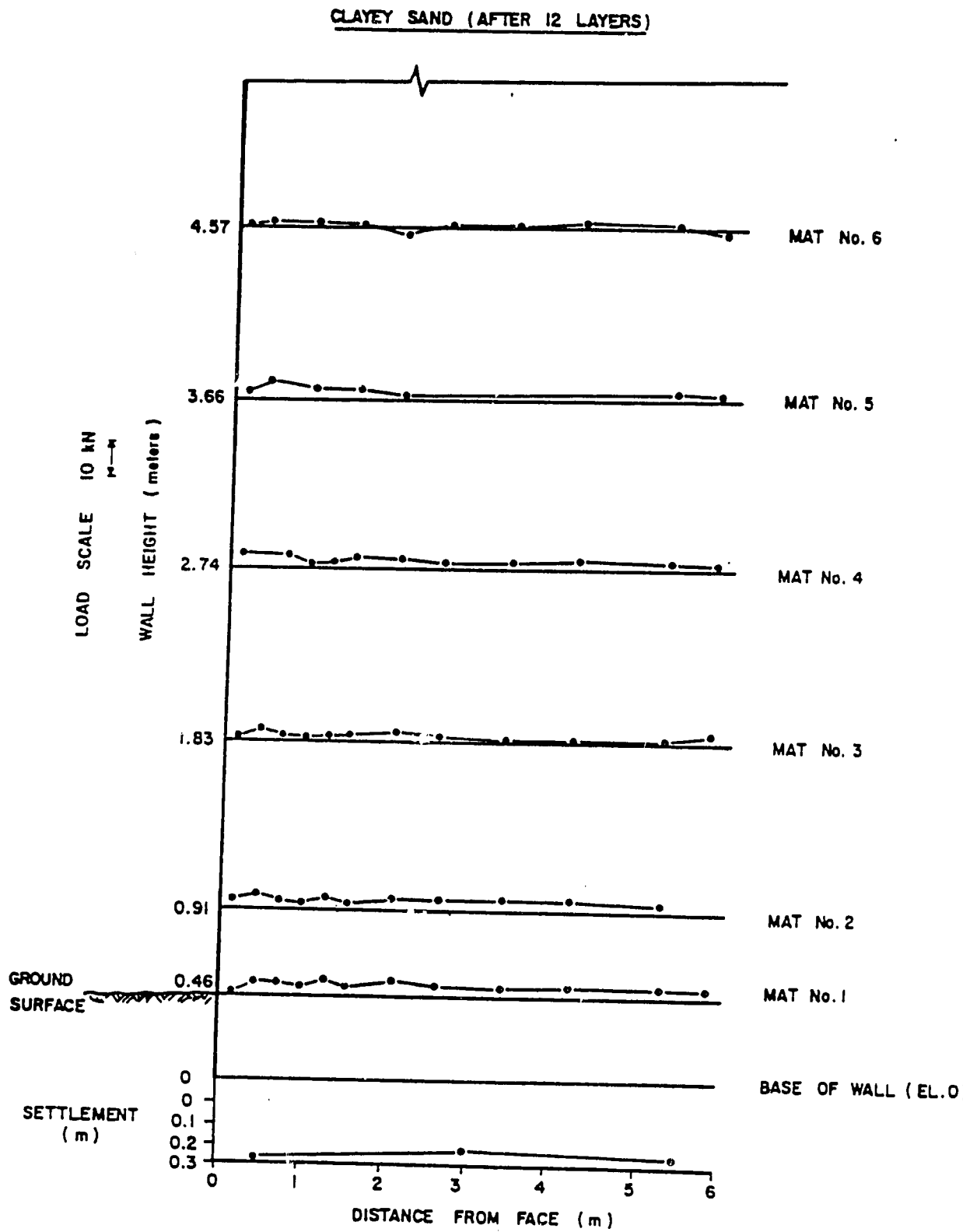

Fig.85 Reinforcement Tensions During Construction

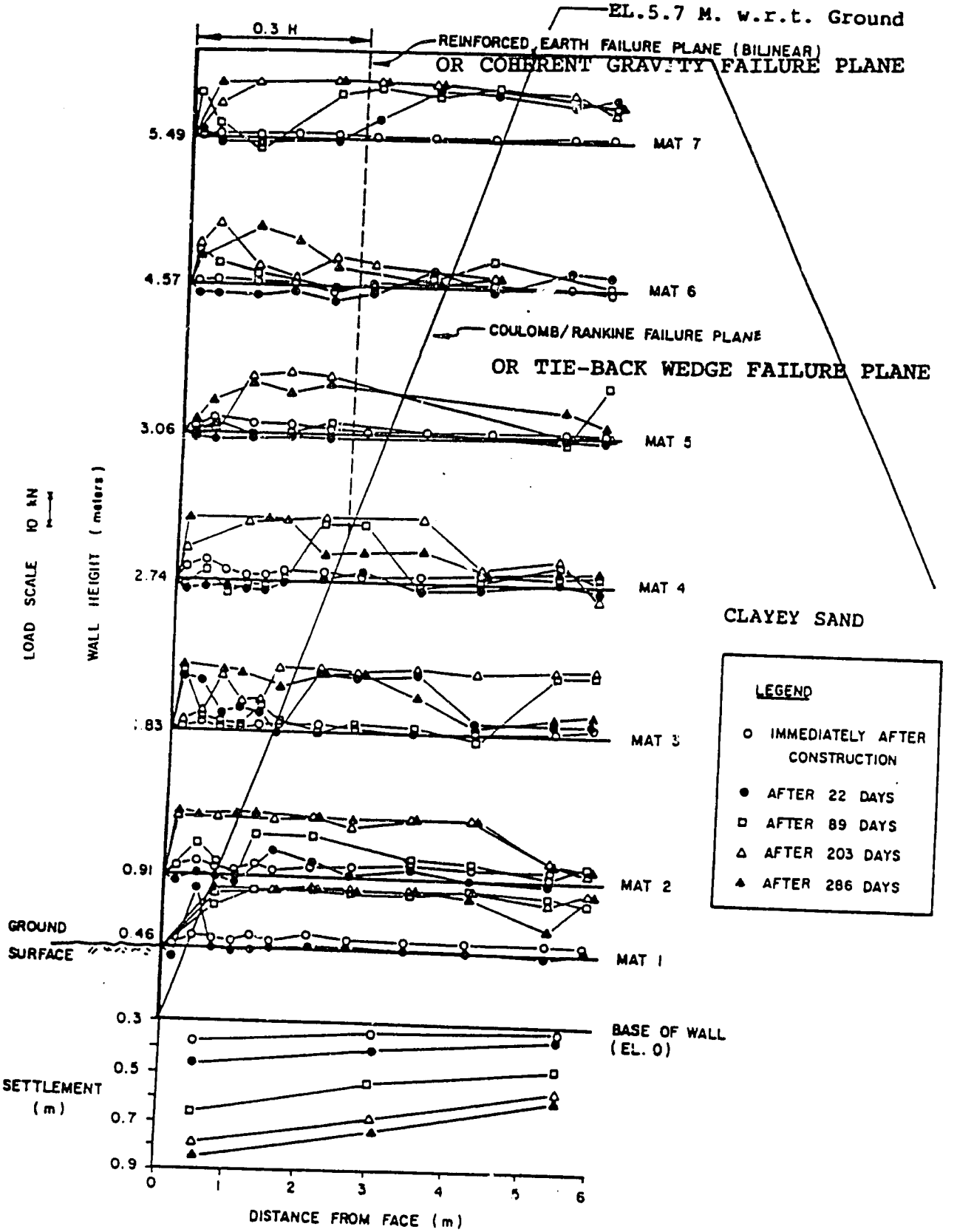

Fig.86 Reinforcement Tensions Immediately and For Four Different Periods After Construction

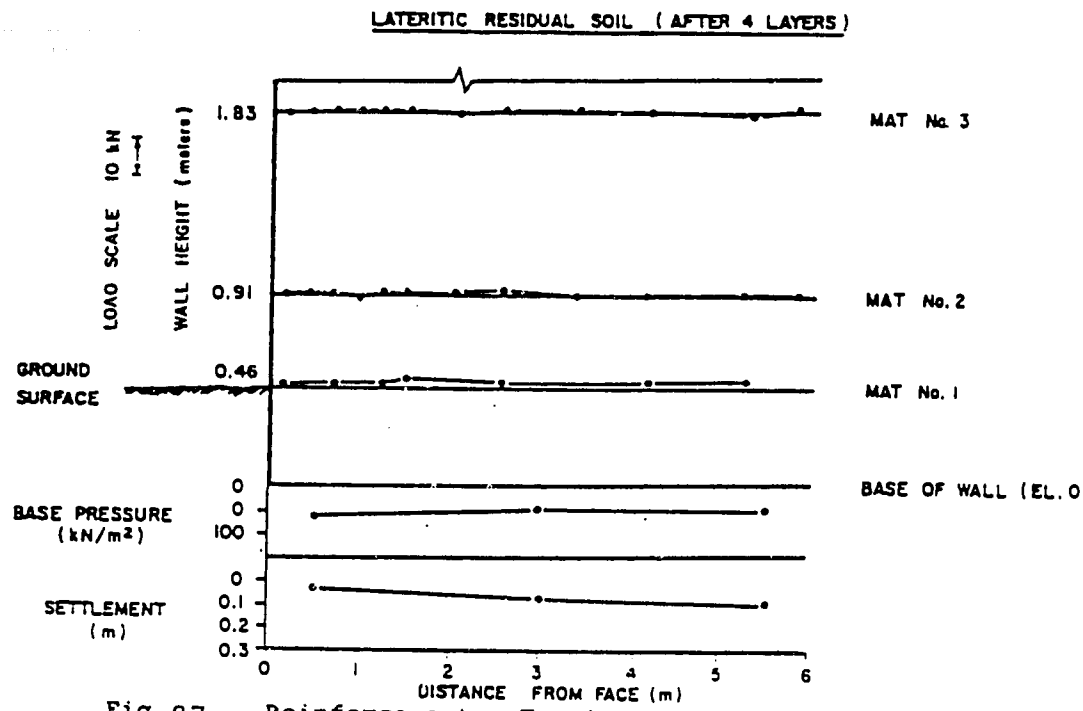

Fig. 87 Reinforcement Tensions During Construction

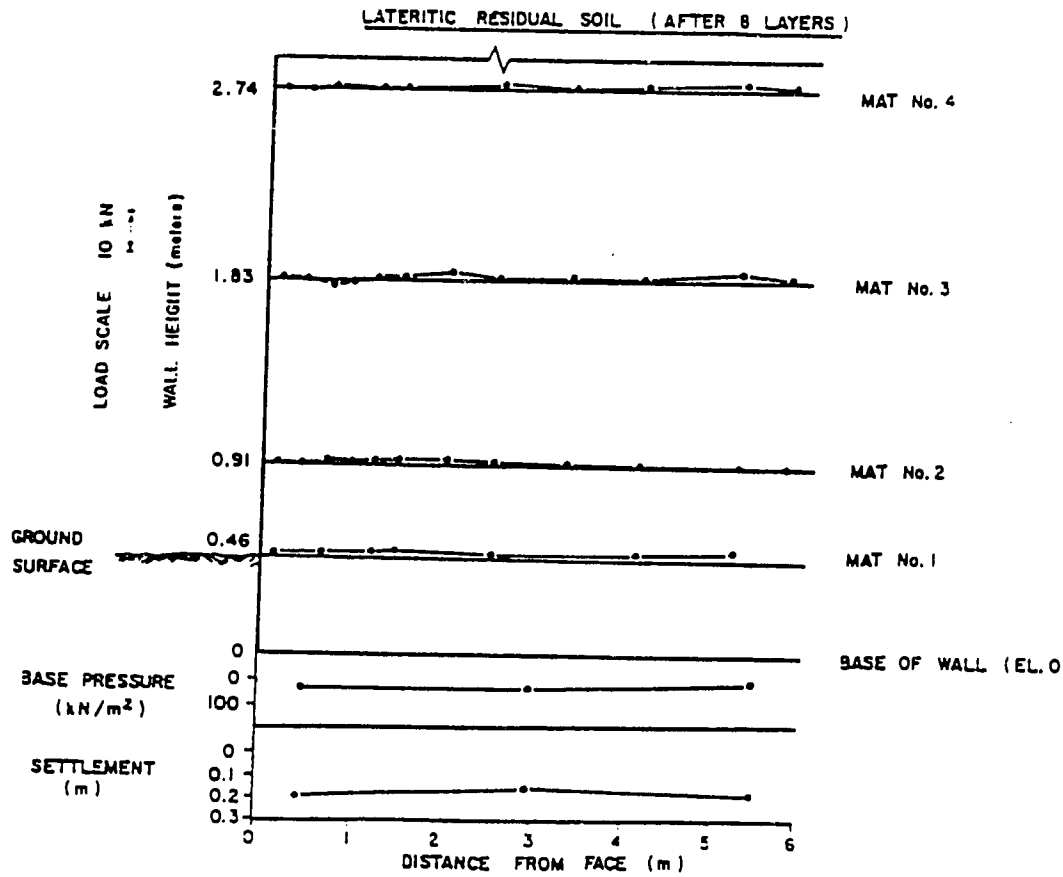

Fig. 88 Reinforcement Tensions During Construction

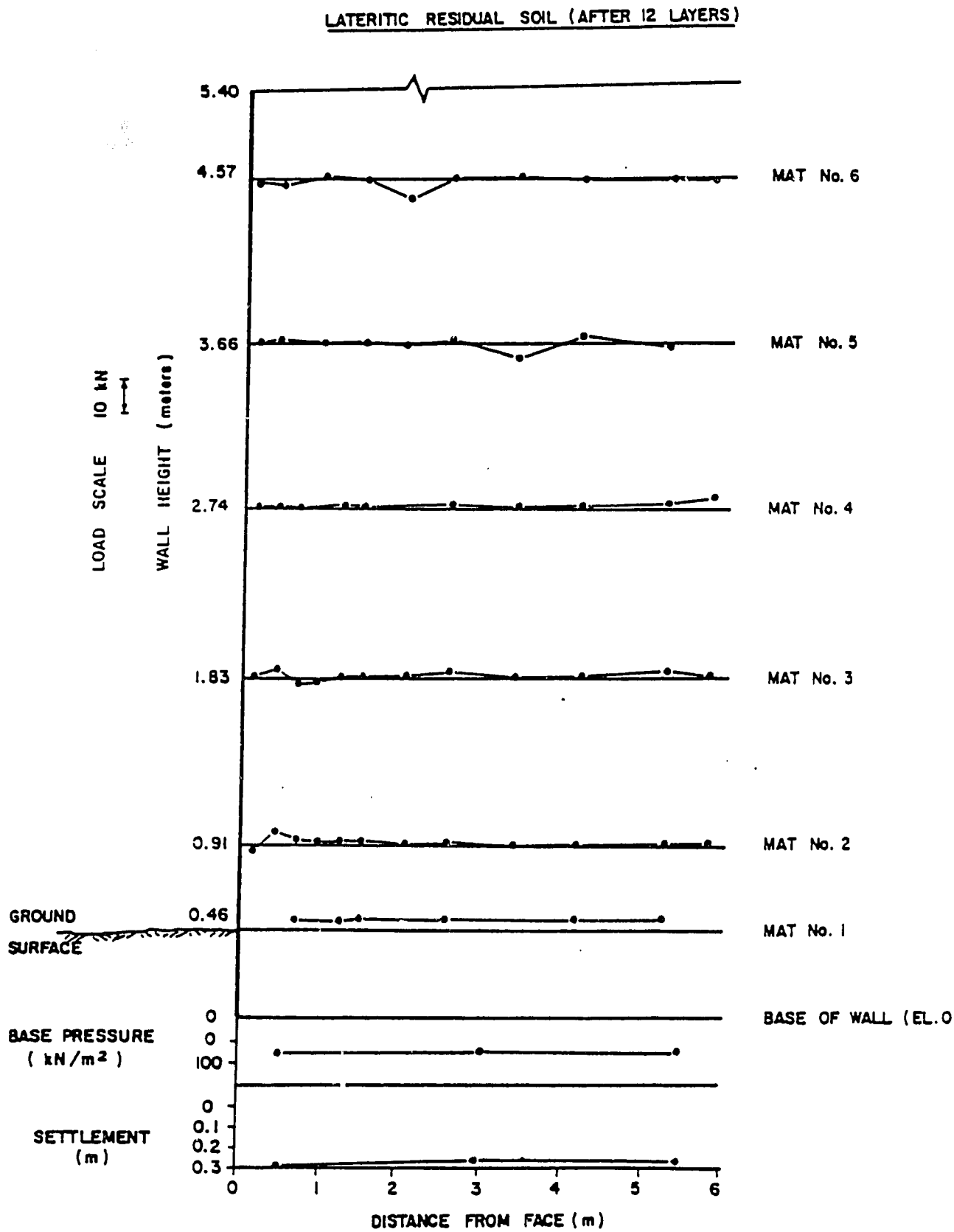

Fig. 89 Reinforcement Tensions During Construction

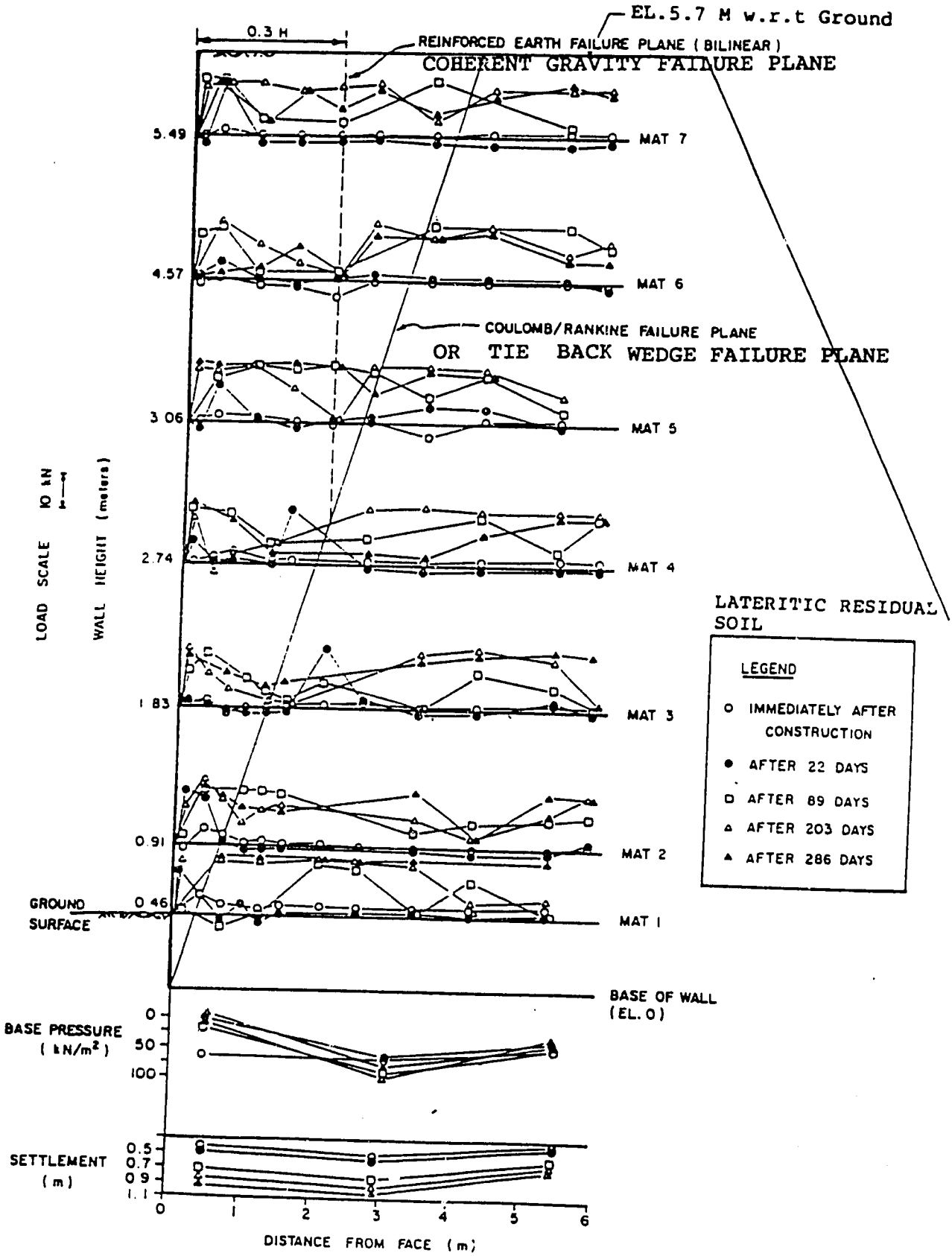

Fig. 90 Reinforcement Tensions Immediately and For Four Different Periods After Construction

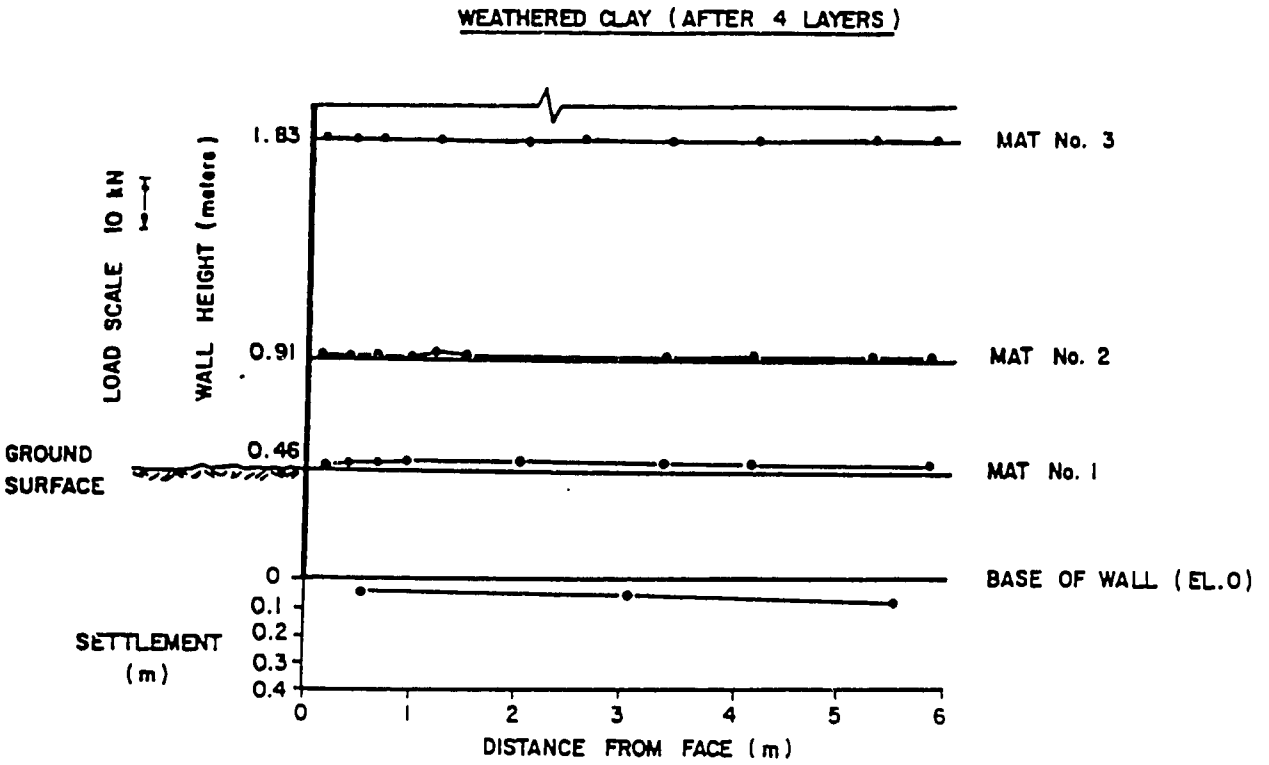

Fig.91 Reinforcement Tensions During Construction

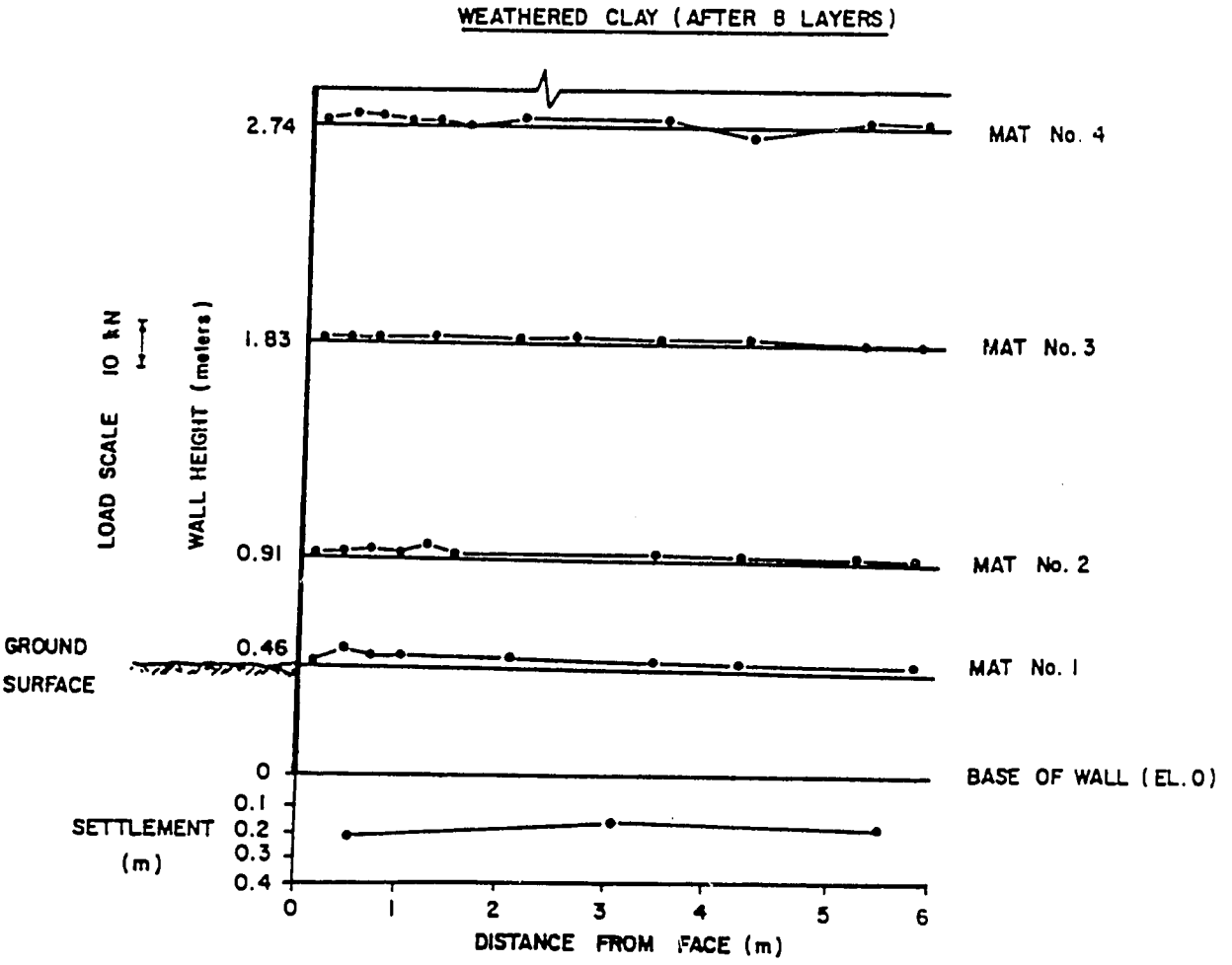

Fig.92 Reinforcement Tensions During Construction

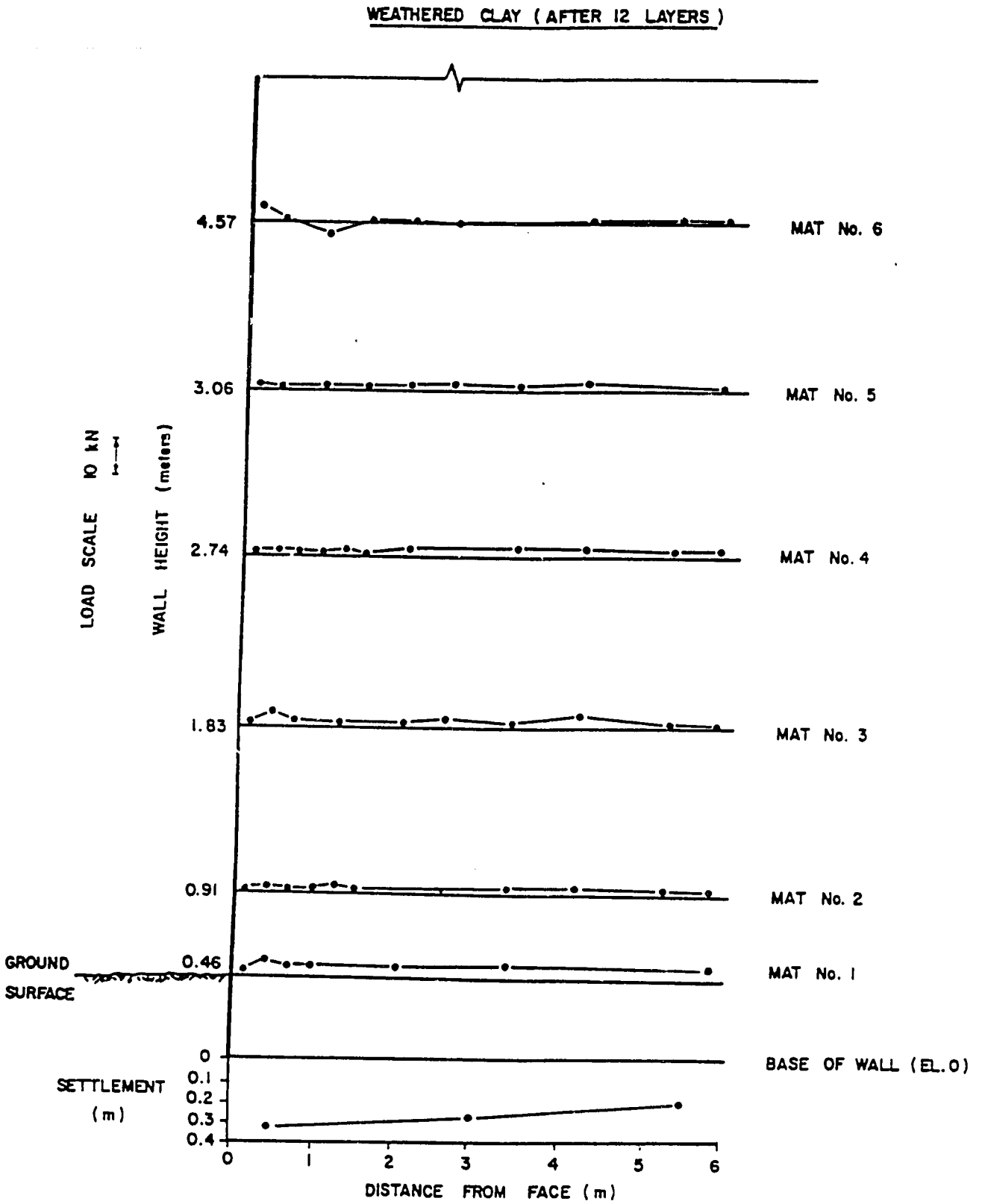

Fig. 93 Reinforcement Tensions During Construction

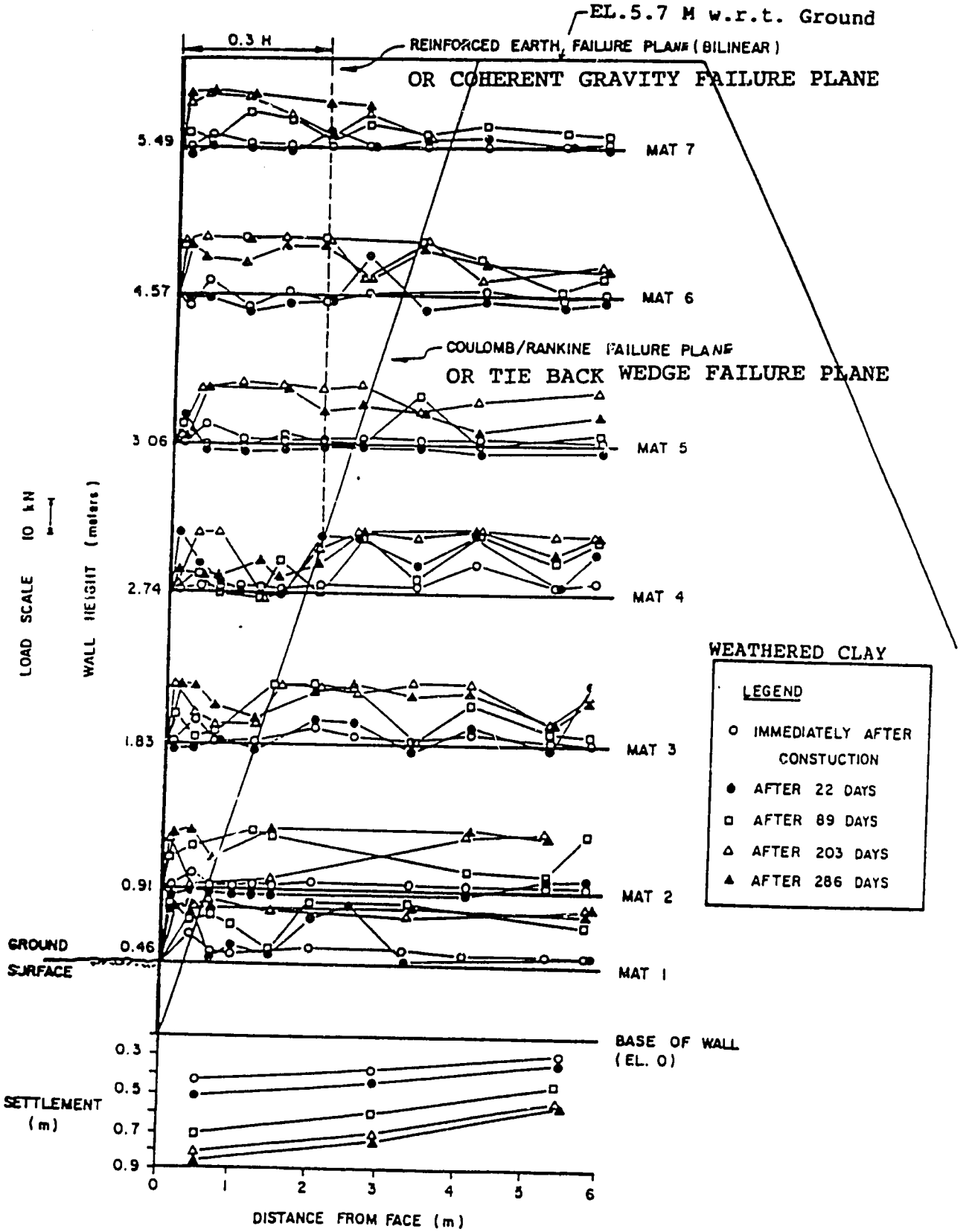

Fig. 94 Reinforcement Tensions Immediately and For Four Different Periods After Construction

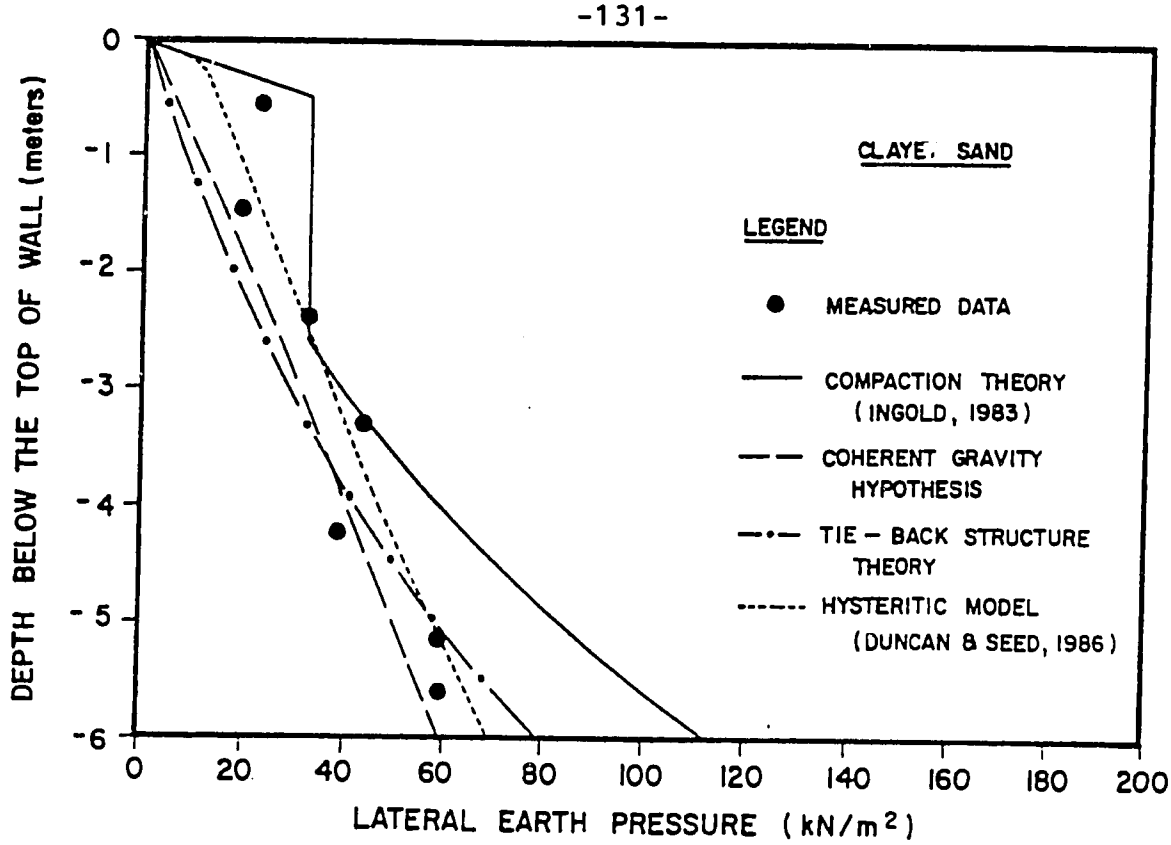

Fig.95 Measured and Predicted Lateral Earth Pressures Immediately After Construction (Clayey Sand)

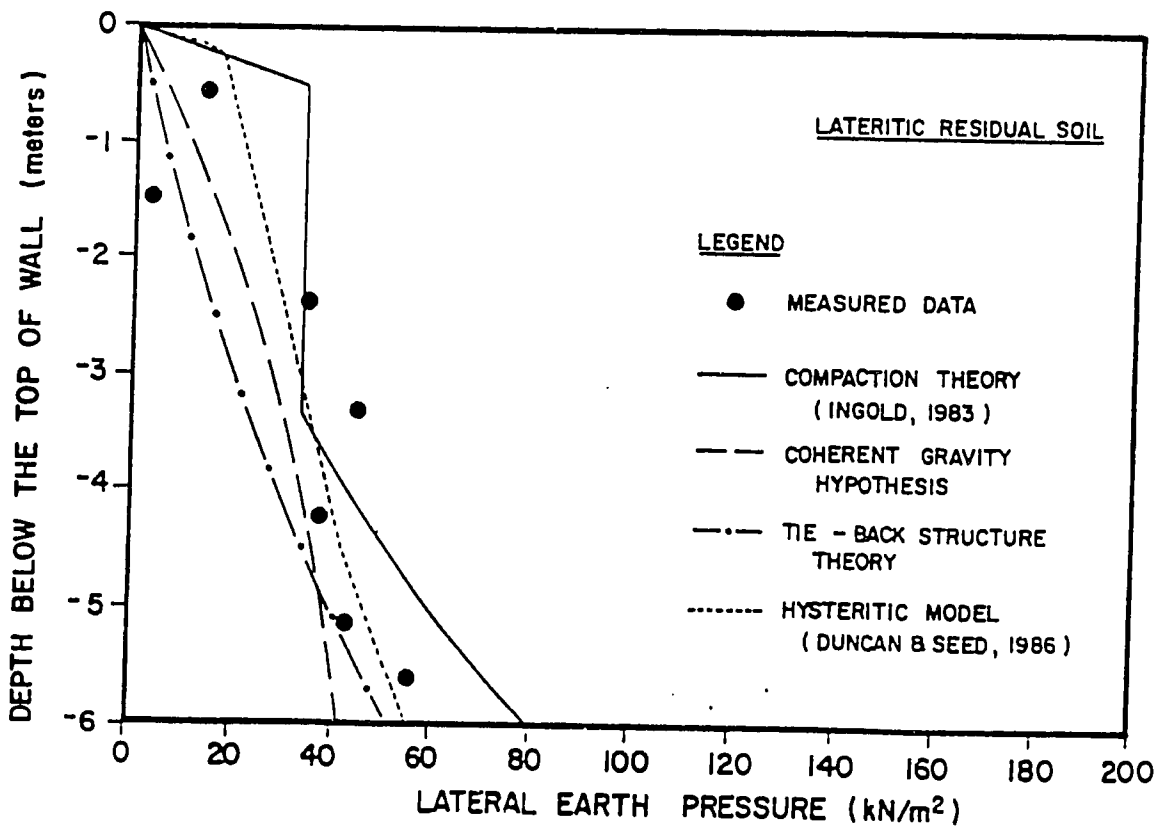

Fig.96 Measured and Predicted Lateral Earth Pressures Immediately After Construction (Lateritic Soil)

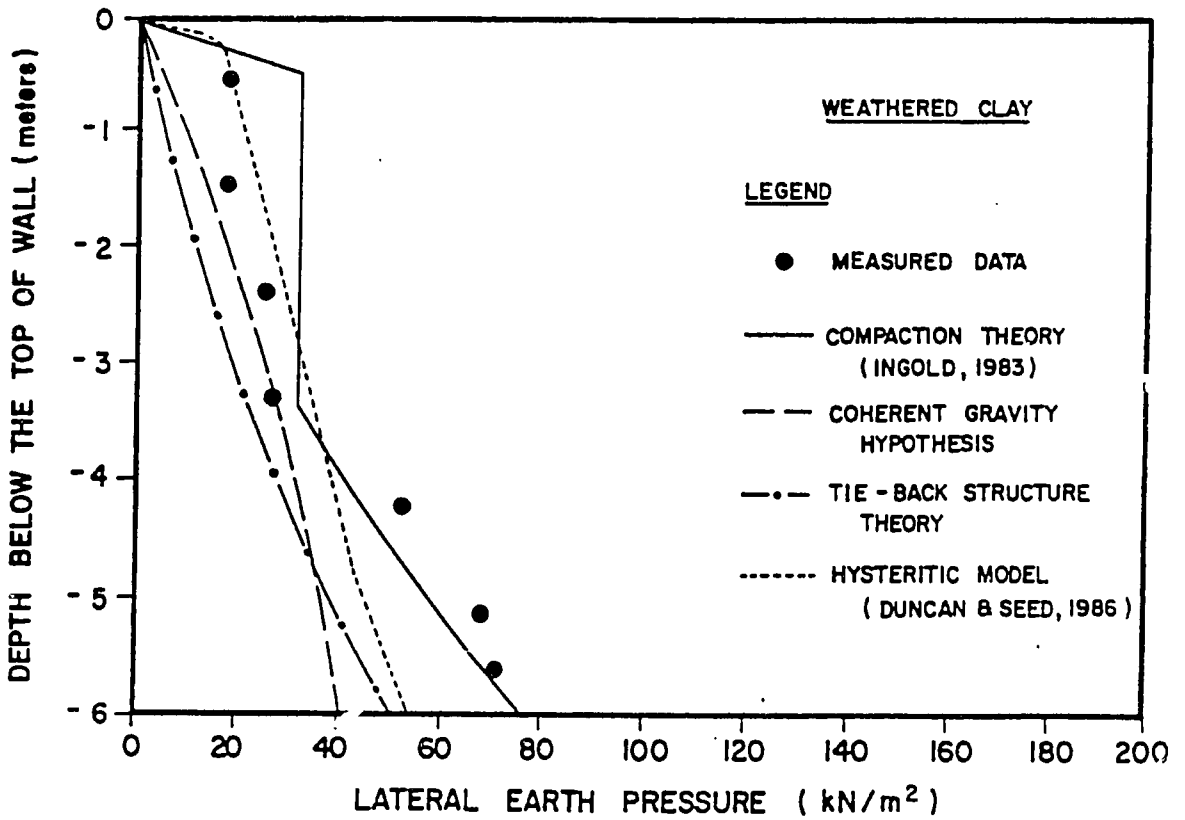

Fig.97 Measured and Predicted Lateral Earth Pressures Immediately After Construction (Weathered Clay)

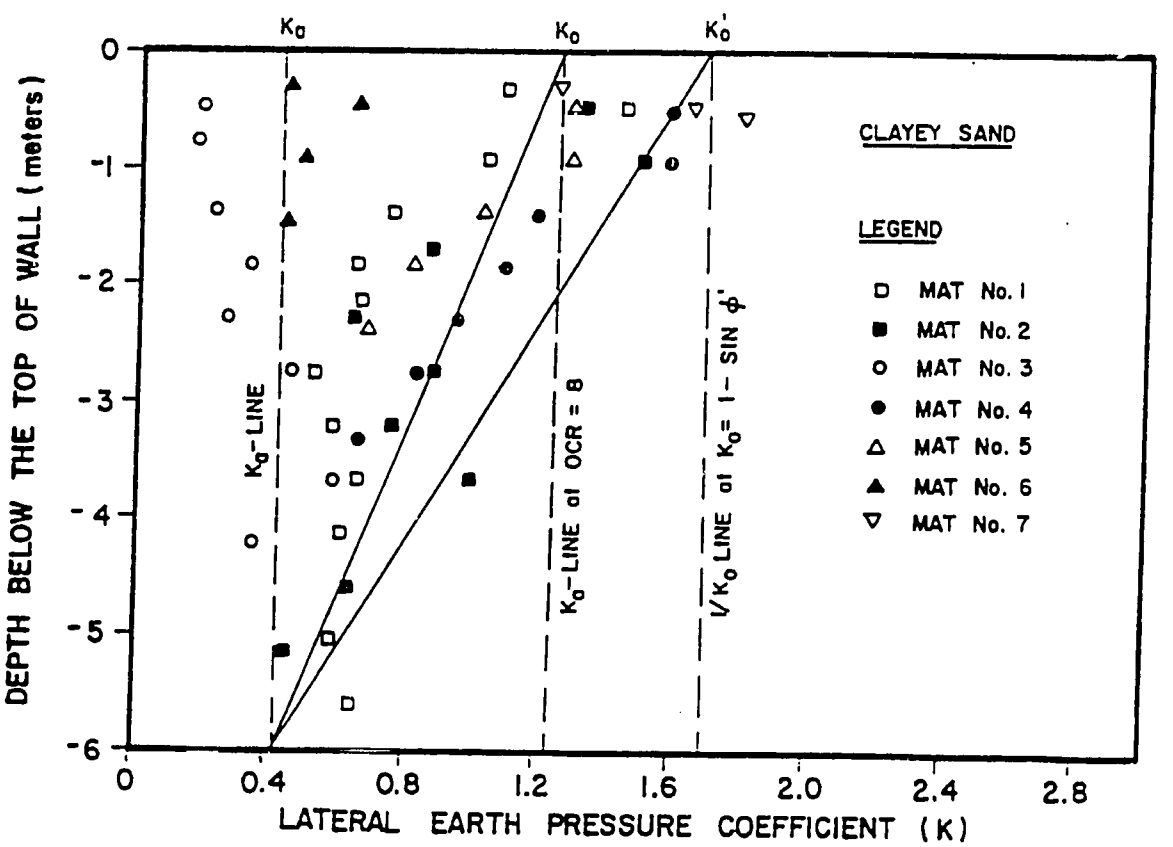

Fig.98 Maximum Values of K During Construction (Clayey Sand)

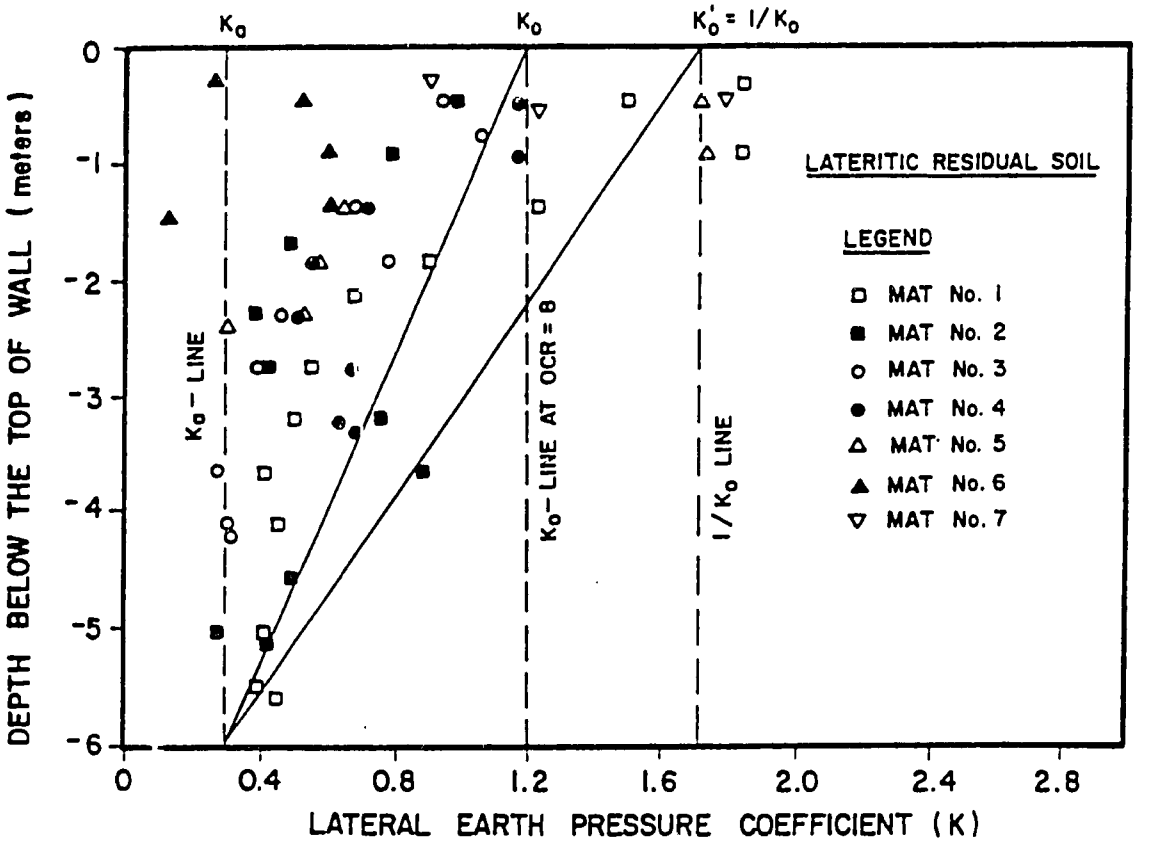

Fig.99 Maximum Values of K During Construction (Lateritic Soil)

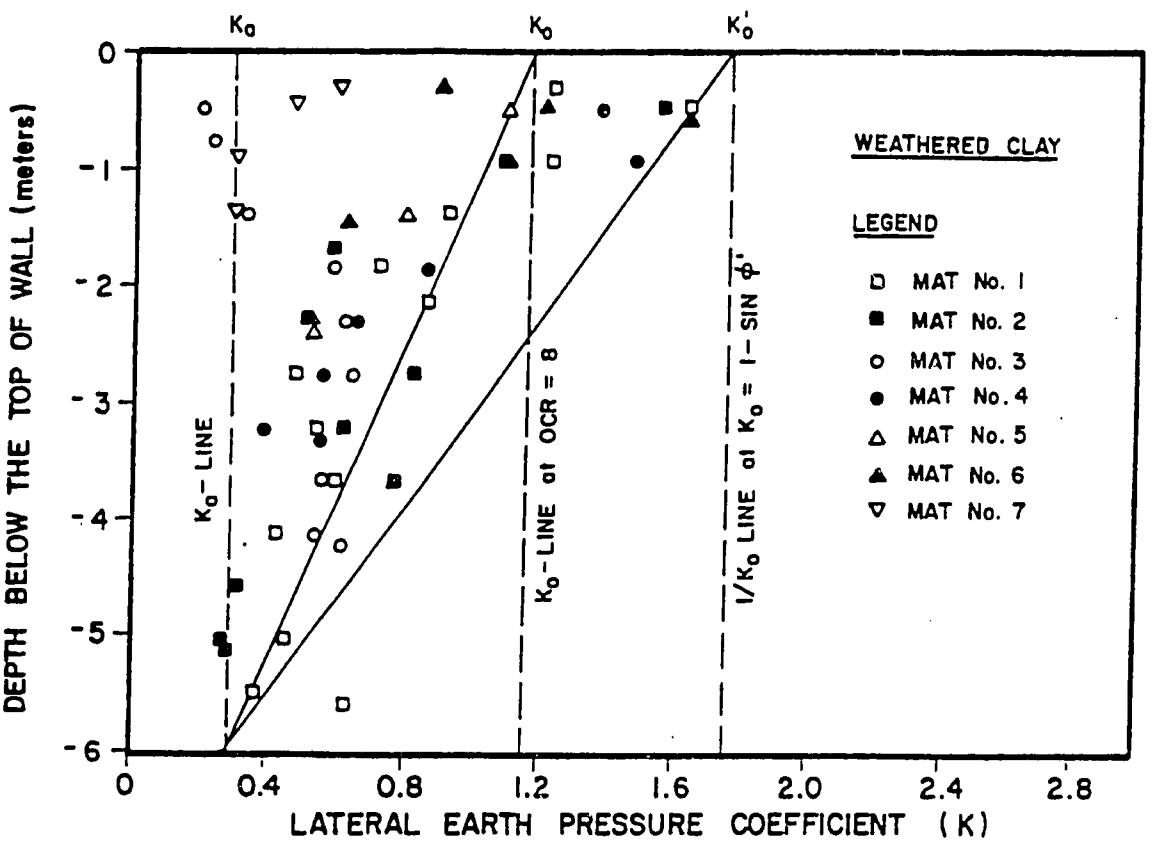

Fig.100 Maximum Values of K During Construction (Weathered Clay)

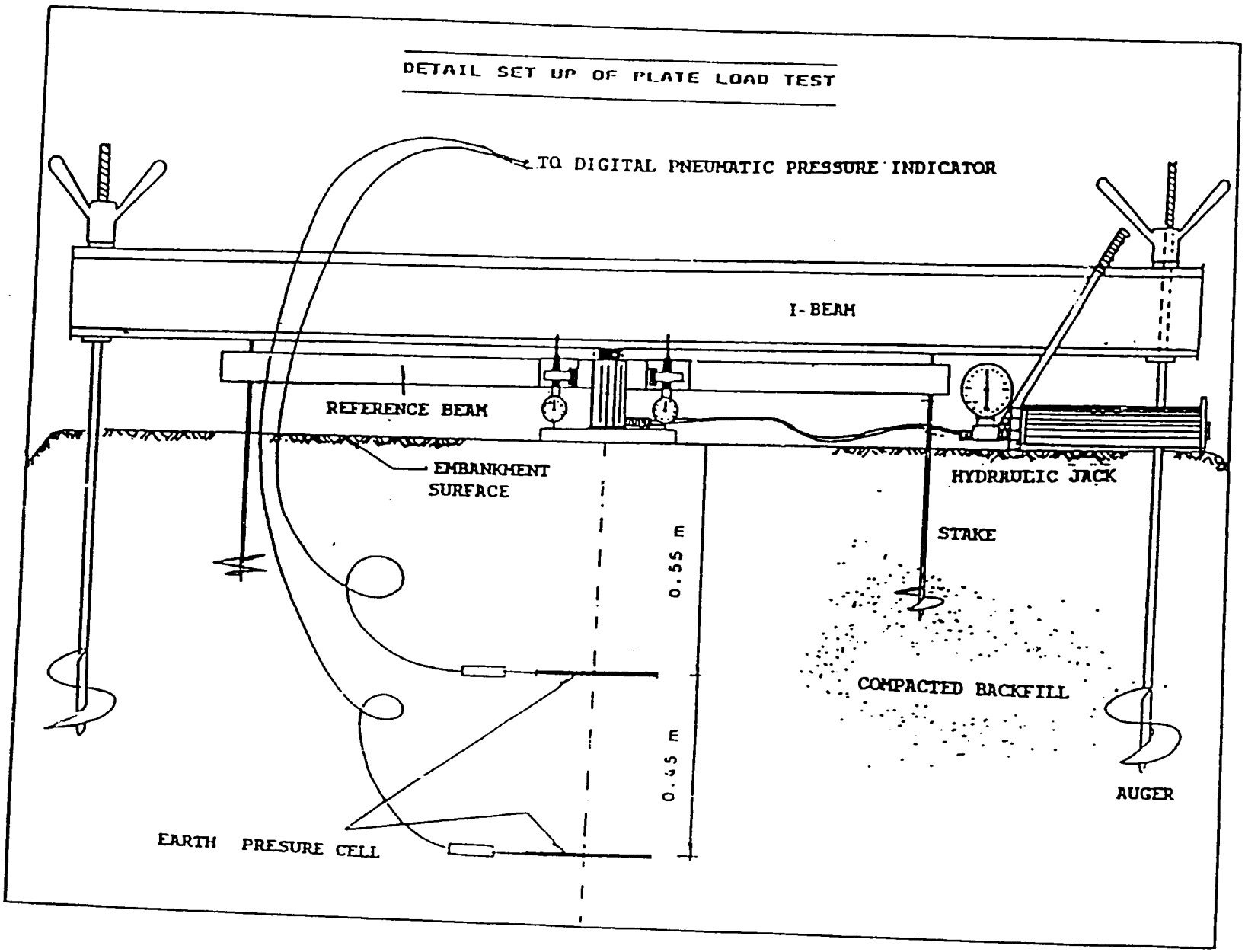

Fig. 101 Set-Up of the Plate Load Test

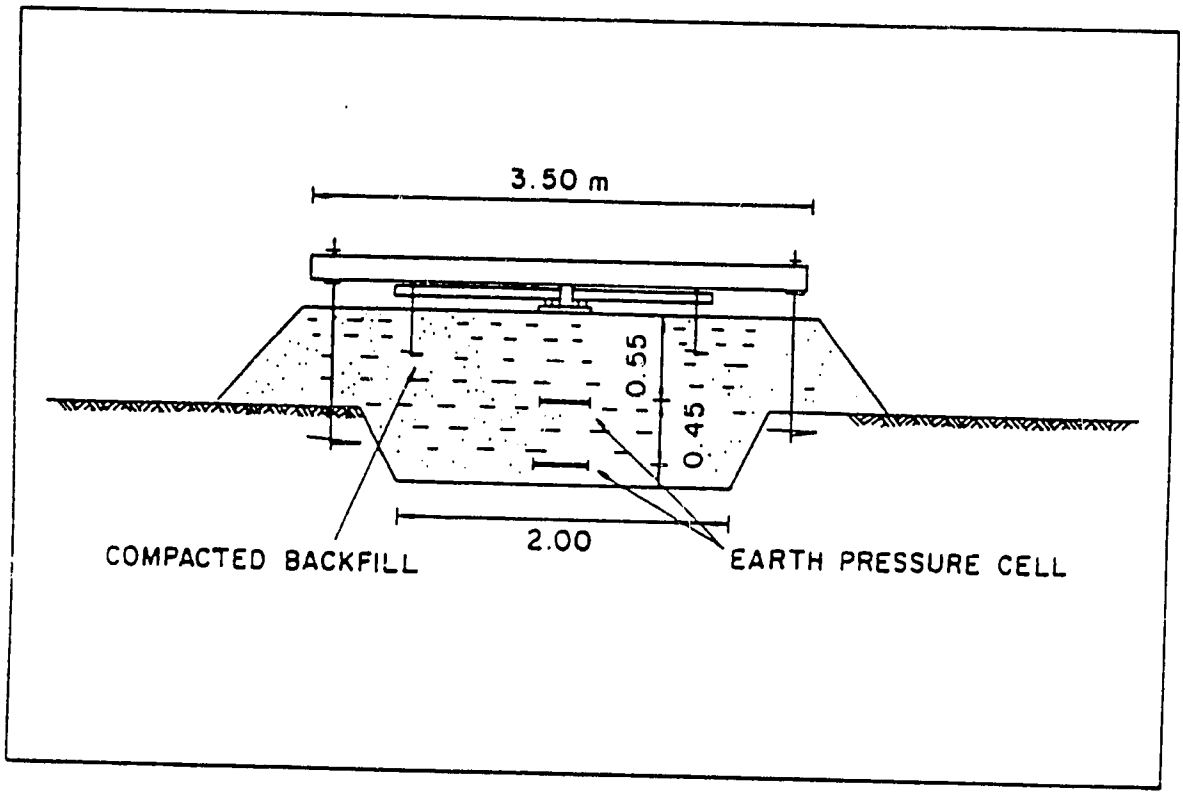

Fig. 102 Set-Up of the Plate Load Test on Unreinforced Embankment

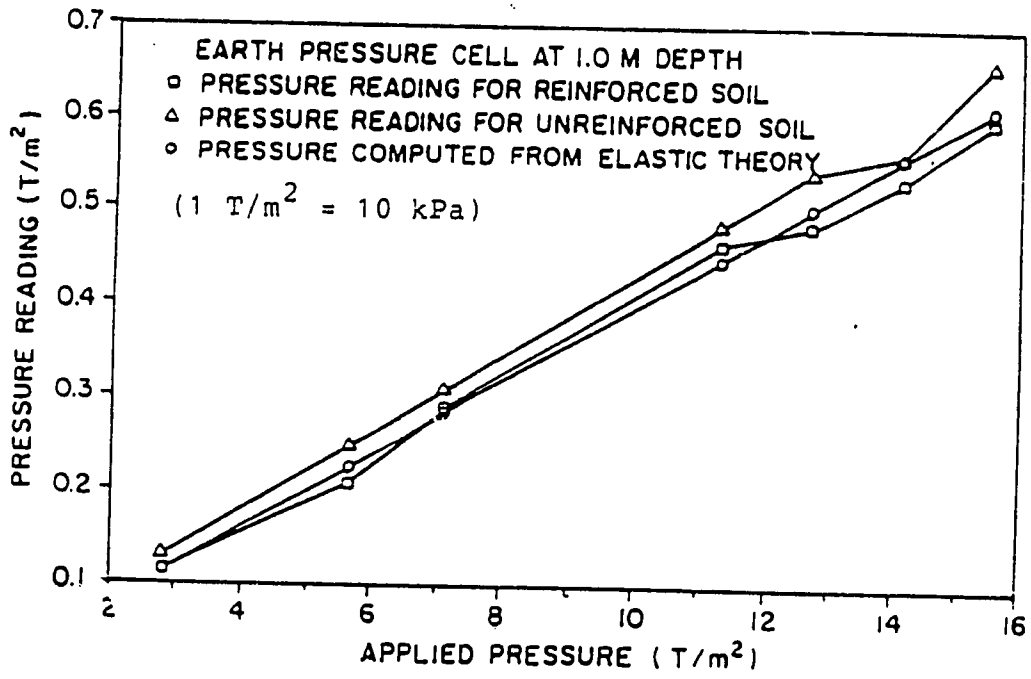

Fig. 103 Comparison of Cell Pressure Beneath Reinforced and Unreinforced Fills at Depth of 1.0 m

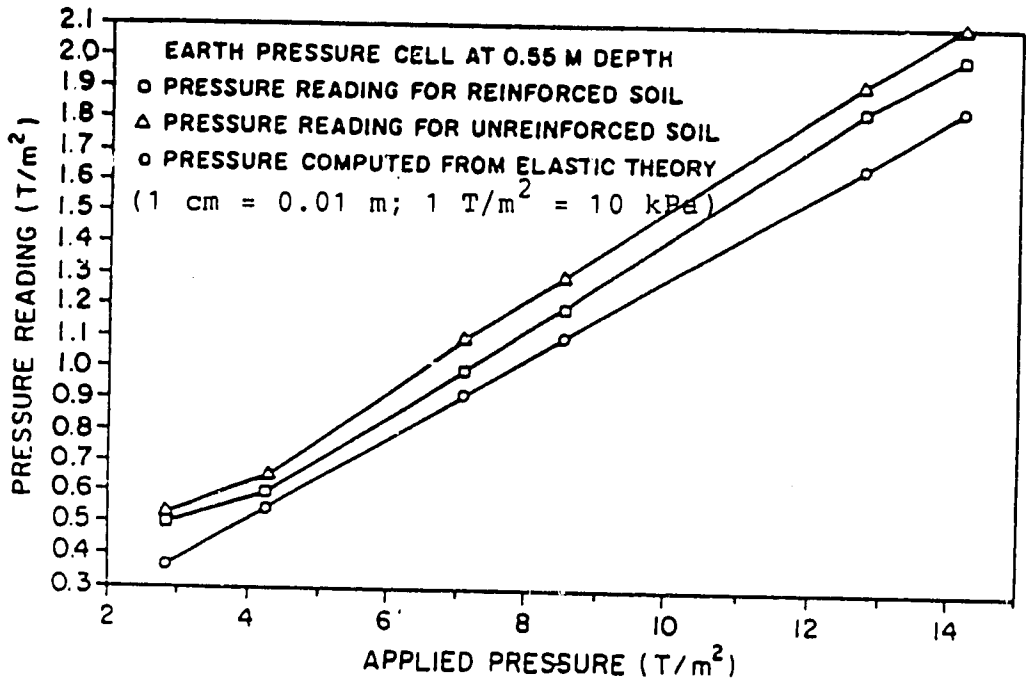

Fig. 104 Comparison of Cell Pressure Beneath Reinforced and Unreinforced Fills at Depth of 0.55 m

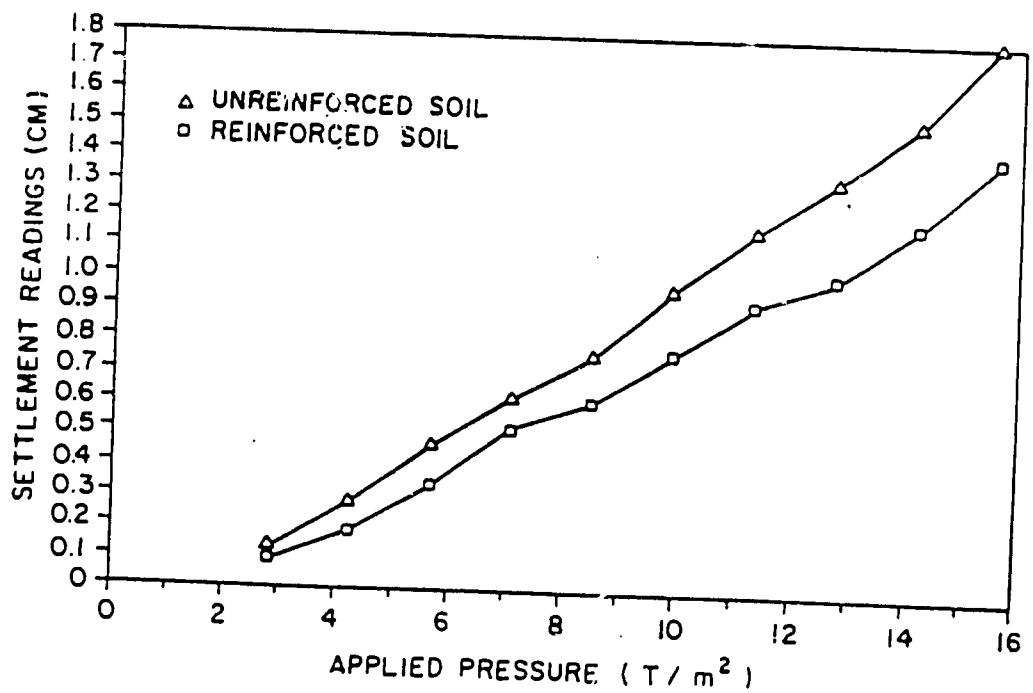

Fig.105 Comparison of Settlements Beneath Reinforced and Unreinforced Fills Due to Applied Pressures

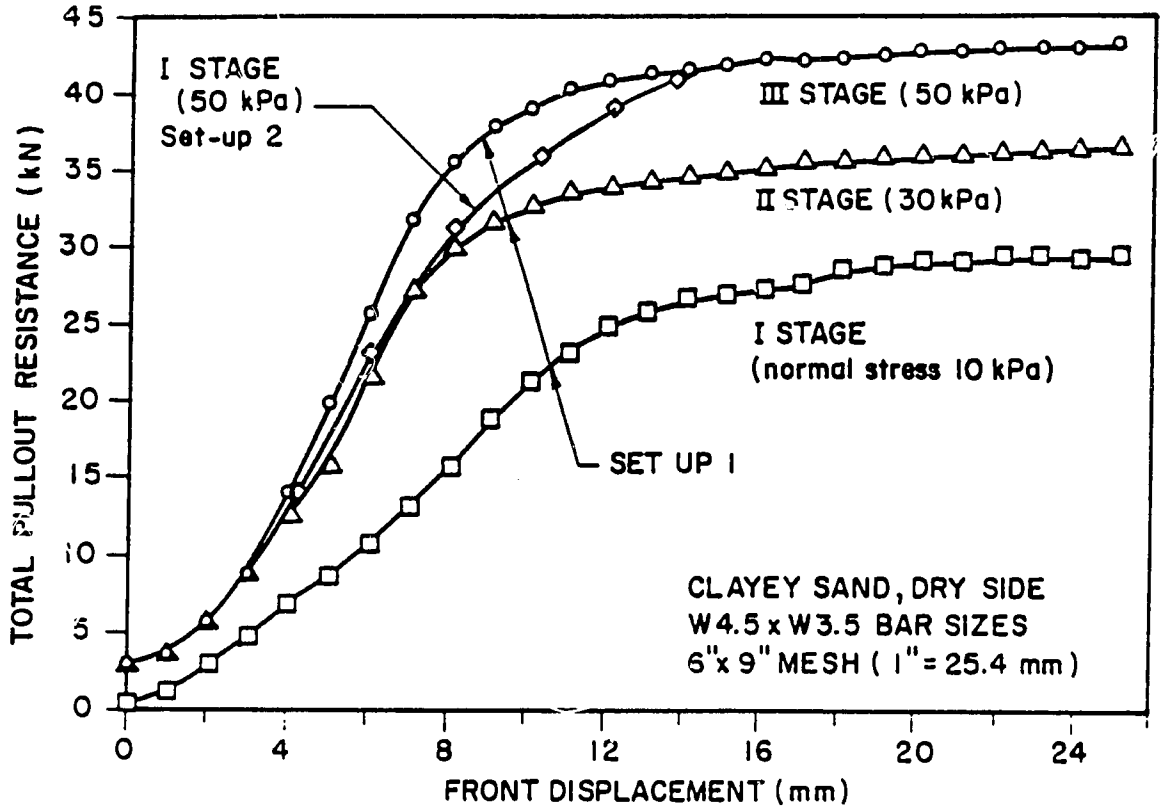

Fig.106 Effect of Stage Loading on Load-Displacement Curves During Laboratory Pullout

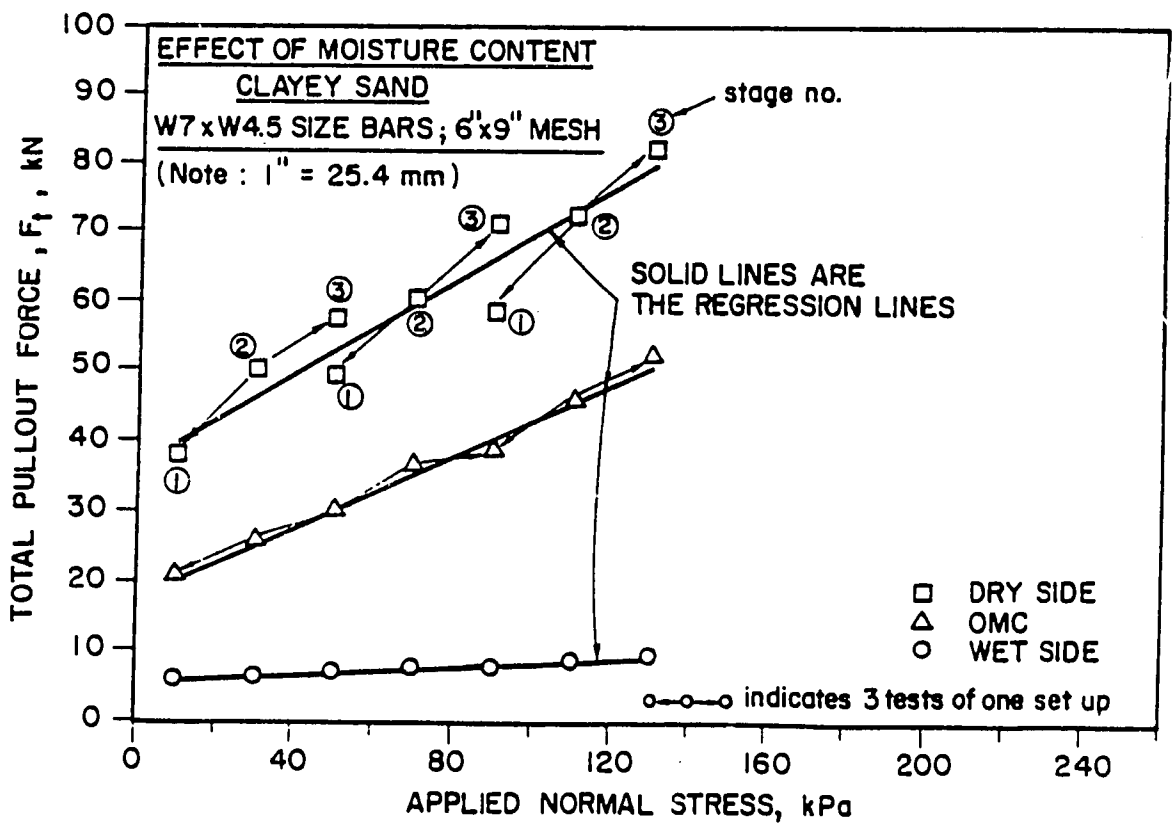

Fig.107 Effect of Moisture Content and Stage Loading on the Pullout Capacities

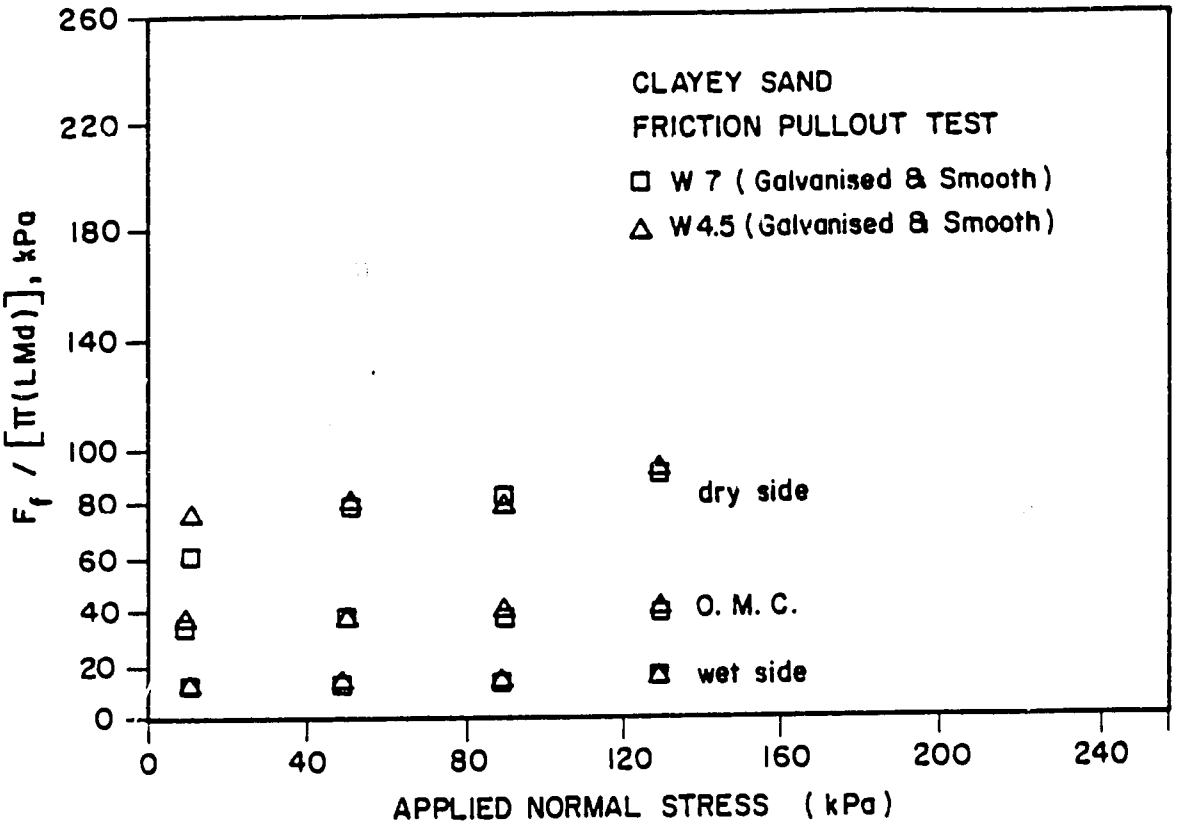

Fig.108 Friction Pullout Test Results in Clayey Sand

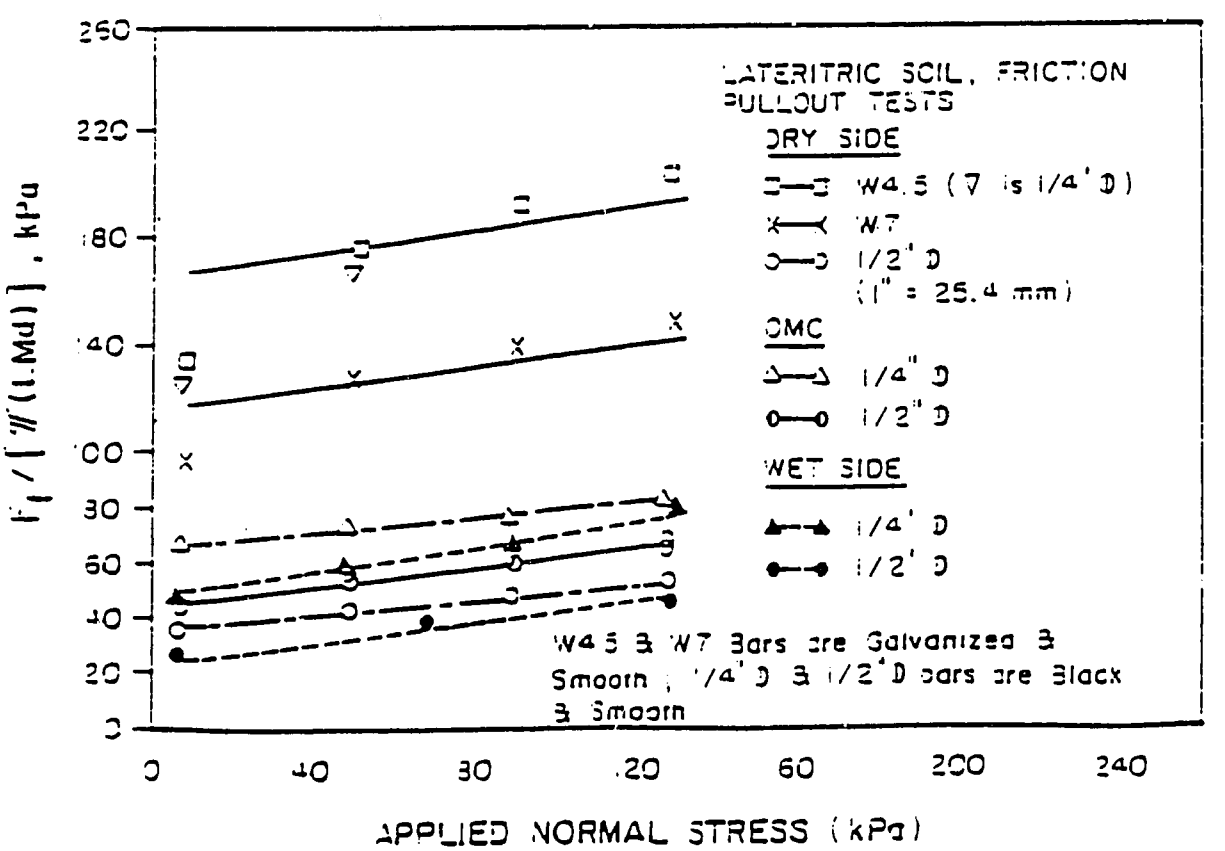

Fig.109 Friction Pullout Test Results in Lateritic Soil

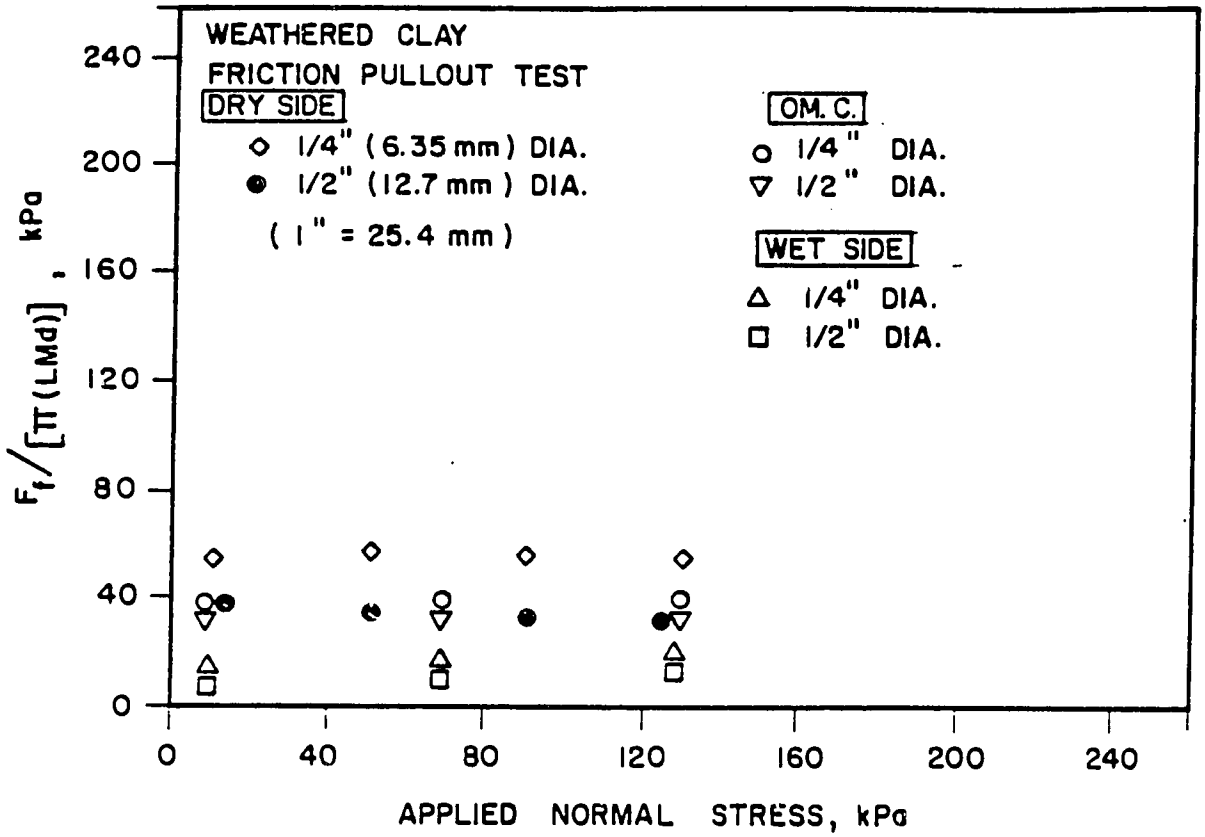

Fig.110 Friction Pullout test Results in Weathered Clay

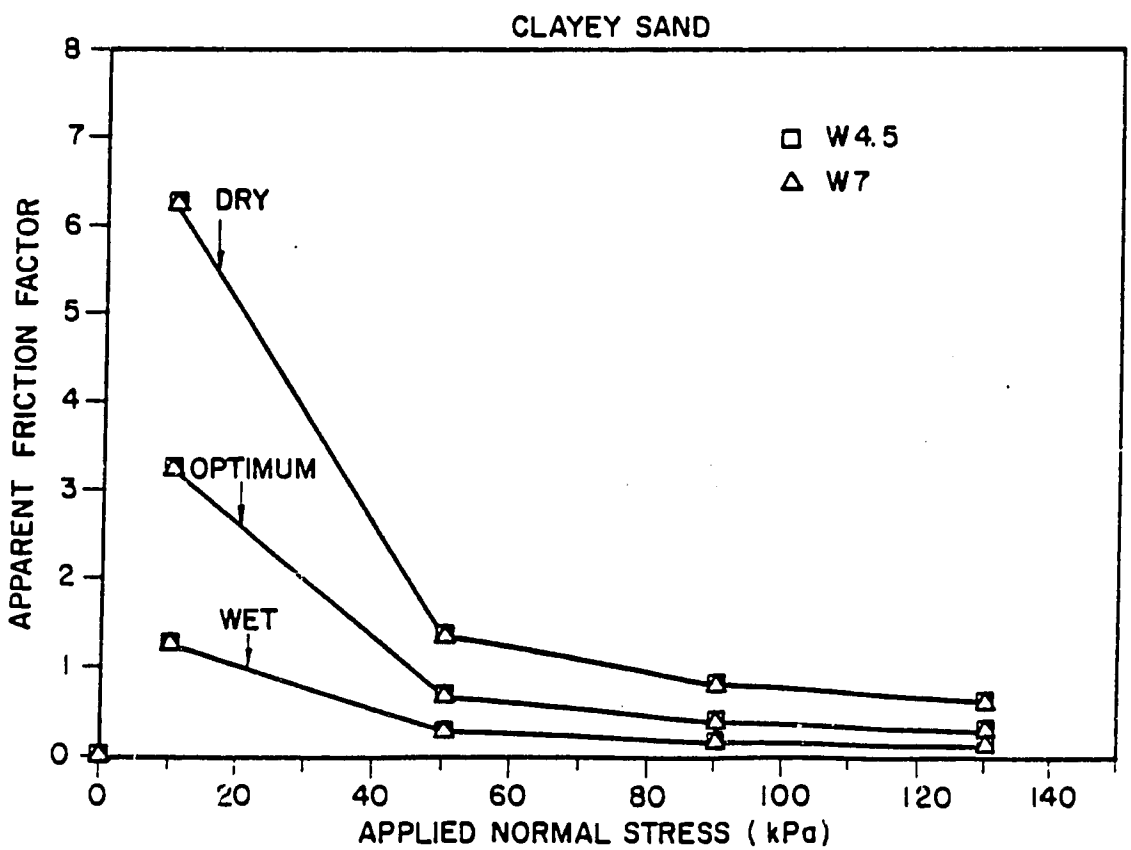

Fig.111 Variation of Apparent Friction Coefficient With Applied Normal Stress (Clayey Sand)

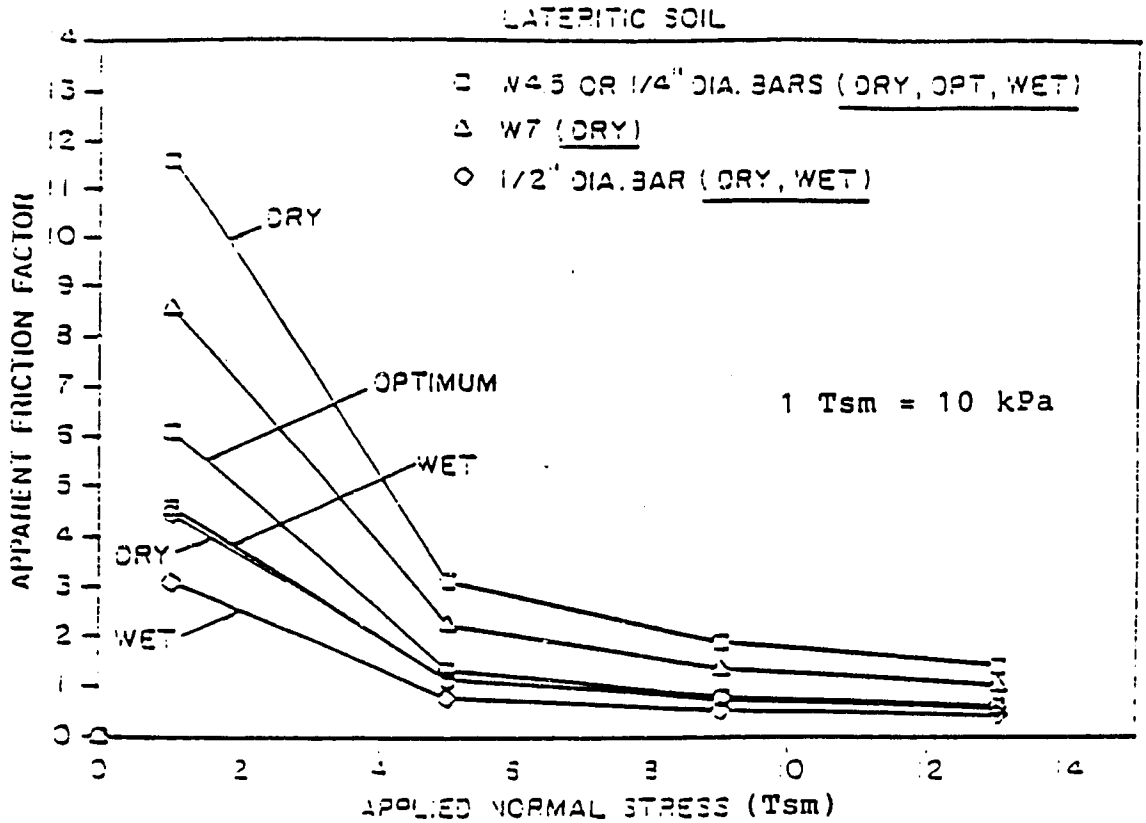

Fig.112 Variation of Apparent Friction Coefficient With Applied Normal Stress (Lateritic Soil)

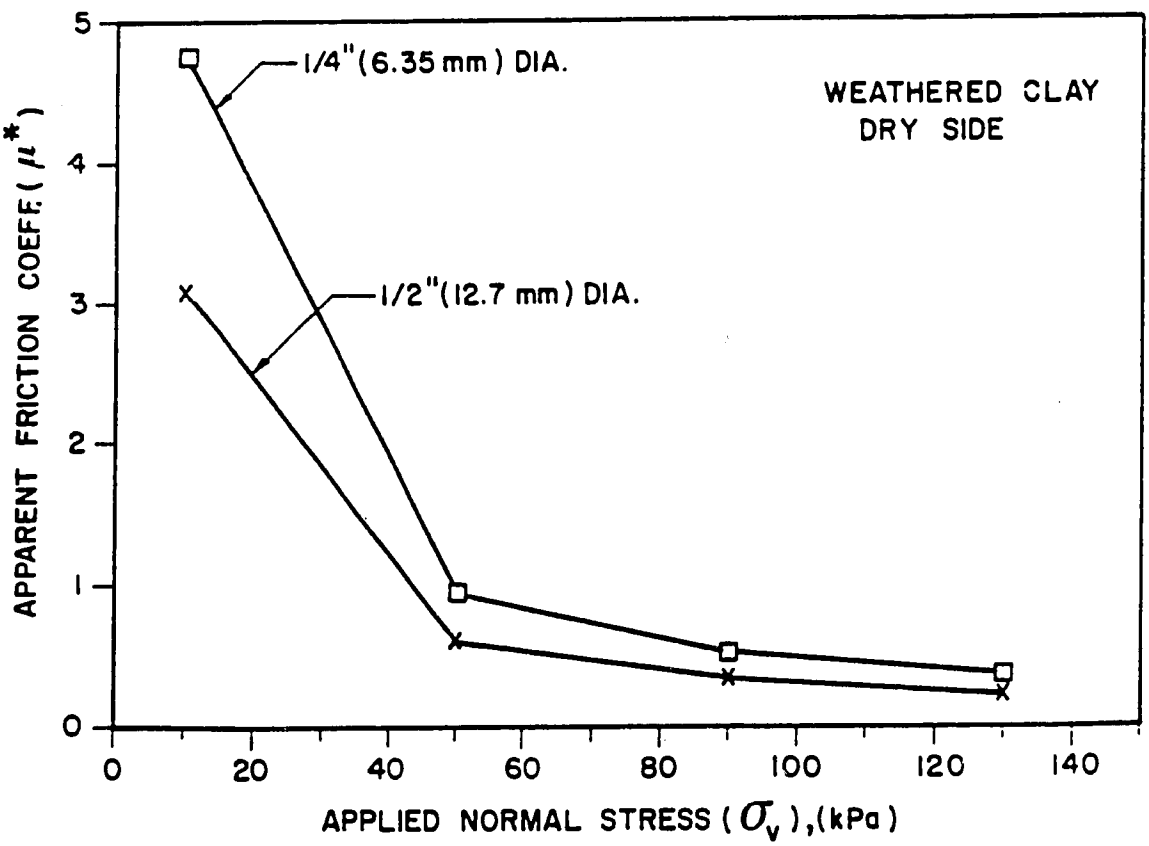

Fig.113 Variation of Apparent Friction Coefficient With Applied Normal Stress (Weathered Clay)

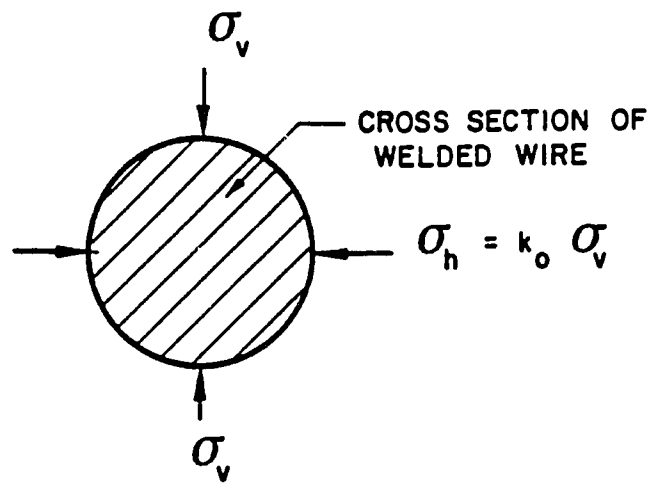

Compacted Soil ≡ Overconsolidated Soil (OCR = 8, k_c = 1.3 for Weathered Clay)

$$\sigma_{ave} = \frac{\sigma_v + \sigma_h}{2} = 1.15\,\sigma_v$$

Fig.114 Average Overburden Pressure on Bars of Circular Cross-Section

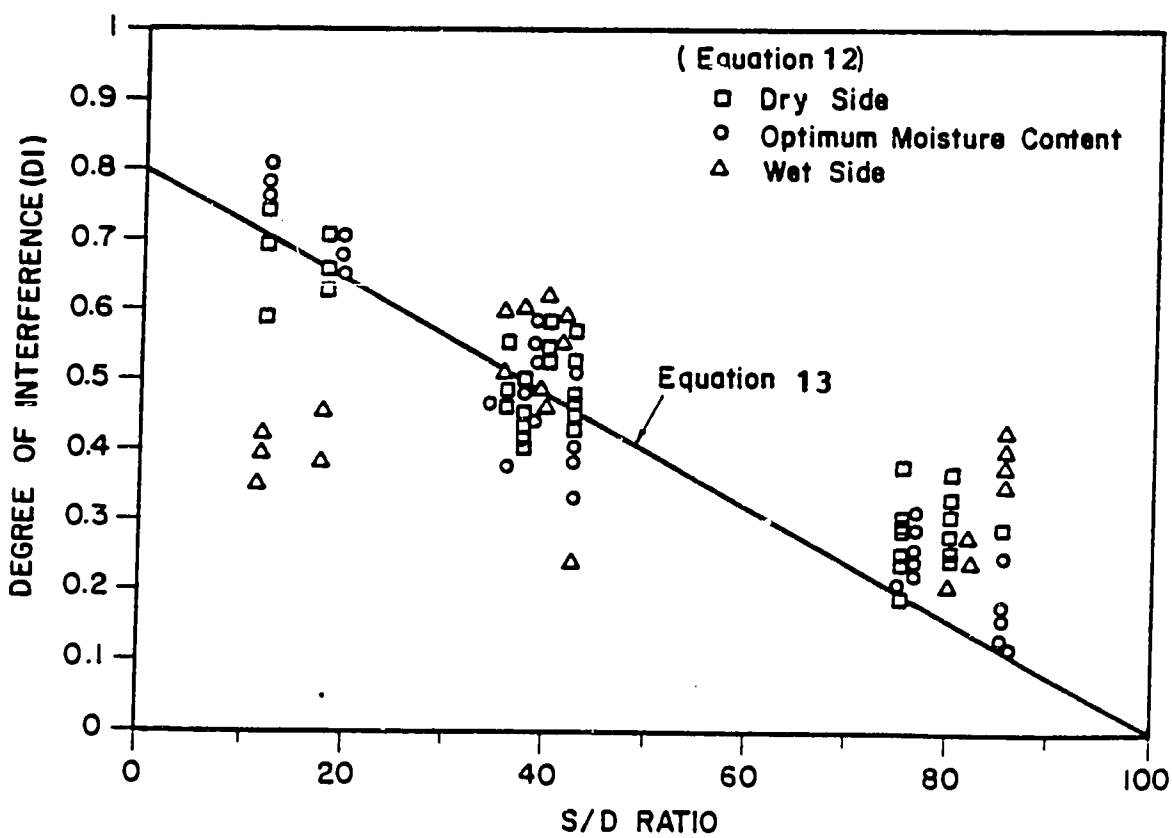

Fig.115 Degree of Interference (DI) versus S/D Ratio (Clayey Sand)

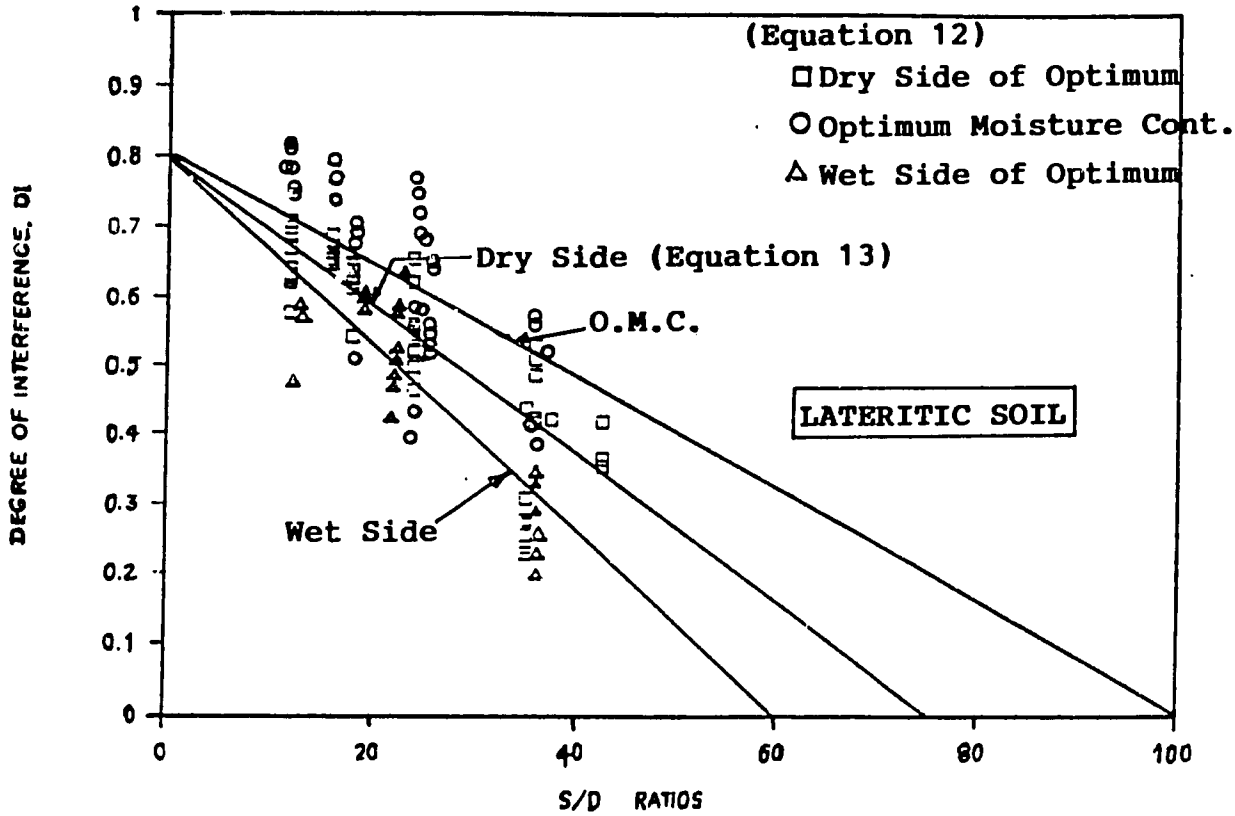

Fig. 116 Degree of Interference (DI) versus (S/D) Ratio (Lateritic Soil)

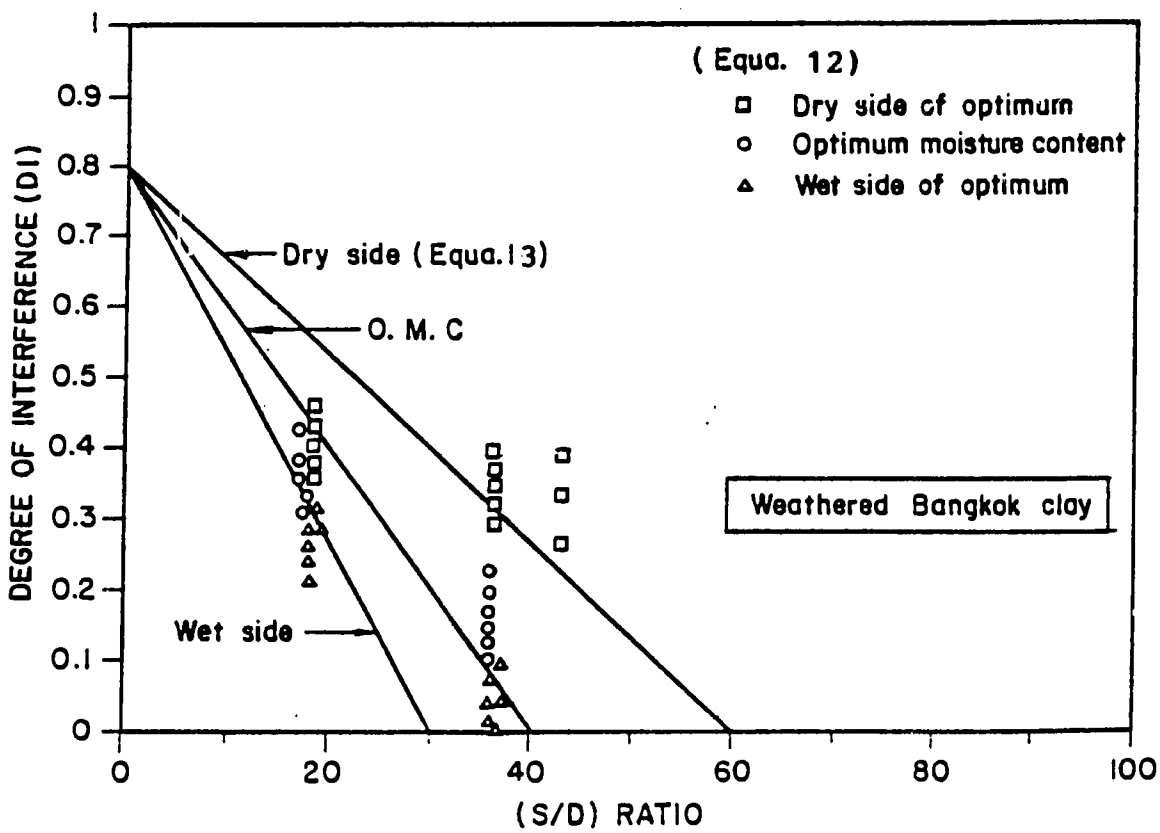

Fig.117 Degree of Interference (DI) versus (S/D) Ratio (Weathered Clay)

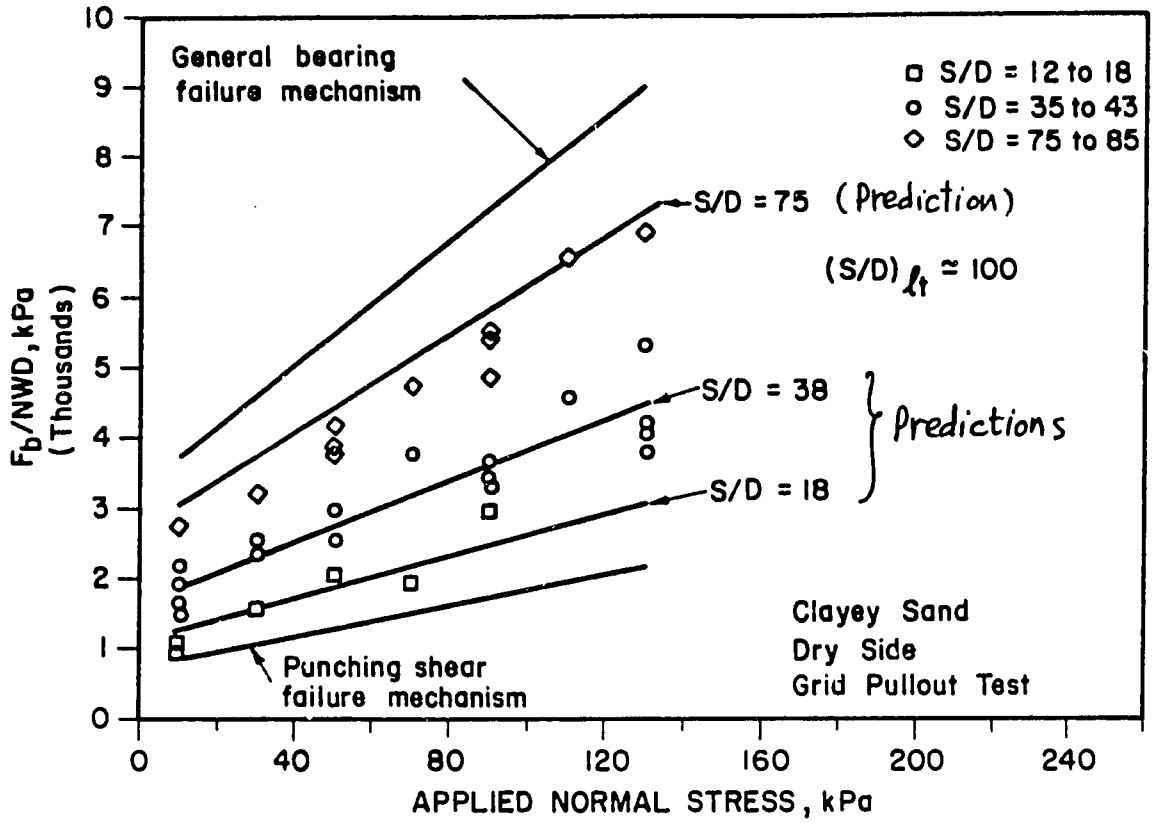

Fig.118 Grid Pullout Test Results on the Dry side of Optimum (Clayey Sand)

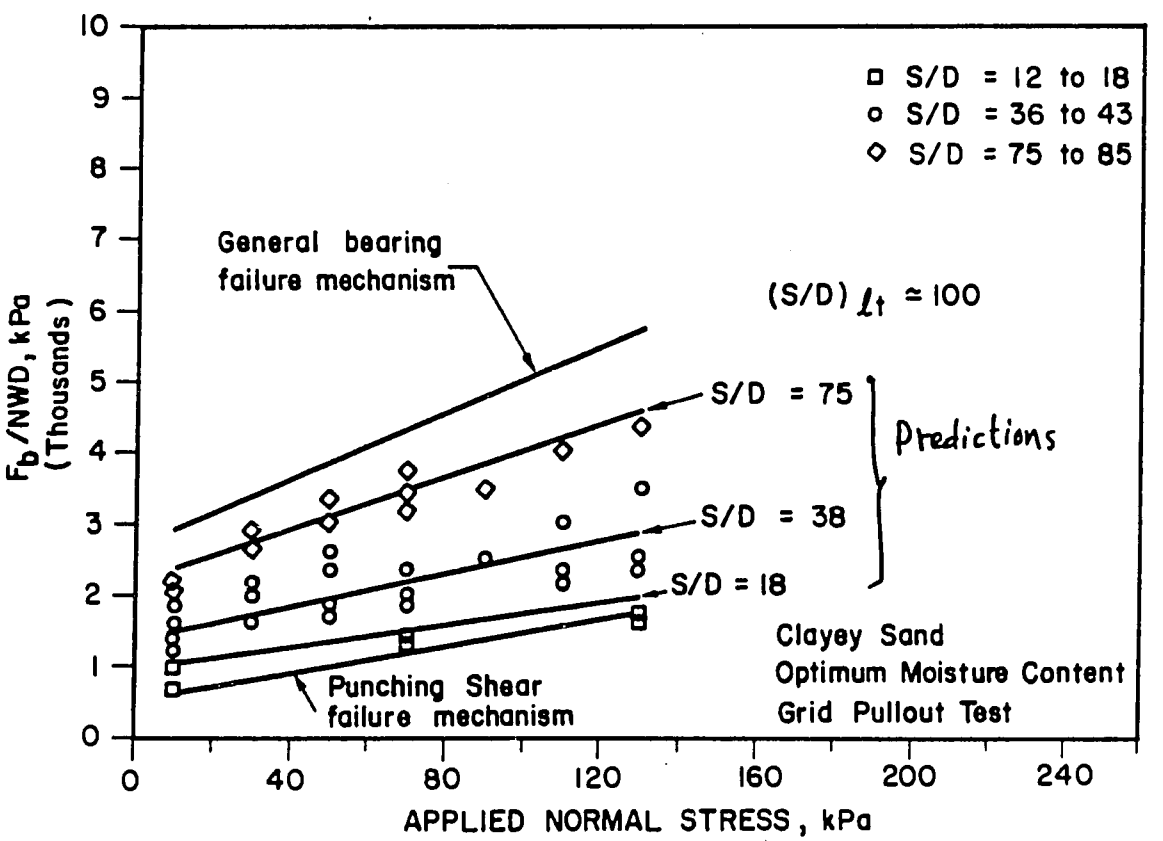

Fig.119 Grid Pullout Test Results at Optimum Moisture Content (Clayey Sand)

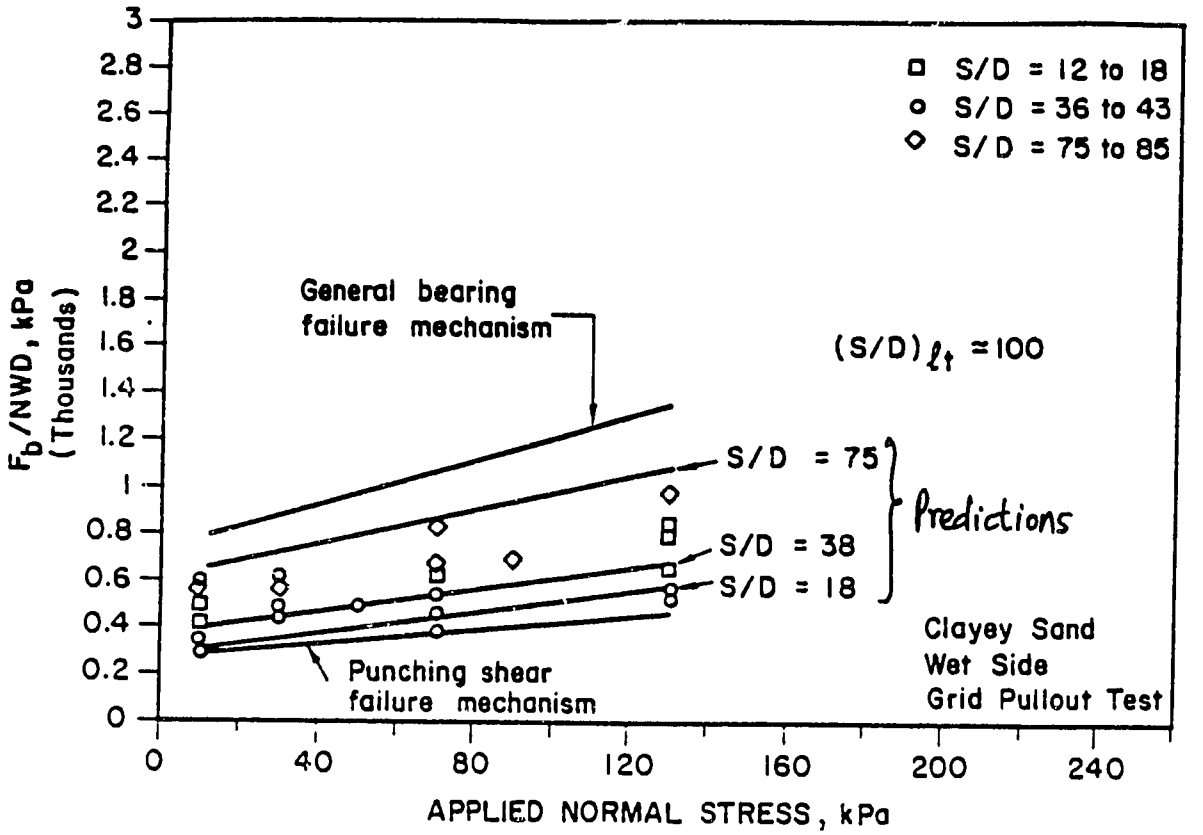

Fig.120 Grid Pullout Test Results on the Wet Side of Optimum (Clayey Sand)

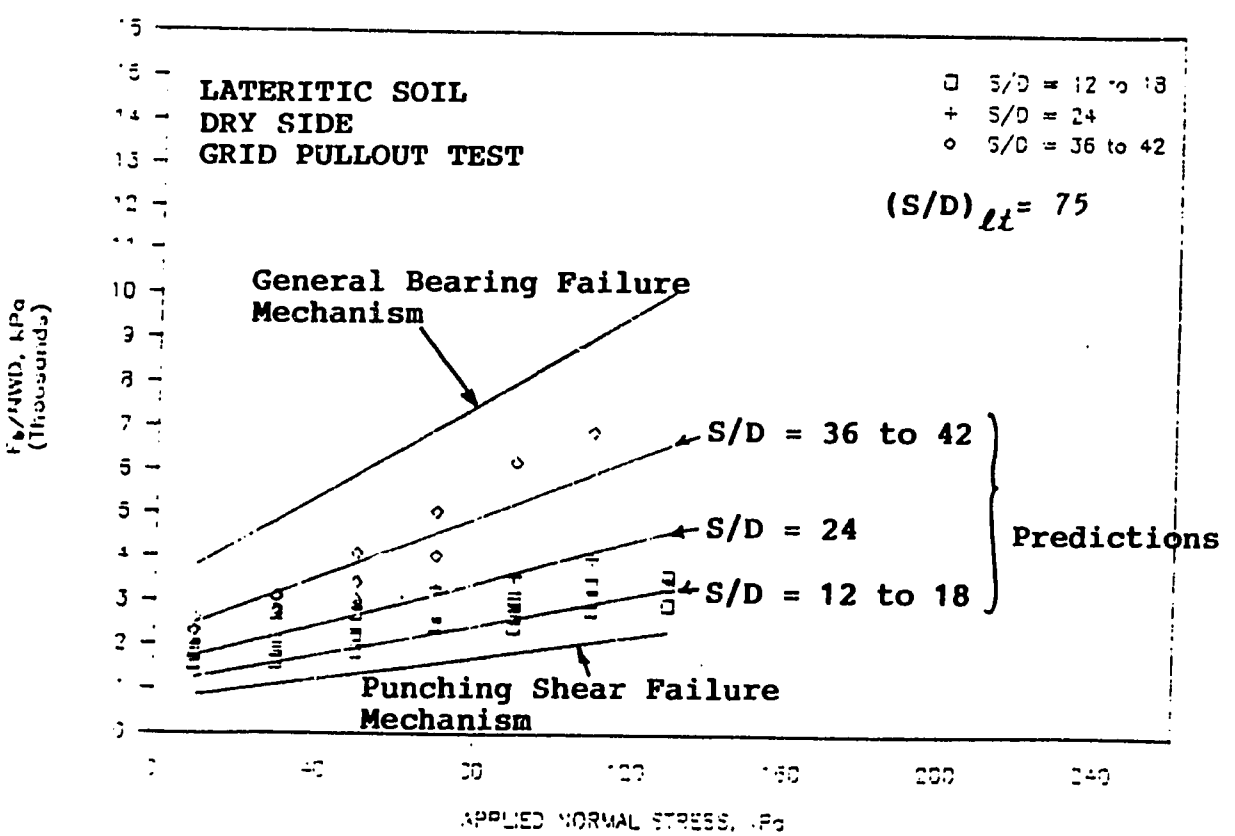

Fig.121 Grid Pullout Test Results on the Dry Side of Optimum (Lateritic Soil)

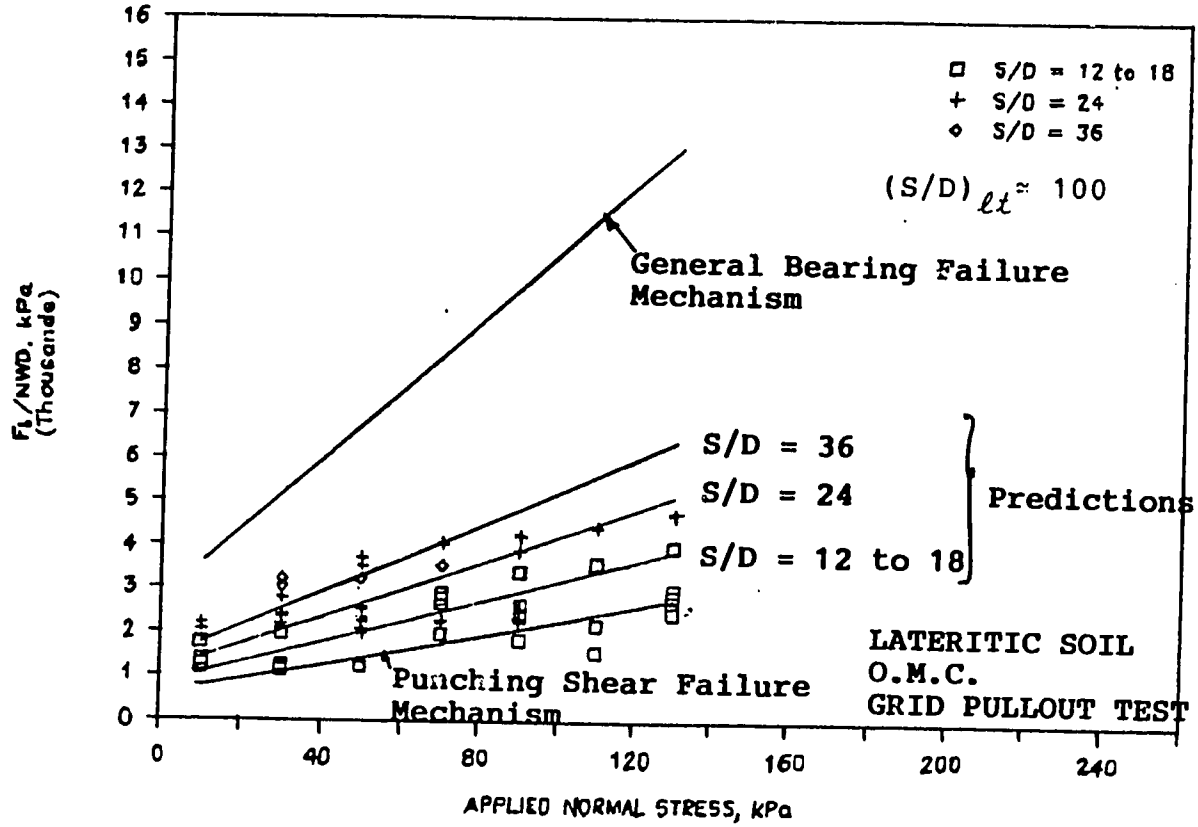

Fig.122 Grid Pullout Test Results at Optimum Moisture Content (Lateritic Soil)

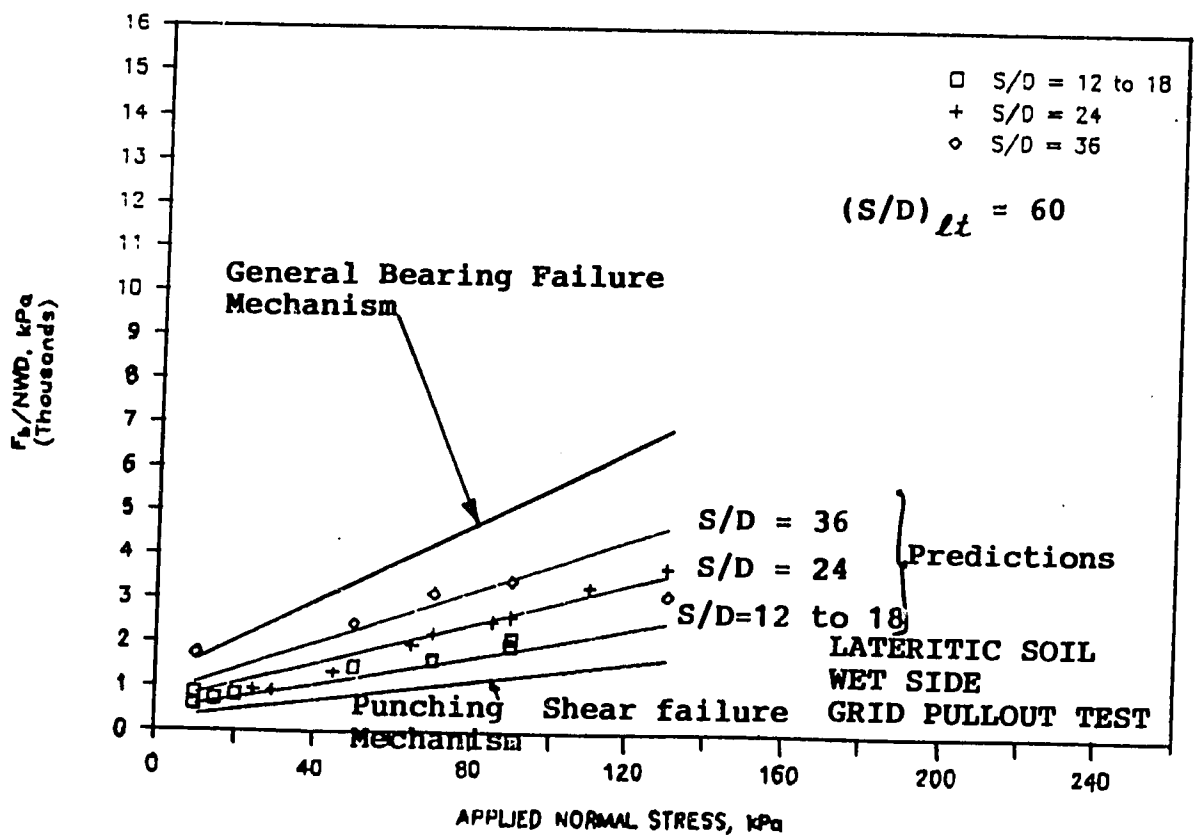

Fig.123 Grid Pullout Test Results on the Wet Side of Optimum (Lateritic Soil)

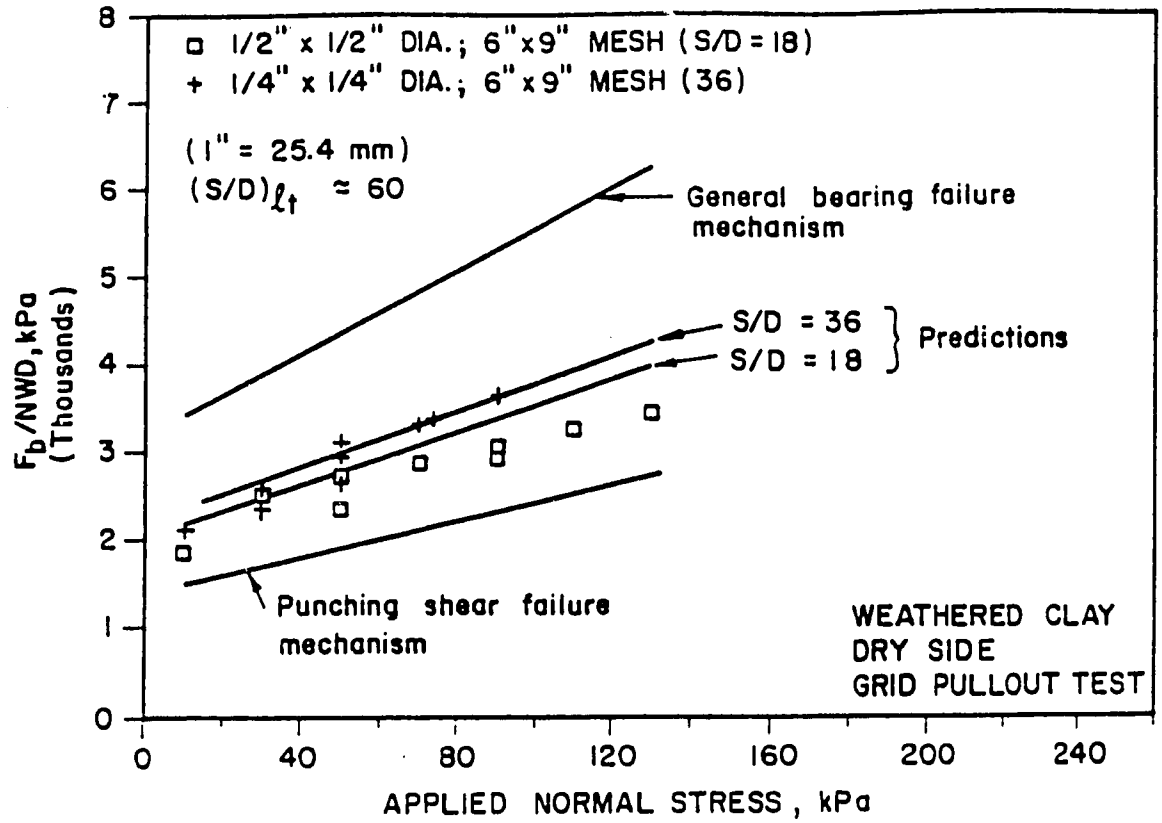

Fig.124 Grid Pullout Test Results on the Dry Side of Optimum (Weathered Clay)

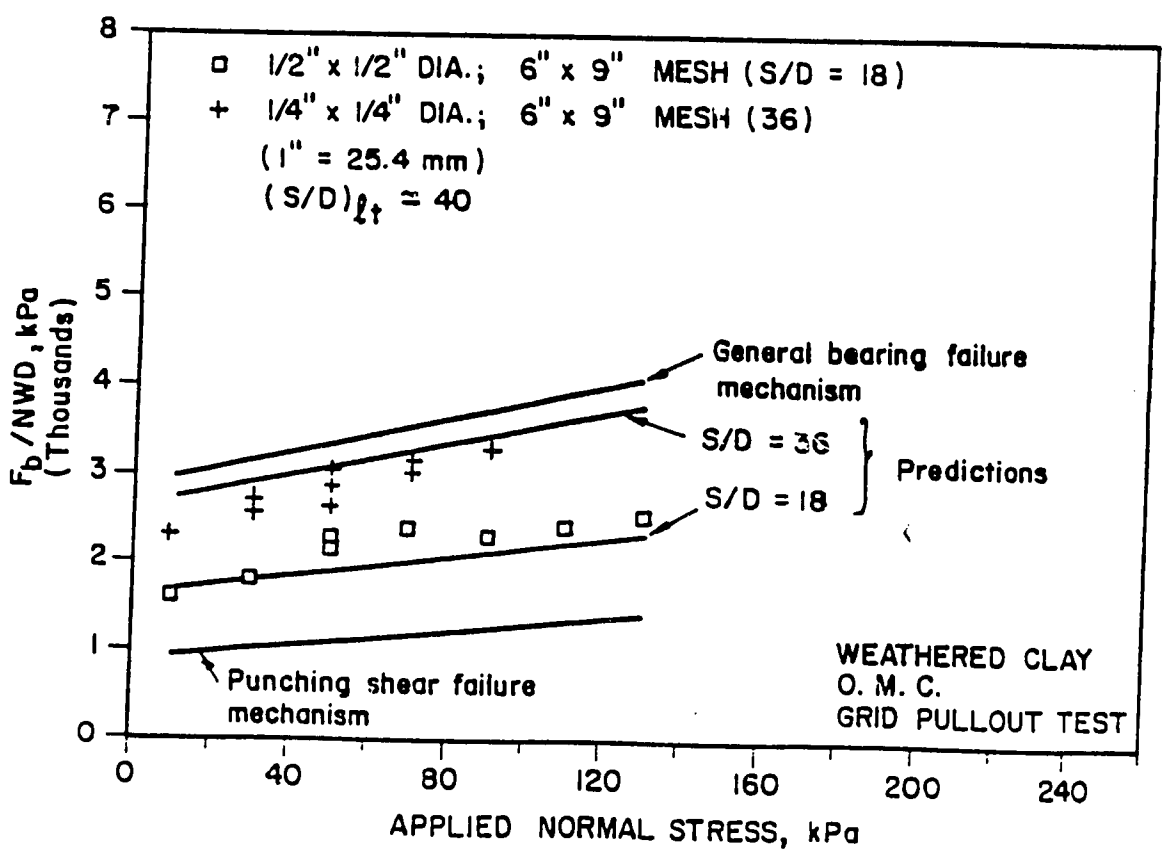

Fig.125 Grid Pullout Test Results at Optimum Moisture Content (Weathered Clay)

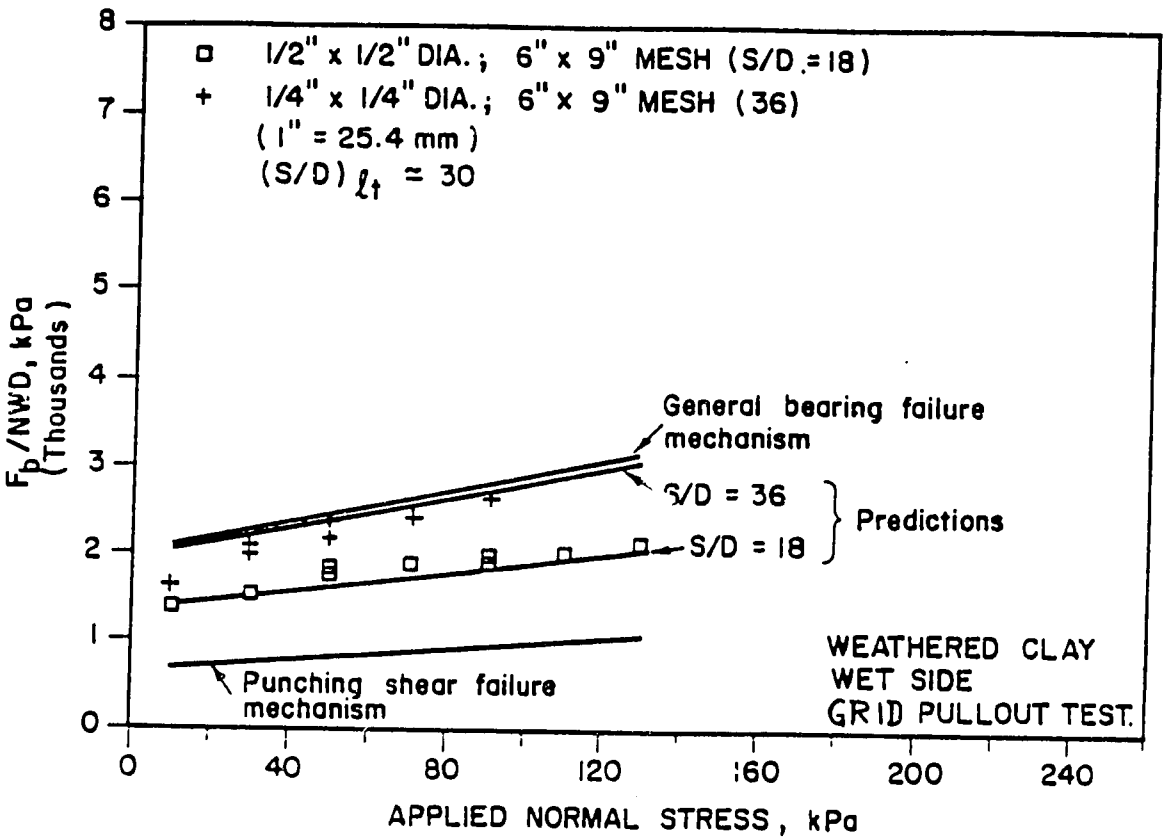

Fig.126 Grid Pullout Test Results on the Wet Side of Optimum (Weathered Clay)

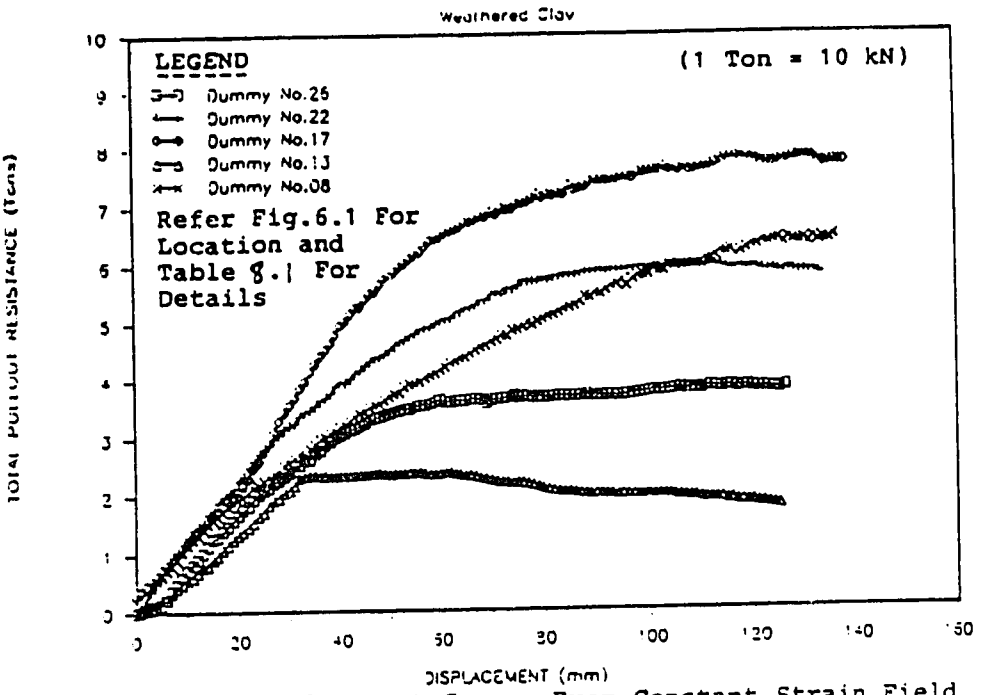

Fig .127 Load-Displacement Curves From Constant Strain Field Pullout Tests in Weathered Clay

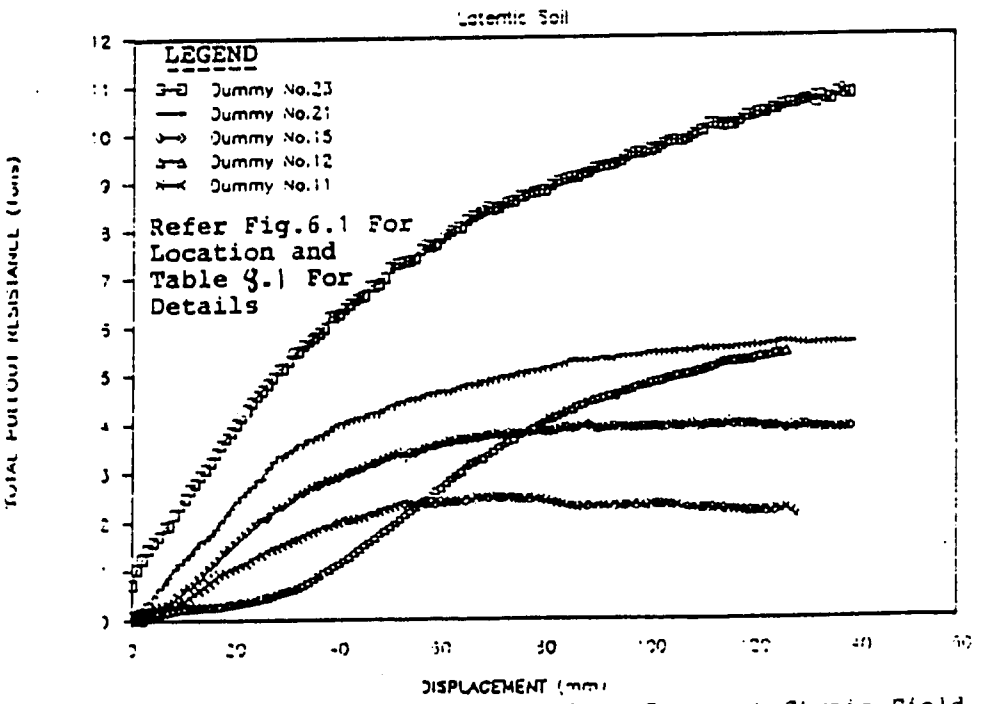

Fig. 128 Load-Displacement Curves From Constant Strain Field Pullout Tests in Lateritic Soil

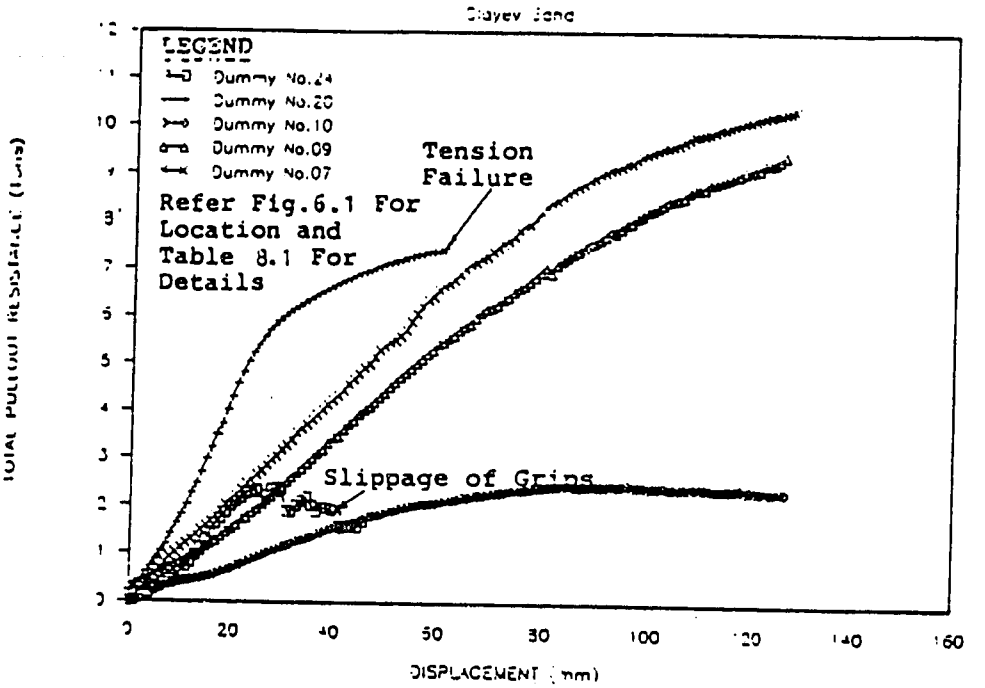

Fig.129 Load-Displacement Curves From Constant Strain Field Pullout Tests in Clayey Sand

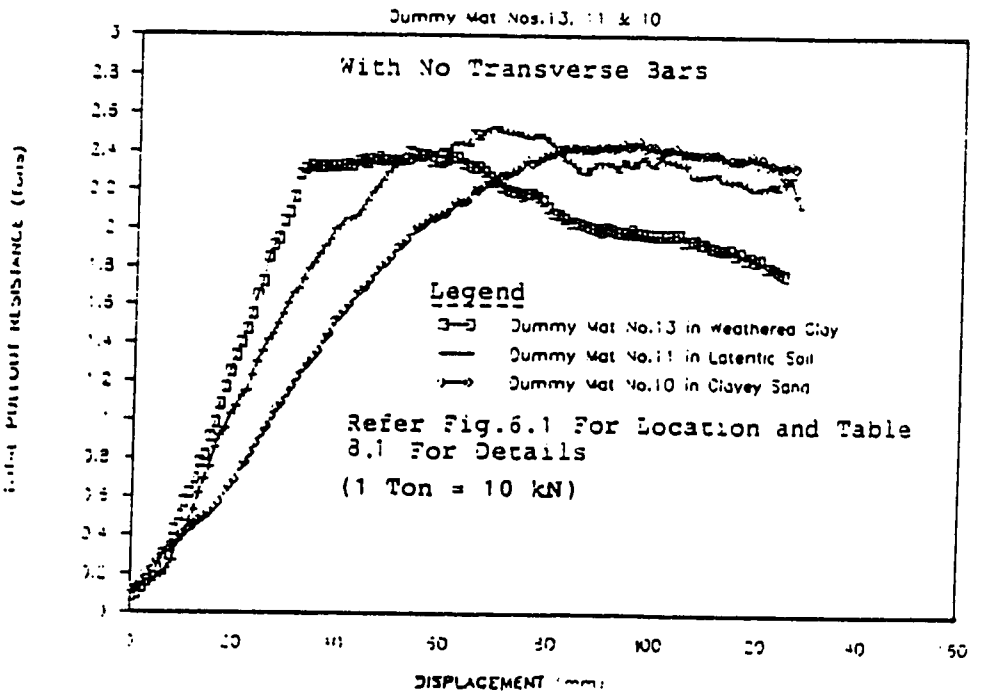

Fig. 130 Load-Displacement Curves From Constant Strain Field Pullout Tests of Dummy Mats With No Transverse Bars

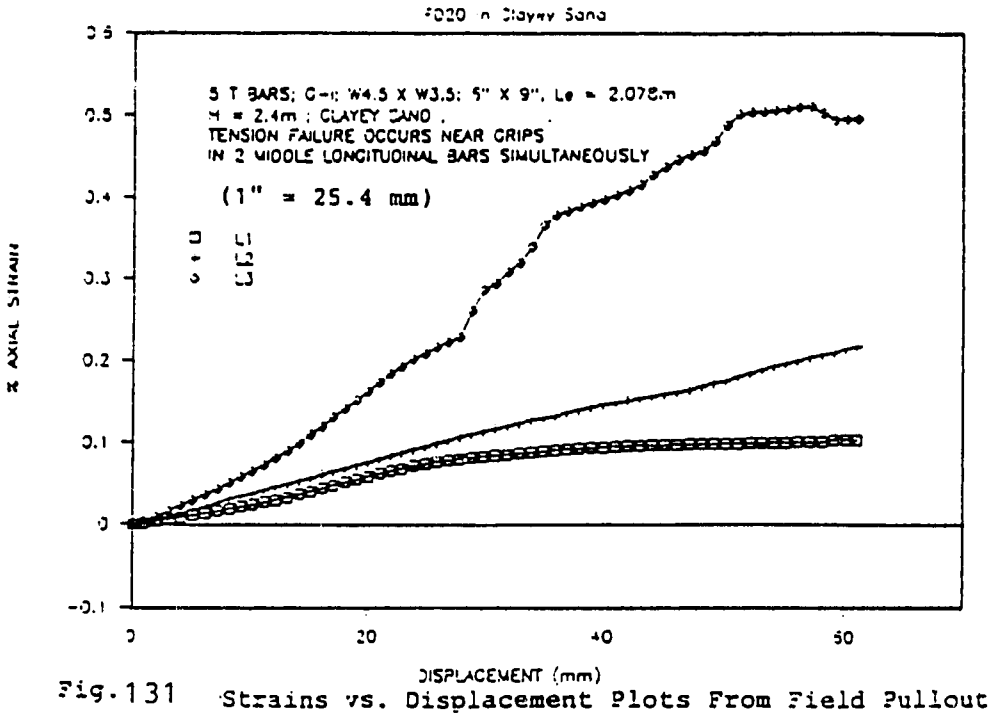

Fig.131 Strains vs. Displacement Plots From Field Pullout Test on Dummy No.20 in Clayey Sand

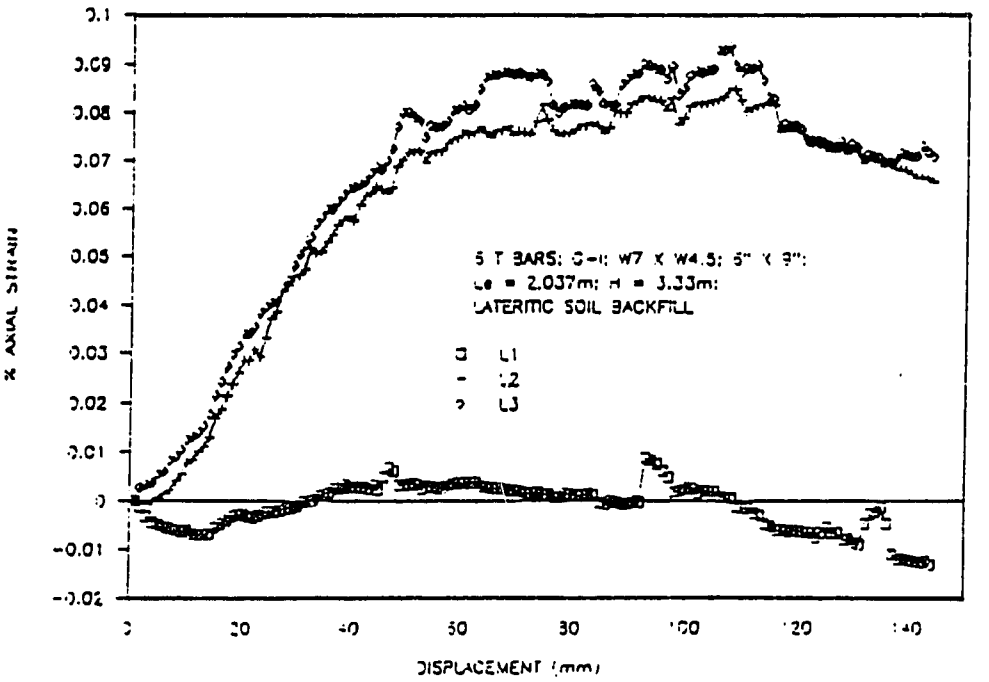

Fig.132 Strains versus Displacement Plots From Field Pullout Test On Dummy No.15 in Lateritic Backfill Soil

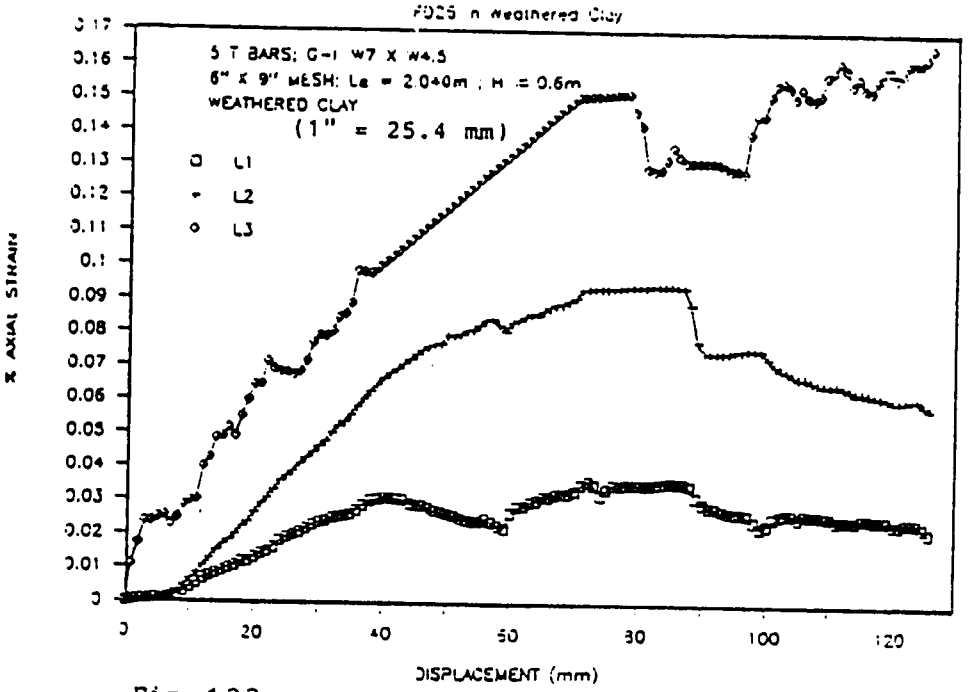

Fig. 133 Strains vs. Displacement Plots From Field Pullout Test of Dummy No.26 in Weathered Clay

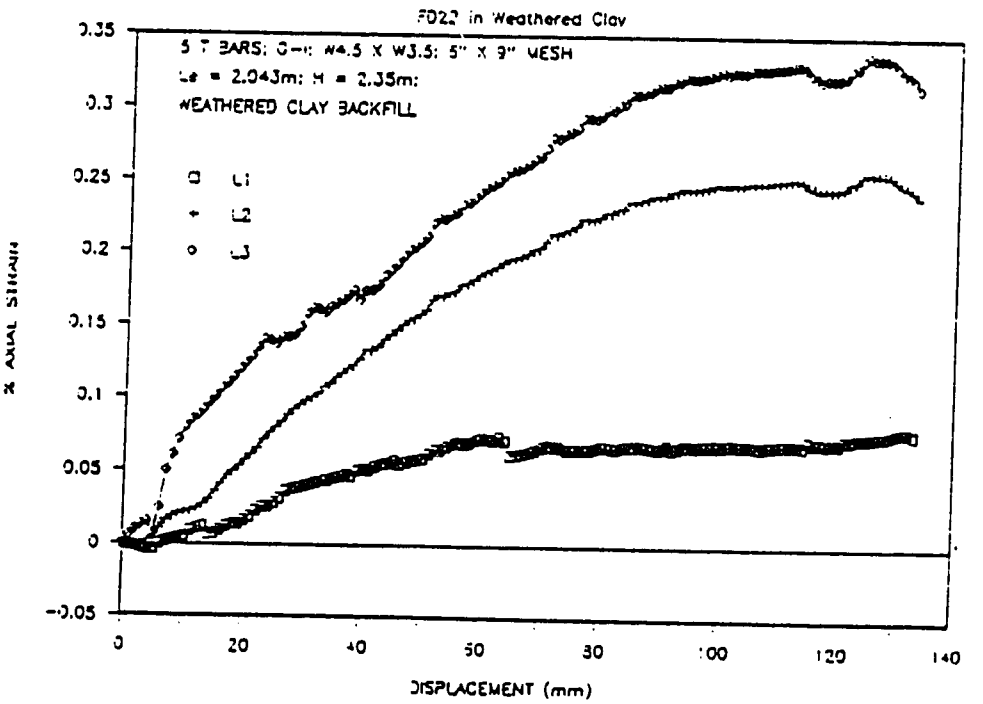

Fig. 134 Strains vs. Displacement from Field Pullout Test of Dummy No.22 in Weathered Clay

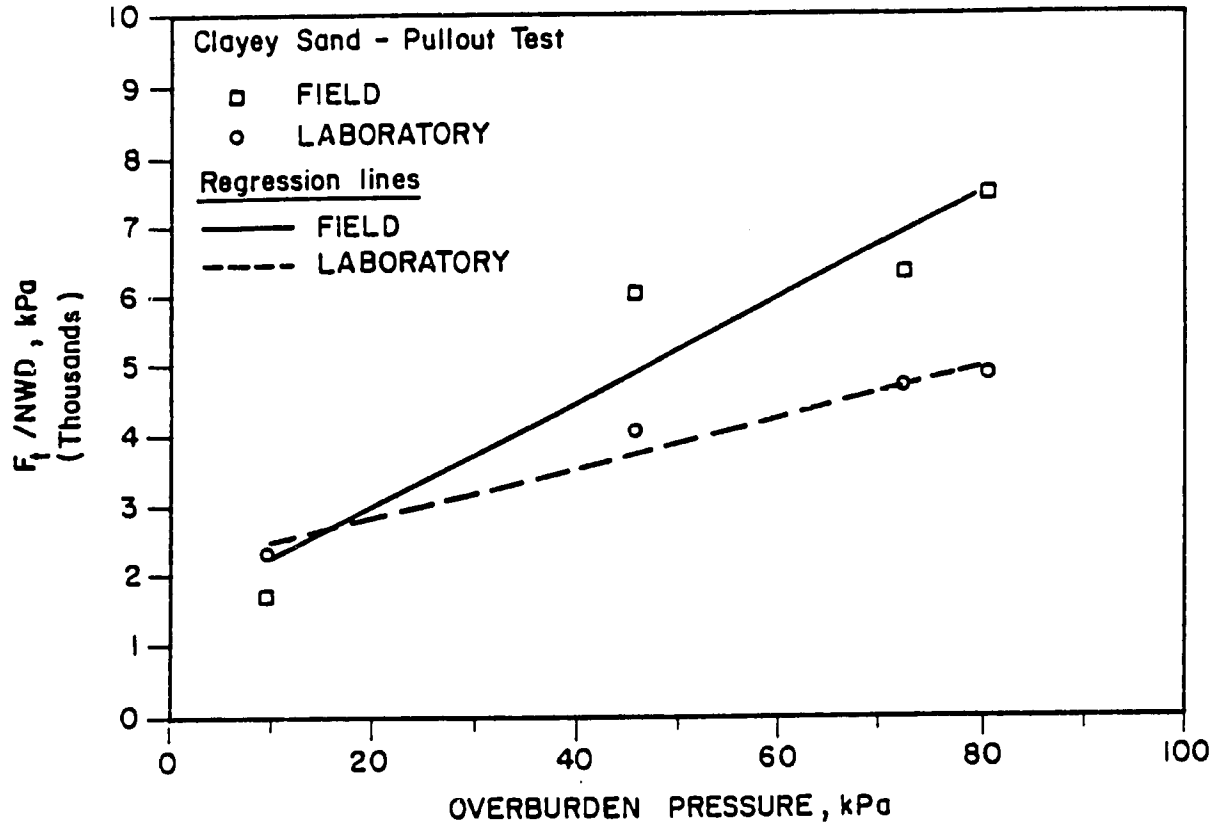

Fig.135 Comparison Between Laboratory and Field Pullout Test Results (Clayey Sand)

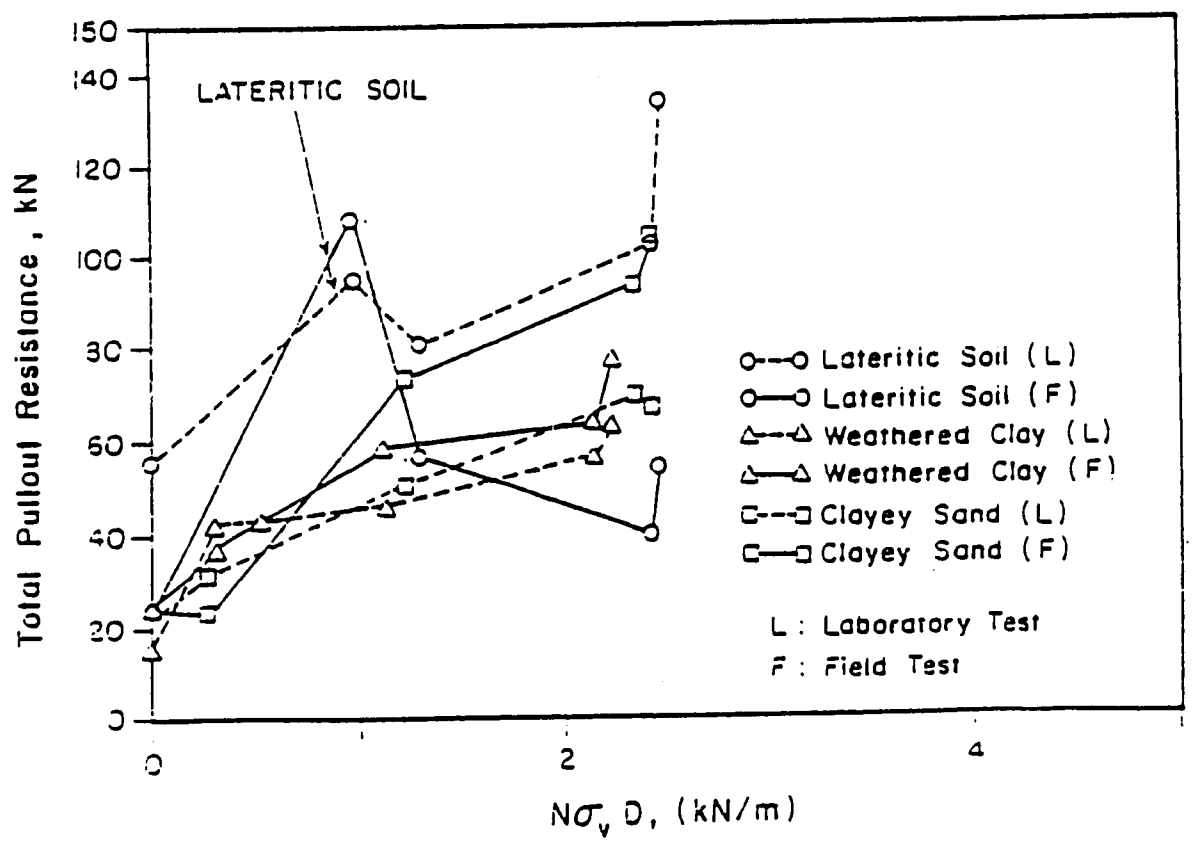

Fig.136 Comparison Between Laboratory and Field Pullout Test Results (Lateritic Soil)

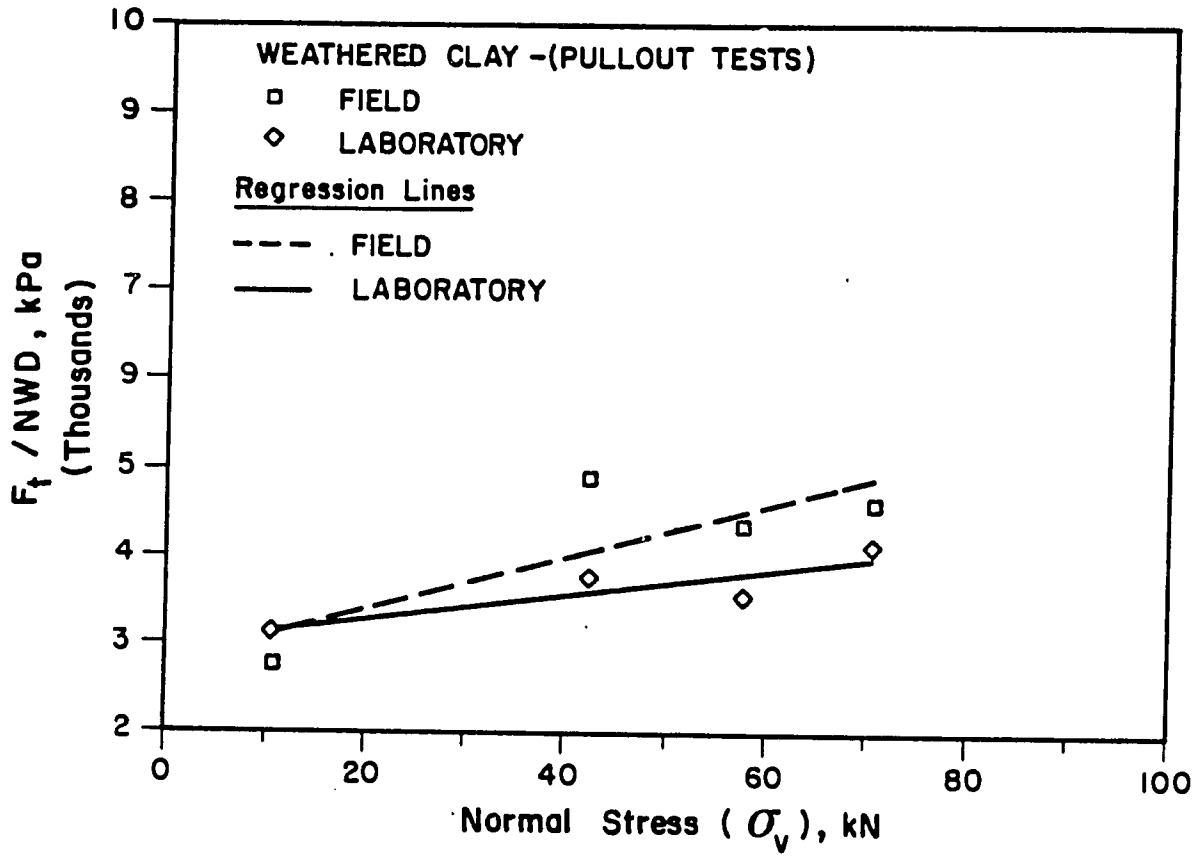

Fig.137 Comparison Between Laboratory and Field Pullout Test Results (Weathered Clay)

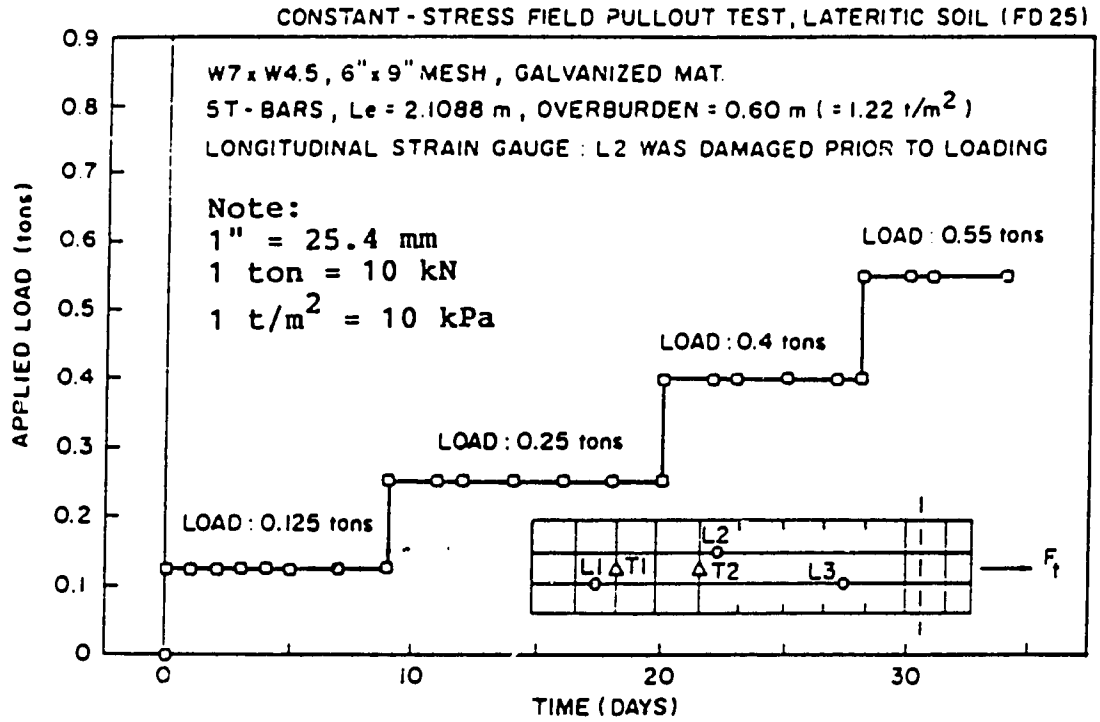

Fig. 138 Plot of Applied Load Against Time in Constant Stress Field Pullout Test For Dummy Mat No.25 in Lateritic Backfill Soil

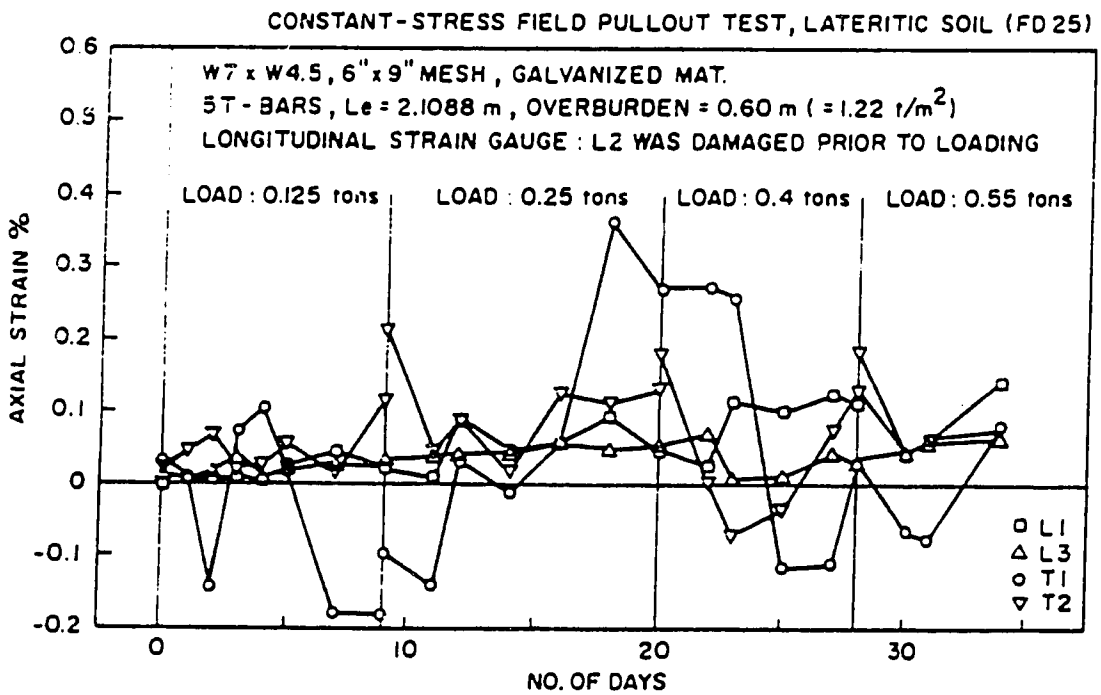

Fig. 139 The Variation of Axial Strains With Time in Constant Stress Field Pullout Test For Dummy No.25 in Lateritic Backfill Soil

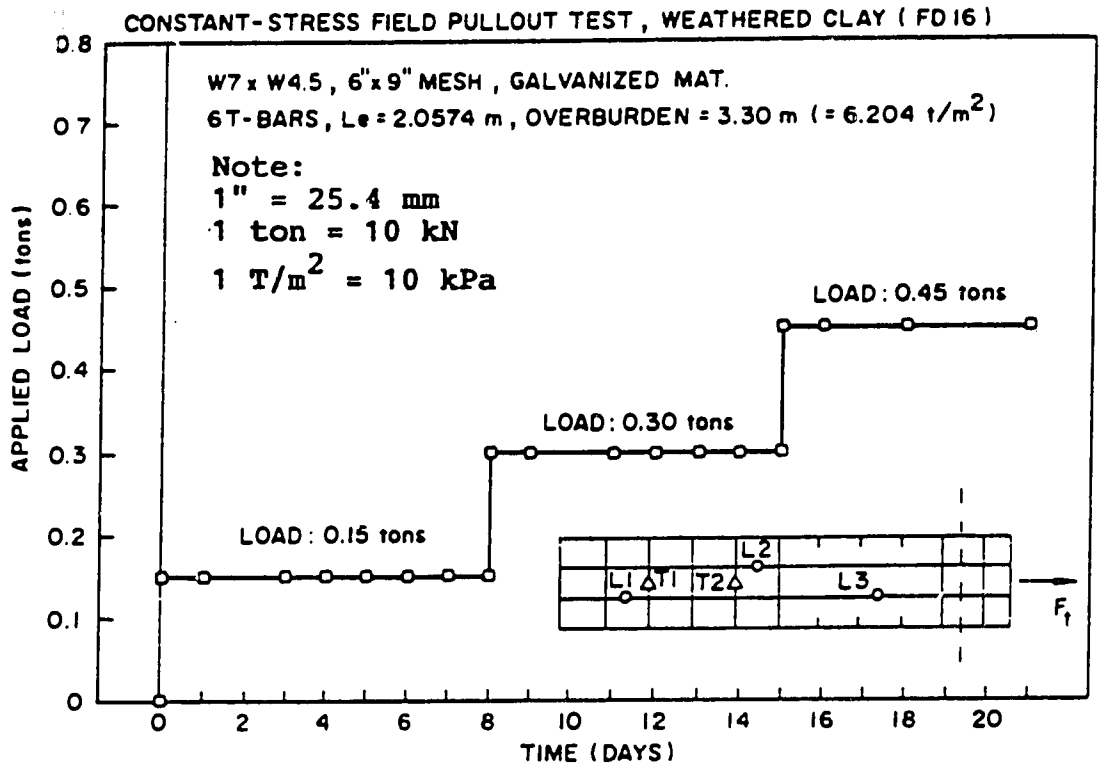

Fig.140 Plot of Applied Load Against Time in Constant Stress Field Pullout Test For Dummy No.16 in Weathered Clay Backfill

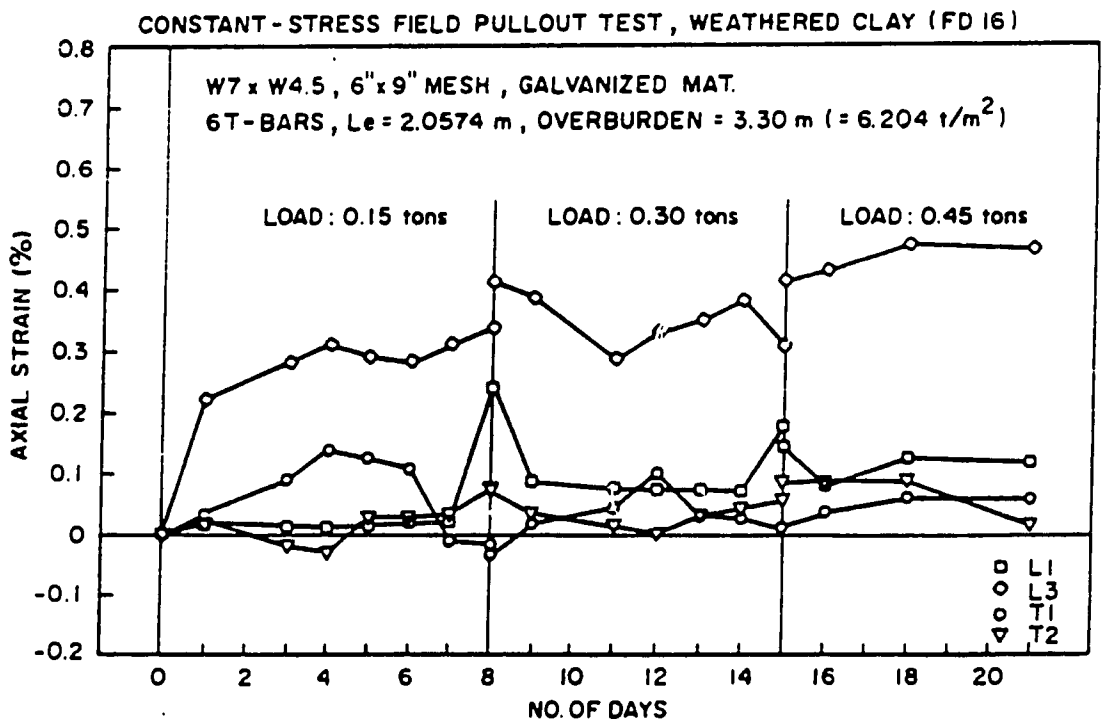

Fig. 141 The Variation of Axial Strains With Time in Constant Stress Field Pullout Test For Dummy No.16 in Weathered Clay Backfill

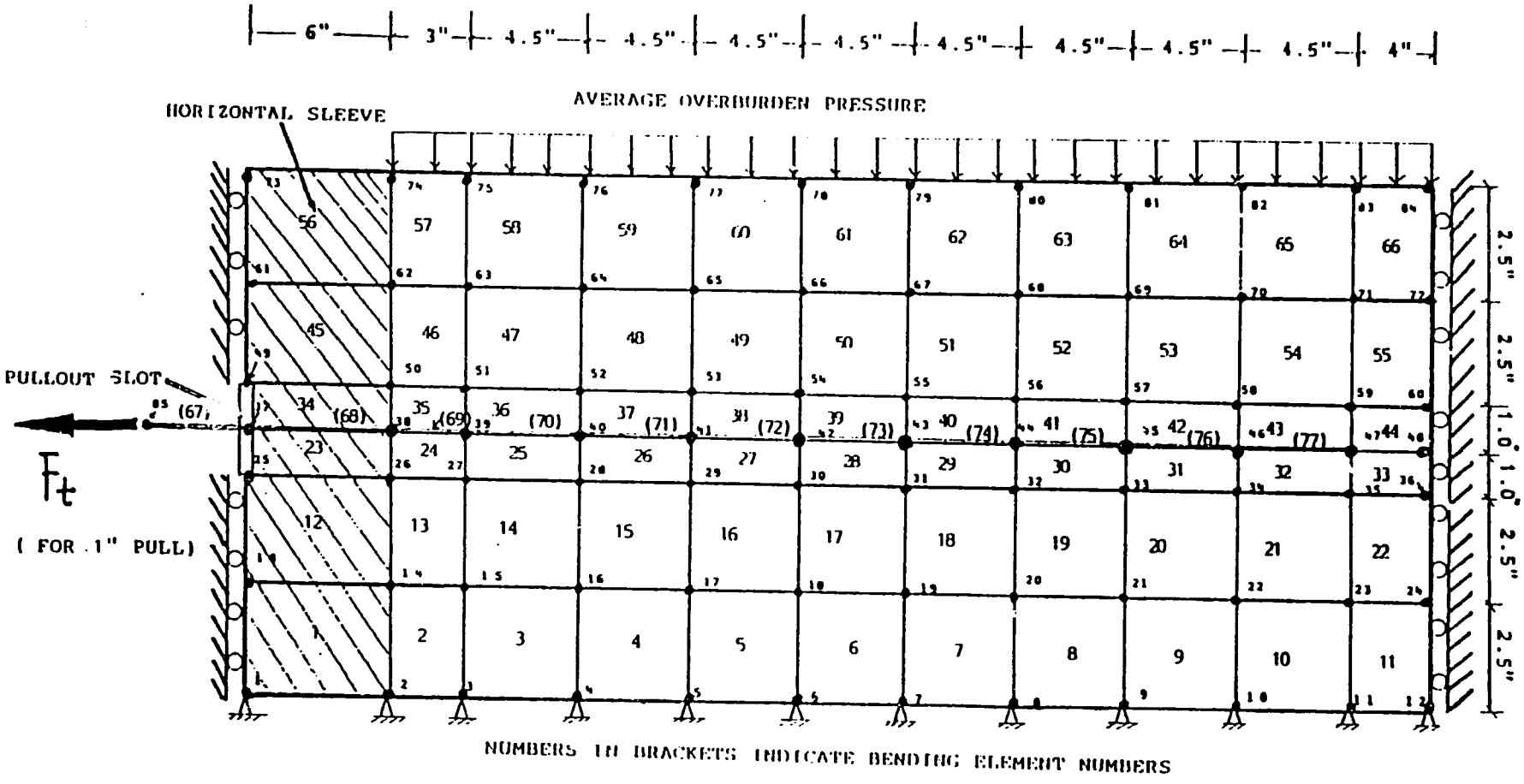

FIG.142 Finite Element Mesh Used to Model the Laboratory Pullout Test (Using the Program REA) (1" = 25.4 mm)

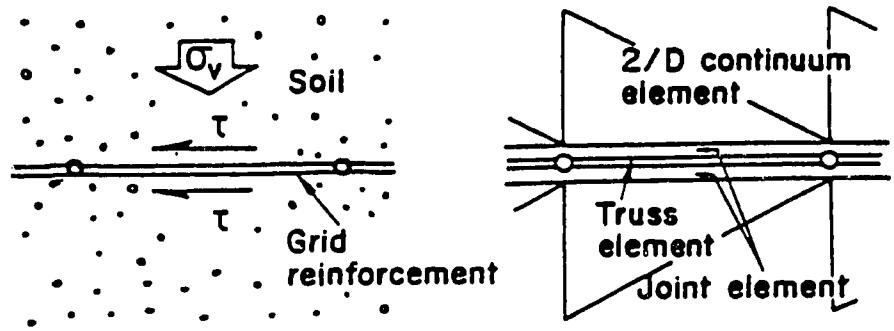

Fig.143 Modelling of Reinforcement and Soil/Reinforcement Interface (NONLIN 1)

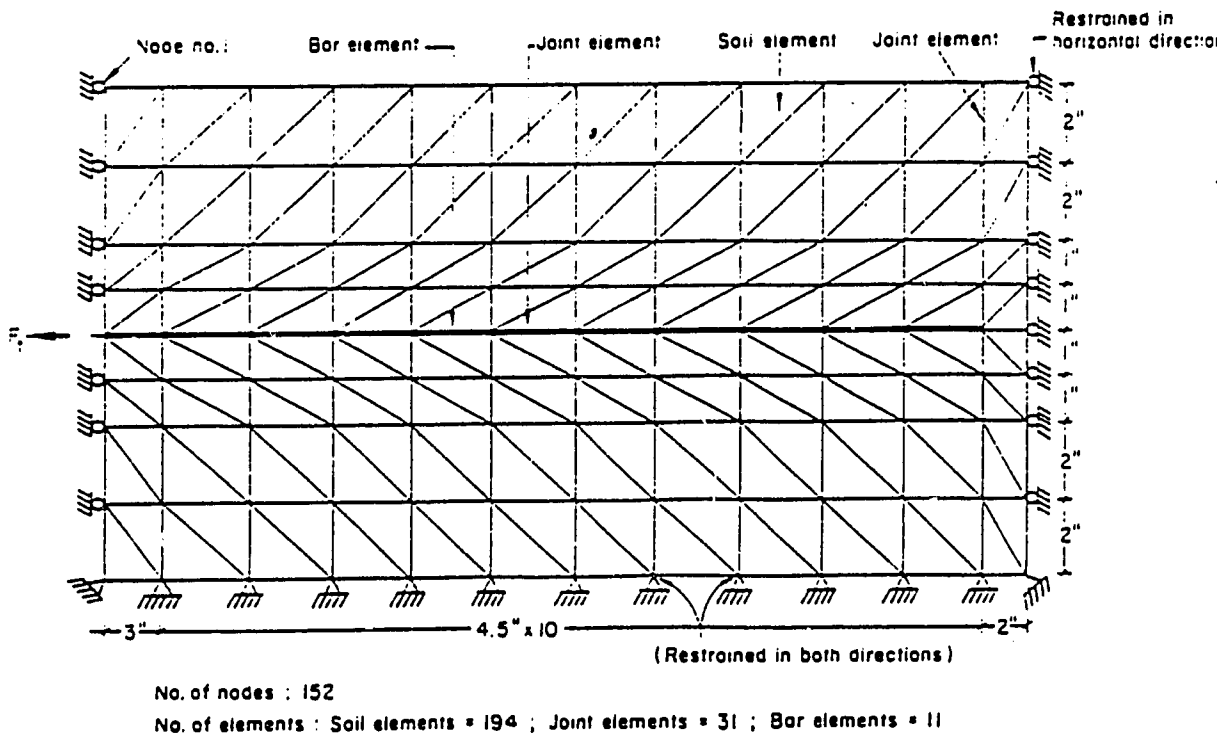

Fig.144 Finite Element Mesh Used to Model the Laboratory Pulllout Test by a Discrete Analysis (NONLIN 1)

(1" = 25.4 mm)

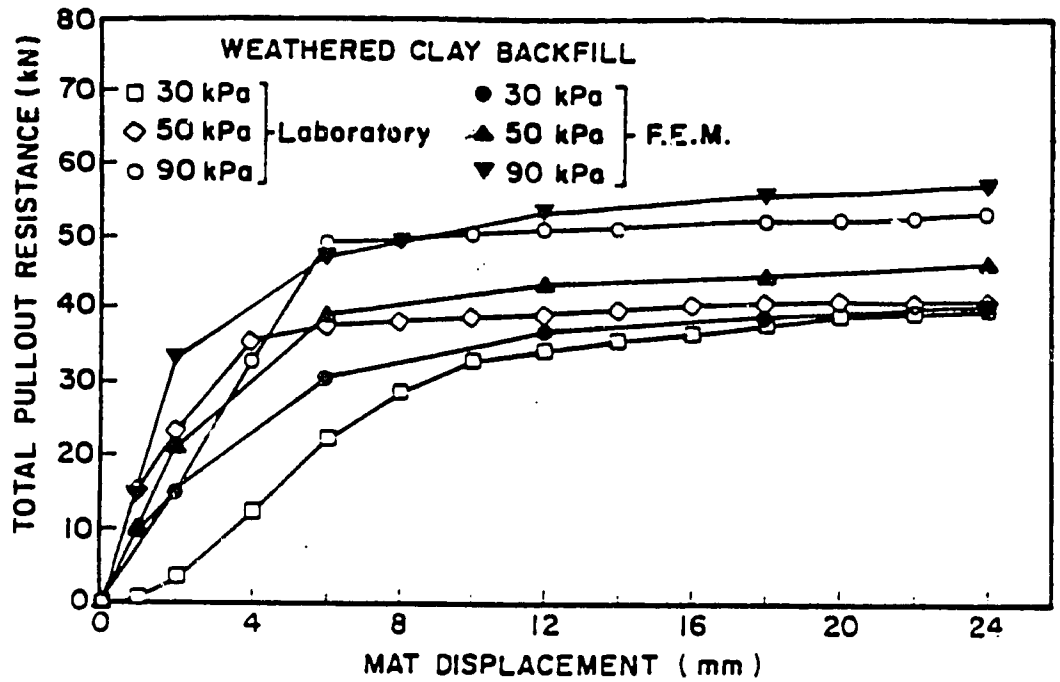

Fig.145 Comparison Between Experimental and Predicted (NONLIN 1) Load-Displacement Curves For Weathered Clay

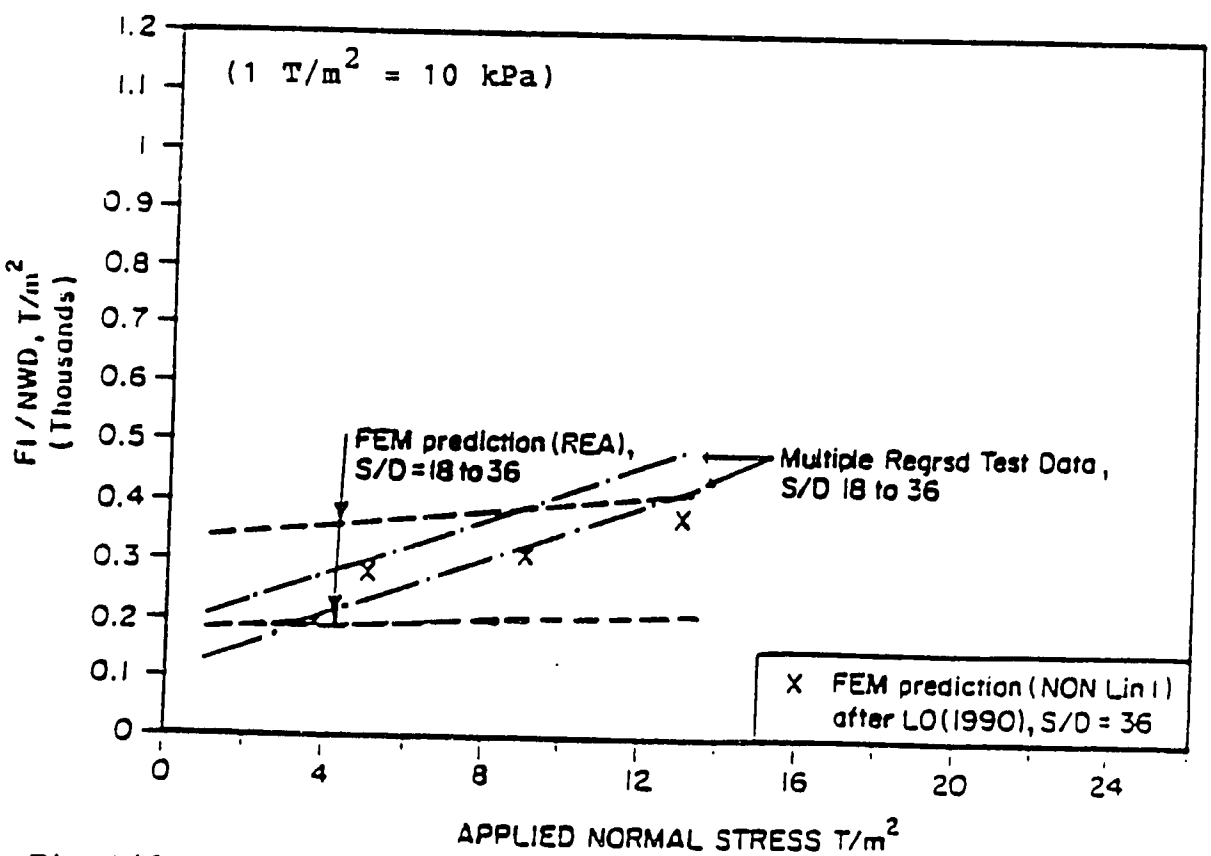

Fig.146 Comparison of the Pullout Resistances From the Finite Element Analyses and Observed Values (Clayey Sand)

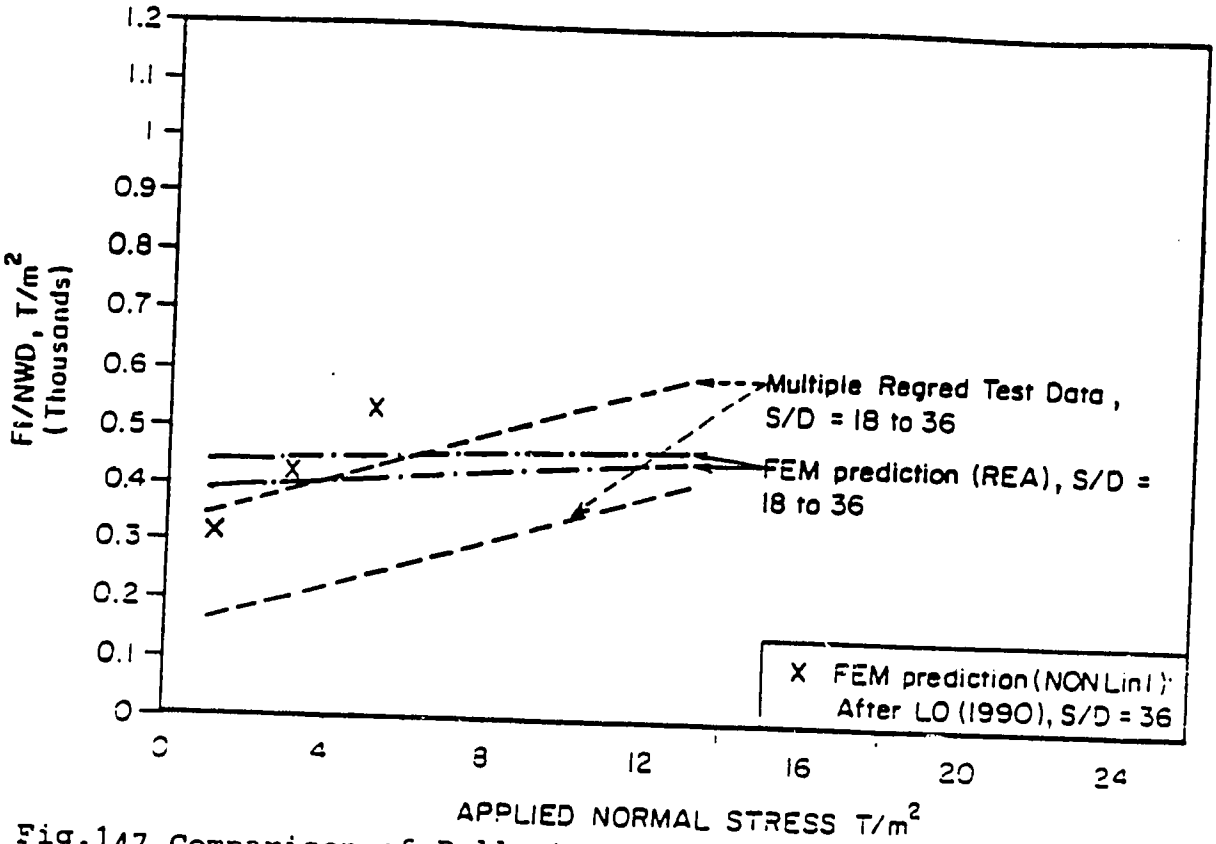

Fig.147 Comparison of Pullout Capacities From the Finite Element Analyses and Observed Values (Lateritic Soil)

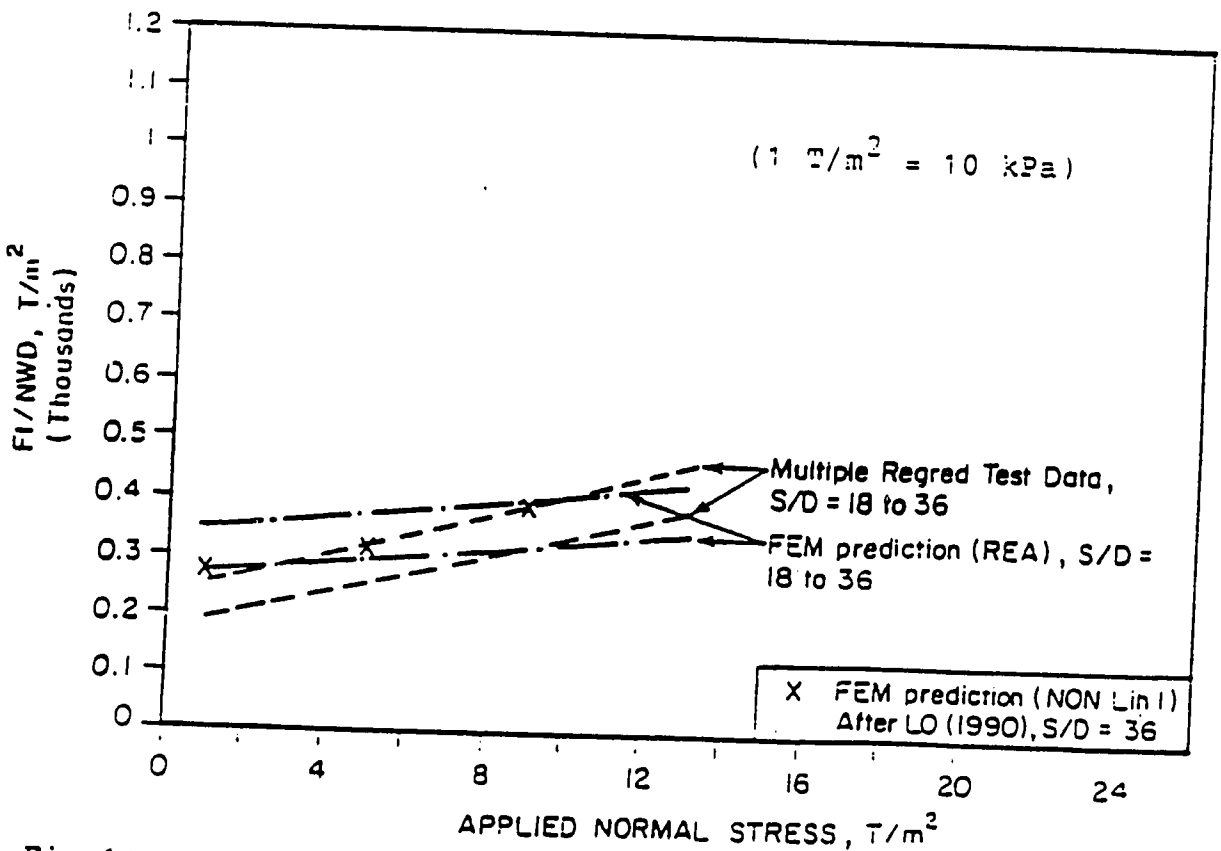

Fig.148 Comparison of Pullout Capacities From the Finite Element Analyses and Observed Values (Weathered Clay)

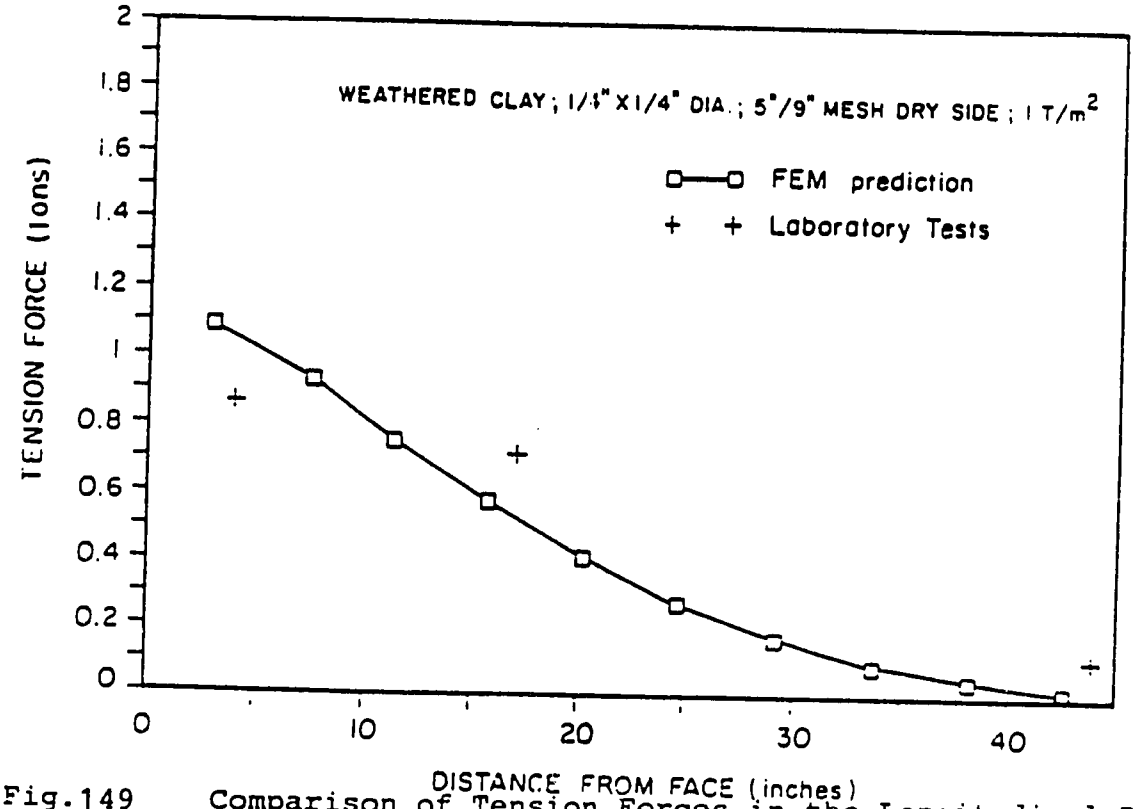

Fig.149 Comparison of Tension Forces in the Longitudinal Bars of the Grid with Distance From the Face From FEM Prediction (REA) and Observed Values, For Weathered Clay, 1/4"x1/4" Dia. Bar Sizes, 6"x9" Mesh, Dry Side, at 1 T/m^2

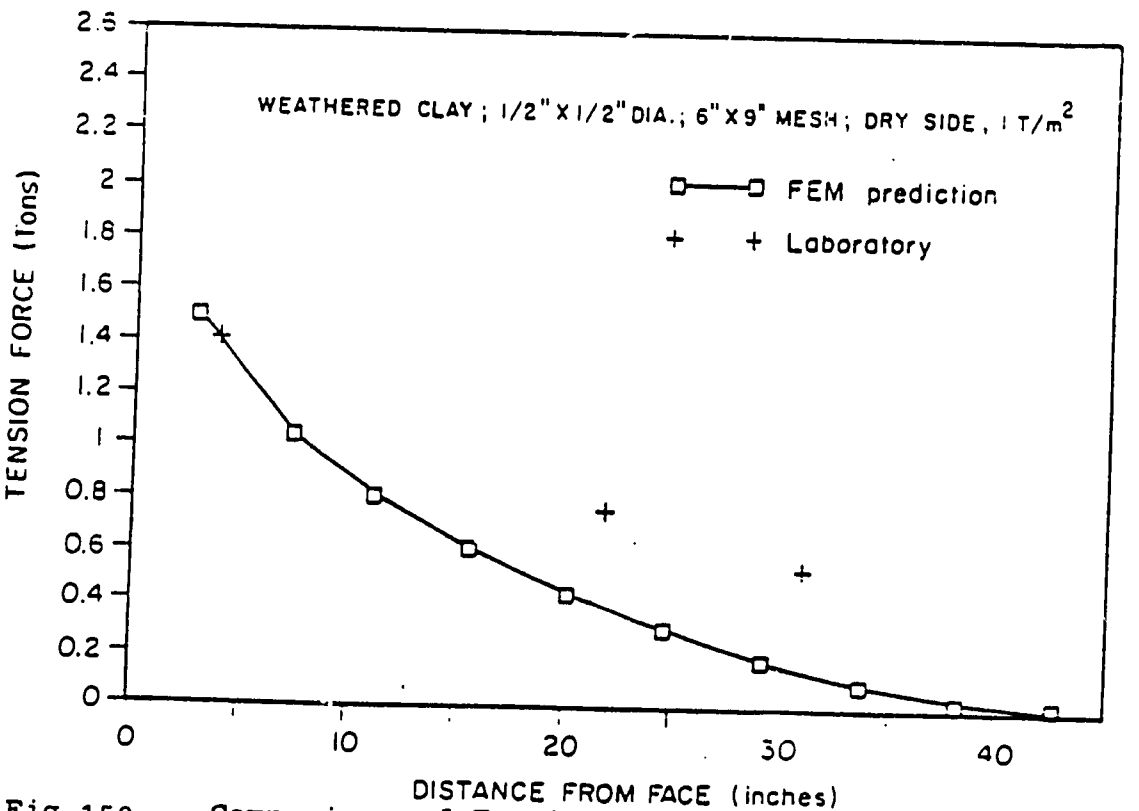

Fig.150 Comparison of Tension forces in the Longitudinal Bars of the Grid With distance From Face From REA and Observed Values, For Weathered Clay, 1/2"x1/2" Dia. Bar Sizes, 6"x9" Mesh, Dry Side, at 13 T/m^2

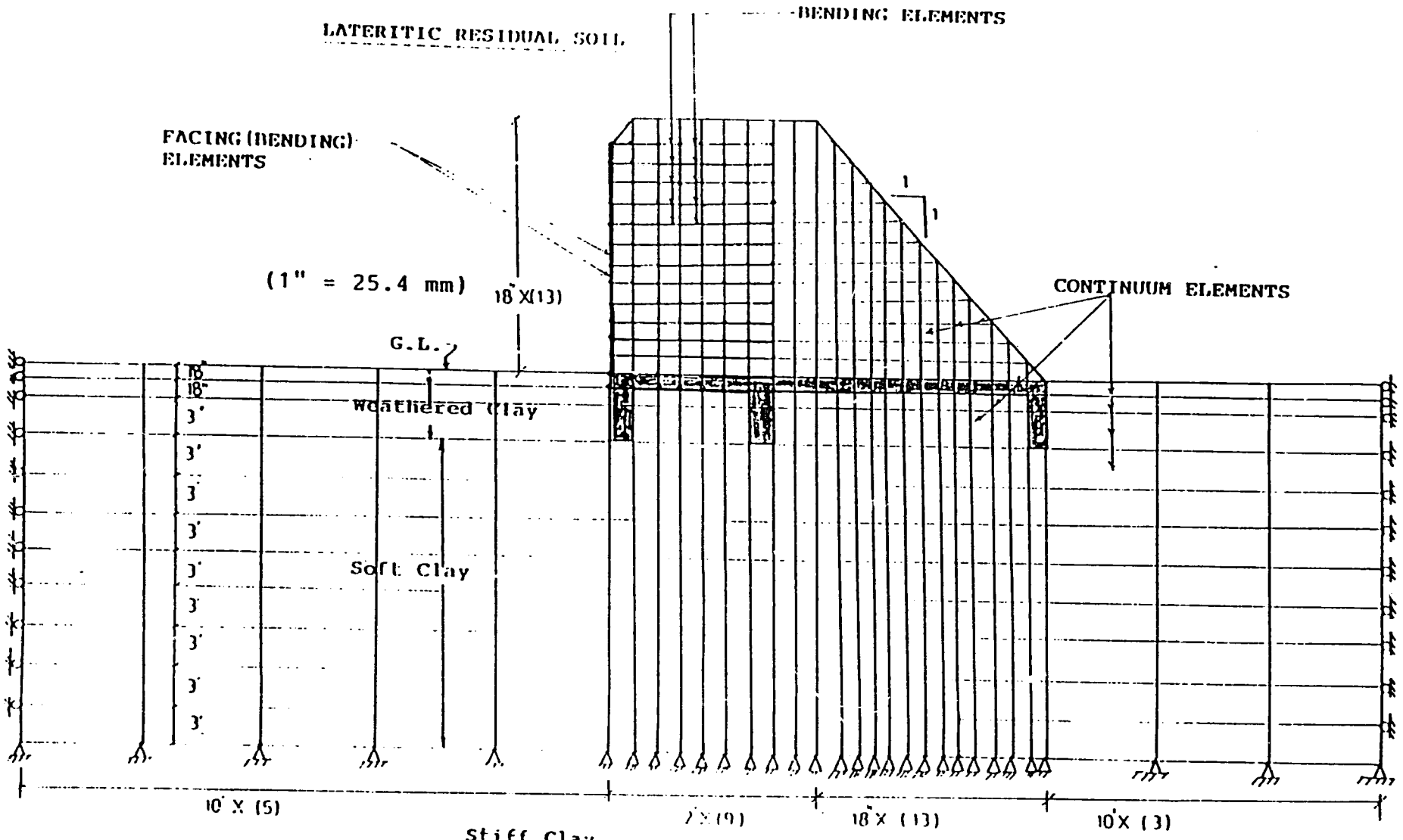

Fig. 151 Finite Element Mesh Used to Model the Welded-Wire Wall (REA)

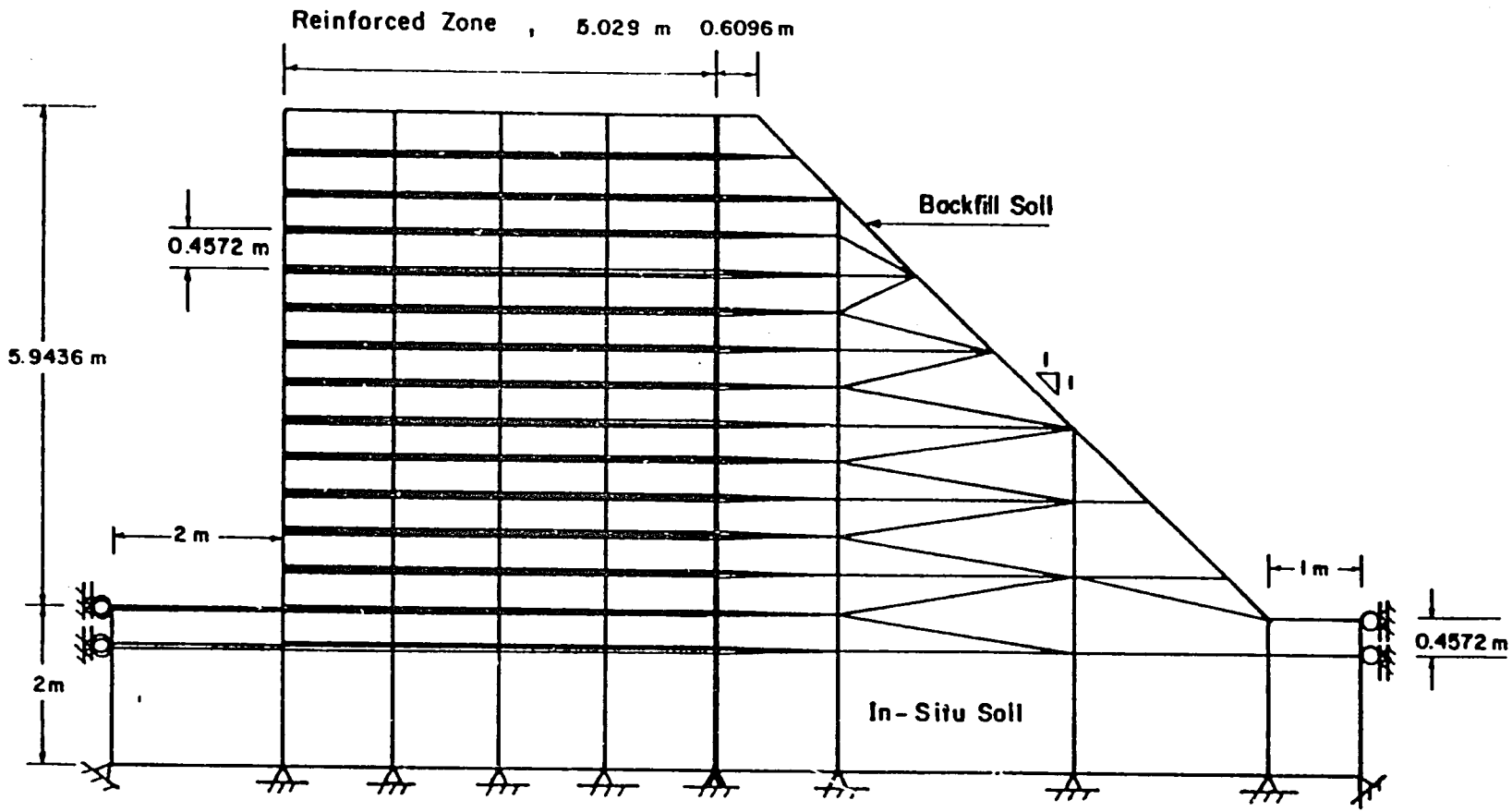

No. of Nodes : 299
No. of Elements : a) Beam Element = 14
b) Bar Element = 56
c) Joint Element = 137
d) Soil Element = 93

Fig.152 Typical Finite Element Mesh For Analyses of the MSE Test Embankment Using NONLIN 1 Program (After LO, 1990)

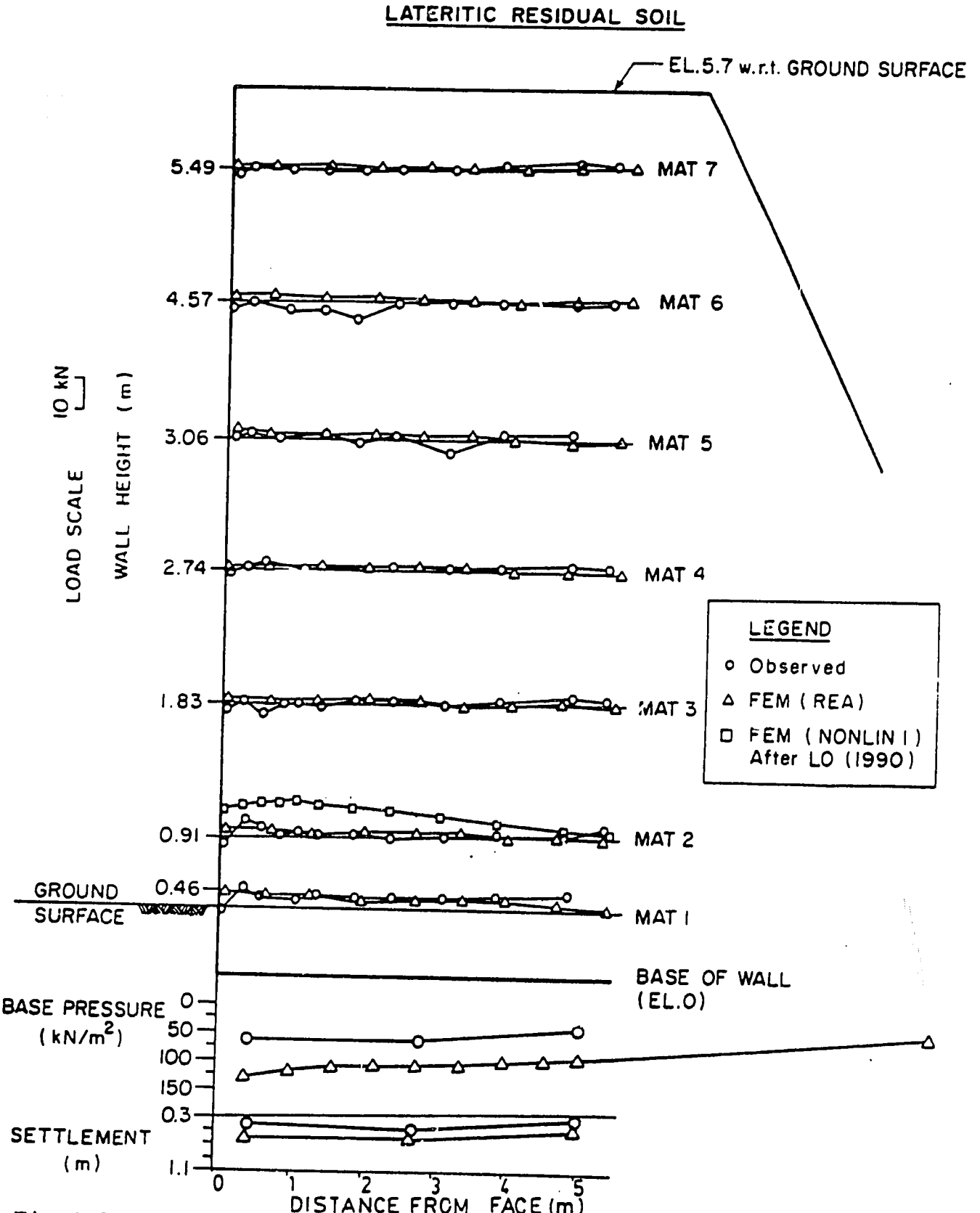

Fig.153 Comparison of Tensile forces in the Reinforcements From Finite Element Analyses (REA & NONLIN 1) With Observed Values

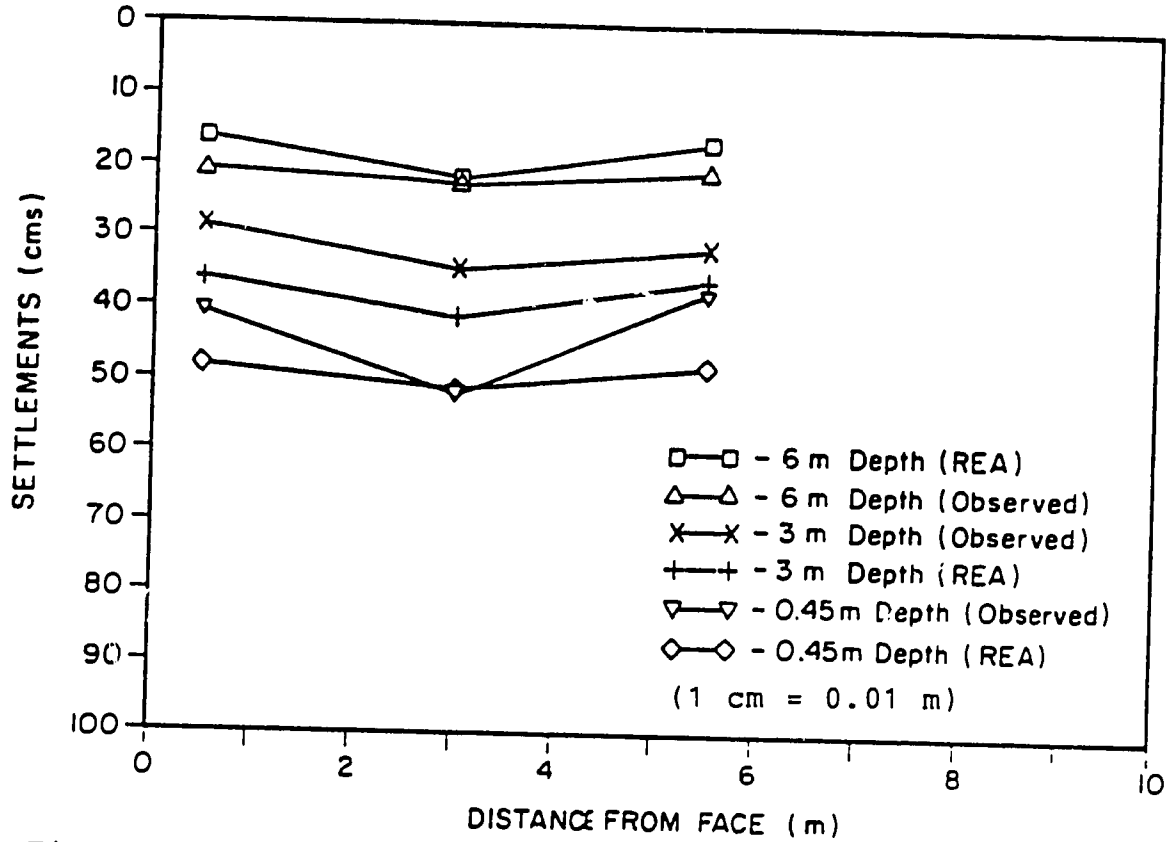

Fig.154 Observed and Predicted (REA) Surface and Subsurface Settlements

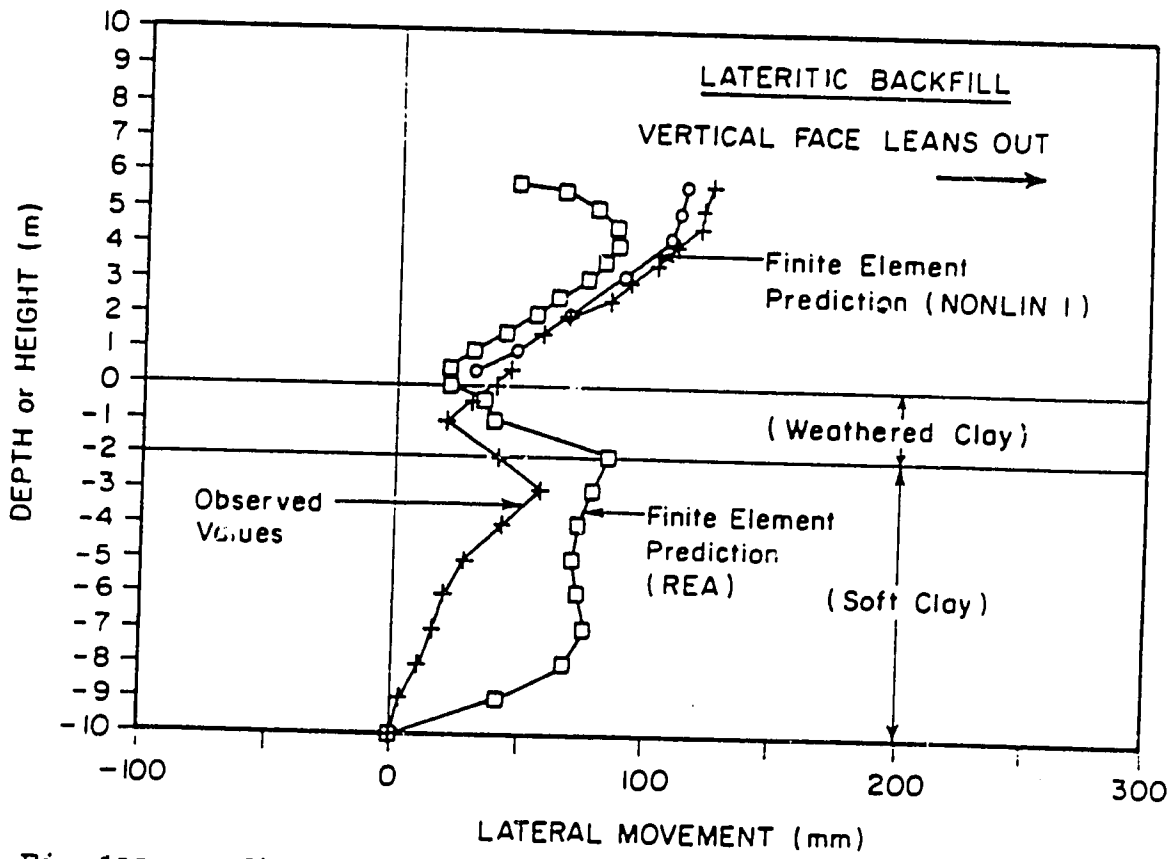

Fig.155 Observed and Predicted (REA & NONLIN 1) Lateral Movements at the Face

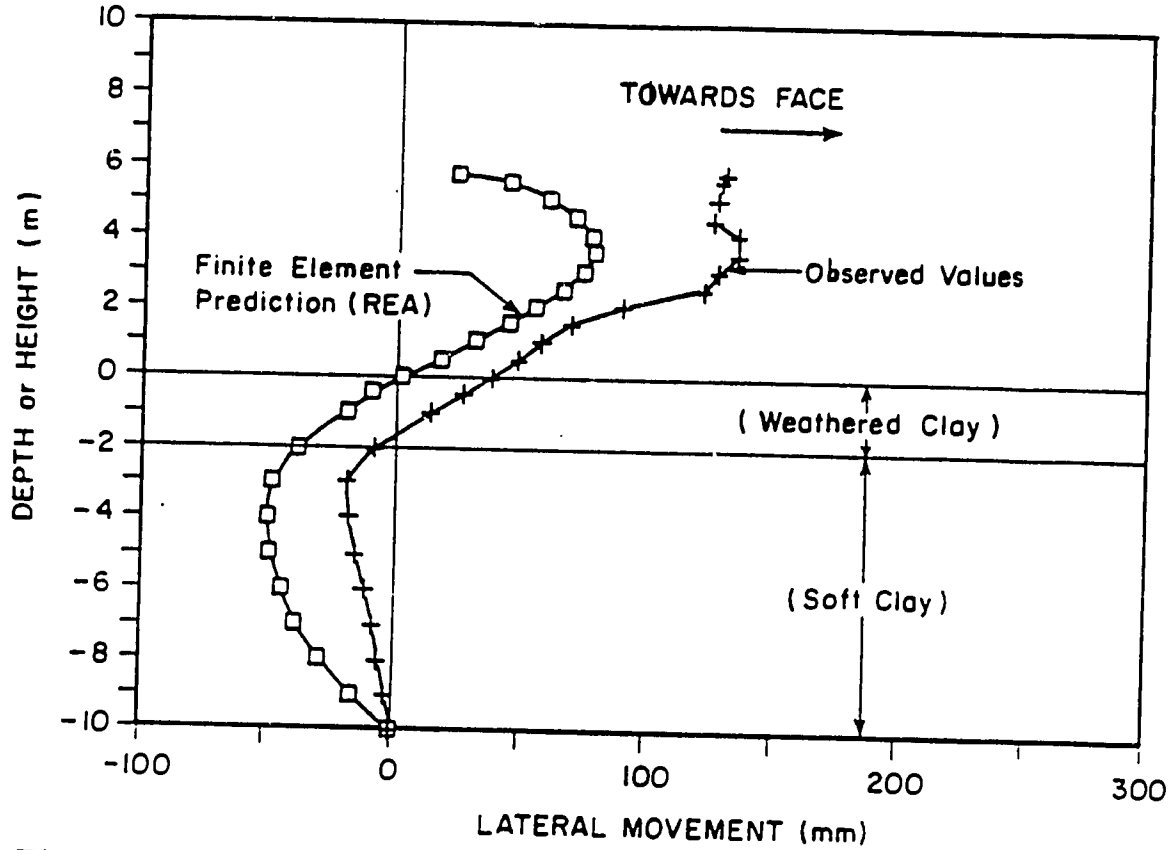

Fig.156 Observed and Predicted (REA) Lateral Movements at Location of I4.

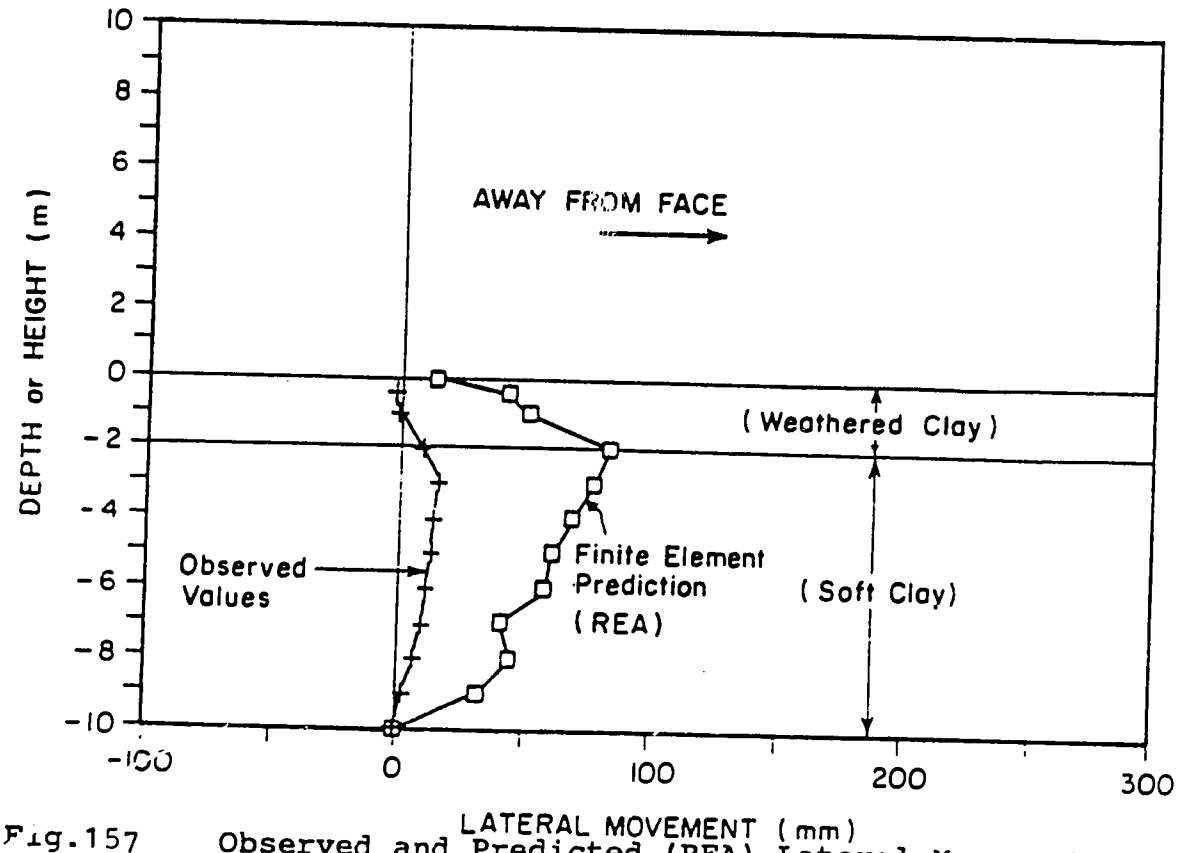

Fig.157 Observed and Predicted (REA) Lateral Movements at the Back, at Location I5